

2020 Review of the Instrument Suite for Spectroscopy at the Spallation Neutron Source and High Flux Isotope Reactor



September 17–18, 2020

CONTENTS

CONTENTS.....	iii
LIST OF FIGURES.....	xi
LIST OF TABLES.....	xviii
1. Introduction to the Spectroscopy Suite at SNS / HFIR.....	1
1.1 Recommendations from the 2017 Suite Review	2
1.2 Triple-Axis Spectrometers.....	3
1.3 Direct Geometry Spectrometers.....	4
1.4 Chemical Spectroscopy	6
1.5 Upgrades and Developments.....	8
Triple-Axis Spectroscopy	8
Direct Geometry Spectroscopy	9
Chemical Spectroscopy	10
1.6 Critical needs for new instruments.....	11
New instruments for HFIR.....	11
New instruments for FTS	12
New instruments for STS	13
1.7 Software.....	14
Data Reduction	14
Data Acquisition.....	14
Data Visualization and Analysis	15
1.8 Staffing	16
2. HFIR HB-1 Polarized Triple-axis Spectrometer Beamline Status and Planning Summary	18
2.1 Overview/Current Status	18
2.2 Scientific Focus.....	19
2.3 Scientific Highlights.....	20
New capabilities in high-resolution neutron Larmor diffraction at ORNL	20
High-resolution phonon energy shift measurements with the inelastic neutron spin echo technique	21
Dual nature of Magnetism in a uranium heavy-fermion system.....	22
Origin of net magnetic moment in LaCoO_3	23
Unique helical magnetic order and field-induced phase in trillium lattice antiferromagnet EuPtSi	24
2.4 General User Program	25
2.5 Update on Instrument Development Activities	25
2.6 Sample Environment.....	26
2.7 Software.....	26
2.8 Update on Impact of Discretionary Beamtime	26
2.9 Outreach and Expansion Activities	26
2.10 Vision.....	26
2.10.1 Near-term Vision (1-3 years).....	26
2.10.2 Strategic Vision (3-10 years) and Alignment with NSCD/ORNL Strategic Plans	27
2.11 Funding/Resource Needs.....	27
2.11.1 Future Funding Opportunities	27
2.12 Self-assessment.....	28
Strengths.....	28

	Weaknesses (Limitations)	28
	Opportunities	28
	Threats 28	
2.13	Executive Summary	29
2.13.1	Comparison of instrument specifications to similar instrument worldwide	30
2.13.2	Comparison of sample environment capabilities with similar instruments worldwide	31
2.13.3	Data and computing capabilities	31
3.	HFIR HB-3 Triple Axis Spectrometer Beamline Status and Planning Summary	33
3.1	Overview/Current Status	33
	Team Structure	33
3.2	Scientific Focus	34
3.3	Scientific Highlights	35
	Temperature dependence of low-E magnetic fluctuations in nearly optimally doped $\text{NaFe}_{0.9785}\text{Co}_{0.0215}\text{As}$	35
	Supersonic propagation of lattice energy by phasons in fresnoite	36
	f-Electron States in PrPd_5Al_2	37
	Low-T anharmonicity and the thermal conductivity of cesium iodide	38
	Anharmonic Eigenvectors and Acoustic phonon Disappearance in Quantum Paraelectric SrTiO_3	39
3.4	General User Program	40
3.5	Update on Instrument Development Activities	41
	Omega shielding around the sample position.	41
	Velocity Selector	42
	New analyzer tank wedge lifter system	42
3.6	Sample Environment	42
3.7	Software	42
3.8	Impact of Discretionary Beam Time	43
3.9	Outreach and Expansion Initiatives	43
3.10	Vision	43
	Near-term Vision (1-3 years)	43
	Strategic Vision (3-10 years)	44
3.11	Funding/Resource Needs	45
3.12	Self-Assessment	45
	Strengths	45
	Weaknesses	45
	Opportunities	46
	Threats 46	
3.13	Executive Summary	46
3.13.1	Comparison of instrument specifications with similar instrument worldwide	47
4.	HFIR HB-1A, FIE-TAX, Fixed-Incident-Energy Triple-Axis Spectrometer Beamline Status and Planning Summary	48
4.1	Overview/Current Status	48
4.2	Team Structure	49
4.3	Scientific Focus and Publications	49
4.4	Scientific Highlights	49
	Revisiting the Kitaev material candidacy of Ir^{4+} double perovskite iridates	50
	Spin canting and orbital order in spinel vanadate thin films	51

	Destabilization of magnetic order in a dilute Kitaev spin liquid candidate	52
	Novel strongly spin-orbit coupled quantum dimer magnet: $\text{Yb}_2\text{Si}_2\text{O}_7$	52
4.5	General User Program	53
4.6	Update on Instrument Improvement Project	53
4.7	Sample Environment	54
4.8	Software	55
4.9	Update on Impact of Discretionary Beamtime	55
4.10	Outreach and Expansion Activities	56
4.11	Vision	56
	Near-term Vision (1-3 years)	56
	Strategic Vision (3-10 years) and Alignment with NScD/ORNL Strategic Plans	56
4.12	Funding / Resource Needs	57
4.13	Future Funding Opportunities	58
4.14	Self-assessment	58
	Strengths	58
	Weaknesses (Limitations)	58
	Opportunities	58
	Threats	59
4.15	Executive Summary	59
	4.15.1 Comparison of instrument specifications to similar instruments worldwide	60
	Comparison of sample environment capabilities with similar instruments worldwide	61
	Data and computing capabilities	61
4.16	References	62
5.	HFIR CG4-C Cold Neutron Triple-Axis Spectrometer Beamline Status and Planning Summary	62
5.1	Overview/Current Status	63
	Team Structure	63
5.2	Scientific Focus	64
5.3	Scientific Highlights	65
	Field-induced quasiparticle breakdown in a quantum antiferromagnet	65
	Time dependence of the magnetic structure in a triangular lattice magnet $\text{Ca}_3\text{Co}_2\text{O}_6$	66
	Large spin-orbit torque efficiency enhanced by the magnetic structure of a collinear antiferromagnet in epitaxial IrMn thin films	67
	Novel excitations near quantum criticality in geometrically frustrated antiferromagnet CsFeCl_3	68
5.4	General User Program	69
5.5	Update on Instrument Development Activities	69
5.6	Sample Environment	69
5.7	Software	70
5.8	Update on Impact of Discretionary Beamtime	70
5.9	Vision	70
	Near-term Vision (1-3 years)	70
	Strategic Vision (3-10 years) and Alignment with NScD/ORNL Strategic Plans	70
5.10	Funding/Resource Needs	70
5.11	Future Funding Opportunities	70
5.12	Self-assessment	71
	Strengths	71
	Weaknesses (Limitations)	71
	Opportunities	71

	Threats	71
5.13	Executive Summary.....	71
5.13.1	Comparison of instrument specifications with similar instrument worldwide	72
5.13.2	Data and computing capabilities	72
5.13.3	Comparison of sample environment capabilities with similar instruments worldwide	73
6.	SNS BL-18, The wide Angular-Range Chopper Spectrometer (ARCS): Beamline Status and Planning Summary Document	74
6.1	Overview/Current Status	74
	Team Structure	75
	Scientific Focus.....	76
6.2	Scientific Highlights.....	76
	Beyond quasi-harmonic theory: Silicon anharmonicity and quantum effects	76
	Vibrational studies of ionic transport materials	78
	Single crystal magnetism: Highly frustrated square-lattice itinerant magnet $\text{CaCo}_{2-\gamma}\text{As}_2$	79
6.3	General User Program	80
6.4	Update on Instrument Development Activities.....	81
	ARCS detector array upgrade.....	81
	New DAS controls	81
	Optimized CCR	82
	Automatic helium exchange gas handling	82
	Multi-sample stick.....	82
	Software.....	82
6.5	Update on the Impact of Discretionary Beam Time	83
6.6	Outreach and Expansion Initiatives	83
6.7	ARCS Vision	84
	Near-term Vision (1-3 years).....	84
	Strategic Vision (3-10 years) and Alignment with NScD/ORNL Strategic Plans	84
6.8	Funding/Resources Needs	84
6.9	Self-Assessment	85
	Strengths.....	85
	Weaknesses	85
	Opportunities.....	85
	Threats	85
6.10	Executive summary	86
6.10.1	Comparison of instrument specifications to similar instrument worldwide	87
6.10.2	Comparison of sample environment capabilities with similar instruments worldwide	87
6.10.3	Data and computing capabilities	88
7.	SNS BL-17, The SEQUOIA Fine-Resolution Fermi Chopper Spectrometer: Beamline Status and Planning Summary Document	89
7.1	Overview/Current Status	89
	Team Structure	90
7.2	Scientific Focus.....	91
7.3	Scientific Highlights.....	91
	Three-Magnon Bound State in the Quasi-One-Dimensional Antiferromagnet $\alpha\text{-NaMnO}_2$	92
	Frustrated Magnetism in a Mott Insulator	93

	Complexity of Intercalation in MXenes: Destabilization of Urea by Two-Dimensional Titanium Carbide.....	94
	Water and Intercalated Protons Exhibit Limited Dynamics in Tungsten Oxide Hydrates for Electrochemical Energy Storage.....	95
7.4	General User Program	96
7.5	Update on Instrument Development Activities.....	97
7.6	Update on IDT and Discretionary Beam Time.....	98
7.7	Outreach	99
7.8	Vision.....	100
	Near-term Vision (1-3 years).....	100
	Strategic Vision (3-10 years) and Alignment with NScD/ORNL Strategic Plans	103
7.9	Funding/Resources Needs	103
7.10	Future funding opportunities.....	104
7.11	Self-Assessment	104
	Strengths	104
	Weaknesses	104
	Opportunities.....	105
	Threats 105	
7.12	Executive summary	105
	7.12.1 Comparison of instrument specifications to similar instrument worldwide	106
8.	SNS-BL5, CNCS, Cold Neutron Chopper Spectrometer, Status and Planning Summary.....	107
8.1	Overview and Current Status.....	107
	Team Structure	108
8.2	Scientific Focus.....	109
8.3	Scientific Highlights.....	110
	Anharmonic lattice dynamics and superionic transition in AgCrSe ₂	110
	Competing Magnetic Interactions in the Antiferromagnetic Topological Insulator MnBi ₂ Te ₄	111
	Novel Strongly Spin-Orbit Coupled Quantum Dimer Magnet: Yb ₂ Si ₂ O ₇	112
	Tomonaga–Luttinger liquid behavior and spinon confinement in YbAlO ₃	113
	Fast Rotational Diffusion of Water Molecules in a 2D Hydrogen Bond Network at Cryogenic Temperatures.....	114
8.4	General User Program	115
8.5	Update on Instrument Development Activities.....	115
8.6	Update on Impact of Discretionary Beamtime	118
8.7	Outreach and Expansion Initiatives	118
8.8	Vision.....	118
	Near term vision (1-3 years)	118
	Strategic vision (3-10 years).....	119
8.9	Funding Resource Needs.....	120
8.10	Self-Assessment	120
	Strengths.....	120
	Weaknesses (Limitations)	120
	Opportunities.....	120
	Threats 120	
8.11	Executive Summary.....	120
	8.11.1 Comparison of instrument specifications to similar instrument worldwide.....	121

8.11.2	Comparison of sample environment capabilities with similar instruments worldwide	121
8.11.3	Data and computing capabilities	122
9.	SNS BL-14B, HYSPEC, Neutron Direct Geometry Spectrometer Status and Planning Summary	123
9.1	Overview / Current Status	123
	Team Structure	124
9.2	Scientific Focus.....	124
9.3	Scientific Highlights.....	125
	Continuum of quantum fluctuations in a three-dimensional $S = 1$ Heisenberg magnet	126
	Exotic Magnetic Field-Induced Spin-Superstructures in a Mixed Honeycomb-Triangular Lattice System	127
	Intrinsic anharmonic localization in thermoelectric PbSe	128
	Excitations in the field-induced quantum spin liquid state of α -RuCl ₃	129
	Anharmonic Eigenvectors and Acoustic Phonon Disappearance in Quantum Paraelectric SrTiO ₃	130
	Reentrant spin glass state induced by structural phase transition in La _{0.4} Ce _{0.6} Co ₂ P ₂	131
9.4	General User Program	132
9.5	Update on Instrument Development Activities.....	132
9.6	Update on Impact of Discretionary Beamtime	138
9.7	Outreach and Expansion Initiatives	139
9.8	Mapping recent activities to the previous 3-year VISION.....	140
9.9	Vision.....	140
	Near-term Vision (1-3 years).....	140
	Strategic Vision (3-10 years) and Alignment with NSCD / ORNL Strategic Plan.....	143
9.10	Funding / Resource Needs	145
9.11	Self-Assessment	145
	Strengths.....	145
	Weaknesses (Limitations)	145
	Opportunities.....	146
	Threats	146
9.12	Executive Summary.....	146
	9.12.1 Comparison of HYSPEC polarized capabilities to other instruments.....	147
10.	SNS BL-2, The BASIS Backscattering Spectrometer: Beamline Status and Planning Summary Document	148
10.1	Overview/Current Status	148
	Team Structure	149
10.2	Scientific Focus.....	150
10.3	Scientific Highlights.....	150
	Mixed Ionic Liquid Improves Electrolyte Dynamics in Supercapacitors	151
	Spatial-Temporal Characteristics of Confined Polymer Motion Determine Proton Conduction of Polyoxometalate-Poly(ethylene glycol) Hybrid Nanocomposites.....	152
	Elucidating the Mobility of H ⁺ and Li ⁺ Ions in (Li _{6.25-x} H _x Al _{0.25})La ₃ Zr ₂ O ₁₂ via Correlative Neutron and Electron Spectroscopy	153
	Abnormally Low Activation Energy in Cubic Na ₃ SbS ₄ Superionic Conductors	154
10.4	General User Program	154
10.5	Update on Instrument Development Activities.....	155
10.6	Update on Partner and Discretionary Beam Time.....	155
10.7	Outreach	155

10.8	Vision.....	156
	Near-term (1-3 years) and strategic (3-10 years)	156
10.9	Funding/Resources Needs	158
10.10	Future funding opportunities.....	158
10.11	Self-Assessment	158
	Strengths.....	158
	Weaknesses	159
	Threats	159
10.12	Executive Summary.....	159
11.	SNS BL-16B, The VISION Vibrational Spectrometer Beamline Status and Planning Summary Document	160
11.1	Overview and Current Status.....	160
	Team Structure	161
11.2	Scientific Focus.....	161
11.3	Instrument Productivity.....	162
11.4	Science Examples	165
	Orientational Glass Formation in Substituted Hybrid Perovskites	165
	Production of arenes via direct lignin upgrading over a niobium-based catalyst	166
	Nuclear modes limiting charge mobility in molecular semiconductors	168
	Quantum dynamics of H ₂ trapped within organic clathrate cages	170
	Nature of Reactive Hydrogen for Ammonia Synthesis over a Ru/C ₁₂ A ₇ Electride Catalyst	171
11.5	Beam Line Development Activities	172
	Diffraction	172
	Pair Distribution Function	173
	High-pressure cells.....	174
	Furnace.....	176
	Software.....	177
11.6	Outreach	177
11.7	Strategic Vision	178
11.8	Resources Needed	178
	VISION Staffing.....	178
	More space for the chemistry lab.....	178
	Complete BL16A.....	179
	New CCR/cooling system	179
	Sample Changer	179
	Testing beam time	179
11.9	Self-Assessment	179
	Strengths.....	179
	Weaknesses (limitations).....	179
	Opportunities.....	180
	Threats	180
11.10	Executive summary	180
12.	SNS BL-15, Neutron Spin Echo Spectrometer at SNS (SNS-NSE)	182
12.1	Overview and Current Status.....	182
	Team Structure	182
12.2	Scientific Focus.....	183
12.3	Scientific Highlights.....	183

Mechanical properties and transport processes in lipid membranes	184
Dynamics of Proteins	187
12.4 User Program of the SNS-NSE spectrometer	190
12.5 General User Program	190
12.6 Updates on Discretionary and Partner-User Program	191
12.7 Outreach and Expansion Initiatives	191
12.8 Update on Instrument Development Activities	192
New reduction software	194
12.9 Vision.....	194
Near-term Vision (1-3 years).....	194
Strategic Vision (3-10 years) and Alignment with NScD/ORNL Strategic Plans	195
12.10 Funding/Resource needs	196
12.11 Self-assessment.....	197
Strengths	197
Weaknesses/Limitations	197
Opportunities.....	198
12.12 Future funding opportunities.....	198
12.13 Executive summary	198

LIST OF FIGURES

Figure 1.1. Planned instrument configuration for HFIR cold guide hall post Be reflector change (2024).....	11
Figure 1.2. McSTAS incident flux estimation for MANTA. Note that MANTA and Thales (ILL) have similar incident beam divergences resulting in comparable wave vector resolution.	12
Figure 2.1. HB-1 publication statistics.....	19
Figure 2.2. The measured $\Delta d/d$ as a function of temperature for CuFeO ₂ . The solid and open circles are the values obtained by Larmor diffraction and X-ray diffraction, respectively. J. Applied Crystallography 2018.....	20
Figure 2.3. Schematic of the double-arm Larmor diffraction	20
Figure 2.4. (left) Neutron intensity measured as a function of current inside the outgoing arm of the Wollaston Prism at various temperatures. (right) The measured phonon energy change as a function of temperature for the same sample of ⁷⁶ Ge at HB-1 and TRISP. J. Applied Crystallography 2019.....	21
Figure 2.5. (a) Total magnetic scattering at 5 K and 12 meV. (b) Transverse and longitudinal components of the magnetic scattering. Phys. Rev. Lett. 2018	22
Figure 2.6. Magnetic scattering intensity as a function of temperature. (b) H scans of the magnetic peak (1 0 0) at 4 and 50 K. Phys. Rev. B 2018.	23
Figure 2.7. Incident polarization dependence of scans along (h, h, 0). across (0, -0.2, -0.3) measured at (c) 1.5 K, (d) 1.5 K with reversed guide field, and (e) 3.0 K with original guide field. J. Phys. Soc. Jpn. 2019.....	24
Figure 2.8. HB-1 user program statistics.....	25
Figure 3.1. HB-3 triple-axis spectrometer.....	33
Figure 3.2. The HB-3 instrument team. From left to right: Jaime Fernandez-Baca, Travis Williams, Mike Cox, and Songxue Chi	33
Figure 3.3. HB-3 publication statistics.....	34
Figure 3.4. (a) Constant-Q scans at Q = (1,0,1). (b) Comparison of the difference between 4 K and 35 K for constant-Q scans	35
Figure 3.5. Phason formation measured on HB-3, which provide a detailed assessment of the T-dependence of the phason and incommensurate reflection.	36
Figure 3.6. Neutron inelastic scattering spectra of PrPd ₅ Al ₂ measured using HB-3. The solid lines are the model calculation based on HCFHCFE. The CEF scheme is shown on the right.....	37
Figure 3.7. Phonon dispersions and phonon DOS of CsI.....	38
Figure 3.8. HB-3 data shows the temperature dependence of TA mode vs simulation.....	39
Figure 3.9. HB-3 user program statistics.....	40
Figure 3.10. Shielding design around the HB-3 sample position.	41
Figure 3.11. Neutron velocity selector with goniometer.....	42
Figure 3.12. Design of the neutron velocity selector in the cubicle	44
Figure 3.13. A concept of the new HB-3 secondary spectrometer.....	45
Figure 4.1. Schematic view of HB-1A. The instrument operates from a side port on HB-1.	48
Figure 4.2. HB-1A team, from Left: Wei Tian, Adam Aczel and Shirley Xu.	49
Figure 4.3. HB-1A publication statistics	49
Figure 4.4. (a), (b) The HB-1A data collected at low scattering angles for Sr ₂ CeIrO ₆ and Ba ₂ CeIrO ₆ . The solid and dotted curves represent magnetic refinements to models with A-I and A-II antiferromagnetic order, with the latter providing a superior fit in both cases. (c), (d)	

Order parameter scans of the strongest magnetic Bragg peak for each material, indicative of 21 K and 17 K transition temperatures respectively.....	50
Figure 4.5. Elastic neutron scattering measurement of a 300 nm thin film of CoV_2O_4 . (a) (111) Bragg peak intensity as a function of temperature. The red curve is a power-law fit. (b) (-2-20) and (202) Bragg peak intensities as a function of temperature.....	51
Figure 4.6. Scan at 1.5 K collected at HB-1A along the $[1/2\ 0\ L]$ direction through characteristic magnetic reflections $Q1 = (1/2\ 0\ 1)$ and $Q2 = (1/2\ 0\ 3/2)$ for a 50 mg single crystal with $x = 0.035$. 20 K ($T > T_N$) data are subtracted as background. (b) Temperature scans of the scattering intensity at $Q1$ and $Q2$. Scans along $[1/2\ 0\ L]$ at (c) 4 K and (d) 0.3 K in a 20 mg single crystal with $x = 0.06$. 50 K data are subtracted as a background	52
Figure 4.7. (a) Ultrasound velocity with longitudinally polarized sound waves along the c-axis. (b) H vs T phase diagram for $\text{Yb}_2\text{Si}_2\text{O}_7$ with the points on the phase diagram determined by ultrasound velocity (pink circles and blue crosses), and specific heat (yellow squares). The field was applied along the c-axis (specific heat) and c^* axis (ultrasound). (c) Evolution of the (200) magnetic Bragg peak intensity (blue) vs field, $I(H)$, which is proportional to the square of the net magnetization. Additionally, the derivative of the (200) magnetic Bragg peak intensity (square symbols) and the inverse of the ultrasound velocity data (solid line) are superimposed, showing excellent agreement between the two measurements.....	53
Figure 4.8. HB-1A user program statistics.....	54
Figure 5.1. Instrument team members (left to right): Travis Williams, Jaime Fernandez-Baca, Tao Hong, and Mike Cox.....	63
Figure 5.2. CTAX publication statistics.....	64
Figure 5.3. Top: Background-subtracted peak intensity as a function of field at $q=(0.5,0.5,-0.5)$. Inset: the size of the staggered moment as a function of field. Bottom: Evidence of spontaneous magnon decays at the magnetic zone center. Data were collected at $T=250$ mK.....	65
Figure 5.4. Magnetic field variations of neutron scattering intensity along the (1, 0, l) at $T=1.9$ K in the (a) increasing, (b) decreasing field processes and of (c) the integrated amplitude, (d) the peak position δ , and (e) the width (FWHM).....	66
Figure 5.5. Neutron scattering patterns measured in zero field along (a) (1, 0, l) and (b) (h, 0, 0) at various elapsed times in $T=5.5$ K after removing the magnetic field of 6.0 T.....	66
Figure 5.6. Neutron diffraction θ - 2θ scans for several nuclear and magnetic reflections in the epitaxial IrMn thin film. (A) (001). (B) (110). (C) (100). (D) (-100). (E) (101). (F) (10-1).....	67
Figure 5.7. Left: Constant- q scans at $(-1/3, 2/3, 0)$ showing evolution of the gap energies as a function of applied hydrostatic pressure. The black dashed curve is a Gaussian function of the incoherent scattering at 1.4 GPa with the FWHM of 0.17 meV. Right: Pressure dependence of the excitation energies at $(-1/3, 2/3, 0)$ calculated by the extended spin-wave theory. Above 0.9 GPa, the blue and red curves are the excitations of gapless and gapped modes, respectively. The circles are peak energies obtained from the above constant- q scans.....	68
Figure 5.8. CTAX user program statistics	69
Figure 6.1. Schematic view of the ARCS layout. Inset: Radial collimator on lift.....	74
Figure 6.2. The ARCS instrument team. From left to right: Doug Abernathy (point-of-contact), Garrett Granroth (neutron scattering scientist), Rick Goyette (scientific associate) and Victor Fanelli (SEQUOIA SA). Not shown – Andrei Savici (computational instrument scientist).....	75
Figure 6.3. ARCS cumulative publication statistics	76

Figure 6.4. ARCS publication and experiment statistics	76
Figure 6.5. Experimental phonon dispersions of silicon. Inelastic neutron scattering data of silicon were measured on ARCS at (A) 100 K, (B) 200 K, (C) 300 K, (D) 900 K, (E) 1,200 K, and (F) 1,500 K. The 4D phonon dynamical structure factors, $S(Q,E)$, were reduced, multiphonon-subtracted, and “folded” into one irreducible wedge in the first Brillouin zone. Phonon dispersions are shown along high-symmetry lines and through the zone L–X.	77
Figure 6.6. AgCrSe ₂ phonon DOS from experiments and simulations. (A) INS powder measurements at ARCS with $E_i = 20$ and 80 meV. Blue, green, orange, and red lines are measured at 300, 450, 520, and 650 K. (B) Calculated neutron-weighted DOS. Black dashed line is labeled as DFT, and AIMD at 300 and 600 K are blue and red dashed lines. (C and D) Site-projected DOS from DFT for the c-axis polarized (C) and in-plane (D) motions in the a–b plane. Ag motions mainly contribute the strong peak around 3.5 meV for the in-plane vibration and a weaker peak near 10 meV for c polarizations.	78
Figure 6.7. Spin fluctuations in CaCo _{2-y} As ₂ : Experimental INS data ($E_i = 75$ meV) vs diffusive model. (a)–(c) Constant-energy slices of the background-subtracted data averaged over the energy ranges of 50–60, 40–50, and 10–20 meV, respectively. (d)–(f) Corresponding constant-energy slices calculated using the diffusive model. (g),(h) Transverse slices of the background-subtracted data. (i),(j) Corresponding energy dependence of the scattering obtained using the diffusive model.	80
Figure 6.8. ARCS user program statistics	81
Figure 6.9. Prototype six sample holder.	82
Figure 7.1. Illustration of the SEQUOIA instrument and its components. The flight path of the neutrons travels from left to right in this figure.	89
Figure 7.2. The SEQUOIA Instrument team photographed inside the SEQUOIA instrument ‘sample cave’. From left to right: Alexander “Sasha” Kolesnikov (Instrument Scientist), Matthew Stone (Lead Instrument Scientist) and Victor Fanelli (Scientific Associate (SA)).	90
Figure 7.3. SEQUOIA publication metrics from 2014 through July of 2020.	90
Figure 7.4. SEQUOIA publication statistics	91
Figure 7.5. Inelastic neutron scattering intensity measured for α -NaMnO ₂ . Data are shown on a logarithmic intensity scale. (a) spectrum as a function of energy transfer (vertical axis) and wave-vector transfer along the K direction of reciprocal space (horizontal axis). (b) Constant wave-vector scan through the $K=0.5$ position as a function of energy transfer.	92
Figure 7.6. (a),(b) Calculated neutron scattering intensity using SpinW[7] for exchange constants determined from the low-temperature $T=5$ K measurements (c). Panel (d) corresponds to measurements at $T=205$ K. Data were acquired with $E_i=100$ meV at SEQUOIA and averaged over multiple Brillouin zones and divided by the squared magnetic form factor for presentation with an azimuthally averaged incoherent background subtracted.[8]	93
Figure 7.7. INS spectra for Urea treated MXene, and NH ₄ ⁺ intercalated MXene reference sample show excellent agreement for the NH ₄ ⁺ modes. ReaxFF was used to provide insights for pathways for urea decomposition on MXenes. INS and IR measurements showed that urea interact with MXene results in ammonium intercalation and CO ₂ evolution. [S.H. Overbury, et al. <i>J. Am. Chem. Soc.</i> 140 , 10305 (2018)]	94
Figure 7.8. (a) QENS in the pristine (WO ₃ ·H ₂ O, black) and proton intercalated (H _{0.1} WO ₃ ·H ₂ O, red) states at $T = 300$ K. INS of the same electrodes at $T = 5$ K with incident energies (b) 600 and (c) 250 meV. Generalized vibrational density of states (GDOS) from INS and ab initio MD simulations of the vibrational density of states (VDOS, (d)) show the effect of intercalated protons at the bridging oxygen atoms to the overall spectrum.	95

Figure 7.9. SEQUOIA user program statistics.....	97
Figure 7.10. First page of issue 2 (January 2017) of the SEQUOIA newsletter, The Syllabary. The newsletter is sent by email to more than 300 SEQUOIA stakeholders. It contains information on recent science at the instrument, publications, and how to apply for beamtime at the instrument.	99
Figure 7.11. Kinematically accessible region of momentum transfer and energy transfer space for several incident energies. Lines are shown for detectors located at 5 degrees and at 0.5 degrees scattering angle. The region above each line is the portion accessible by inelastic neutron scattering. The current proposal is to extend the detector coverage at SEQUOIA to 0.5 degrees in scattering angle.....	101
Figure 7.12. : Detector upgrade path for SEQUOIA, BL17, at the SNS. The Brillouin Scattering upgrade will add detectors in the vicinity of the beam-stop, shown in red.....	102
Figure 8.1. CNCS Instrument layout.....	107
Figure 8.2. CNCS team (left to right): Gabriele Sala (postdoc working on CNCS - transitioned to STS in 2019), Andrey Podlesnyak, Daniel Pajerowski, Chris Schmitt.	108
Figure 8.3. CNCS publication statistics.....	109
Figure 8.4. $S(Q , E)$ maps of AgCrSe_2 from CNCS in the (A) ordered phase and the (B) superionic phase. (C) Integration over momentum shows the temperature dependence of the flat phonon. (D) Quasi-elastic scattering shows the activated hopping.	110
Figure 8.5. (a) Inelastic neutron scattering data from CNCS of MnBi_2Te_4 and (b) model calculations. (c) Less parameterized models (e.g. J_1 or J_1 - J_2) are unable to reproduce the experimental data.....	111
Figure 8.6. Inelastic neutron scattering data from CNCS for $\text{Yb}_2\text{Si}_2\text{O}_7$ at $T = 50$ mK and the magnetic field along the c-axis. Slices are integrated ± 0.1 reciprocal lattice units in the perpendicular direction.	112
Figure 8.7. Inelastic neutron scattering data from CNCS for YbAlO_3 at (a) $T = 1\text{K}$ and (b) $T = 50$ mK, compared to density functional renormalization group calculations in (c and d). At $T = 50$ mK with an applied field of 0.6 T, the (e) experimental data and (f) density functional renormalization group calculations are shown.....	113
Figure 8.8. (a) The quasi-elastic scattering of $\text{Zn}_4\text{Si}_2\text{O}_7(\text{OH})_2 \cdot \text{H}_2\text{O}$ measured at CNCS with the data as black circles, the “fast” process as blue dashed line, the “slow” process as green dash-dotted line, and the solid red line being all components plus a linear background. (b) An Arrhenius plot of the proton relaxation times, with the “fast” process as blue circles and the “slow” process as orange squares.....	114
Figure 8.9. CNCS user program statistics	115
Table 3. CNCS instrument developments	116
Figure 9.1. Layout of the HYSPEC instrument, with insets showing the Fermi chopper package, and both vertical focusing arrays.....	123
Figure 9.2. HYSPEC team members B. Winn, M. Graves-Brook, and O. Garlea, standing in front of the HYSPEC detector vessel.	124
Figure 9.3. HYSPEC publication statistics	125
Figure 9.4. Polarized and unpolarized neutron scattering data at 1.8 K (top panels) compared with a calculation (bottom panel) based on self-consistent Gaussian approximation. Polarized neutron measurements labelled by NSF (non-spin-flip) measures components of the dynamic spin correlation function that are perpendicular to the (h, h, ℓ) scattering plane, and SF (spin-flip) measures the component of the spin correlation function polarized within the (h, h, ℓ) scattering plane.....	126

Figure 9.5 Left panel: Models of the static magnetic order in $K_2Mn_3(VO_4)_2CO_3$ compound consisting of alternately stacked triangular and honeycomb magnetic layers. Right panel: INS spectra measured on 0.3 g coaligned crystals to characterize the magnetic interactions of completely different energy scales in the triangular and honeycomb sublattices.	127
Figure 9.6. Time-of-flight neutron scattering data from HYSPEC (a, b) resolving fine energy structure in the spectral distribution for comparison with the ab initio simulations (c, d, e)	128
Figure 9.7. Inelastic scattering of α - $RuCl_3$ along (H,0,0) at 2 K ((a)-(e)) and 15 K (f). At 2 K the field is varied between 0 T and 8 T along the (-1,2,0) direction in the honeycomb plane. The application of a magnetic field suppresses the magnetic order and the spin waves, leaving a gapped continuum spectrum of magnetic excitations.....	129
Figure 9.8. $S(Q,E)$ of $SrTiO_3$ along $Q=[2\ 2\ L]$ directions measured at HYSPEC at 300, 120, and 2 K (d-f) show simulation results obtained from combined ab initio molecular dynamics (AIMD) with the temperature-dependent effective potential (TDEP) method. All are plotted on a log10 scale.....	130
Figure 9.9. The flipping difference of neutron scattering ($I^+ - I^-$) recorded on a powder sample of $La_{0.4}Ce_{0.6}Co_2P_2$ at different temperatures and the temperature dependence of the neutron depolarization factor by the sample.....	131
Figure 9.10. HYSPEC user program statistics	132
Figure 9.11. The new elevator / oscillator assembly with radial collimator at beam elevation and the supermirror above it. Side shielding has been removed to show the pneumatic lift system. This assembly includes a new table and rotary bearing underneath the 3D coil system, which is loosely mechanically connected to the oscillator assembly.....	135
Figure 10.1. The BASIS Instrument team. From left to right: Naresh Osti (Instrument Scientist), Niina Jalarvo (Instrument Scientist), Eugene Mamontov (Point of Contact) and Richard Goyette (Instrument Scientific Associate (SA) until 2019. Not shown: Chris Schmitt (current SA).....	148
Figure 10.2. BASIS publication statistics	150
Figure 10.3. Top: classical DFT results. Left panel: excess absorption of cations near the electrode surface as a function of anion concentration in EmimTFSI-EmimBF ₄ ionic liquid mixture. Right panel: ion distributions for 0, 13, and 100 vol. % of EmimBF ₄ . Bottom: QENS results. The optimal composition is characterized by the highest fraction of the immobile cations (left panel) and the highest diffusivity of the remaining mobile cations (right panel).	151
Figure 10.4. Left: conformation of the PEG inside the 1D nanochannel defined by the framework of POMs. Top panel: PEG chain is seen to stay as a distorted helix. Bottom panel: illustration of the meanings of the QENS fitting parameters. The cylinder with a length of L and a radius of R denotes the space that an atom with a diffusivity, D, can explore. The double-headed arrow denotes the direction of the 1D nanochannel. Right: correlation between the diffusivity (red) and conductivity (blue) temperature dependence.	152
Figure 10.5. Mean-squared displacements (top) and QENS signal broadening (middle) in proton-bearing (Hx-LLZO) and proton-free (LLZO) materials indicating a changing diffusion mechanism for the protons at higher temperatures. Bottom: a schematic illustration of structural and chemical modifications in c-LLZO after intensive proton exchange.	153
Figure 10.6. Temperature dependence of the conductivity (left) and the mean-squared displacements (top, right) and QENS signal broadening (bottom, right) in Na_3SbS_4	154
Figure 10.7. BASIS user program statistics.....	155

Figure 10.8. Left: the neutron scattering signal from gamma-picoline N-oxide at 9 K as a function of time-of-flight. Red line: choppers operated at 10 Hz with a band center at 3.15 Å, Si(333) elastic reflection at 46,870 μs and Si(311) elastic reflection at 73,450 μs and Si(111) elastic reflection at 140,630 μs. The three insets on the left show zoomed-in TOF ranges near the Si(333), Si(311), and Si(111) elastic peaks to emphasize the quantum tunneling peaks that can be detected using each of these reflections. The inset on the right shows the quantum tunneling data converted from the TOF to energy transfer, where the peaks from different reflections are now at the same positions, but are of different widths due to the variable energy resolution associated with the Si(333), Si(311), and Si(111) reflections. Right: Temperature dependence of the neutron elastic scattering intensity from (H₂O)_{0.88}(LiCl)_{0.12} (symbols) measured at Q = 1.3 Å⁻¹ using Si(333) reflection (bottom), Si(311) reflection (middle), and Si(111) reflection (top). The temperatures of the intensity decay to one-half of its low-temperature value are indicated by the vertical thin red lines. [From: E. Mamontov, *Nuclear Instruments and Methods in Physics Research A* **949**, 162534 (2020)] 157

Figure 10.9. Left: Black symbols: average relaxation times previously measured from QENS data for (H₂O)_{0.88}(LiCl)_{0.12}. Red symbols: relaxation times as obtained from the present analysis. Right: relaxation times vs. temperature for (H₂O)_{0.88}(LiCl)_{0.12} and the corresponding Arrhenius plots (lines) for the Q values accessible through the Si(333), Si(311), and Si(111) reflections. [From: E. Mamontov, *Nuclear Instruments and Methods in Physics Research A* **949**, 162534 (2020)]..... 158

Figure 11.1. The VISION spectrometer (BL16B) at SNS..... 160

Figure 11.2. VISION team: (left to right) Luke Daemen, Timmy Ramirez-Cuesta, Eric Novak, Yongqiang Cheng. 161

Figure 11.3. The VISION community of users by specialties in 2019..... 162

Figure 11.4. VISION publication statistics 163

Figure 11.5. VISION unique users. The 2015-2019 (5-year) average is 40..... 163

Figure 11.6. VISION user program statistics 164

Figure 11.7. Reorientational dynamics of the methylammonium cation as a function of Cs doping as measured at VISION. (a) INS spectra collected at T = 5 K of (CH₃NH₃)_{1-x}Cs_xPbBr₃ over the energy range 2–40 meV. (b) The centroid of the low-lying optic phonons (4–5 meV) as a function of x. (c) The average energy of the CH₃NH₃⁺ torsion (33–37 meV) as a function of x. Error bars in (b) and (c) are taken from the instrument resolution, respectively. The centroid of the peaks was determined by fitting the peak in the INS spectra to a Gaussian function and extracting the center..... 166

Figure 11.8. Comparison of the INS spectra for the adsorbed and reacted phenol molecules on Ru/Nb₂O₅ (a), Ru/ZrO₂ (b), Ru/Al₂O₃ (c) and Ru/TiO₂ (d). The second reacted phenol curve in panel (a) shows the conversion of phenol to benzene and cyclohexanol, which does not occur on other supports in panels (b)-(d)..... 167

Figure 11.9. Schematic showing the connection between hole mobility, thermal disorder, crystal, and chemical structure in BTBT. The spectrum of motions leading to thermal disorder is measured using inelastic neutron scattering, which agrees with simulated modes over the full energy range measured (410–3500 cm⁻¹). 168

Figure 11.10. (a–f) Experimental INS spectrum, and corresponding optPBE simulation for BTBT, c8-BTBT, m8-BTBT, TIPS-pentacene, TES-ADT, and TIPS-ADT, respectively. Crystal structures used for each simulation are displayed above each plot for the BTBT series. Crystal structures for TIPS-pentacene, TES-ADT, and TIPS-ADT are shown below the plots. 169

Figure 11.11. Experimental INS spectra collected at VISION from sample formed using n-H ₂ recorded at 5 K. Pure ortho and para contributions were obtained by measuring two different samples with known concentrations. Inset shows the probability distribution of a rotating hydrogen molecule trapped inside the organic clathrate cage.	170
Figure 11.12. Illustration of the reaction of N ₂ and H ₂ to form NH ₃ . The reaction is catalyzed by Ru particles atop the C12A7 electride. The engaged H atoms do not play a significant role in the reaction.	171
Figure 11.13. Left panel: A two-phase Rietveld fit (solid line) to the VISION neutron data (open circles) in the d-spacing range 2.0 to 0.8 Angstrom (upper panel) and 4.0 to 0.8 Angstrom (lower panel). Blue tick marks indicate the reflection positions for cryolite, w whilst green tick marks indicate the reflections associated with the aluminium sample can. An excellent fit to data is obtained, even though the atomic positions and temperatures factors of the cryolite have not been refined. Right panel: Vibrational spectra of cryolite: (a) infrared at room temperature, (b) Raman at room temperature (1064 nm excitation), (c) Raman at 13 K (785 nm excitation) and (d) INS at 5 K recorded on VISION. The lower panel shows the lattice mode region on expanded scales. Relative to the top panel the spectra are ordinate expanded: (a) x10, (b) x40 and (d) x1.5. Ref. S. Parker <i>et al.</i> , RSC Advances, in press.....	172
Figure 11.14. Neutron diffraction pattern and PDF G(r) for α -quartz from (left) VISION at 5 K and (right) LAD (ISIS) at 20 K from Ref. 1. Note, D(r) is scaled by a weighted density compared to G(r).	173
Figure 11.15. Photos of a CuBe gas pressure capable of 3 kbar available on VISION. The gas pressure cells is also H ₂ /D ₂ compatible.....	174
Figure 11.16. CuBe clamped diamond cells with Versimax [®] anvils.....	175
Figure 11.17. Three images of VISION clamped DAC: (a) mounted on the new sturdy stick, via (b) two bolt holes on the DAC cap and (c) a close-up of the DAC with its cadmium shielding.....	175
Figure 11.18. 3D model of the new Mini-McWhan cell. The sample is contained inside the (light yellow) ceramic biconical cylinder and pressurized using the (light grey) pistons made from polycrystalline diamond.....	176
Figure 12.1. The SNS-NSE Team. From left to right: Piotr Adam Zolnierczuk (Lead Instrument Scientist), Mary Odom (Scientific Associate), and Laura-Roxana Stingaciu	182
Figure 12.2. NSE publication statistics since entering the User Program.....	183
Figure 12.3. Proposed mechanism of transient trapping and mean square displacement $\langle \Delta r(t)^2 \rangle_N$ as a function of Fourier time.....	184
Figure 12.4. Left: The cover of Journal of Physical Chemistry B 123 (2019), issue 9 illustrating J. Nickels <i>et al.</i> , research; Right: The lateral diffusion of the lipid DMPC/DSPC bilayer measured using neutron spin echo	185
Figure 12.5. Diagram of the observed mechanical properties of native WT and inhibited WTDCMU membranes. The green circles represent Synechocystis 6803 cyanobacterial cells with one pair of thylakoid membranes, under different illumination conditions. The distance d represents the interthylakoidal distance = the local length scale where thickness and shape fluctuations are sampled. The red arrows show the direction of increase flexibility.	186
Figure 12.6. Diagram of the assumed protein internal energy landscape and polymer-like dynamics behavior of MBP during osmolyte-denaturation.	187
Figure 12.7. Diffusion coefficient as example of dynamics in PNIPAM microgels. While MG10P (green triangles) shows a constant value over the entire Q-range, and the linear PNIPAM	

solution (red squares) shows a continuous increase, MG10F (blue circles) has a constant value up to $Q = 0.11 \text{ \AA}^{-1}$ and increases afterwards.	188
Figure 12.8. Diagram of the bicontinuous microemulsions fluidity and its dependence on the antimicrobial peptide concentration.	189
Figure 12.9. NSE user program statistics	191
Figure 12.10. Group picture of the “Soft and Bio-Materials Dynamics at the Nano- to Meso-Scale” the NSE & XPCS Workshop @SNS.	192
Figure 12.11. Sample reduction data obtained with DrSpine, the new data reduction software at SNS-NSE.	194

LIST OF TABLES

Table 1. List of spectroscopy instruments at SNS / HFIR including the current staffing on each beamline. The three colors correspond to the three teams: Triple-Axis, Direct Geometry, and Chemical Spectroscopy.	1
Table 2. Summary of publication numbers, publications in journals with impact factor greater than 7 and PhD dissertations from CY 2018, CY 2019, and CY 2020 (until 5-Aug-20). The percentage of publications with impact factor greater than 7 is also indicated.	2

1. INTRODUCTION TO THE SPECTROSCOPY SUITE AT SNS / HFIR

The suite of 11 spectroscopy instruments at the two neutron sources at Oak Ridge National Laboratory (ORNL) provide to users the unprecedented ability to study excitations in materials over 8 orders of magnitude in energy transfer (from 10s of neV to ~ 1 eV). The scientific program enabled by this instrument suite is diverse covering areas such as quantum materials, energy related materials, soft matter, chemistry, and biology. The instrument suite is composed of four triple-axis spectrometers, four direct geometry spectrometers, two indirect geometry spectrometers, and one spin-echo spectrometer. The source / moderator and the current staff supporting each spectrometer are summarized in Table 1.

Instrument	Source / Moderator	Instrument Scientists	Scientific Associate
HB-1A (FIE-TAX)	HFIR / thermal H ₂ O	Adam Aczel, Wei Tian	Shirley Xu
HB-1 (PTAX)	HFIR / thermal H ₂ O	Masa Matsuda, Travis Williams, Jaime Fernandez-Baca	Shirley Xu
HB-3 (TAX)	HFIR / thermal H ₂ O	Songxue Chi, Travis Williams, Jaime Fernandez-Baca	Mike Cox
CG-4C (CTAX)	HFIR / cold H ₂	Tao Hong, Travis Williams, Jaime Fernandez-Baca	Mike Cox
BL-5 (CNCS)	SNS / cold coupled H ₂	Daniel Pajerowski, Andrey Podlesnyak	Christopher Schmitt
BL-14B (HYSPEC)	SNS / cold coupled H ₂	Barry Winn, Ovidiu Garlea	Melissa Graves-Brook
BL-17 (SEQUOIA)	SNS / thermal decoupled H ₂ O	Matthew Stone, Sasha Kolesnikov	Victor Fanelli
BL-18 (ARCS)	SNS / thermal decoupled H ₂ O	Doug Abernathy, Garrett Granroth	Rick Goyette
BL-2 (BASIS)	SNS / cold decoupled H ₂	Eugene Mamontov, Niina Jalarvo, Naresh Osti	Christopher Schmitt
BL-15 (NSE)	SNS / cold coupled H ₂	Laura Stingaciu, Piotr Zolnierczuk	Mary Odom
BL-16B (VISION)	SNS / thermal decoupled H ₂ O	Luke Daemen, Timmy Ramirez-Cuesta	Eric Novak

Table 1. List of spectroscopy instruments at SNS / HFIR including the current staffing on each beamline. The three colors correspond to the three teams: Triple-Axis, Direct Geometry, and Chemical Spectroscopy.

This review document describes the 11 spectroscopy instruments which are divided into Triple-Axis Spectroscopy (HB-1A, HB-1, HB-3, CG-4C), Direct Geometry Spectroscopy (CNCS, HYSPEC, SEQUOIA, ARCS), and Chemical Spectroscopy (BASIS, NSE, VISION). Each instrument chapter provides a detailed description of the instrument capabilities, the science program enabled on each spectrometer, and planned developments to keep this suite of instruments world-leading in neutron spectroscopy.

The instruments within the spectroscopy suite are now mature and have largely obtained steady

publication output. The details of publication output are included in the instrument specific sections. As a high-level summary, considering CY 2018, CY 2019, and CY 2020 (until 5-Aug-20), the 11 instruments included in the assessment have produced 378 unique publications. Of these 103 have been published in journals with impact factor greater than 7 (27%). Included in these 103 publications were 2 in Science, 3 in Nature Materials, 7 in Nature Physics, 12 in Nature Communications, 7 in Journal of the American Chemical Society, and 24 in Physical Review Letters. Additionally, during this time, these instruments contributed to 37 PhD dissertations. The publication metrics per instrument are summarized in Table 2 (note that the total in this table is more than the 378 total publications as numerous papers included more than 1 spectroscopy instrument).

Instrument	Publications	Pubs in journal with IF > 7	PhD dissertations
HB-1A (FIE-TAX)	40	6 (15%)	8
HB-1 (PTAX)	35	9 (26%)	2
HB-3 (TAX)	22	7 (31%)	2
CG-4C (CTAX)	22	4 (18%)	4
BL-5 (CNCS)	59	15 (25%)	7
BL-14B (HYSPEC)	25	10 (40%)	3
BL-17 (SEQUOIA)	75	20 (27%)	12
BL-18 (ARCS)	52	18 (35%)	9
BL-2 (BASIS)	59	13 (22%)	6
BL-15 (NSE)	21	3 (14%)	0
BL-16B (VISION)	58	26 (45%)	9

Table 2. Summary of publication numbers, publications in journals with impact factor greater than 7 and PhD dissertations from CY 2018, CY 2019, and CY 2020 (until 5-Aug-20). The percentage of publications with impact factor greater than 7 is also indicated.

1.1 RECOMMENDATIONS FROM THE 2017 SUITE REVIEW

The 2020 instrument suite review is the second triennial review of the spectroscopy suite with the prior review being held November 14-15, 2017. There were a number of specific recommendations in the 2017 report. Some recommendations were instrument specific and some were more broadly applicable. A description of progress made towards these recommendations are included in the separate document.

1.2 TRIPLE-AXIS SPECTROMETERS

Since the development of the first triple-axis spectrometer by Brockhouse in the 1950's this type of instrument has remained a versatile tool to study the elementary excitations of solids, such as phonons and magnons. This versatility arises from the ability to measure with high flux at a specified point in momentum-energy space. The current set of triple-axis spectrometers at HFIR consists of three thermal instruments (The Polarized Triple Axis Spectrometer (PTAX) at HB-1, the Triple Axis Spectrometer (TAX) at HB-3, and the Fixed Incident-Energy Triple Axis Spectrometer (FIE-TAX) at HB-1A) and one cold neutron instrument (Cold Triple-Axis Spectrometer (CTAX) at CG-4C). These four instruments complement the suite of direct geometry spectrometers at SNS because of their ability to map out small volumes of Q and ω space quickly and efficiently in a variety of sample environments. The high flux and a range of incident energies (2 - 120 meV) makes these instruments particularly well suited for condensed matter physics problems including studies of magnetic excitations in unconventional superconductors, multiferroics, frustrated and quantum magnets, heavy fermion materials, itinerant magnets, magnetic multilayers, and commercial magnetic alloys, as well as studies of lattice excitations in thermoelectrics and other energy related materials. The triple-axis spectrometers are ideally suited to parametric studies and all instruments are compatible with a wide range of sample environment equipment, including closed-cycle helium (Displex) refrigerators, ^4He cryostats (with a ^3He or dilution inserts), cryomagnets, furnaces, clamp pressure cells, gas pressure cells, and measurements with applied electric field.

For two of the thermal instruments, HB-1 (PTAX) and HB-3 (TAX), the monochromator drums and vertically focusing monochromator assemblies were upgraded during the last HFIR beryllium reflector replacement shutdown of the year 2000. However, the secondary spectrometers (analyzer / detector shields) were not rebuilt and their upgrades are still pending. The HB-1A (FIE-TAX) monochromators and drum were recently upgraded to improve the incident beam focus resulting in approximately a 3x increase in incident flux. An ongoing project will also upgrade the secondary spectrometer to take full advantage of the vertical beam divergence. The cold neutron instrument CG-4C (CTAX) is a refurbished version of the old H4M triple axis spectrometer formerly located at the High Flux Beam Reactor at Brookhaven National Laboratory (BNL) and was installed in 2011. CTAX is part of the US-Japan Cooperative Program in Neutron Scattering.

HFIR HB-1, PTAX is designed for polarized beam measurements, but it is also an efficient general-purpose unpolarized neutron spectrometer. The high flux and a wide range of incident energies, 5–120 meV, make the instrument particularly well-suited for polarized studies of spin excitations in magnetic materials. The choice of two monochromator plugs gives this instrument great versatility. The polarizing plug accommodates a large 18-cm tall and 25-cm wide fixed vertical focusing Heusler alloy monochromator with a vertical guide field. The unpolarized plug accommodates a pyrolytic graphite (PG) monochromator with variable vertical focusing. The instrument offers a choice of Heusler alloy (for polarized experiments) and PG (unpolarized or half-polarized) analyzers. A recent addition to the capabilities of PTAX is the development of Wollaston prisms for ultra-high-resolution spectroscopy. These prisms have already been used successfully to perform Larmor diffraction with a $\Delta d/d$ resolution of the order of 10^{-5} and spectroscopy with ultra-high-resolution of $<10 \mu\text{eV}$. Ongoing developments include a novel high- T_c based spherical neutron polarimetry device. The expanded capabilities on HB-1 are hindered by the current Heusler monochromator and analyzer and a project is underway to upgrade these devices. Plans are being developed to upgrade the secondary spectrometer to enable better signal to noise measurements and enhanced instrument flexibility.

HFIR HB-3, TAX is designed to operate as a versatile high-intensity unpolarized-neutron instrument. Its versatility is achieved by the availability of three monochromators on a single plug, that can be changed

by computer control. Currently, these are PG (002), Be (002), and plastically deformed Si (111); all are vertically focusing, and their focal length is adjusted automatically as the monochromator scattering angle changes. The PG monochromator provides the highest neutron intensity because of its high neutron reflectivity. The high-quality beryllium monochromator allows measurements with good energy resolution at higher energy transfers. The Si (111) monochromator has the advantage of eliminating second-order ($\lambda/2$) contamination. The availability of these three monochromator crystal choices makes this spectrometer extremely versatile for a wide range of studies of the properties of materials.

HFIR HB-1A, FIE-TAX is a fixed incident-energy ($E_i = 14.5$ meV) instrument. This fixed E_i is selected using a double crystal monochromator system consisting of two PG (002) monochromators. PG filters after these two monochromators are used to reduce $\lambda/2$ contamination. The double bounce monochromator system and PG filters were recently upgraded resulting in better focus of the incident beam and a tripling of the incident flux. The incident beam has very little higher order contamination ($I_{\lambda/2} \approx 10^{-4} \times I_\lambda$). This is an excellent instrument for measuring low-lying excitations, elastic studies of lattice or magnetic structures and transitions, and elastic studies on thin film or small samples where high flux on sample and very low higher order contamination of the beam are critical issues. This instrument was originally constructed by the Ames Laboratory and is now owned and operated by ORNL. Due to the high-flux, low-background, and very low higher-order contamination of the beam, HB-1A is an ideal instrument for measuring weak magnetic signals from small single crystals ($m > 2$ mg) and thin film samples using a variety of sample environments.

HFIR CG-4C, CTAX is a cold neutron triple-axis spectrometer with variable incident energy and sample-analyzer distances. The Cold Guide 4 bender and guide hall shielding reduce background levels at CG-4C, and the 15-cm-tall guide profile is well matched by CG-4C's focusing monochromator (PG 002). To enhance accommodation of strong magnetic fields at the sample position and simplify future polarization analysis, the amount of ferromagnetic material has been minimized in the construction of this instrument. CG-4C enables high signal-to-noise measurements due to the low background and is ideal for high-resolution measurements of low-energy, atomic-scale dynamics of crystalline solids, as well as for studies of magnetic phenomena exploiting the energy range that matches achievable applied fields. This instrument is part of the US-Japan Cooperative Program in Neutron Scattering. As the incident flux of cold neutrons is limited on the CG-4 beamline, our future strategy calls for replacing CTAX with a new, high flux cold triple-axis spectrometer, MANTA.

1.3 DIRECT GEOMETRY SPECTROMETERS

For pulsed neutron source such as SNS, direct geometry spectrometers with a fixed incident neutron energy and highly pixelated arrays of position sensitive detectors, have proven to be ideal for spectroscopic measurements where good wave vector resolution is required. As such, they have become the instrument of choice to map collective excitations such as phonons and magnons over a wide range of momentum-energy space and diffuse magnetic signals characteristic of quantum disordered materials. The current suite of spectrometers at SNS includes two thermal spectrometers, ARCS (BL-18) and SEQUOIA (BL-17) and two cold neutron spectrometers, CNCS (BL-5) and HYSPEC (BL-14B). The ability to map out wide ranges of momentum-energy space while preserving good resolution results in a science program dominated by quantum materials research; typical problems of interest include studies of quantum magnets (including quantum spin liquids), multiferroics, frustrated magnets, high- T_c superconductors, itinerant magnets, quantum criticality, and quantum fluids. Additionally, these instruments enable studies of lattice dynamics in both polycrystalline and single crystal samples and topics of interest include relaxor ferroelectrics, thermoelectrics, and negative thermal expansion materials. Finally, for chemical spectroscopy, these instruments complement the indirect geometry spectrometers;

VISION (BL-16B) in cases where wave vector dependence is of interest and the quasielastic instrument BASIS (BL-2) providing expanded dynamic range with coarser resolution.

The first two direct geometry instruments were funded through separate DOE construction projects. ARCS was the first instrument to enter the user program in 2008 and was followed by CNCS in 2009. The remaining two instruments, SEQUOIA and HYSPEC, were part of the SING (SNS Instruments – Next Generation) project. SEQUOIA entered the user program in 2010 and HYSPEC entered in 2013. ARCS, CNCS, and SEQUOIA all followed a similar trajectory from entering the user program to relatively steady-state scientific productivity. For HYSPEC, it should be noted that the instrument was available to users for unpolarized measurements in 2013, and the expanded scope of adding polarized neutron capabilities was made available to users in 2016. The polarized capabilities required significant additional development time and resources.

SNS BL-18, ARCS is a thermal neutron direct geometry spectrometer viewing the decoupled ambient water moderator. It is optimized for high flux and a large solid angle detector coverage. The source to sample distance is 13.6m and the sample to detector distance is 3.0-3.4 m with a cylindrical array of 920 position sensitive ^3He tubes. The detector array is composed of three rows of $\sim 1\text{m}$ tubes covering horizontal angles of -28° to 135° and vertical angles of -27° to 26° . The chopper system consists of a T0 chopper to suppress the prompt radiation from the source and a fermi chopper located 2m from the sample. The fermi choppers sit on a translation stage that allows two different slit packages to be interchanged in a computer-controlled manner. The incident energy can be varied from 10 meV to about 1.5 eV and the energy resolution at the elastic line is 2-5% of E_i . The wide angular coverage on ARCS makes it ideal for lattice dynamics measurements and the high flux is well suited to many problems in magnetism and these two areas dominate the science program on the beam line.

SNS BL-17, SEQUOIA is also a direct geometry spectrometer viewing the decoupled ambient water moderator providing high flux of neutrons in the thermal to epithermal range. SEQUOIA serves as the high-resolution complement to the ARCS spectrometer. The source to sample distance is 20m and the sample to detector distance varies from 5.5m to 6.3m. The chopper configuration is identical to ARCS with a T0 chopper and a Fermi chopper (on a two-chopper translation stage) located 2m before the sample. Incident energies of ~ 5 meV to 2 eV can be used on SEQUOIA and the elastic energy resolution is 1-5% of E_i . The detector array is composed of three rows of 1.2m ^3He linear position sensitive detectors covering a horizontal angular range of -30° to 60° and a vertical coverage of $\pm 18^\circ$. The SEQUOIA vacuum tank was designed to accommodate 5 rows of detectors and, hence, the current coverage represents 60% of the original design. The higher resolution and smaller angular coverage make SEQUOIA ideal for studies of magnetic excitations in a variety of quantum materials and this represents most of the user community for the instrument. There is also an active program studying hydrogen and water in confined geometries and SEQUOIA represents an excellent complement to the chemical spectroscopy capabilities of VISION in cases where wave vector dependence is of interest.

SNS BL-5, CNCS is our workhorse cold neutron direct geometry spectrometer. Neutrons from a coupled hydrogen moderator pass through a series of choppers, a Fermi chopper at 6.41m, bandwidth choppers at 7.52m and 33.02 m and a double disk chopper at 34.78m. The sample is at 36.2m from the source. This incident energy is defined by the Fermi chopper and double disk chopper and can be tuned from 0.5 – 80 meV with a resulting energy resolution ranging from 10 – 100 μeV . The detector array is composed 400 linear position sensitive ^3He tubes (length of 2m) covering 1.7 sr of solid angle. These detectors cover -50° to 135° degrees horizontally and $\pm 16^\circ$ degrees vertically. There is room for as much as 3 sr of detectors by occupying empty rows above and below the central row. The sample position is in air and the detector tank is filled with argon with a collimator removing unwanted sample environment background. Most

experiments are performed using an orange cryostat and magnetic fields are also important for the science on CNCS (^3He or dilution temperatures are frequently required). The new 14T magnet combined with the new collimator will provide a critical new capability for this instrument. Most of the science on CNCS is focused on studies of magnetic excitations in quantum materials and some studies of lattice dynamics in energy materials. In addition, CNCS complements the quasielastic scattering capabilities of BASIS enabling coarser resolution measurements over a larger dynamic range.

SNS BL-14B, HYSPEC is a direct geometry spectrometer that incorporates some of the advantages of crystal spectrometers at continuous sources. The sample is located 40.4 m from the source and the incident energy is selected by a fermi chopper located 3.2 m upstream of the sample. The instrument incorporates a crystal array in the incident beam which can either be pyrolytic graphite or Heusler. In both cases, the crystal array serves as a vertically focusing optical element increasing the intensity on the sample and the Heusler array serves as an incident beam polarizer. HYSPEC views a coupled hydrogen moderator and the incident energy can be tuned from 3.8 – 60 meV. The detector array is composed of 20 8-packs of ^3He linear position sensitive detectors which are 1.2m tall and this array covers 60° horizontally and $\pm 7.5^\circ$ vertically with a nominal sample-detector distance of 4.5 m. This detector array is contained in an argon-filled tank which can be rotated to cover angles from 2° to 135° . As mentioned above, HYSPEC entered the user program with unpolarized neutrons in 2013 but development continued to implement polarized neutron capabilities. Several key developments were required the most significant of which was the arrival of a supermirror array designed and constructed at the Paul-Scherrer Institut which is now used to polarize the scattered beam. Together with the development of a set of coils at the sample position to rotate the polarization, and the polarized incident beam, we can now perform spectroscopy measurements including polarization analysis. These polarized capabilities were available to users in 2016 and work continues to optimize software routines for such measurements. Currently, roughly 44% of the experiments on HYSPEC use polarized neutrons. Scientifically, the focus of the research performed on HYSPEC centers around magnetism in quantum materials with some effort concentrating on lattice dynamics in energy related materials. The polarized neutron scientific program is developing, and problems of interest include cases where lattice and magnetic degrees of freedom interact (for example, multiferroics) and cases where separation of components of $S(\mathbf{Q},\omega)$ can shed light on complex problems (for example, quantum spin liquid candidates).

1.4 CHEMICAL SPECTROSCOPY

Indirect geometry spectrometers employ a fixed final neutron energy and, to improve measurement efficiency, often employ large analyzer crystal arrays in focusing geometries. This results in an optimization with excellent energy resolution, but relaxed wave vector resolution and these instruments are ideally suited to studies of a variety of problems across diverse scientific areas including soft matter, biology, chemistry, and complex fluids. At SNS, BL-2 (BASIS) is an indirect geometry quasielastic neutron scattering spectrometer which typically measures diffusive dynamics in problems such as biological and polymeric systems, fluids either in bulk or confined geometries, and hydrogen in confinement. BL-16B (VISION) is a neutron chemical spectroscopy instrument which provides an excellent complement to the more traditional optical spectroscopy. Specific advantages include high sensitivity to hydrogen, absence of selection rules, ease of computation of the vibrational spectrum, isotopic sensitivity, no energy deposition in sample, and high neutron penetrability through complex sample environment equipment. The science program on VISION is diverse but the ability to study small quantities of hydrogenous material has led to a focus on chemistry and soft matter – specific topics of interest include water in confinement, hydrogen storage, catalysis, polymers, fuel cells, proton conductors, etc. Finally, to achieve the best energy resolution, BL-15 (NSE) is a neutron spin echo spectrometer capable of measuring excitations with

times up to ~ 150 ns (corresponding to about 30 neV). The science on NSE is mostly focused on soft matter and biological systems.

Of the SNS spectrometers, BL-2, BASIS was first constructed entering the user program in December 2007. BL-16B, VISION was part of SING-II and was the last spectrometer to enter the user program in 2015. Finally, as mentioned below, BL-15, NSE was constructed and commissioned as a joint venture between SNS and Juelich Centre for Neutron Science (Forschungszentrum Juelich, Germany) in record time (3 years and 7 months) and entered the user program in 2010.

SNS BL-2, BASIS is an inverse geometry spectrometer located on a decoupled hydrogen moderator. The final energy is selected using either Si (111) and Si (311) analyzers configured in a near backscattering geometry. The resulting final energy is 2.08 meV ($\lambda_F=6.267$ Å) for Si (111) crystals and 7.64 meV ($\lambda_F=3.273$ Å) for Si (311). The addition of Si (311) crystals to the original array of Si (111) allows measurements to be performed over an expanded dynamic range at the expense of coarser energy resolution. The accessible range of energy transfers can be tuned with bandwidth choppers and symmetric configurations up to ± 0.2 meV can be selected for Si (111) and ± 1.7 meV for Si (311). The current analyzer array can be separated into four quarters, two of which are occupied by the originally designed Si (111) crystals, one of which is occupied by Si (311) crystals and the remaining quarter contains a new design for Si (111) crystals. This new design incorporates cadmium coated Si crystals to remove background contributions from the aluminum support structure. This modification eliminates a shoulder in the elastic resolution function which is problematic for certain weak scattering samples. An upgrade of the remaining Si (111) crystals to incorporate this new design would expand the scientific capabilities of the instrument.

SNS BL-16B, VISION is an inverse geometry spectrometer optimized for chemical spectroscopy measurements. To deliver sharp pulses and an appropriate range of incident energies, neutrons are generated by a decoupled water moderator and choppers deliver 30 Hz pulses of neutrons to the sample. Neutrons with a final energy of 3.5 meV ($\lambda_F=4.835$ Å) are selected by 13 focusing arrays of PG (002) analyzer crystals positioned in the forward and backward scattering directions. This results in an elastic energy resolution of 120 μ eV and the typical 30 Hz operation provides energy transfers from -2 to 1000 meV. As mentioned above, the scientific areas explored by VISION are diverse and to enable this range of science, the VISION team has been involved in several sample environment developments. Complementary lab resources are required to enable the robust and growing scientific program on VISION. To enable more rapid data interpretation, modeling has been tightly integrated into the scientific program on VISION. First principles calculations are performed using a dedicated cluster (VirtuES). As a component of the ICEMAN project, the OCLIMAX software was developed to calculate vibrational spectra from these first principles calculations and allow for direct comparison to experimental results.

SNS BL-15, NSE is the world's first neutron spin echo spectrometer to be located on a pulsed neutron source. It was designed, built and operated by the Forschungszentrum Juelich through the Juelich Centre for Neutron Science during the review period. Preparations have been made to transition the instrument to ORNL at the end of the operational agreement that expired at the end of March 2020. The instrument views a coupled hydrogen moderator and incident beam polarization is achieved using a kink polarizer which works across the full wavelength band of interest. The main components of the instrument are two symmetric superconducting solenoids, one before and one after the sample and these coupled with appropriate correction coils yield a highly homogeneous field for neutron spin precession. A magnetically shielded enclosure around the spectrometer minimizes sensitivity to stray fields from external sources. NSE enables measurements with ultrahigh resolution and Fourier times between 5 ps and 150 ns can be studied. These slow dynamic processes are characteristic of nanoscopic and mesoscopic materials and the science program on NSE is consequently focused on soft matter, complex fluids and biological materials.

1.5 UPGRADES AND DEVELOPMENTS

As described in detail in the subsequent instrument specific reports, the science program enabled by these instruments can be enhanced by strategic investments in upgrades and expanded capabilities. A listing of some of the completed, ongoing, or identified upgrades are included below:

Triple-Axis Spectroscopy

Recent developments:

- HB-1: Wollaston prisms for Larmor diffraction and ultra-high-resolution spectroscopy
- HB-3: Shield around the sample position
- HB-1A: Upgrade of the double bounce monochromator system and drum
- 6T workhorse magnet for triple-axis and HFIR diffraction instruments
- Liquid helium autofill (LHeF) system tested at HB-1A, CTAX, and HB-3
- HB-1A: sample stick with in-situ rotation (>90 degrees to enable changes in scattering plane)
- CTAX: 11T uncompensated magnet moved to HFIR

Developments in progress:

- HB-1: new spherical neutron polarimetry device using high-Tc superconductors
- HB-1: new elliptical focusing device for small samples
- HB-1: upgrade of Heusler monochromator and analyzer
- HB-3: Velocity selector in incident beam to eliminate higher order contamination (installation to coincide with Be reflector change)
- HB-1A: upgrade of secondary spectrometer enabling use of full beam divergence

Identified needs:

- World class cold neutron triple-axis spectrometer at HFIR (MANTA)
- HB-1: new secondary spectrometer with flexibility to change distances
- HB-3: new secondary spectrometer enabling use of focusing analyzer geometries
- HB-3: rebuild sample goniometer
- HB-3: permanent boundary wall to reduce background impact on neighboring instrument and improve radiological conditions
- HB-1A: new sample table including accommodation of a four-circle goniometer
- HB-1A: area detector for diffraction experiments
- Additional magnet (6 T) to handle demand
- Wide-angle horizontal field magnet (most need is from HB-1A and HB-1)
- Expand liquid helium autofill system to work on all triple-axis spectrometers
- Uniaxial pressure stick with ability to change pressure in situ

Direct Geometry Spectroscopy

Recent Developments:

- ARCS: upgrade of detector electronics (eliminate vulnerability and improved tunability of array)
- ARCS & CNCS: transition to EPICS based data acquisition system
- SEQUOIA: vacuum system upgrade
- SEQUOIA: additional 6 8-packs of detectors
- CNCS: radial collimator that is compatible with magnets
- CNCS: boron absorber bandwidth chopper to eliminate spurious scattering
- HYSPEC: permanent magnet yokes to enable half polarized measurements
- HYSPEC: purchased supermirror array which was on loan from PSI
- HYSPEC: elevator oscillator for radial collimator / polarizing supermirror array
- HYSPEC: incident beam RF flipper
- HYSPEC: compact 3D coils
- 14T magnet (currently being commissioned across the DGS suite)
- CNCS: Ruby fluorescence pressure determination for clamp cells
- CNCS: vertical translation stick
- Uniaxial pressure device for detwinning crystals

Developments in progress:

- ARCS: multi-sample stick to enable 6 polycrystalline samples to be loaded simultaneously
- CNCS: add out-of-plane detector coverage using Pharos detectors
- ARCS / SEQUOIA: new 70mm top-loading CCR
- Automatic helium exchange gas handling for top loader
- Additional 100mm bore ³He insert
- 50/35mm bore ³He insert compatible with magnets

Identified needs:

- ARCS: additional chopper (could be for background suppression or pulse shaping chopper)
- SEQUOIA: radial collimator
- SEQUOIA: complete detector array
- SEQUOIA: Brillouin scattering option
- SEQUOIA: addition of neutron shielding for floor and lower rear wall of detector tank
- CNCS: elevator for last section of guide
- HYSPEC: horizontal field magnet with open geometry
- HYSPEC: shielding to reduce time independent background

Chemical Spectroscopy

Recent Developments:

- BASIS: transition to EPICS based data acquisition system
- BASIS: implemented use of higher order Si (333) reflection to study relaxation dynamics
- BASIS: Performed first dynamic PDF experiment on BASIS using Si (333) reflection
- VISION: addition of collimators for diffraction banks enabling simultaneous spectroscopy and diffraction / PDF
- VISION: 3 kbar hydrogen compatible gas pressure cells
- VISION: large volume diamond anvil cells enabling chemical spectroscopy up to 10 GPa (sample volume of 1 mm³)
- VISION: rigid sample stick allowing for repeatable placement of pressure cells
- NSE: replace polarizing bender with new kink polarizer

Developments in progress:

- NSE: transition operation of instrument and maintenance of all associated equipment to ORNL
- VISION: new “mini McWhan” cell enabling pressure up to 5 GPa (sample volume of 3 mm³)
- VISION: new furnace, based on MICAS design, compatible with VISION with versatile sample sticks and a maximum temperature of 1000 C.

Identified needs:

- New high resolution NSE spectrometer at HFIR
- New BeFAST Be filter spectrometer at SNS (BL-16A)
- VISION: expanded capabilities in labs for pre- and post-experiment characterization
- VISION: new CCR with increased sample chamber diameter
- NSE: expand available sample environment equipment including shear cells and rheometer, pressure cells, and ³He cryostat

1.6 CRITICAL NEEDS FOR NEW INSTRUMENTS

While the suite of spectroscopy instruments at HFIR and FTS represent an impressive set of capabilities covering a wide range of scientific areas, there are gaps that can be addressed by new instruments at these two sources and the Second Target Station (STS). STS will provide beams of cold neutrons with unsurpassed peak brightness which are ideally suited to many spectroscopy applications. Several workshops have been carried out to discuss community needs for spectroscopy and this has led to several proposed instruments for STS. The remainder of this section will outline proposed instruments at HFIR, FTS, and STS.

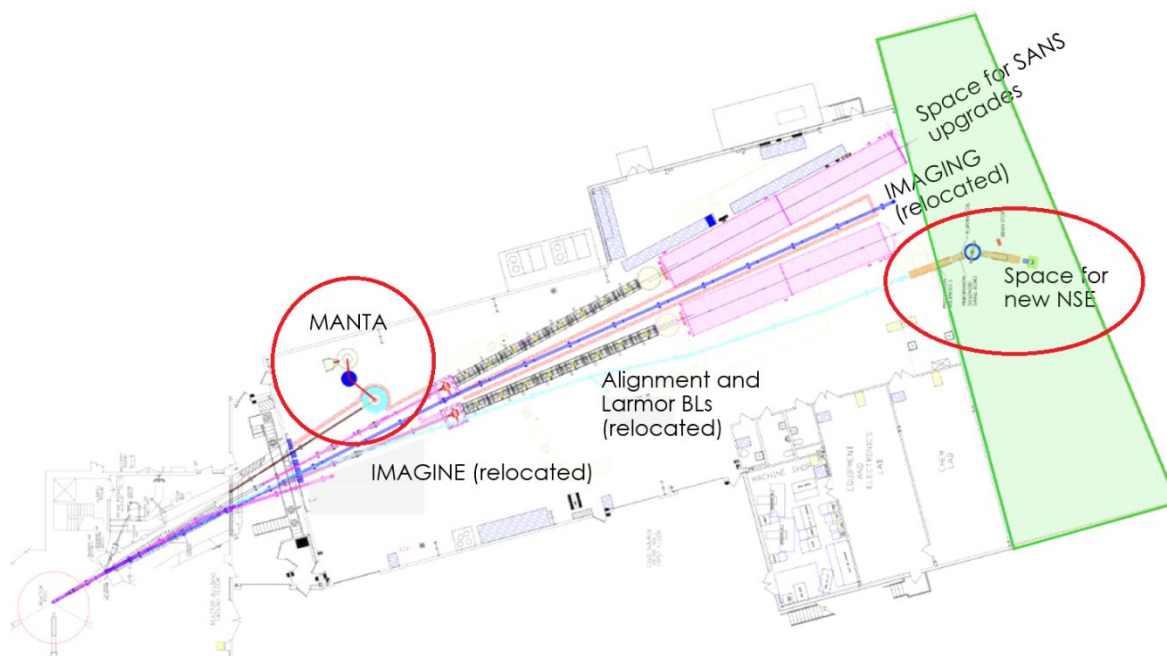


Figure 1.1. Planned instrument configuration for HFIR cold guide hall post Be reflector change (2024)

New instruments for HFIR

The HFIR beryllium reflector change outage, scheduled to begin in 2024, provides an opportunity to reoptimize the cold neutron instrument suite at HFIR. Guided by community feedback and our Instrument Advisory Board, the current plans for the HFIR cold guide hall are shown in Figure 1.1. This includes two spectrometers, MANTA and a high-resolution neutron spin echo spectrometer.

There is strong community demand for expanded, new capabilities in cold neutron spectroscopy and BL-2, BASIS and BL-5, CNCS are two of the most oversubscribed instruments at either facility. One clear weakness in the spectroscopy suite is the absence of a high-flux cold neutron triple-axis spectrometer at HFIR. **MANTA**, proposed for the current CG-1 guide at HFIR, will fill this gap and provide complementary capabilities for cold neutron spectroscopy studies of quantum materials. The incident beam optics of MANTA are being optimized and will utilize double focusing and a virtual source to deliver an incident flux of cold neutrons comparable to the highest flux instruments in the world (see Figure 1.2). MANTA will be designed with exchangeable secondary spectrometers. For measurements best optimized for a single analyzer / detector, the current CTAX secondary spectrometer will be utilized.

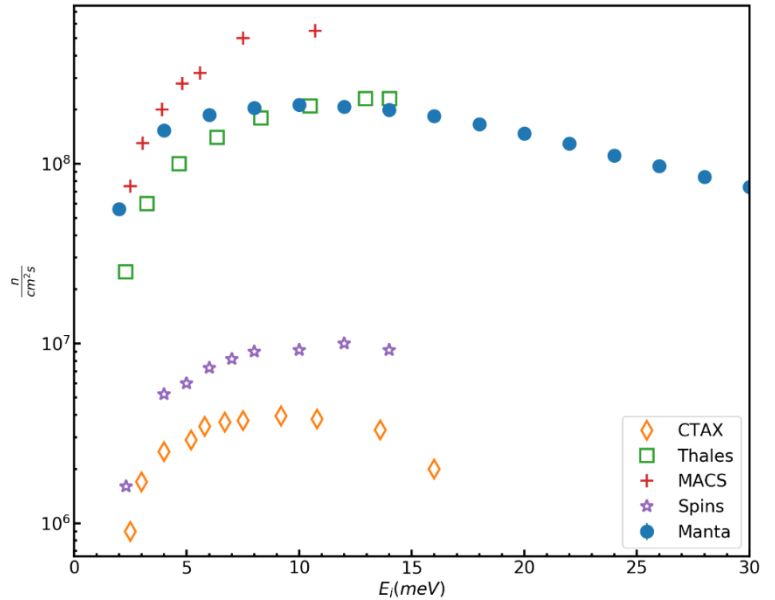


Figure 1.2. McStAS incident flux McStAS simulation for MANTA. Note that MANTA and Thales (ILL) have similar incident beam divergences resulting in comparable wave vector resolution.

Examples of this would include the use of Wollaston prisms for ultra-high-resolution spectroscopy. This can be exchanged for a multiplexed secondary spectrometer allowing for measurements over a wide range of scattering angles and with multiple final energies. The instrument will be optimized for complex environments including high magnetic fields which could include high-T_c based magnets depending on technological advances in magnet design.

HFIR-NSE will be a high-flux-high-resolution Neutron Spin Echo spectrometer that is optimized for small sample volumes, high energy resolution and a large dynamical range that leverages the planned upgrades at the High Flux Isotope Reactor during the Be change out. The design will seek to provide Fourier times up to 500 ns over an extended Q-range of 0.02Å⁻¹ - 2Å⁻¹ for user experiments. In summary, it will:

- possess world-class flux at long wavelengths ($\lambda > 11\text{\AA}$)
- possess excellent flux for measurements in the high Q-range
- employ state-of-the art optics to provide low intrinsic field integral inhomogeneity
- leverage the best available field integral correction coils
- provide short counting times per sample with a significant reduction in sample volume
- provide the best stability and reliability over long counting times during challenging experiments

New instruments for SNS First Target Station (FTS)

There are limited available beamlines at FTS but there have been two spectroscopy instruments proposed to expand our current capabilities.

BL-16A is a shared beamline with VISION which is geometrically restricted by the two neighboring instruments. One proposed instrument that could be incorporated in this space is **BeFAST**, a filter spectrometer which would complement the chemical spectroscopy capabilities of VISION. This instrument uses a Be filter to define a broad ΔE_F (~ 5 meV), and the compact nature of the spectrometer results in large solid-angle coverage. These combined factors result in better performance in the higher energy

transfer region when compared to VISION. Although VISION collects data up to $8,000\text{ cm}^{-1}$, the intensity is weak above $3,000\text{ cm}^{-1}$. This region of the vibrational spectrum contains chemical bond stretches, which are important to the identification of functional groups and their chemical transformation in chemical reactions. As such, this instrument would provide an important complement to VISION expanding our chemical spectroscopy capabilities.

A second proposed for the BL-8A is an indirect geometry spectrometer, **HIGGS** (High Intensity Indirect Geometry Graphite Spectrometer) optimized for measurements with fine wave vector resolution enabling studies of quantum materials in the presence of complex sample environments. The final energy will be selected by a planar array of PG (002) analyzer crystals scattering through a common focal point located below the sample. An array of position sensitive detectors together with appropriate collimation will provide fine Q resolution and an aperture at the focal point will be used for background and spurious scattering suppression. This beamline is on a decoupled water moderator and the resulting resolution for PG (002) is about $40\text{ }\mu\text{eV}$ (if PG (004) could also be used, this gives a resolution of $150\text{ }\mu\text{eV}$). This instrument could also be suitable for chemical spectroscopy measurements, particularly in complex environments allowing for a broad science case for this spectrometer.

New instruments for SNS Second Target Station

STS is nearing selection of the 8 instruments to be included in the project. Spectroscopy staff have been working with the user community to understand their needs and provide concepts. Science cases for the following instruments are being developed:

1. BWAVES - Indirect geometry spectrometer with high energy resolution and a very broad dynamic range of energy transfers (point-of-contact: Eugene Mamontov)
2. CHESS - Chopper spectrometer for small samples (point-of-contact: Gabriele Sala)
3. JANUS - Hybrid indirect/direct geometry spectrometer optimized for irreversible phenomena and in situ sample manipulation (point-of-contact: Timmy Ramirez-Cuesta)
4. Extreme environments spectrometer / diffractometer (point-of-contact: Barry Winn)
5. EXPANSE – Wide angle neutron spin echo (point-of-contact: Changwoo Do)

BWAVES is a small beam size, broadband inverse geometry spectrometer optimized for small (below 10 microliter in volume) biological and soft-matter samples that utilizes a novel wide-angle velocity selection device (WAVES) instead of traditional crystal analyzers, for the final energy selection of scattered neutrons. BWAVES alone will cover almost 5 orders of magnitude in energy transfer, from about $10\text{ }\mu\text{eV}$ to several hundred meV, providing unprecedented capabilities to study, simultaneously, relaxational and vibrational dynamics in biological and soft-matter systems. BWAVES will provide access to the low-Q range (particularly relevant to soft-matter and biology systems) because of the long final wavelength of $15\text{ }\text{\AA}$.

CHESS is a cold neutron direct geometry spectrometer for STS which will take advantage of the high brightness, optimized coupled hydrogen moderators to yield significant gain factors over current instruments. CHESS will employ focusing optics with moderate energy resolution to enable measurements on small samples (cross-sectional area of 1 mm^2 to 1 cm^2). The instrument will enable inelastic measurements to be performed with polarization analysis. The current optimization for CHESS suggests gain factors of ~ 200 when compared to the current CNCS instrument under equivalent energy resolution conditions (including credit for solid angle coverage and repetition rate multiplication).

JANUS is a medium-high resolution, broadband, indirect geometry spectrometer coupled together with a medium resolution direct geometry spectrometer. JANUS is optimized for materials chemistry and catalytic studies involving hydrogenous materials.

Extreme environment spectrometer / diffractometer: This instrument will be optimized for simultaneous diffraction and indirect geometry spectroscopy. The analyzer array will be optimized for planar measurements with a multiplexing secondary spectrometer allowing for measurements with multiple final energies. This planar geometry is well matched to vertical split bore magnets and high-pressure cells. As such, the instrument will provide high flux measurements in a variety of extreme environments. The instrument will be optimized to expand to the highest fields possible allowing for future upgrades as high-Tc magnet technology develops. This versatile instrument will be optimized for the quantum materials community but could also provide unique capabilities to diverse communities such as materials science and geophysics.

EXPANSE is an NSE spectrometer which will enable simultaneous access to wide ranges in both momentum transfer Q and Fourier time. EXPANSE will incorporate wide angle detector banks that will provide approximately two orders of magnitude in Q -range, and a wavelength band that can provide approximately four order of magnitude in Fourier times. The instrument will enable Fourier transform of the typical intermediate scattering function, $F(Q,\tau)$, so that the real space – time correlation, $g(r,t)$, can be extracted from the data. This instrument will provide a unique capability that has not been available in the currently existing NSE instruments, which is not only to visualize local slow-dynamics in real-space and time but also to enable time-resolved studies with NSE.

1.7 SOFTWARE

Data Reduction

For direct geometry spectrometers and BASIS, data reduction transforms collected data from time-of-flight events into $S(Q,\omega)$. For VISION, the double-focusing analyzers integrate the intensity over a range of scattering angle (or Q), thus the product of reduction is $S(\omega)$. The four direct geometry spectrometers use Mantid to perform mostly automatic reduction to $S(\text{detector},\omega)$ – the transformation to $S(Q,\omega)$ is performed manually in either MSlice, Horace, or Mantid. The automatic reduction at BASIS uses Mantid to directly obtain $S(Q,\omega)$ with default Q and energy binning. At VISION, two $S(\omega)$ spectra corresponding to the backscattering banks (120-150 degree) and forward scattering banks (30-60 degree) are automatically produced with Mantid. For the triple-axis spectrometers, the data collected is already in the appropriate $S(Q,\omega)$ form assuming counts were collected to a fixed incident beam monitor and only small, simple corrections are required (like accounting for higher order contamination in the beam monitor). For BL-15, NSE, new reduction software was deployed on the analysis cluster to make it available to users. DrSPINE (Data Reduction for SPIN Echo experiments) enables the reduction of neutron spin echo data produced at both reactor and pulsed neutron sources.

Data Acquisition

The data acquisition systems on CNCS, SEQUOIA, HYSPEC, ARCS, VISION and BASIS employ the new EPICS based system. Most instruments transitioned before this review period, ARCS and BASIS transitioned in 2018, and the NSE instrument data acquisition systems will transition after the instrument is taken over

by ORNL. There is a need to standardize user interfaces across common instruments, for example the four direct geometry spectrometers, to provide a more consistent experience for users. As a step in this Direction CNCS and ARCS tested python scripting control of Data Acquisition in the last cycle. The syntax of commands is common among all instruments and will be common across HFIR as well. The scripting will be rolled out to HYSPEC during the next cycle. The new data acquisition system communicates more information to facilitate the reduction process, such as lattice parameters and crystal orientation, and has the potential to allow reduced data to be more easily and rapidly visualized and analyzed.

For the triple-axis spectrometers, the data acquisition system was rewritten as part of the year-2000 beryllium reflector change at HFIR. LabVIEW-based software, SPICE (Spectrometer and Instrument Control Environment) was structured around a command-line interface and included an intuitive graphical user interface providing easy access to the commands. Several structures were included to enhance flexibility including aliases, macros and full scripting using Python. An additional capability provided with SPICE is the use of a UB matrix on the triple-axes which allows for handling of arbitrary sample symmetry and for movements in reciprocal space out of the scattering plane. These instruments will transition to the EPICS based control system in the future for consistency across the instrument suite.

Data Visualization and Analysis

A unique feature of the neutron scattering sources at ORNL is that we offer the analysis cluster to our users to do much of the work to analyze data for publication. The following paragraphs summarize how these resources are used for the various instruments.

For the four direct geometry spectrometers, data is typically visualized using DAVE MSlice, HORACE, or Mantid. Most users employ MSlice for visualization of the data during the experiment and either MSlice or HORACE for more detailed visualization and analysis. A major effort is underway to develop visualization tools in Mantid. This allows more statistically correct combining of runs in a rotation scan. This event-based method has the advantage of reducing the memory usage and has better options for symmetrization and cuts in non-standard directions. These tools are currently available for use, and a growing number of users are taking advantage of them. Nevertheless, work is required to make them more broadly accessible to the user community. To improve efficiency, a set of planning tools was implemented within Mantid (DGSPanner). Other projects underway include more user-friendly density-of-states generation and comparison with modeling and preparing an implementation of MSlice in Mantid in collaboration with ISIS. From a modeling perspective, the OCLIMAX program in the ICEMAN project enables first-principles calculations of single crystal and powder averaged $S(Q,\omega)$ from phonons for all the direct-geometry spectrometers including both coherent and incoherent scattering. A novel use of software for the Direct Geometry Spectrometers is using Monte Carlo Ray tracing instrument simulation to make closer comparisons between simulation and experiment with the MCViNE package. These simulations implicitly convolve resolution and take care of multiple scattering effects, even those between the sample and the sample environment. The interface to these tools is being expanded to make these tools more accessible to the users. More broadly, tools for allowing models to be convolved with the full resolution function and compared to single crystal data are in the planning stage.

For BASIS, data analysis is most frequently performed using DAVE. The inexperience of the diverse user community places a heavy load on the instrument team to assist users with data analysis and this is a limitation on the overall instrument output. Single crystal measurements were recently processed in Mantid using a similar workflow to MSlice/Horace. In the near term we would like to extend the event-

based processing to indirect geometry instruments as well. Recently, advances in quasielastic neutron scattering software, QCLIMAX, as part of the ICEMAN project, enables parameterized fits for users that were previously only available through expert users. Molecular dynamics simulations are making an impact on the data from BASIS but, currently, this suffers from user accessibility issues.

VISION is the instrument where modeling is most closely integrated into the science program. Tools are available to perform first-principles calculations and to generate simulated spectra which can be compared to measured data. A dedicated cluster (VirtuES) was purchased in FY 2015 to allow these calculations to be performed routinely and potentially in real-time during an experiment. Finally, the ICEMAN project was started using FY 2016 LDRD funds to develop tools that will aid in data analysis and interpretation. This is meant to streamline workflows enabling analysis of data from multiple neutron techniques together with complementary simulations and to provide a user-friendly interface reducing barriers to efficiently extract scientific content from measurements.

For SNS-NSE, the final shape of the intermediate scattering function $S(Q, \tau)$ obtained from reduction with DrSpine is ASCII and/or .csv format. This allows the analysis to be performed by curve fitting using packages of the users' choice, e.g. Origin, Matlab, Python...etc. Locally, data visualization and analysis are performed using the analysis/visualization Python-based package implemented in the reduction software DrSpine. The core named stapler-drspine consists of a Python routine, available on the SNS analysis cluster, that can be easily modified to adapt to both NSE-spallation and NSE-reactor reduced data. The package scripts can also be provided to users' personal computers upon request. The package for visualization and analysis uses Matplotlib and Scipy library function for fitting. The fitting routine includes the most commonly used models to treat NSE data (e.g. KWW, Zilman-Granek, Diffusion, Power law, liner, exponential, cumulant fit ...etc.). Users present on site during the NSE experiment get in-person full training on both reduction and analysis software. The remote users are also provided with instructions how to access and use these routines. The complete SNS-NSE reduction-visualization-analysis package software is available for users on the SNS analysis cluster and is actively updated with new functions upon users' request. Molecular dynamics simulations can have a significant impact on understanding data from SNS-NSE but, currently, this is not implemented at the beam line.

For most triple axis users, analysis is performed by simple curve fitting using packages of their choice, e.g. Origin. Many users rely on Grafitti, a portion of the Spice suite, however Grafitti is in dire need of replacement. Meanwhile, since the DAVE software from NIST contains a similar interface, we provide users with a simple file converter. For experiments where resolution convolution is required Reslib (MATLAB-based) is the most commonly used package and we are encouraging the use of neutronpy (a Python version of the Reslib package) as it has identical functionality and fits more in our overall software paradigm.

1.8 STAFFING

List of staff for all the spectroscopy instruments, including instrument scientists and scientific associates are shown in Table 1. An appropriate staffing level is required to meet the demands of the user program, instrument upgrade projects, and development of new instruments and techniques. Staffing on the four direct geometry spectrometers has been steady at two instrument scientists per instrument which is adequate. Staffing for the triple-axis spectrometers had been 1.67 instrument scientists per instrument

which falls below an ideal of two per instrument. Adding one instrument scientist to the triple-axis team would provide additional resources which are particularly important with planned upgrades and the development of MANTA. BASIS staffing level is at three instrument scientists which is appropriate for the demands of this instrument. The throughput of VISION together with the transition of Yongqiang Cheng to the Computational Instrument Scientist role clearly requires the addition of another instrument scientist to the VISION team and this is the highest priority for the Spectroscopy group. NSE staffing with two instrument scientists is appropriate.

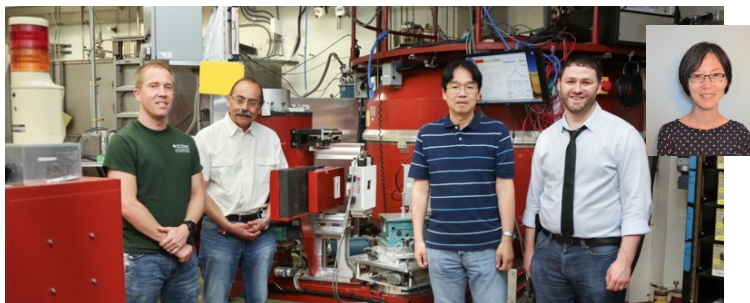
2. HFIR HB-1 POLARIZED TRIPLE-AXIS SPECTROMETER BEAMLINE STATUS AND PLANNING SUMMARY

2.1 OVERVIEW/CURRENT STATUS

Of the four triple-axis spectrometers installed at HFIR, the HB-1 PTAX instrument is specifically designed for polarized beam measurements, but it is also a highly efficient general-purpose unpolarized neutron spectrometer. The high flux and a wide range of incident energies, 5–120 meV, make the instrument particularly well-suited for polarized studies of magnetic excitations in colossal magnetoresistance (CMR) and high-temperature superconductivity (HTSC) materials, “bad” metals, quantum magnets, magnetic multilayers, and commercial magnetic alloys. In unpolarized mode, HB-1 becomes a state-of-the-art tool for studying various types of excitations and critical phenomena in a broad variety of materials, from shape memory and super elastic alloys to thin films and heavy fermion systems. The choice of two monochromator plugs gives this instrument great versatility. The polarizing plug accommodates a fixed vertical focusing Heusler alloy monochromator with a vertical guide field. The unpolarized plug accommodates a pyrolytic graphite (PG) monochromator with variable vertical focusing. The instrument offers a choice of Heusler alloy (for polarized experiments) and PG (unpolarized or half-polarized) analyzers. Polarized beam experiments can use a set of Mezei-type “flipper” devices that are fully controlled by the instrument software and achieve a nominal flipping ratio of 10-15. The magnetic guide field at sample position is generated by a Helmholtz-type coil system. The field can be rotated in three dimensions electronically by adjusting the current distribution in the coils, which is also fully automated. The polarized setup is designed to be compact enough to accommodate all available sample environment equipment, including $^4\text{He}/^3\text{He}$ dilution refrigerators, standard ^4He flow cryostats, cryofurnaces, and a variety of closed-cycle refrigerators.

HB-1 has seen a large increase in the polarized neutron experiments in the past few years. The novel scientific highlights and sustained output of HB-1 in the following pages is clear evidence of its success and importance to the neutron scattering user program. At the same time, new capabilities such as Wollaston Prisms were implemented, which enable us to measure excitations and diffraction with very high energy and Q resolution, respectively. However, the current polarized setup suffers from insufficient polarization and beam flux, which limits growth of the user community. For these reasons, the short-term goal is to improve the polarization capabilities by upgrading Heusler monochromator and analyzer with appropriate focusing mechanism using high quality crystals. The long-term goal is to build the new secondary spectrometer with having flexibility of monochromator-sample and sample-analyzer distances to accommodate large sample environments and accessories, such as cryomagnets that can reach above 8 T. The current compact Wollaston Prism can also be replaced by a larger one with higher Q and energy resolutions. Using nonmagnetic materials will improve the spin transport, which is beneficial for accurate and efficient polarization analysis. The fully upgraded HB-1 will be a world-leading polarized triple-axis spectrometer. The polarized neutron capability on HB-1 is complementary to that on HYSPEC at SNS, with HB-1 being more suitable for parametric studies in a narrow region of energy and momentum space with higher beam flux.

Team Structure. HB-1 is part of the Triple-axis Team in the Spectroscopy Group, which is in turn part of the Neutron Scattering Division. Staff instrument scientists, Masaaki Matsuda, Travis Williams and Jaime Fernandez-Baca, contribute a total of 1 FTE, 0.33 FTE and 0.33 FTE, respectively, and the scientific associate (John Carruth before April 2020 and Shirley Xu from April 2020) a total of 0.5 FTE to the effort. The computational instrument scientist providing software support for HB-1 is Andrei Savici.



2.2 SCIENTIFIC FOCUS

Since 2017, 76 general user proposals were submitted to the HB-1 instrument, of which 51 were selected to run as proposed, resulting in 103 unique users utilizing HB-1 and 39 papers published based on HB-1 data, of which 26% are in high impact journals. The following paragraphs summarize the results of selected highlights, showcasing the diverse capabilities of the high-flux polarized triple-axis spectrometer. Examples presented include research on neutron Larmor diffraction and spin echo techniques, a heavy fermion system UPt_2Si_2 , weak ferromagnetism in $LaCoO_3$ and a spintronics material $EuSiPt$.

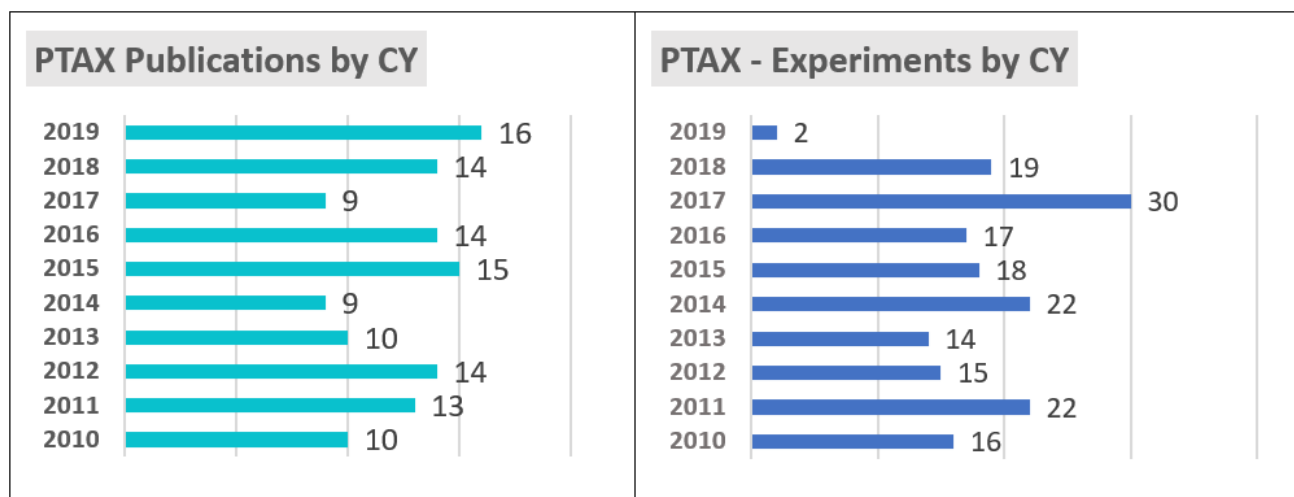


Figure 2.1. HB-1 publication statistics

2.3 SCIENTIFIC HIGHLIGHTS

New capabilities in high-resolution neutron Larmor diffraction at ORNL.

Fankang Li, Hao Feng, Alexander N. Thaler, Steven R. Parnell, Lowell Crow, Masaaki Matsuda, Feng Ye, Tsuyoshi Kimura, Jaime A. Fernandez-Baca and Roger Pynn, *Journal of Applied Crystallography* 51, 584 (2018)

Using superconducting magnetic Wollaston prisms (Figure 2.3), high-resolution neutron Larmor diffraction has been implemented. This technique allows the inverse relationship between the achievable diffraction resolution and the usable neutron flux to be overcome. Instead of employing physically tilted radio-frequency spin flippers, the method uses magnetic Wollaston prisms which are electromagnetically tuned by changing the field configurations in the device. As implemented, this method can be used to measure lattice-spacing changes induced, for example, by thermal expansion or strain with a resolution of $\Delta d/d \sim 10^{-6}$, and the splitting of sharp Bragg peaks with a resolution of $\Delta d/d = 3 \times 10^{-4}$. The resolution for discerning a change in the profile of a Bragg peak is $\Delta d/d < 10^{-5}$. This is a remarkable degree of precision for a neutron diffractometer as compact as the one used in this implementation. The sample used for this measurement was CuFeO_2 , which undergoes a first-order structural phase transition induced by the magnetic transition at 11 K and a second-order symmetry-lowering lattice distortion at 14 K, seen using high-resolution synchrotron X-ray scattering performed on station 11-ID-C at the Advanced Photon Source, Argonne National Laboratory. As shown in Figure 2.2, the minute change of the lattice distortion was clearly observed with high accuracy. Higher precision could be obtained by implementing this technique in an instrument with a larger footprint. The availability of this technique will provide an alternative when standard neutron diffraction methods fail and will greatly benefit the scientific communities that require high-resolution diffraction measurements.

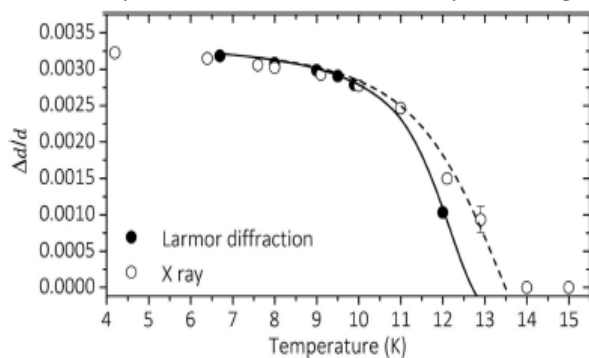


Figure 2.2. The measured $\Delta d/d$ as a function of temperature for CuFeO_2 . The solid and open circles are the values obtained by Larmor diffraction and X-ray diffraction, respectively. *J. Applied Crystallography* 2018.

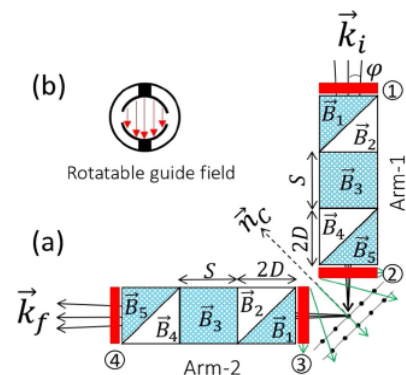


Figure 2.3. Schematic of the double-arm Larmor diffraction

High-resolution phonon energy shift measurements with the inelastic neutron spin echo technique.

F. Li, J. Shen, S. R. Parnell, A. N. Thaler, M. Matsuda, T. Keller, O. Delaire, R. Pynn and J. A. Fernandez-Baca, *Journal of Applied Crystallography* 52, 755 (2019)

The energy resolution of the conventional way of measuring a small change in a phonon dispersion curve using neutron scattering is restricted by the relatively coarse intrinsic resolution ellipsoid of the neutron triple-axis spectrometer (TAS). By implementing inelastic neutron spin echo on the host TAS using the Larmor precession of the neutron spin, the energy resolution of such measurements can be further improved without reducing the resolution ellipsoid. The sample measured was pure isotopic ^{76}Ge of 30 g. The transverse acoustic (TA) phonon at $[0, 0, 0.8]$ was studied in the $[2, 2, 0]$ Brillouin zone.

Measurements of the temperature-dependent phonon energy change are demonstrated using superconducting magnetic Wollaston prisms, and the achievable resolution is $<10 \mu\text{eV}$ (Figure 2.4).

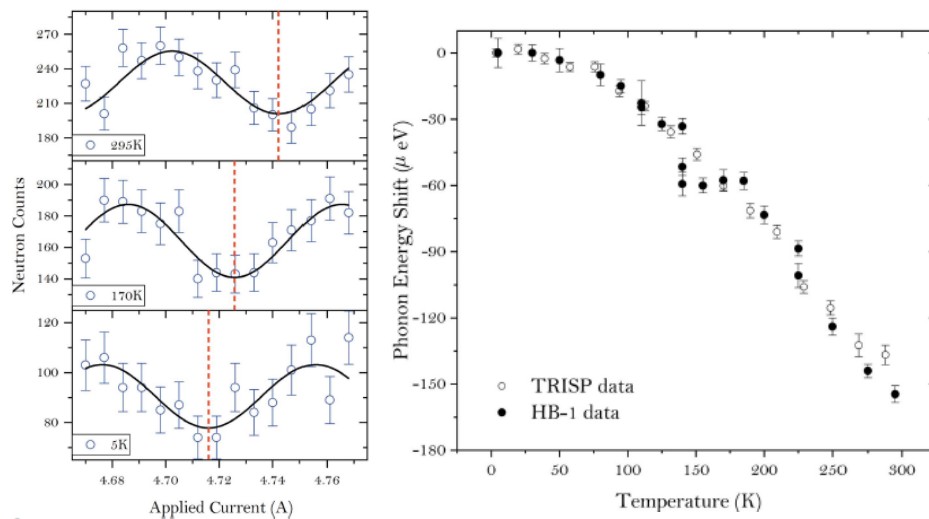


Figure 2.4. (left) Neutron intensity measured as a function of current inside the outgoing arm of the Wollaston Prism at various temperatures. (right) The measured phonon energy change as a function of temperature for the same sample of ^{76}Ge at HB-1 and TRISP. *J. Applied Crystallography* 2019.

Dual nature of Magnetism in a uranium heavy-fermion system

Jooseop Lee, Masaaki Matsuda, John A. Mydosh, Igor Zaliznyak, Alexander I. Kolesnikov, Stefan Süllow, Jacob P. C. Ruff, and Garrett E. Granroth, *Physical Review Letters* 121, 057201 (2018)

The duality between the localized and itinerant nature of magnetism in 5f-electron systems has been a long-standing puzzle. In this study inelastic neutron scattering measurements, which reveal both local and itinerant aspects of magnetism in a single-crystalline system of UPt_2Si_2 , are reported. In the antiferromagnetic state, a broad continuum of diffuse magnetic scattering with a resonance-like gap of ~ 7 meV and the surprising absence of coherent spin waves were observed, suggestive of itinerant magnetism. While the gap closes above the Neel temperature, strong dynamic spin correlations persist to a high temperature. Nevertheless, the size and temperature dependence of the total magnetic spectral weight can be well described by a local moment with $J=4$. Furthermore, polarized neutron measurements revealed that the magnetic fluctuations are mostly transverse, with little to none of the longitudinal component expected for itinerant moments (Figure 2.5). These results suggest that a dual description of local and itinerant magnetism is required to understand UPt_2Si_2 and, by extension, other 5f systems, in general.

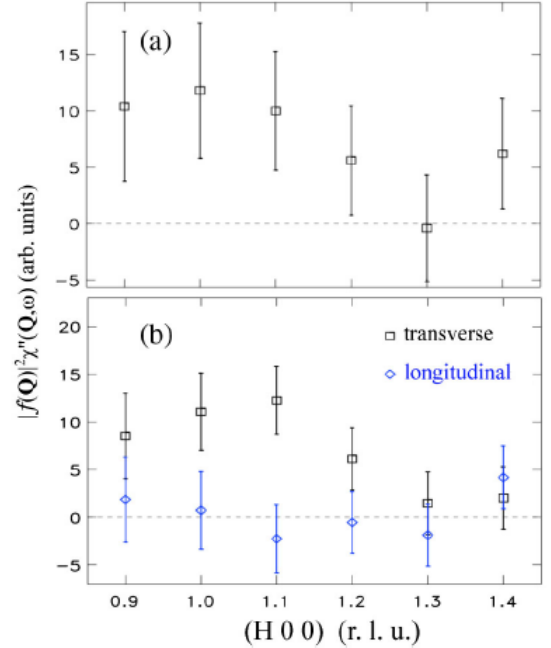


Figure 2.5. (a) Total magnetic scattering at 5 K and 12 meV. (b) Transverse and longitudinal components of the magnetic scattering. Phys. Rev. Lett. 2018

Origin of net magnetic moment in LaCoO₃

G. M. Kaminsky, D. P. Belanger, F. Ye, J. A. Fernandez-Baca, J. Wang, M. Matsuda, and J.-Q. Yan, *Physical Review B* 97, 024418 (2018)

The unusual magnetic behavior of bulk LaCoO₃ below $T = 100$ K is well known but has not been well understood microscopically. Magnetization measurements clearly show that the dominant interaction between spins is antiferromagnetic for $T > 100$ K. Polarized neutron diffraction measurements were used to characterize the Bragg scattering intensity below $T_c = 89.5$ K at the (1,0,0) pseudocubic nuclear Bragg point of LaCoO₃. Upon cooling in a field of 18 Oe (FC), a net magnetic moment is apparent in Bragg scattering intensity, as shown in Figure 2.6, just as it was in previous magnetization measurements. Critical behavior associated with the net moment near T_c upon cooling in small applied fields rapidly rounds with increasing field strength. Using a mean-field calculation, it was shown that this net moment can develop in a metastable state that forms upon FC, even when all the interactions in the system are antiferromagnetic. The work was selected as an Editor's selection.

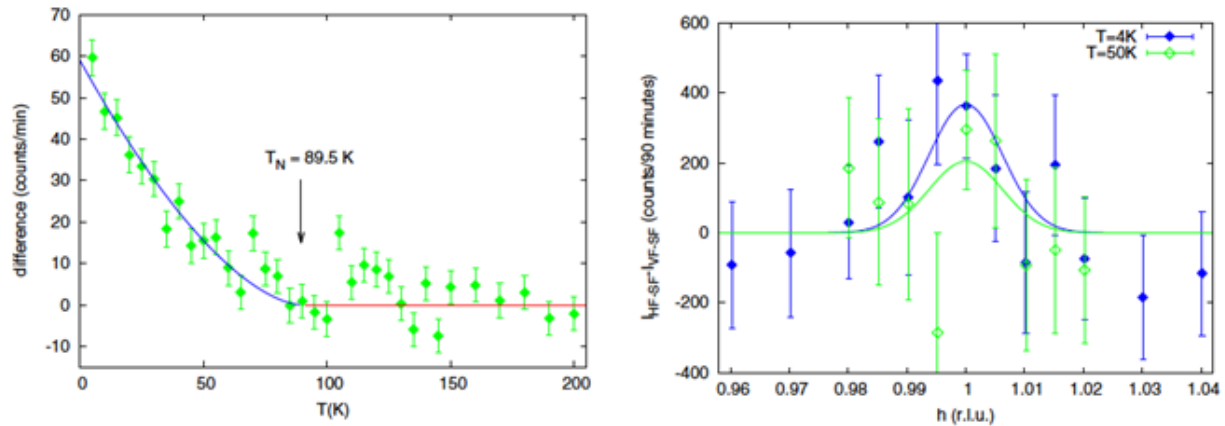


Figure 2.6. Magnetic scattering intensity as a function of temperature. (b) H scans of the magnetic peak (1 0 0) at 4 and 50 K. Phys. Rev. B 2018.

Unique helical magnetic order and field-induced phase in trillium lattice antiferromagnet EuPtSi.

Koji Kaneko, Matthias D. Frontzek, Masaaki Matsuda, Akiko Nakao, Koji Munakata, Takashi Ohhara, Masashi Kakihana, Yoshinori Haga, Masato Hedo, Takao Nakama, and Yoshichika Ōnuki, *Journal of the Physical Society of Japan* **88**, 013702 (2019)

Magnetic transition phenomena in cubic chiral antiferromagnet EuPtSi with $T_N = 4.0\text{K}$ were investigated by means of single crystal neutron diffraction. At 0.3 K in the ground state, magnetic peaks emerge at positions represented by an ordering vector $q_1 = (0.2, 0.3, 0)$ and its cyclic permutations. Upon heating, an additional magnetic peak splitting with hysteresis was uncovered at around $T_N^* \sim 2.5\text{K}$, indicating the presence of a first-order commensurate-incommensurate transition with $q_1^* = (0.2, 0.3, \delta)$. ($\delta_{\max} \sim 0.04$) at T_N^* . A half-polarized neutron scattering experiment (Figure 2.7) for polarization parallel to the scattering vector revealed that polarization antiparallel to the scattering vector has stronger intensity in both magnetic phases. This feature clarifies the single chiral character of the helical structure with moments lying perpendicular to the ordering vector in both ordered states. Under a vertical magnetic field of 1.2 T for $B//[1, 1, 1]$ at 1.9 K entering into the so-called A phase, magnetic peaks form characteristic hexagonal patterns in the equatorial scattering plane around nuclear peaks. An ordering vector $q_A \sim (+0.09, +/-0.20, +/-0.28)$ of the A-phase has similar periodic length as q_1 and could be the hallmark of a formation of skyrmion lattice in EuPtSi. The work was published in the *Journal of the Physical Society of Japan* **88**, 013702 (2019) and selected as an Editors' choice.

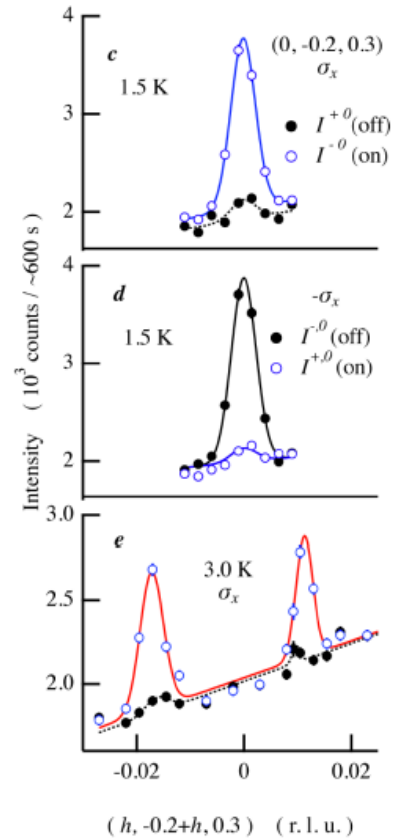


Figure 2.7. Incident polarization dependence of scans along $(h, h, 0)$ across $(0, -0.2, -0.3)$ measured at (c) 1.5 K, (d) 1.5 K with reversed guide field, and (e) 3.0 K with original guide field. *J. Phys. Soc. Jpn.* 2019.

2.4 GENERAL USER PROGRAM

About 60% of the HB1 beamtime is operated in unpolarized -neutron mode, with the remaining 40% operating in polarized-neutron mode. There are active user groups connected with hard condensed matter physics, energy materials, and functional materials. The performance of the unpolarized setup is extremely reliable and productive. The sample environments (high/low temperature, magnetic field, electrical field, and pressure) also satisfy most of the user demands. Further growth of the user community is largely limited by the instrument polarized neutron performance, i.e. insufficient beam flux and polarization. The science impact of the instrument is also limited by the polarized neutron performance. Thus, polarization and beam flux of the polarized neutron beam and the spin transport need to be improved significantly.

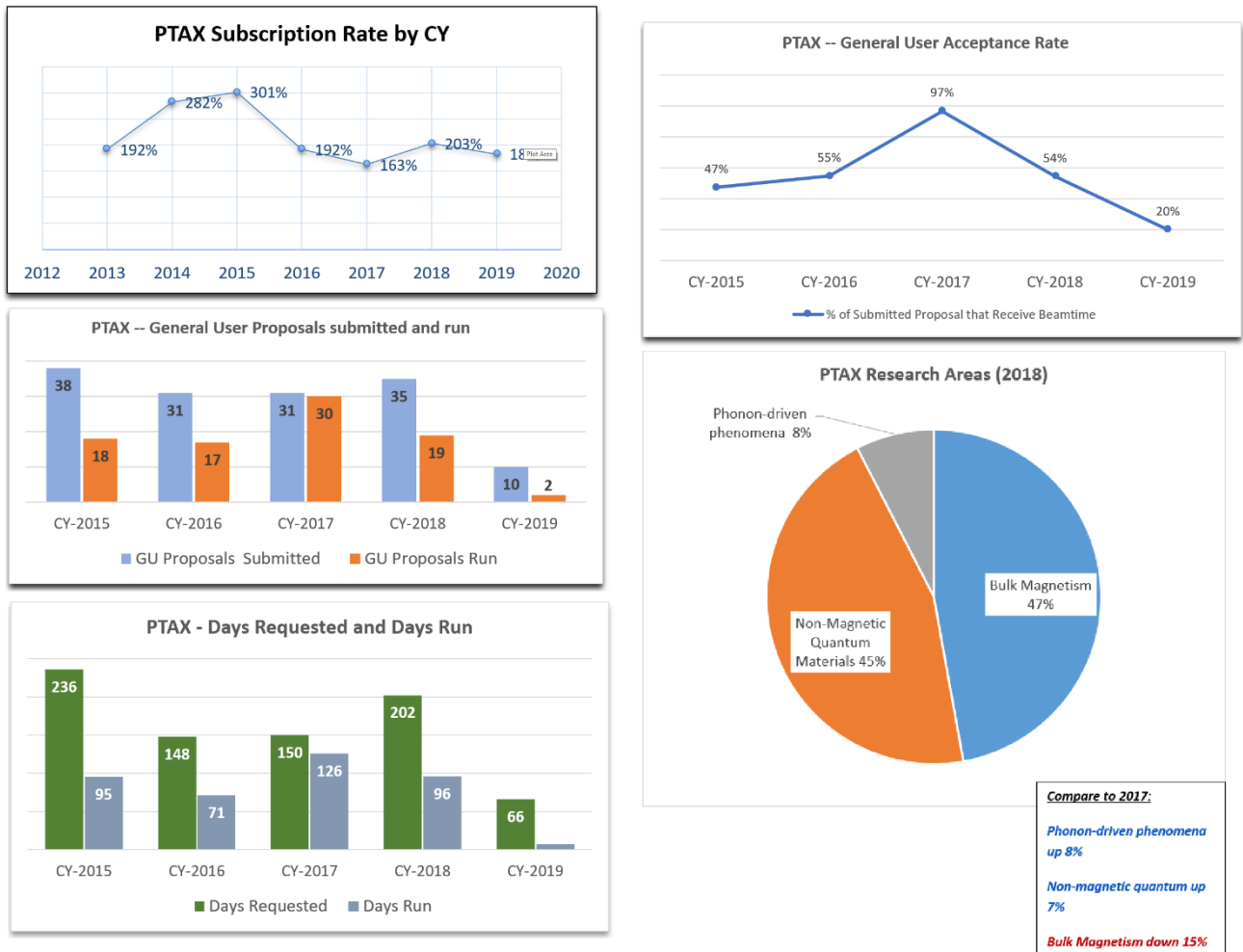


Figure 2.8. HB-1 user program statistics

2.5 UPDATE ON INSTRUMENT DEVELOPMENT ACTIVITIES

A Wollaston prism setup for ultra-high-resolution spectroscopy at HB-1 was developed as a part of a LDRD initiative (2014-16). This new capability made measurements with high Q and energy resolution possible. It is now possible to observe minute lattice distortions ($\Delta d/d \sim 10^{-5}$) using neutron Larmor

diffraction and excitation widths and shifts with $\sim\mu\text{eV}$ resolution using neutron spin-echo. This setup was implemented, and several experiments have been performed successfully. The Larmor diffraction capability has been open for the general user program since 2018.

2.6 SAMPLE ENVIRONMENT

The triple axis spectrometers at HFIR benefit from the availability of a quite diverse collection of sample environment equipment for low and high temperatures, high magnetic fields and high pressure. This allows routine measurements at high magnetic fields (up to 8 T), low temperatures (down to 30 mK), and high temperatures (up to 1600 C). High pressure experiments with CuBe clamp cells are feasible in the pressure range below 2 GPa, although this is mostly used for diffraction measurements due to small sample space. A 10 kV electrical field capability in the temperature range of $4 < T < 700$ K has newly been added in 2016.

2.7 SOFTWARE

The data acquisition software is SPICE. Graffiti has been used for the data transfer and analysis of raw data. Reslib for MATLAB has mostly been used for resolution convolution. Additionally, users often use a wide variety of software tools for later-stage data analysis and simulation.

2.8 UPDATE ON IMPACT OF DISCRETIONARY BEAMTIME

Discretionary beamtime (DT) is used to build collaborations, to attract new users and new research projects, to test new instrument capabilities, and further the science program of NScD staff. 50% of the DT are allocated through the science initiative program, and a majority of the initiative DT on HB-1 is connected to the Quantum Materials initiative.

2.9 OUTREACH AND EXPANSION ACTIVITIES

HB-1 has participated in the National School on Neutron and X-ray Scattering (<http://neutrons.ornl.gov/nxs>) every two years. In September 2019, the HB-1 instrument team also participated in a neutron polarization workshop, where lectures and facility visits took place. These and other outreach efforts are important to help grow a skill user community.

HB-1 has been used in support of two Ph.D. theses since 2017.

2.10 VISION

2.10.1 Near-term Vision (1-3 years)

Ensure HB-1 reaches its full potential as a world class polarized triple-axis spectrometer beamline.

The flipping ratio of the current polarized setup is ~ 15 at 13.5 meV and decreases to ~ 10 at 30 meV, which is far below the world standard (20 or larger in the energy range of $13.5 < E_i < 50$ meV). The current

Heusler analyzer is flat so that the scattered beam is not transported to the detector efficiently. The low flipping ratio and the insufficient intensity make some polarized inelastic experiments unsuccessful. We will build a new Heusler monochromator with variable vertical focusing mechanism, using high quality (polarization and reflectivity) crystals. We also plan to build the vertical focusing Heusler analyzer. These upgrades will greatly improve HB-1's capabilities and will attract a broader user community. The budget has been approved. The upgrades are ongoing.

A Spherical Neutron Polarimetry setup is being developed as a part of a LDRD initiative (PI: Peter Jiang at Neutron Technologies Division). This new capability will make it possible to determine complicated magnetic structures, in which spin chirality or magnetic/nuclear cross term is involved. The project is delayed due to an unexpected long-term reactor shutdown in 2019 and the COVID-19 pandemic. We hope that this capability will be tested and open for the general user program soon.

An elliptical focusing device, which focuses the unpolarized neutron beam to the sample position both vertically and horizontally, is also being implemented. This device will be used for measuring very small crystals of $\sim\text{mm}^3$ dimensions efficiently. We expect that the high-pressure experiments using piston cylinder cells and cubic anvil cells with tiny crystals can be performed with several-time enhanced intensities. We have procured the device and are ready to test it.

2.10.2 Strategic Vision (3-10 years) and Alignment with NScD/ORNL Strategic Plans

HB-1 is competitive with the best polarized triple-axis spectrometer in the world, suited for exploring new materials and sciences.

The current secondary spectrometer is outdated, compared to similar instruments at other facilities. A new secondary spectrometer should be built to have flexibility of monochromator-sample and sample-analyzer distances to accommodate large sample environments and accessories and to fully accept the vertical divergence of the scattered neutron beam. This also helps enhance the energy and Q resolution of the Wollaston Prism setup. The secondary spectrometer should be designed to use nonmagnetic materials for better spin transport of the polarized beam. The upgrade expands the possibility of new sample environments and also makes more accurate and efficient polarization analysis possible.

2.11 FUNDING/RESOURCE NEEDS

To maximize the potential scientific productivity of the HB-1 PTAX, several important near- and long-term investments are needed. Already underway is a Heusler monochromator and analyzer upgrade projects that will improve the beam flux and polarization of the polarized beam. This upgrade project has been funded and is ongoing.

A long-term upgrade project is to rebuild the secondary spectrometer. The tentative schedule for the projects calls for completion around the beryllium reflector change-out, and the funding source will be internal.

2.11.1 Future Funding Opportunities

In addition to advocating for internally funded instrument upgrades, the instrument team is actively

engaged and committed to both partnering and leading funding proposals to advance the strategic science mission of HB-1 and the full suite of polarized neutron instrument at ORNL.

2.12 SELF-ASSESSMENT

Strengths

Unpolarized neutron inelastic measurements with high beam flux are feasible under variable sample environment conditions including, T (30 mK-1873 K), H (0-8 T), P (0-2 GPa) and E (0-10kV/cm). Q and energy resolutions can be tuned by changing collimators and energies. Using the polarized neutron option, polarization analysis of the elastic and inelastic neutron scattering can be performed. This is a unique capability at HFIR. The Wollaston Prisms are also available for measurements with high Q and energy resolution. This is a unique capability in North America. The ongoing upgrade on Heusler monochromator and analyzer will make the polarized neutron measurements more efficient and make the observed data more reliable. The polarized neutron capability on HB-1 is complementary to that on HYSPEC at SNS. HB-1 is more suitable for parametric studies in a narrow region of energy and momentum space.

Weaknesses (Limitations)

The current polarized setup has deficiencies due to insufficient monochromator crystal quality, lack of the analyzer focusing mechanism, and imperfect spin transport. Insufficient beam flux and polarization are ascribed to these factors. Some of the previous polarized experiments, mostly inelastic scattering measurements, were unsuccessful because of these deficiencies. In order to improve performance, we aim to install new monochromator crystals, design a focusing mechanism for analyzer and use non-magnetic materials for the secondary spectrometer. The first two will be performed in the ongoing upgrade project. Since the last one is also vital for the good spin transport to improve the polarization, it should be done with high priority.

Opportunities

If the polarized neutron setup with high beam flux and polarization is realized, HB-1 will be a world-class polarized triple-axis spectrometer and further growth of the user community is expected.

The implementation of the Spherical Neutron Polarimetry setup will attract more users and contribute to further growth of the user community.

Larmor diffraction and inelastic measurements are now possible using the Wollaston Prism setup. The energy resolution for the inelastic measurements and the Q resolution for the Larmor diffraction can be improved by expanding the distances between monochromator and sample and between sample and analyzer. To accommodate this capability, we need to redesign the secondary spectrometer.

Threats

Lack of resources (funding), lack of added staff (full, 1.0FTE, second instrument scientist), and the possible inability to retain staff.

2.13 EXECUTIVE SUMMARY

The current polarized setup was implemented in 2013. In 2014-2019, thirty-one papers (46%) out of sixty-eight papers in total are from the polarized neutron studies. Seven (23%) out of the thirty-one papers were in journals with high impact factors (> 7). Unfortunately, due to the limitation of the polarized neutron beam flux, only six papers (19%) are about the inelastic neutron scattering studies. The upgrade project to improve the performance (beam flux and polarization) of the polarized setup will enhance the scientific productivity of inelastic studies. With the upgrade, HB-1 will be among the top instruments of its kind worldwide.

2.13.1 Comparison of instrument specifications to similar instrument worldwide

	HB-1	PUMA (FRMII)	BT7 (NIST)	TAIPAN (ANSTO)
Velocity Selector	No	No	No	No
Monochromator Crystals	PG(002), Heusler(111)	PG(002), Cu(220), Cu(111)	PG(002), Cu(220)	PG(002), Cu(200)
Monochromator size	PG: 30X18 cm ² Heusler: 20X18 cm ²	26X16.2 cm ²	20X20 cm ²	20X20 cm ²
Mono. focusing	Vertical only	Double focusing	Double focusing	Double focusing
Mono. Takeoff angle	14° to 75°	15° to 115°	16° to 75°	15° to 85°
Incident energy	5 to 120 meV	5 to 160 meV	5 to 500 meV	5 to 160 meV
Max. Flux (n cm⁻² s⁻¹)	5e7@41meV	1e8 VF; 4.5e8 DF	3.4e7 @Ei=14.7 meV	2e8 @Ei=50 meV
Beam size	5X3 cm ²		3.8X5 cm ²	
Scattering angle	0° to 120°	-70° to 120°	0 to 120°	0 to 120°
Multianalyzer availability	No	Yes	Yes	No
Analyzer crystals	PG(002), Heusler(111)	PG(002), Ge(311)	PG(002)	Double Focusing PG(002)
Analyzer size	PG: 18 X13 cm ² Heusler: 10X7.5 cm ²	27.5X15 cm ²	30X15 cm ²	16X14 cm ²
Analyzer angles	0° to 140°	-120° to 120°		0° to 110°
No. of detectors	1 single detector (SD)	11 SD; 1 PSD	SD group and PSD	1 SD
Detector dimension	W:5.08 cm H:~15 cm		SD:2.5X15 cm ² PSD: 16.5 cm tall	2.5X10 cm ²
Polarized beam	Heusler mono&analyzer		³ He in situ drop in polarizers	³ He polarizers

2.13.2 Comparison of sample environment capabilities with similar instruments worldwide

	HB-1	PUMA (FRMII)	BT7 (NIST)	TAIPAN (ANSTO)
Temperature range	30 mK (DR), 1500 C (vacuum)	0.03K to 2200 K	0.03K to 1600C	0.03K to 1600C
Max magnetic field	8 T (VF)	14 T VF	15 T VF	12 T VF
Max pressure	~2 GPa	PE cell:7 GPa	0.6 G Pa with helium intensifier	No

2.13.3 Data and computing capabilities

	HB-1	PUMA (FRMII)	BT7 (NIST)	TAIPAN (ANSTO)
Data reduction	SPICE		DAVE	SICS
Data visualization	SPICE/Graffiti		ICE/DAVE	
Data analysis packages	Graffiti Reslib for MATLAB		DAVE	RESTRAX
Data Modeling				
Simulation and data correction tools		MAX-1	DAVE	
Planning tools		MAX-1;paprika	DAVE	
Computing resources				

3. HFIR HB-3 TRIPLE AXIS SPECTROMETER BEAMLINE STATUS AND PLANNING SUMMARY

3.1 OVERVIEW/CURRENT STATUS

The thermal triple axis spectrometer (TAS) HB-3 was originally designed and installed in the 1960's. The beam tube and the monochromator system were upgraded during the last HFIR Be changeout in the year 2000. This instrument currently provides the highest thermal TAS flux in the U.S. Its monochromator system provides 3 crystal choices: PG(002), Be(002) and Si(111). The PG (002) monochromator provides a neutron flux as high as $\sim 2.5 \times 10^8$ n/cm²/s. The Si (111) has the advantage of an absent second-order reflection, providing a higher order contamination-free beam. The high-quality beryllium monochromator is unique, which allows measurements with good energy resolution at higher energy transfers. All 3 monochromators have variable vertical focus which is optimized for a 1 inch tall beam at the sample position.



Figure 3.1. HB-3 triple-axis spectrometer

With its high flux, large beam size and the versatility in choosing the incident neutron beam, HB-3 has been very productive in various research areas such as spin and lattice dynamics in high-temperature superconductors and related compounds; spin waves in magnetically ordered materials; and phonons in thermoelectric materials, multiferroics, and relaxors. The total publications generated by HB-3 is comparable to most of its peer instruments around the world. More details of the instrument and the related publications can be found on the official webpage of the instrument (<http://neutrons.ornl.gov/tax>).

Team Structure

HB-3 is one of the neutron spectrometers in the Triple-Axis team in the NSD Spectroscopy Group. Staff instrument scientists Songxue Chi (1.00 FTE), Travis Williams (0.33 FTE) and Jaime Fernandez-Baca (0.33 FTE), and a scientific associate, Mike Cox (0.5 FTE) contribute to the effort. The computational instrument scientist providing software support for HB-3 is Andrei Savici.



Figure 3.2. The HB-3 instrument team. From left to right: Jaime Fernandez-Baca, Travis Williams, Mike Cox, and Songxue Chi .

3.2 SCIENTIFIC FOCUS

During calendar years 2017-2019, 85 general user proposals were submitted to the HB-3 instrument, of which 53 were selected to run as proposed, resulting in 89 unique users (FY-17 and 18) utilizing HB-3 and 26 papers published based on HB-3 data, of which 8 are in 'DOE high impact' journals.

Publication Impact: **23%** publications with a high impact factor (recent 3 years)

Results from use of both facilities: **32%**

Results from use of multiple instruments: **64%**

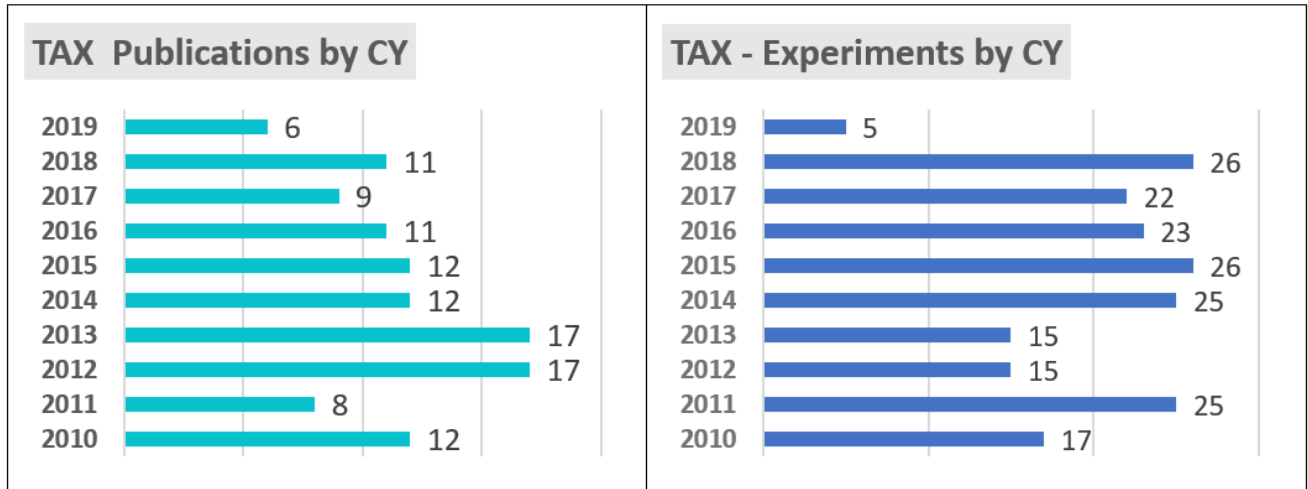


Figure 3.3. HB-3 publication statistics

3.3 SCIENTIFIC HIGHLIGHTS

The following paragraphs summarize the results of selected scientific highlights, showcasing the diverse capabilities of the high-flux triple axis spectrometer. Examples presented include research on quasi-2D antiferromagnets, high- T_c superconducting materials, quantum magnets, and thermoelectric materials.

Temperature dependence of low-E magnetic fluctuations in nearly optimally doped $\text{NaFe}_{0.9785}\text{Co}_{0.0215}\text{As}$

Yu Song, Weiyi Wang, Chenglin Zhang, Yanhong Gu, Xingye Lu, Guotai Tan, Yixi Su, Frédéric Bourdarot, A. D. Christianson, Shiliang Li, and Pengcheng Dai, *Physical Review B*, 96, 184512 (2017)

Unpolarized inelastic neutron scattering measurements on the optimally Co-doped NaFeAs, with coexisting superconductivity ($T_c \approx 19$ K) and weak antiferromagnetic order ($T_N \approx 30$ K, ordered moment $\approx 0.02 \mu\text{B}/\text{Fe}$) were performed at HB-3. A single spin resonance mode with intensity tracking the superconducting order parameter was observed, although the energy of the mode only softens slightly upon approaching T_c . A separate polarized neutron scattering revealed that the single resonance is mostly isotropic in spin space, similar to overdoped $\text{NaFe}_{0.935}\text{Co}_{0.045}\text{As}$ but different from optimal electron-, hole-, and isovalently doped BaFe_2As_2 compounds, which feature an additional prominent anisotropic component. The HB-3 measurements revealed that spin anisotropy in $\text{NaFe}_{0.9785}\text{Co}_{0.0215}\text{As}$ is instead present at energies below the resonance, which becomes partially gapped below T_c , similar to the situation in optimally doped $\text{YBa}_2\text{Cu}_3\text{O}^{6,9}$. These results indicate that anisotropic spin fluctuations in $\text{NaFe}_{1-x}\text{Co}_x\text{As}$ appear in the form of a resonance in the underdoped regime, become partially gapped below T_c near optimal doping, and disappear in overdoped compounds.

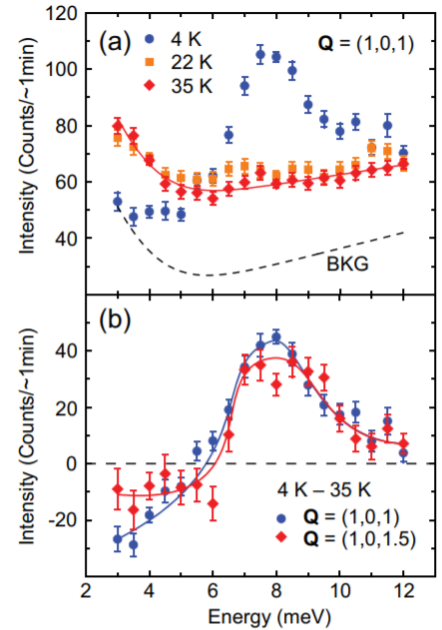


Figure 3.4. (a) Constant-Q scans at $Q = (1,0,1)$. (b) Comparison of the difference between 4 K and 35 K for constant-Q scans

Supersonic propagation of lattice energy by phasons in fresnoite

M. E. Manley, P. J. Stonaha, D. L. Abernathy, S. Chi, R. Sahul, R. P. Hermann and J. D. Budai, *Nature Communications*, 9,1823 (2018)

To remove heat without shorting electrical connections, heat must be carried in the lattice of electrical insulators. Phonons are limited to the speed of sound, which, compared to the speed of electronic processes, puts a fundamental constraint on thermal management. This study reports a supersonic channel for the propagation of lattice energy in fresnoite ($\text{Ba}_2\text{TiSi}_2\text{O}_8$) using neutron scattering. Lattice energy propagates 2.8–4.3 times the speed of sound in the form of phasons, which are caused by an incommensurate modulation in the flexible framework structure of fresnoite. The phasons enhance the thermal conductivity by 20% at room temperature and carry lattice-energy signals at speeds beyond the limits of phonons. Highly supersonic propagation of pure lattice energy in fresnoite in thermal equilibrium, breaking the conventional limit set by the speed of sound. The supersonic phasons carrying this thermal energy are exposed in the HB-3 neutron scattering measurements by a wave vector rotation that moves the phason dispersion cones away from interference from the soft phonon mode. This rotation challenges established ideas on how incommensurate structural modulations develop from soft phonon modes and suggests unexpected phason reorientation instability. Taken together these remarkable findings open a new venue for understanding and controlling.

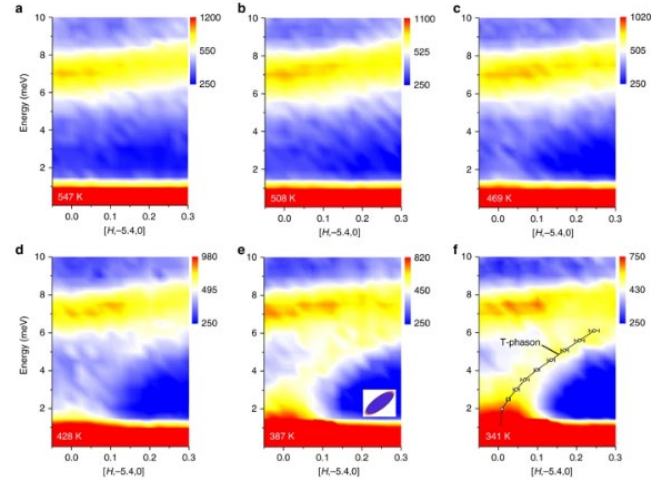


Figure 3.5. Phason formation measured on HB-3, which provide a detailed assessment of the T-dependence of the phason and incommensurate reflection.

f-Electron States in PrPd₅Al₂

Naoto Metoki, Hiroki Yamauchi, Hiroyuki S. Suzuki, Hideaki Kitazawa, Masato Hagihara, Takatsugu Masuda, Adam A. Aczel, Songxue Chi, Tao Hong, Masaaki Matsuda, Daniel Pajerowski, and Jaime A. Fernandez-Baca, *J. Phys. Soc. Jpn.* **87**, 094704 (2018)

The crystalline electric field (CEF) excitation spectrum of PrPd₅Al₂ has been studied using HB-3 and CTAX in order to reveal the *f*-electron states. PrPd₅Al₂ is a Pr-based isostructural compound of the heavy-fermion superconductor NpPd₅Al₂. We observed clear CEF excitations up to ~25 meV. The CEF Hamiltonian of the Pr³⁺ ion (³H₄) under tetragonal point symmetry was orthogonalized analytically and the CEF parameters were determined from the excitation energies. The *f*-electron states reproduce the distinctive temperature dependence of the magnetic excitation spectra as well as the macroscopic properties. A point charge model is effective in understanding the systematic change in the *f*-electron states in RPr₅Al₂. The Ising anisotropy in CePd₅Al₂, PrPd₅Al₂, and NdPd₅Al₂ originates from the flat orbitals with large *J_z* due to the CEF potential developed in the crystal structure. We found that the temperature dependence of the magnetic susceptibility in NpPd₅Al₂ can be explained qualitatively on the basis of the identical charge distribution in RPr₅Al₂. *XY*-type anisotropy is expected from the positive Stevens factors α_l for the Pr³⁺ ion. Thus, this study concluded that the local properties of the *f*-electron states are important for the physical properties of RPr₅Al₂ compounds, including the heavy-fermion superconductivity in NpPd₅Al₂.

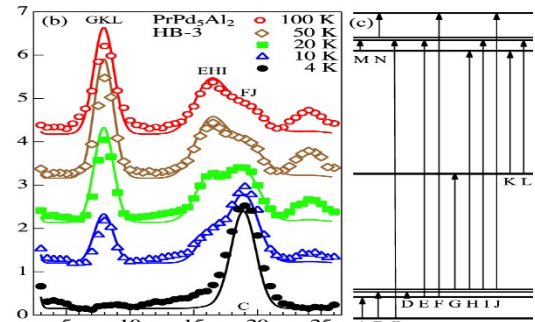


Figure 3.6. Neutron inelastic scattering spectra of PrPd₅Al₂ measured using HB-3. The solid lines are the model calculation based on HCEF/HCEF. The CEF scheme is shown on the right

Low-T anharmonicity and the thermal conductivity of cesium iodide

Bin Wei, Xiaoxia Yu, Chao Yang, Xin Rao, Xueyun Wang, Songxue Chi, Xuefeng Sun, and Jiawang Hong, *Physical Review B* 99, 184301 (2019)

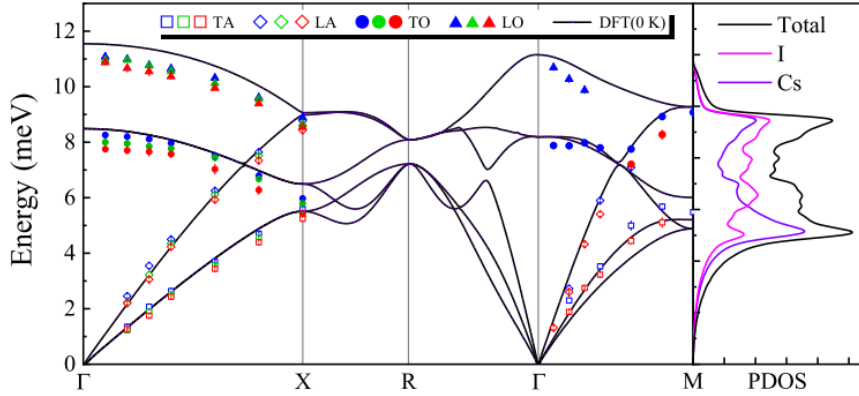


Figure 3.7. Phonon dispersions and phonon DOS of CsI

Cesium halide has a simple cubic crystal structure and hosts low thermal conductivity, but its microscopic mechanism has not been fully understood. In the present work, we took cesium iodide (CsI) single crystal as an example, to investigate the lattice dynamics and thermal conductivity by performing inelastic neutron scattering (INS), heat transport measurements, and first-principles calculations. The temperature dependent phonon dispersions of CsI were obtained from INS and the low temperature anharmonicity of transverse optic (o) and transverse acoustic (a) phonon modes in CsI was observed. By performing the thermal conductivity measurement and first-principles calculations, it is shown that the low thermal conductivity of CsI originates from the combined effect of the small phonon group velocities and the large phonon scattering rates, which is dominated by the (a, a, a) and (a, a, o) phonon scattering processes. This work highlights the importance of phonon anharmonicity in lattice dynamics, which sheds light on the design of materials with low thermal conductivity.

Cesium halide has a simple cubic crystal structure and hosts low thermal conductivity, but its microscopic mechanism has not been fully understood. In the present work, we took cesium iodide (CsI) single crystal as an example, to investigate the lattice dynamics and thermal conductivity by performing inelastic

Anharmonic Eigenvectors and Acoustic phonon Disappearance in Quantum Paraelectric SrTiO₃

Xing He, Dipanshu Bansal, Barry Winn, Songxue Chi, Lynn Boatner, and Olivier Delaire, *Physical Review Letters*, 124, 145901 (2020)

Pronounced anomalies in the SrTiO₃ dynamical structure factor, $S(Q,E)$, including the disappearance of acoustic phonon branches at low temperatures, were uncovered with inelastic neutron scattering (INS) and simulations. The striking effect reflects anharmonic couplings between acoustic and optic phonons and the incipient ferroelectric instability near the quantum critical point (QCP). This is rationalized using a first-

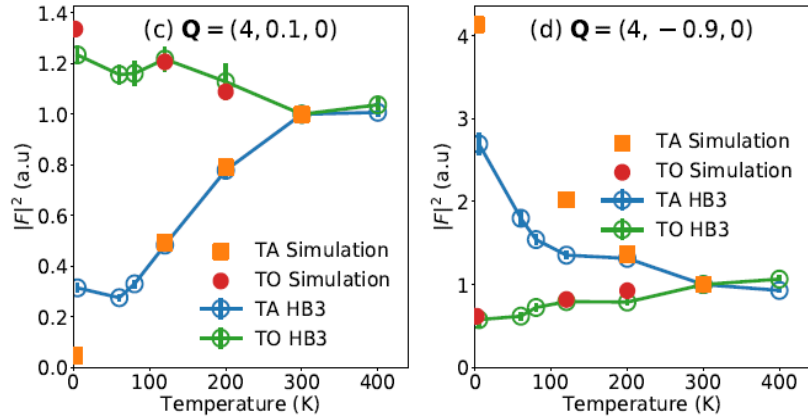


Figure 3.8. HB-3 data shows the temperature dependence of TA mode vs simulation.

principles renormalized anharmonic phonon approach, pointing to non-linear Ti-O hybridization causing unusual changes in real-space phonon eigenvectors. This method is general and establishes how T-dependences beyond the harmonic regime, assessed by INS mapping of large volumes, provide real-space insights into anharmonic atomic dynamics near phase transitions in complex oxides.

Note that the same paper was highlighted in the HYSPEC section of the document – an example of effective utilization of the relative strengths of direct geometry and triple-axis spectrometers.

3.4 GENERAL USER PROGRAM

During calendar years 2017-2019, a total of 523 beam days were requested for the general user program at HB-3, as shown in Figure 3.9. During the same period, 270 days were allocated for the general user program (51.6% of the demand). The total number of completed user experiments during that time span was 124. The user base is diverse but mostly at ORNL (40% of the beam time used). 20% of the users are from foreign institutions.

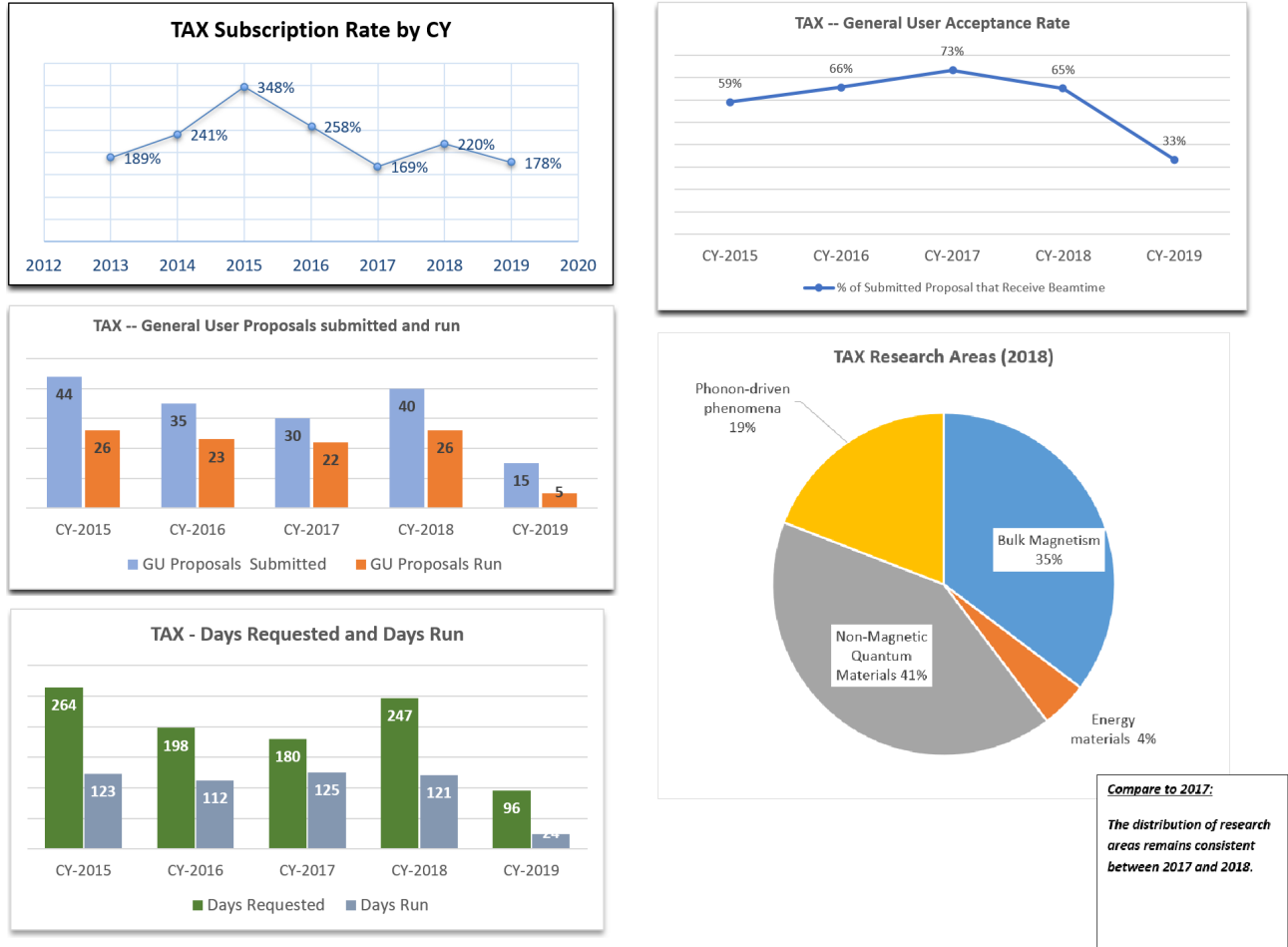


Figure 3.9. HB-3 user program statistics

3.5 UPDATE ON INSTRUMENT DEVELOPMENT ACTIVITIES

Omega shielding around the sample position.

HB-3's high-neutron flux also leads to a high radiological and neutronic background. To ensure the radiation does not exceed the posted level, we have come up with a design to shield the sample area. This design uses an Omega-shaped track around the sample position (Figure 3.10). A frame with a neutron window is fixed to the analyzer arm. Shielding pieces, linked together and mounted on the tracks, are tied to both sides of the moving frame. As S2 moves, the shielding pieces are pushed or dragged on the tracks whose far ends extend toward the monochromator drum. The linkage between the shielding pieces can be easily unlocked so that fraction of the shielding can be moved out of the way for sample loading or high-Q measurements. We have performed test using collimation 48'-60'-Sample-60'-120' and a plastic sample are chosen to create high neutron flux. The radiation detectors were held at the boundary of the instrument proximity alarm. The test results are shown in the table below. Both neutron and Gamma radiation have been cut by half. The new shielding also help reduce the erroneous counts on HB-2B and HB-3A.



Figure 3.10. Shielding design around the HB-3 sample position.

Location	Radiation	Without the shielding	With the shielding
North side (HB-2B side)	Neutron (millirem)	20	10
	Gamma (millirem)	100	45
South side (HB-3A side)	Neutron (millirem)	14	5
	Gamma (millirem)	60	34
HB-2B detector			50% reduction in background counts

Velocity Selector

A neutron velocity selector upstream of the HB-3 monochromator will eliminate the neutron higher-order wavelength contamination in the main beam. Eliminating these undesired neutrons will provide a clean beam, alleviate the radiological background problems and enhance HB-3's performance. Neutron velocity selector is a rotary device with helically curved neutron absorbing blades. The resultant clean beams will significantly improve the signal/noise ratio which is essential for samples with small volume or intrinsically weak signal. Clean beams will also broaden the choices for fixed final energies constrained by filters, and consequently increase the range of energy transfer and momentum transfer. In addition scattering artifacts caused by incident higher order neutrons can be avoided. A neutron velocity selector with goniometer is shown in Figure 3.11. The estimated total cost for this project is \$1,394 K. We have finished the evaluation of the cubicle where this velocity selector will be located, the design criteria document and the translation stage procurement, and signed the Final Design report with Airbus.

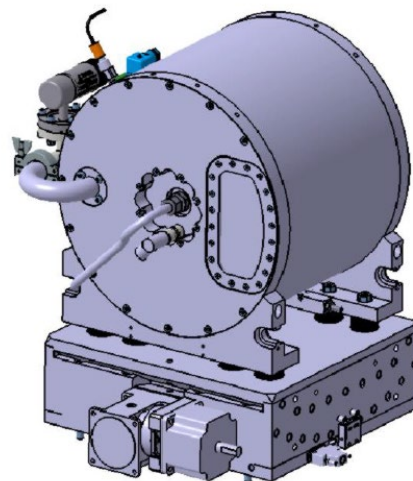


Figure 3.11. Neutron velocity selector with goniometer

New analyzer tank wedge lifter system

To replace the obsolete lifter, a new analyzer wedge lifter system has been installed. The new system follows the same design as the obsolete system, and so does not affect the instrument performance. However, the new system will provide prolonged operation of the wedge lifter without the risk of malfunctions when changing the final neutron energy.

3.6 SAMPLE ENVIRONMENT

The current sample environments inventory allows measurements in the temperature range between 0.03 K and 2000 K. In 2014 high magnetic field (8 T) became available for HB-3 thanks to the sample table upgrade. High pressure experiments, both elastic and inelastic, have been tried with CuBe clamp cells, pressure cells from a collaboration with Russian scientist, and a palm-cubic cell developed by the US-Japan collaboration on neutron scattering. The highest pressures of these cells are 2 GPa, 3 GPa and 7 GPa, respectively. A 10 kV electrical field capability in the temperature range of $4 < T < 700$ K has newly been added in 2016.

3.7 SOFTWARE

The data acquisition software is SPICE. Graffiti has been used for the data transfer analysis of raw data. Graffiti recently has encountered an incompatibility with the latest MAC OS deployment. In the long term a Graffiti replacement with extended functionalities is desirable, while in the short term we have made a request to the IDAC team for a fix. Reslib for MATLAB has mostly been used for resolution deconvolution. ScanMapper on Dave is used to identify the sources of spurious scatterings. FullProf is useful in calculation of neutron scattering cross section and determining magnetic structures with triple-axis data. SpinW has been increasingly recognized among the users as a useful tool for spin wave analysis.

3.8 IMPACT OF DISCRETIONARY BEAM TIME

The discretionary time on HB-3 has been allocated to encourage collaborations with US universities, research teams outside the neutron scattering division, neutron instrument scientists, as well as locally sponsored postdoc, students and researchers. The HB-3 instrument team strives to identify worthwhile projects to promote new collaborations, innovations and publications. Half of the discretionary beamtime is being allocated to proposals within ORNL's various Science Initiatives. Most of the beamtime allocated on HB-3 through this program is being used by proposals from the Quantum Materials Initiative.

3.9 OUTREACH AND EXPANSION INITIATIVES

The HB-3 team has been participating regularly in DOE's National School on Neutron and X-Ray Scattering. Hands-on experiment and data reduction/analysis sessions that are given during the workshop provide graduate students and post-doctoral researchers a great opportunity to become familiar with inelastic neutron scattering. When supporting inexperienced users, the instrument team makes an effort to train them in single crystal alignment, spurion identification, resolution calculation and other triple-axis technical skills. We provide data analysis support even after experiment if need to. Instrument team members have volunteered in events such as ORISE/ORNL Virtual Career Fair, APS March meeting neutron booth to promote and advocate the use of neutron scattering.

3.10 VISION

Near-term Vision (1-3 years)

- Optimize the sample area omega shield. The tests on this shield have proved that the design is effective in reducing both neutron and gamma radiation. Currently only one side of the aluminum holder is glued with flexi-Boron sheet. We expect more reduction of radiological background if both sides have flexi-Boron. The details of the design can be improved to avoid mechanical failures.
- Rebuild the sample goniometer: The Huber table is very old the tilt motors get stuck occasionally due to the worn worm gear. Huber has suspended the production of such goniometer. We will try to send it back for rebuild.

Strategic Vision (3-10 years)

Installation of the neutron velocity selector after the beryllium change-out. (Figure 3.12)

Installation of the velocity selector will require that the HB-3 monochromator drum be permanently shifted downstream a few inches. The current estimate of this is 4 – 6 inches.

- a) Rebuilding the cubicle area and the shield wall
- b) Redesign of the Instrument shutter and the monochromator drum saddle shielding.
- c) The HB-3A flight path will be re-aimed, and its exit flight path reconfigured to allow full use of the beam.
- d) Shielding will be reconfigured as necessary to integrate with the new equipment layout.
- e) Required DAS infrastructure/software will be installed to support the new systems.

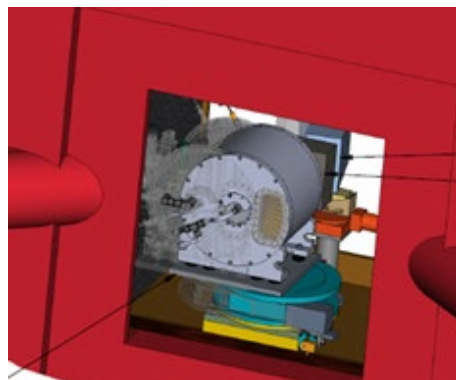


Figure 3.12. Design of the neutron velocity selector in the cubicle

- The scientific benefits from a velocity selector are mainly the following:
 - a) It will considerably reduce the higher-harmonic neutrons and fast neutrons and reduce the background. Better signal/noise ratio makes it possible to study the magnetic excitations in samples with small volume or reduced magnetic moment.
 - b) The resultant clean beam will also allow users to take full advantage of the high flux and big beam size of HB-3. This will also reduce the chance of radiological events.
 - c) The clean beam will obviate the need for filters that constrain the choice of fixed initial or final energies, and consequently give the instrument much more flexibility and more range in energy transfer and reciprocal space.
 - d) Higher-order neutrons create spurious scattering events that are difficult to identify, and a clean beam will eliminate spurious scattering resulting from higher harmonics.

Backend upgrade

The integrated neutron flux limitations of the spallation neutron sources, including the most advanced SNS, highlight the need of the complementary high-flux steady-state neutron sources to probe small regions of (Q,E) space with great detail. Thus, TAS instruments will continue to play a vital role in probing the space and time correlations and their interplay in the behavior of condensed matter systems. While the point-by-point scan strategy has maintained its importance, significant efforts have been made to expand the TAS capabilities and to increase their output using focusing optics and multiplexing techniques. All the TAS at the HFIR are antiquated and are in need of upgrades. We are proposing a new HB-3 backend design that increases flexibility, neutron luminosity, signal/noise ratio, and data acquisition rate. New neutron optics technology such as elliptic focusing guide should be explored to deal with small crystals. Figure 3.13 shows a preliminary concept of the secondary spectrometer including a multiplexing analyzer and detector system and their shielding.

The upgraded HB3 will also accommodate more state-of-the-art sample environments such as high-field magnets. In addition to the enhanced performance in the conventional measurements of elementary

excitations, the expanded capability will make HB-3 a much better tool in probing continuum modes or fluctuations related to ordering processes both on short and long ranges.

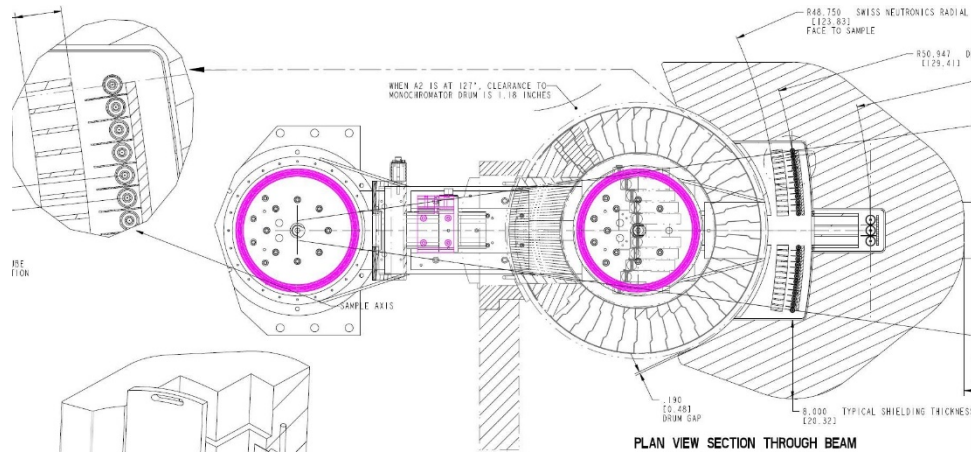


Figure 3.13. A concept of the new HB-3 secondary spectrometer

In addition, an effort shall be made to implement full polarization with in-situ polarized ^3He polarized spin filters to take advantage the intense and clean neutron beam after the neutron velocity selector has been installed. This will be particularly useful for inelastic neutron scattering at high energies.

3.11 FUNDING/RESOURCE NEEDS

The neutron velocity selector (NSV) project has been approved as a A-list project. However, to this date funding and manpower have been provided only for the procurement of the NVS. Its installation has been postponed and an additional \$1,000,000 is needed for this task. We will seek internal funding for the backend upgrade.

3.12 SELF-ASSESSMENT

Strengths

The combination of a large neutron beam opening from the reactor and multiple monochromator choices provide the highest thermal triple axis flux in the US, high energy transfers and a wide variety of energy resolution choices.

Weaknesses

- Low data acquisition rate: The analyzer is one piece with a fixed vertical focus and one rotation axis. There is only one single detector.
- Low signal/noise ratio: HB
- 3 has a high background due to fast neutrons, higher harmonic neutrons and leaky analyzer chamber shielding.
- High radiological background: The current measures to prevent the radiation from exceeding the posted level is time-consuming and undermines the productivity of the instrument.

- Weight limitations: The cantilevered design of the current backend and the old sample stage can support environments up to 1000 lbs and prohibits the use of large cryomagnets and other state-of-the-art sample environments.
- Space limitations: The vertical distance between the mounting surface to the center of the beam is too short to position a modern compensated magnet. The boundary with HB2B limits the angular range of the monochromator arm and limits our ability to probe low energy excitations with the beryllium monochromator.

Opportunities

The beryllium change-out that is scheduled for 2024 brings great opportunities to tackle HB-3's weaknesses head-on.

- 1) The cubicle behind the monochromator drum can be rebuilt to provide better shielding against fast neutrons and Gamma radiation.
- 2) The installation of the neutron velocity selector will greatly reduce the background
- 3) The installation of permanent boundary wall could save the space, provide more low-E range, and reduce the background further. An interlock that comes with it will tremendously improve the radiological safety.

Threats

- The rails on the instrument floor make it impossible to have heavy backend design. This means the low data collection efficiency will be a long-term problem even if we have a chance to upgrade the backend. The similar instruments in other facilities, such as ILL and FRMII, have implemented multiplex concept and gained advantages.
- A variety of x-ray elastic and inelastic scattering techniques have been advancing and competing with neutron scattering.

3.13 EXECUTIVE SUMMARY

HB-3's high flux, versatile monochromators, and large momentum coverage make it a very productive spectrometer in a wide range of science. The instrument team is in a constant pursuit of high-quality research projects and new users. Its main drawbacks such as high background are being addressed by the upgrade projects that are currently underway. Its backend is still in its pristine stage. A major upgrade is needed to increase the data collection rate, improve and signal to noise ratio and to accommodate more capable sample environment. The new design will provide a greater horizontal and vertical acceptance of the scattered beam and allow a multiplexed secondary spectrometer. The new design will also provide enough space to implement He-3 transmission polarizers to perform full polarization analysis.

3.13.1 Comparison of instrument specifications with similar instrument worldwide

	HB-3	PUMA (FRMII)	BT7 (NIST)	TAIPAN (ANSTO)
Velocity Selector	No	No	No	
Mono. Crystals	PG(002) Be(002) Si(111)	PG(002) Cu(220) Cu(111)	PG(002) Cu(220)	PG(002) Cu(200)
Mono. size	15X16 cm ²	26X16.2 cm ²	20X20 cm ²	20X20 cm ²
Mono. focusing	Vertical only	Double focusing	Double focusing	Double focusing
Mono. Takeoff angle	-12° to -88°	-15° to -115°	16° to 75°	15° to 85°
Incident energy	5 to 300 meV	5 to 160 meV	5 to 500 meV	5 to 160 meV
Max. Flux (n cm⁻² s⁻¹)	6.8e7	1e8 VF; 4.5e8 DF	3.4e7 @Ei=14.7 meV	2e8 @Ei=50 meV
Beam size	5X3 cm ²		3.8X5 cm ²	
Scattering angle	-90° to 130°	-70° to 120°	0 to 120°	0 to 120°
Multianalyzer availability	No	Yes	Yes	No
Analyzer crystals	PG(002)	PG(002) Ge(311)	PG(002)	Double Focusing PG(002)
Analyzer size	18.6X14.1 cm ²	27.5X15 cm ²	30X15 cm ²	16X14 cm ²
Analyzer angles	-40° to 90°	-120° to 120°		0° to 110°
No. of detectors	1 single detector (SD)	11 SD; 1 PSD	SD group and PSD	1 SD
Detector dimension	W:5.08 cm H:		SD:2.5X15 cm ² PSD: 16.5 cm tall	2.5X10 cm ²
Polarized beam	³ He in situ polarizers		³ He in situ drop in polarizers	³ He polarizers

4. HFIR HB-1A, FIE-TAX, FIXED-INCIDENT-ENERGY TRIPLE-AXIS SPECTROMETER BEAMLINE STATUS AND PLANNING SUMMARY

4.1 OVERVIEW/CURRENT STATUS

The HB-1A Triple Axis Spectrometer (FIE-TAX) at the High Flux Isotope Reactor operates at a fixed incident energy of $E_i = 14.5$ meV (wavelength $\lambda = 2.38$ Å) by employing a double bounce pyrolytic graphite monochromator system. The first monochromator unit is flat and the second monochromator unit is vertically-focused. Two highly oriented pyrolytic graphite filters are mounted after each monochromator to reduce $\lambda/2$ contamination. The double monochromator system provides HB-1A with a very clean beam free of most higher-order contamination neutrons and an excellent signal-to-noise ratio. Typical energy resolution is ~ 1 meV with a PG002 analyzer. HB-1A is an excellent instrument for elastic neutron scattering studies of magnetic materials, particularly in cases where the signal is very weak and/or complex sample environments are required.

HB-1A has been in the user program since 2007 and during that time has produced a total of 204 publications. Although the instrument is capable of performing inelastic measurements (i.e. studying low-lying magnetic excitations up to ~ 9 meV using neutron energy loss [1] and high-temperature phonons up to ~ 35 meV using neutron energy gain [2, 3]), the majority of the experiments performed using HB-1A are elastic experiments for parametric studies of magnetic single crystals, thin films, and powders. Owing to the intense, clean beam and good signal-to-noise ratio, HB-1A is arguably the best instrument in ORNL's neutron scattering suite for measuring weak magnetic scattering.

HB-1A supports a full range of complex sample environments including high temperature furnaces (< 1773 K), cryostats with ultra-low temperature inserts (> 0.05 K), vertical field cryomagnets (< 8 T), pressure cells (< 2 GPa), and electric field sticks (< 3000 V). The instrument can accommodate single crystal samples with various dimensions ranging from < 1 mm up to 25 mm, polycrystalline samples, or thin films. HB-1A also offers great versatility for challenging experiments. For instance, the first uniaxial pressure study on small BaFe_2As_2 single crystals was carried out on HB-1A successfully [4].

As explained above, the typical experiment on HB-1A involves measuring a sample with a weak scattering signal, measuring the scattering of a sample under extreme conditions, or doing both simultaneously. This experimental program makes the instrument unique and extremely complementary to the suite of diffractometers and spectrometers available at the SNS and HFIR.

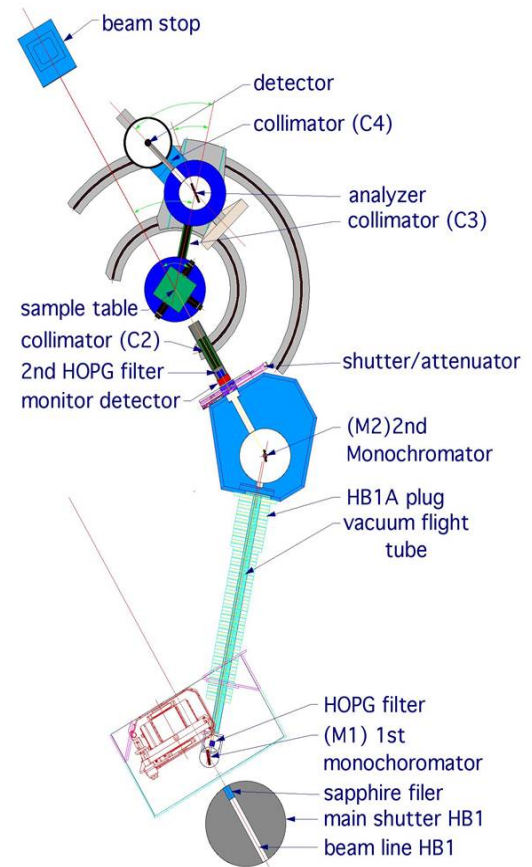


Figure 4.1. Schematic view of HB-1A. The instrument operates from a side port on HB-1.

4.2 TEAM STRUCTURE

HB-1A is managed by the Triple-Axis Spectroscopy Team in the Spectroscopy Group of the Neutron Scattering Division. Staff instrument scientists Adam Aczel (1 FTE) and Wei Tian (1 FTE) contribute a total of 2 FTEs with scientific associate Shirley Xu contributing 0.5 FTE to the effort. The computational instrument scientist providing software support for HB-1A is Andrei Savici.



Figure 4.2. HB-1A team, from Left: Wei Tian, Adam Aczel and Shirley Xu.

4.3 SCIENTIFIC FOCUS AND PUBLICATIONS

The primary focus of HB-1A is to study magnetic transitions in strongly correlated electron materials. Other topics that are pursued much less frequently include structural phase transition and phonon investigations. From CY17 – CY19, 101 general user proposals were submitted to HB-1A and 66 general user experiments ran on the beamline. Note that only one general user experiment ran in CY19 due to the long, unplanned HFIR outage and the uncertainty surrounding reactor restart in late CY19. In FY17 – FY19, 121 unique users performed experiments on the beamline and these efforts culminated in 56 publications from CY17 – CY19. 4 of these papers were published in ‘DOE high impact’ journals, and 9 of these papers were published in a journal with an impact factor > 7.

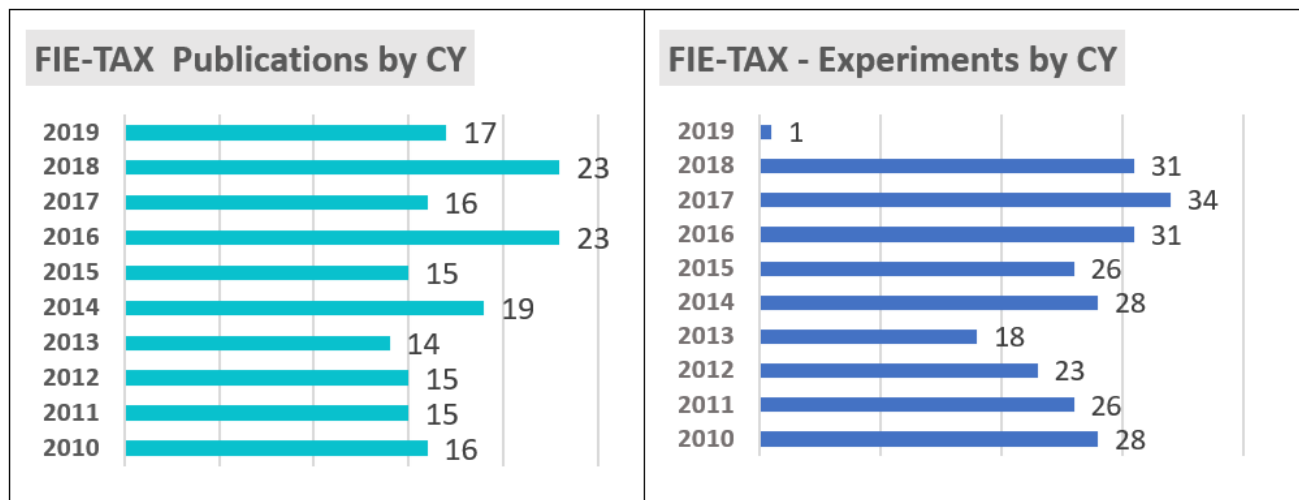


Figure 4.3. HB-1A publication statistics

4.4 SCIENTIFIC HIGHLIGHTS

Selected instrument highlights are presented here, which showcase the capabilities of HB-1A. Four highlights are provided, including one elastic neutron scattering study of a powder, one investigation of a thin film, and two measurements of single crystals.

Revisiting the Kitaev material candidacy of Ir⁴⁺ double perovskite iridates

A. A. Aczel, J. P. Clancy, Q. Chen, H. D. Zhou, D. Reig-i-Plessis, G. J. MacDougall, J. P. C. Ruff, M. H. Upton, Z. Islam, T. J. Williams, S. Calder, and J.-Q. Yan, *Physical Review B* 99, 134417 (2019)

Quantum magnets with significant bond-directional Ising interactions, so-called Kitaev materials, have attracted tremendous attention recently in the search for exotic spin liquid states. Motivated by the exciting work on the honeycomb lattice, one major theme in the field of heavy transition metal magnetism is to identify new Kitaev material candidates with other lattice geometries and characterize their properties. It has been pointed out previously that the face-centered-cubic sublattice is one geometry where the nearest-neighbor Kitaev interaction is allowed by symmetry [5]. In this work, a comprehensive set of measurements was performed to investigate the crystal structures, Ir⁴⁺ single-ion properties, and magnetic ground states of the double perovskite iridates La₂BIrO₆ (B = Mg, Zn) and A₂CeIrO₆ (A = Ba, Sr) with a large nearest-neighbor distance >5 Å between Ir⁴⁺ ions. Neutron powder diffraction data from HB-2A revealed that Ba₂CeIrO₆ crystallizes in the cubic space group *Fm-3m*, while the other three systems are characterized by weak monoclinic structural distortions. Despite the variance in the non-cubic crystal field

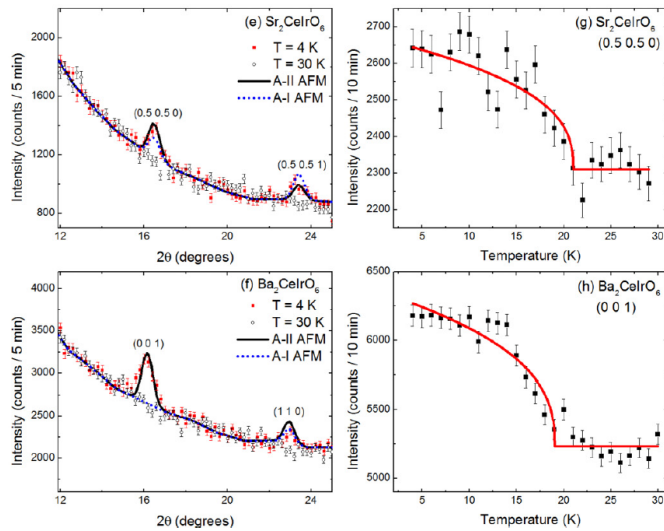


Figure 4.4. (a), (b) The HB-1A data collected at low scattering angles for Sr₂CeIrO₆ and Ba₂CeIrO₆. The solid and dotted curves represent magnetic refinements to models with A-I and A-II antiferromagnetic order, with the latter providing a superior fit in both cases. (c), (d) Order parameter scans of the strongest magnetic Bragg peak for each material, indicative of 21 K and 17 K transition temperatures respectively.

experienced by the Ir⁴⁺ ions in these materials, x-ray absorption spectroscopy and resonant inelastic x-ray scattering are consistent with $J_{\text{eff}} = \frac{1}{2}$ moments in all cases. Complementary HB-1A measurements identified magnetic Bragg peaks in these materials that were not observed with HB-2A. Magnetic refinements were performed by fixing the structural parameters obtained from HB-2A data at the same temperature, and the Ce sample results are shown in Figure 4.4(a) and (b). This analysis is indicative of a common A-type antiferromagnetic order for all four materials, where the moments lie in the plane perpendicular to the ferromagnetic plane stacking direction (i.e. A-II order instead of A-I order) [6]. These electronic and magnetic ground states are consistent with expectations for face-centered-cubic magnets with significant antiferromagnetic Kitaev exchange, which indicates that spacing magnetic ions far apart may be a promising design principle for uncovering additional Kitaev materials.

This work highlights the value of using HB-1A to measure magnetic Bragg peaks in polycrystalline samples with extremely weak scattering signals. As shown in Figure 4.4(c) and (d), the exceptional signal-to-noise of the instrument allowed order parameter scans identifying the magnetic transition temperatures to be performed also.

Spin canting and orbital order in spinel vanadate thin films

Christie J. Thompson, Dalmau Reig-i-Plessis, Lazar Kish, Adam A. Aczel, Biwen Zhang, Evguenia Karapetrova, Gregory J. MacDougall, and Christianne Beekman, *Physical Review Materials* 2, 104411 (2018)

The interplay between spin, lattice, and orbital degree of freedom is an enduring topic in condensed matter physics. The spinel vanadates are an exciting playground for exploring this phenomenon in detail. Previous studies of bulk CoV_2O_4 revealed a ferrimagnetic transition at 156 K, followed by a weak first-order structural transition at 90 K accompanied by a small canting of the V spins and the formation of an orbital glass state [7]. The lack of orbital order arises from the proximity of this material to a localized-itinerant crossover due to the short V-V distance. The primary aim of this work was to understand if the structural and magnetic properties of CoV_2O_4 could be tuned through the application of compressive strain. X-ray results revealed that the symmetry of the unit cell was lowered to orthorhombic from cubic at room temperature and magnetic susceptibility measurements show that this structure change has a drastic impact on the magnetic properties of the system. HB-1A was used to characterize the low-temperature ordered phases in a 300 nm thin film sample. The neutron scattering data shown in Figure 4.5(a) identify a ferrimagnetic transition as observed in the bulk with a similar $T_N = 153$ K, but the additional data presented in Figure 4.5(b) show that the nature of the 90 K transition is quite different. More specifically, there is a major spin reorientation of the Co spins away from the ferrimagnetic easy axis [001] to the [110] direction. Furthermore, the temperature-dependence of the (002) magnetic Bragg peak (not shown here) indicates that the V spins cant away from this direction with extracted perpendicular moments providing evidence of a larger canting angle compared to bulk. These results indicate that compressive strain pushes CoV_2O_4 deeper into the insulating state, away from the localized-itinerant crossover regime. This work highlights the value of HB-1A for measuring magnetic Bragg peaks in thin film samples.

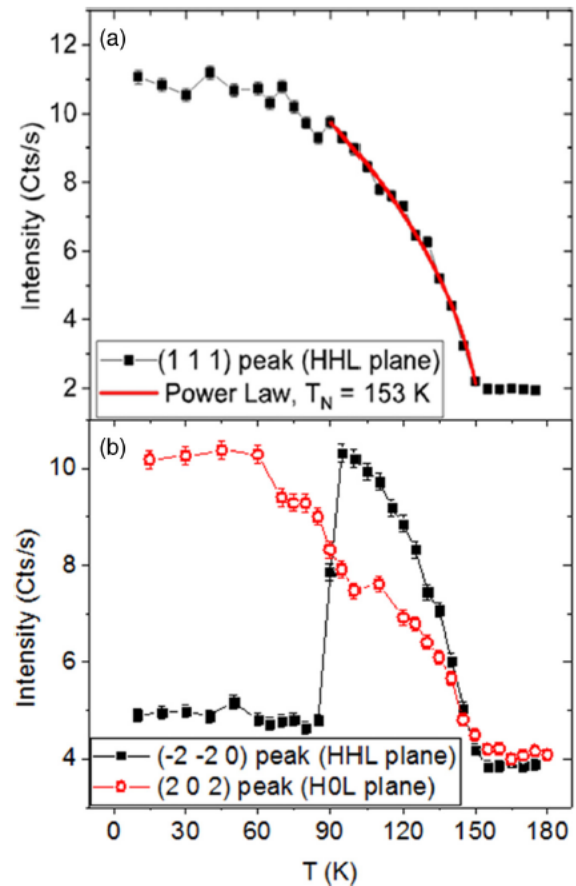


Figure 4.5. Elastic neutron scattering measurement of a 300 nm thin film of CoV_2O_4 . (a) (111) Bragg peak intensity as a function of temperature. The red curve is a power-law fit. (b) (-2-20) and (202) Bragg peak intensities as a function of temperature.

Destabilization of magnetic order in a dilute Kitaev spin liquid candidate

P. Lampen-Kelley, A. Banerjee, A. A. Aczel, H. B. Cao, M. B. Stone, C. A. Bridges, J.-Q. Yan, S. E. Nagler, and D. Mandrus, *Physical Review Letters* 119, 237203 (2017)

The insulating honeycomb magnet α - RuCl_3 with $J_{\text{eff}} = \frac{1}{2}$ magnetic moments exhibits fractionalized excitations that signal its proximity to a Kitaev quantum spin liquid state [8, 9]. However, at low temperatures fragile long-range magnetic order arises from non-Kitaev terms in the Hamiltonian. Spin vacancies in the form of Ir^{3+} substituted for Ru are found to destabilize this long-range order. Elastic neutron scattering data from HB-1A on doped single crystals (masses on the order 10 mgs), combined with bulk characterization measurements, showed that the magnetic ordering temperature of $\text{Ru}_{1-x}\text{Ir}_x\text{Cl}_3$ is suppressed with increasing x , and evidence of zigzag magnetic order is absent for $x > 0.3$. The HB-1A results are summarized in Figure 4.6. Complementary inelastic neutron scattering demonstrated that the signature of fractionalized excitations is maintained over the full range of x investigated. The depleted lattice without magnetic order thus hosts a spin-liquid-like ground state that may indicate the relevance of Kitaev physics in the magnetically dilute limit of RuCl_3 . This work highlights the value of HB-1A for measuring magnetic Bragg peaks in small single crystals with weak magnetic moments.

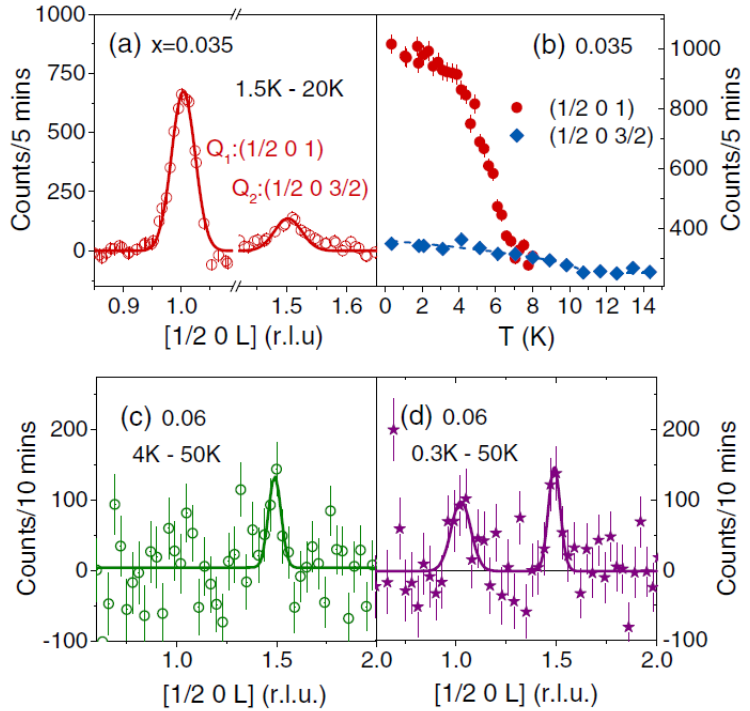


Figure 4.6. Scan at 1.5 K collected at HB-1A along the $[1/2 0 L]$ direction through characteristic magnetic reflections $Q_1 = (1/2 0 1)$ and $Q_2 = (1/2 0 3/2)$ for a 50 mg single crystal with $x = 0.035$. 20 K ($T > T_N$) data are subtracted as background. (b) Temperature scans of the scattering intensity at Q_1 and Q_2 . Scans along $[1/2 0 L]$ at (c) 4 K and (d) 0.3 K in a 20 mg single crystal with $x = 0.06$. 50 K data are subtracted as a background

Novel strongly spin-orbit coupled quantum dimer magnet: $\text{Yb}_2\text{Si}_2\text{O}_7$

Gavin Hester, H. S. Nair, T. Reeder, D. R. Yahne, T. N. DeLazzer, L. Berges, D. Ziat, J. R. Neilson, A. A. Aczel, G. Sala, J. A. Quilliam, and K. A. Ross, *Physical Review Letters* 123, 027201 (2019)

The quantum dimer magnet (QDM) is the canonical example of quantum magnetism. The QDM state consists of entangled nearest-neighbor spin dimers and often exhibits a field-induced triplon Bose-Einstein condensate (BEC) phase. This work shows that $\text{Yb}_2\text{Si}_2\text{O}_7$ is a new QDM in the strongly spin-orbit limit. Single crystal neutron scattering measurements from HB-1A, combined with specific heat and ultrasound velocity measurements, reveal a gapped singlet ground state at zero field and a field-induced magnetically ordered phase reminiscent of a BEC state, with exceptionally low critical fields of $H_{c1} \sim 0.4$

and $H_{c2} \sim 1.4$ T. Complementary inelastic neutron scattering in an applied magnetic field identify a Goldstone mode that persists throughout the entire field-induced magnetically ordered phase, indicative of the spontaneous breaking of U(1) symmetry expected for a triplon BEC. However, in contrast to other well-known cases of this phase, the high-field ($\mu_0 H \geq 1.2$ T) part of the phase diagram in $\text{Yb}_2\text{Si}_2\text{O}_7$ is interrupted by an unusual regime signaled by a change in the field dependence of the ultrasound velocity and magnetization, as well as the disappearance of a sharp anomaly in the specific heat. These measurements raise the question of how anisotropy in strongly spin-orbit coupled materials modifies the field induced phases of QDMs. This highlights the value of HB-1A for performing parametric studies of magnetism in single crystals.

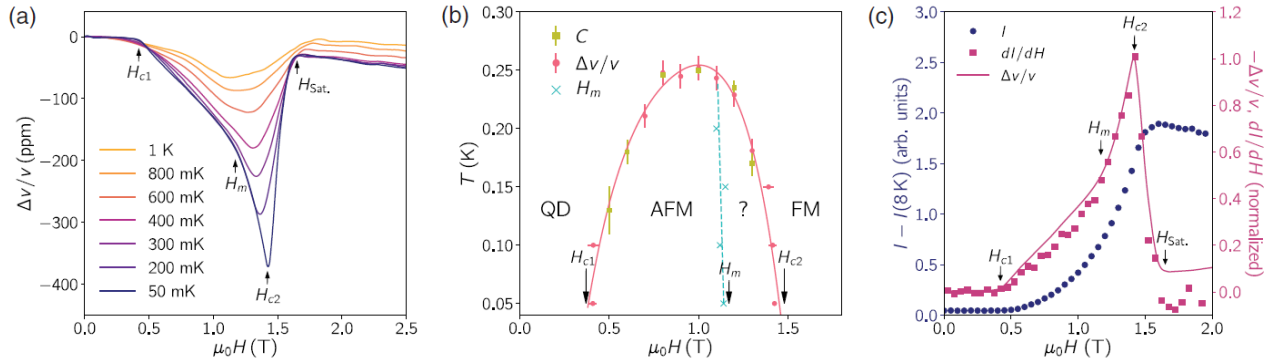


Figure 4.7. (a) Ultrasound velocity with longitudinally polarized sound waves along the c -axis. (b) H vs T phase diagram for $\text{Yb}_2\text{Si}_2\text{O}_7$ with the points on the phase diagram determined by ultrasound velocity (pink circles and blue crosses), and specific heat (yellow squares). The field was applied along the c -axis (specific heat) and c^* axis (ultrasound). (c) Evolution of the (200) magnetic Bragg peak intensity (blue) vs field, $I(H)$, which is proportional to the square of the net magnetization. Additionally, the derivative of the (200) magnetic Bragg peak intensity (square symbols) and the inverse of the ultrasound velocity data (solid line) are superimposed, showing excellent agreement between the two measurements.

4.5 GENERAL USER PROGRAM

HB-1A is most beneficial to the condensed matter and materials science communities. The instrument is recognized by the user community as an ideal place for measuring weak scattering and performing parametric studies covering a wide range of sample environments. The current user community consists of both domestic and international users; about 50% of the users have affiliations with US academic institutions. 75% of HB-1A beamtime is allocated to general user proposals, while the remaining 25% is allocated to discretionary time proposals. The number of unique users at HB-1A has increased over the years, with the obvious exception of FY19 due to the unplanned HFIR outage. There has been an average number of 44 unique users each year since FY10 and members of 22 different institutions used the beamline in FY18.

4.6 UPDATE ON INSTRUMENT IMPROVEMENT PROJECT

An upgrade to the double bounce monochromator system of HB-1A was completed in Nov. 2019, which relocated the vertical focal position of the beam to the desired location at the sample table. This upgrade enhances the flux on sample by a factor of three, while preserving a sizable beam with a $\sim 1''$ height. The backend upgrade is now underway, with appropriate funding and engineering support assigned to the project. This upgrade will involve the installation of a new PG002 analyzer, a new He-3 detector, and appropriate shielding with dimensions that are better matched to the current scattered

beam profile. These modifications will also help to facilitate polarized beam experiments. Finally, a new sample table is being considered that will accommodate a four circle goniometer option for measuring out-of-plane scattering down to 4 K, enable +/- 2 degrees tilting of MAG-E, and facilitate vertical sample translation to ensure that small single crystals can be centered in the beam. An area detector option at the analyzer position is also being considered. This project will improve HB-1A by enhancing its signal-to-noise ratio for the traditional analyzer experiments and improving its flexibility by making complementary diffraction experiments feasible. These upgrades will ensure that HB-1A is a world-leading instrument in elastic neutron scattering and diffraction studies of quantum materials for years to come.

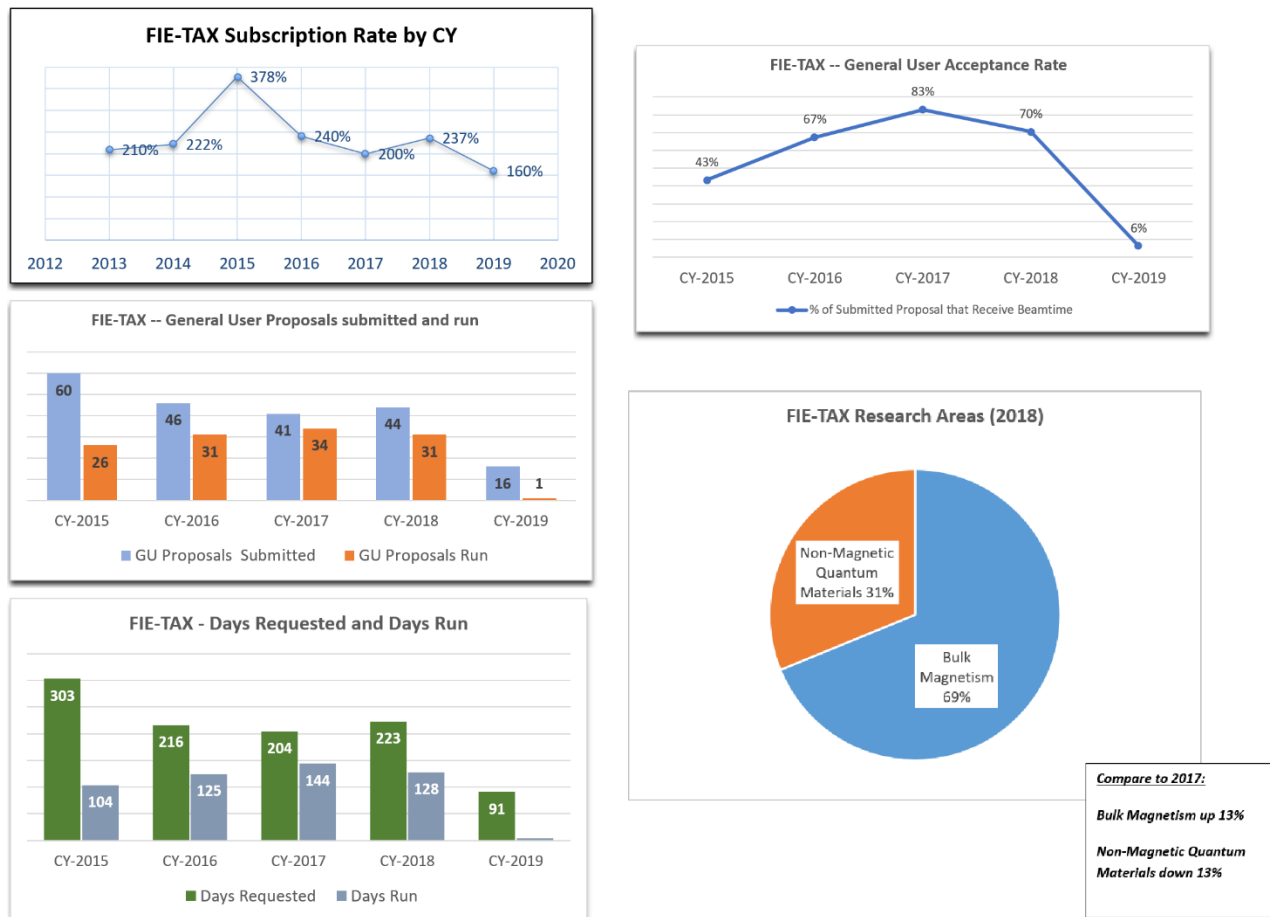


Figure 4.8. HB-1A user program statistics

4.7 SAMPLE ENVIRONMENT

Sample environments are vital to the science performed using HB-1A. This instrument currently supports most of the sample environments available at HFIR, with the small-angle horizontal field magnet that runs primarily on GP-SANS as one notable exception. HB-1A routinely runs bottom-loading closed cycle refrigerators, top-loading closed cycle refrigerators, cryostats, and vertical field cryomagnets. There are three cryomagnets that are available to run on the instrument, including MAG-B (5 T), MAG-E (8 T) and the new MAG-I (6 T). The cryostats and cryomagnets can accommodate both He-3 and dilution fridge inserts. Pressure cells (both gas and clamp cells), electric field sticks, and furnaces also run on the instrument, although they are not used often.

Two new cryomagnets are highly desirable for HB-1A. The first magnet is essentially a clone of the new MAG-I. This capability is required to address severe oversubscription issues already identified in the 2020-B proposal call and rooted in the ability of this magnet to run on seven different beamlines at HFIR (HB-1, HB-1A, HB-3, CTAX, WAND², and DEMAND). A new wide-angle horizontal field magnet for HB-1A (and the other triple axis instruments) is highly desired, as this capability will significantly increase the number of high-impact experiments that can be performed on this instrument. This magnet will likely have a maximum field of 4 T and a four-pole geometry to minimize stray fields.

The liquid helium autofill (LHeAF) system that was developed at ORNL was recently tested at HB-1A with a cryostat. This system works remarkably well and reduces both sample environment manpower requirements and instrument downtime. There are currently plans in place to expand this capability to most cryostats and cryomagnets at HFIR and to implement it at several instruments in the beam room using a multi-point LHeAF system. Development efforts towards these goals are underway.

A few new cryostat sample-sticks have been built for HB-1A, including one that allows >90° in-situ sample rotation and a second one that allows the user to switch between two single crystal samples in-situ. These sticks have both been built and the rotation stick was already commissioned and run on CTAX for a general user experiment. The two-sample single crystal changer will be commissioned soon. Finally, there are plans to buy a uniaxial pressure stick designed and built by a group Rice University that enables in-situ pressure changes. The flat plate samples that are ideal for this cell are compatible with the instrument geometry and don't pose the same alignment problems that arise in clamp cell experiments on HB-1A.

4.8 SOFTWARE

SPICE (Spectrometer Instrument Control Environment) is used to control the HB-1A spectrometer. SPICE is easy to use and very user friendly. The data files can be downloaded via oncat.ornl.gov and plotted in the user's software of choice. Graffiti is legacy software that enables quick data visualization, both at the instrument as part of SPICE or remotely as a standalone software package. Unfortunately, Graffiti is no longer supported by ORNL and therefore a replacement is needed. The Research and Software Engineering Group is aware of this request, but an action plan has not been developed yet.

Other legacy software available for the instrument includes Rescal for resolution calculations and Reslib for performing resolution convolution with a model. However, these tools have not been properly updated in several years and therefore their functionalities should be incorporated in the replacement for Graffiti, preferably using a user-friendly GUI. Other important features that should be incorporated in the new triple axis software package include the ability to implement Lorentz corrections, absorption corrections, and extinction corrections, so performing crystal and magnetic structure refinements with HB-1A data becomes more routine. More generally, we also require the ability to correct for lambda/n contamination of the beam monitor, to correct the resolution volume for constant-Ei inelastic neutron scattering measurements, and to easily manipulate multiple scans simultaneously.

4.9 UPDATE ON IMPACT OF DISCRETIONARY BEAMTIME

Discretionary beamtime now comes in two flavors: one is allocated by the science initiatives while the other one is allocated by the team management. Each type accounts for 12.5% of instrument operations. NScD staff compete for the science initiative time through proposal calls that are concurrent with the

general user calls and beamtime is awarded based on merit after an internal review process. The timing of these proposal calls also enables approved science initiative experiments to be block-scheduled with general user experiments, which ensures that complex sample environments are available. The remaining discretionary time is awarded on an as-needed basis and is used by the instrument team to build collaborations, to attract new users, to test new instrument capabilities, to further their own science programs, to fill in unexpected schedule gaps, or for local graduate student or postdoc development.

4.10 OUTREACH AND EXPANSION ACTIVITIES

In 2018, HB-1A participated in the National School on Neutron and X-ray Scattering (<http://neutrons.ornl.gov/nxs>), and hosted students for hands-on experiments and data analysis. Many HB-1A users are graduate students from US universities and therefore this instrument plays a key role in training new neutron scattering users. In fact, HB-1A data has contributed to 8 Ph.D. theses from US graduate students between CY17 - CY19.

The Quantum Materials Initiative also runs an annual workshop for young investigators at North American universities and national labs interested in performing neutron scattering research at ORNL. This workshop series is organized by Adam Aczel and Stuart Calder. HB-1A features prominently in this workshop series because most of the experiments on this instrument investigate quantum materials. One typical goal of this workshop series is to work with early career scientists to define the compelling scientific questions in quantum materials research driving the development of a successful three source strategy for the Neutron Sciences Directorate at ORNL. This workshop series also offers a forum for NScD to understand the young investigators' current and projected scientific needs in neutron scattering. Other important goals of this workshop series are to foster collaborations between ORNL scientists and the research groups of the external PIs, to provide them with an update on the current state of ORNL's neutron scattering user program, and to solicit their feedback on future instrument priorities and capabilities.

4.11 VISION

Near-term Vision (1-3 years)

Our near-term vision for HB-1A is to ensure that it becomes a world-leading instrument for single crystal, thin film, and powder studies of weak elastic scattering signals using a wide range of sample environments. The hallmarks of this instrument are its high flux combined with its excellent signal-to-noise ratio. These characteristics make HB-1A complementary to other diffractometers and spectrometers in ORNL's instrument suite. The backend upgrade that will be completed in 2021 will ensure that HB-1A is optimized for its main mission, and it is expected that this upgrade will enable HB-1A to reach its full potential and achieve maximum productivity.

Strategic Vision (3-10 years) and Alignment with NScD/ORNL Strategic Plans

Our strategic vision for HB-1A is to ensure that it continues operating as a world-leading instrument for single crystal, thin film, and powder studies of weak elastic scattering signals using a wide range of sample environments. We also anticipate expanding the instrument capabilities to include a polarized beam for

facilitating single axis, XYZ, and spherical neutron polarimetry experiments. This longer-term vision will be achieved by making continuous investments in new sample environments, including a wide-angle horizontal field magnet. New capabilities will also be added to the instrument, including an area detector option for diffraction experiments and a four-circle sample table option to enable measurements of Bragg peaks out of the horizontal scattering plane down to 4 K. The polarized beam option will be implemented using a combination of two He-3 drop-in cells or a He-3 drop-in cell in the incident beam and a Heusler analyzer. Finally, a new triple axis software package will be developed in close collaboration with the Research and Software Engineering group to enable user-friendly experiment planning, data reduction, data visualization, and resolution convolution with models.

4.12 FUNDING / RESOURCE NEEDS

Internal funding has been allocated through NSCD's 'Scientific Productivity' program to re-build the analyzer-detector assembly of HB-1A. As part of this upgrade, a new He-3 detector, a new analyzer, and associated shielding will be installed that are properly matched to the scattered beam profile to ensure an optimal signal-to-noise ratio for the instrument. The instrument team is currently preparing a request to expand the scope of the backend upgrade project. This request includes the following items:

- (1) A new sample table. The justification for this item is to enable vertical translation of small single crystals to ensure that they are centered in the beam, to enable +/- 2 degrees tilting of MAG-E, and to ensure compatibility with a four-circle option that will enable measurements of Bragg peaks out of the horizontal scattering plane down to 4 K. An unused four-circle goniometer has been located at HFIR and reserved for HB-1A.
- (2) An area detector option for diffraction experiments. This option will improve the flexibility of the instrument and enable measurements of larger crystals in 'diffraction' mode. The analyzer-detector re-build will ensure that this capability can be added at any time. The area detector will have a similar footprint to the new analyzer, so changing between the two options should be quite straightforward.

Longer term funding needs are associated with a polarized beam and new sample environments. The fully polarized beam will involve two He-3 drop-in cells or a He-3 drop-in cell in the incident beam and a Heusler analyzer. The latter set-up has been tested at HB-1 using a wavelength like the value of 2.38 Å available at HB-1A and it has been demonstrated that a flipping ratio of 15 or higher can be achieved. A polarized beam will help to facilitate single axis polarization, XYZ polarization, and possibly spherical neutron polarimetry experiments on the instrument. The major sample environment investment required is funding for a wide-angle horizontal field magnet, which will need to be purchased with 'scientific productivity' funds.

Additional longer-term funding will be required for a new alignment station at HFIR to replace the existing CG-1B instrument during the cold guide hall re-optimization scheduled to take place during the next Be outage in 2024-25. The scientific program at HB-1A depends critically on the ability to align single crystal and thin film samples in advance of the experiments. In principle, sample alignments can be completed on the instrument itself, but this has become much more difficult and tedious now that sample environments are routinely block-scheduled. It is important for the new alignment station to have a significantly higher flux than CG-1B, which has about 30x less flux than HB-1A. For small single crystals that cannot be aligned on CG-1B, the only recourse is to perform these sample alignments on HB-1A. This is arguably an inefficient use of HB-1A beamtime and instrument team resources.

Since the last Spectroscopy Suite Review in 2017, the HB-1A instrument team has expanded from 1.5 FTE instrument scientists to 2 FTEs. The team still includes a scientific associate who is shared with HB-1. This

staffing level is appropriate for the high throughput experiments run on the instrument. Although the other triple axis instruments have an instrument scientist staffing level of 1.66 FTEs, it is important to note that they run primarily inelastic scattering experiments with less frequent sample changes. The thermal triple axis instruments HB-1 and HB-3 also run fewer complex sample environments.

4.13 FUTURE FUNDING OPPORTUNITIES

In addition to seeking internally funded instrument upgrades, the HB-1A instrument team is actively pursuing and committed to both, partnering with others and leading funding proposals to advance the strategic science mission of the instrument. Future opportunities within ORNL (LDRD, mid-scale investment, scientific productivity) will be pursued as appropriate.

4.14 SELF-ASSESSMENT

Strengths

HB-1A offers an intense, clean beam and an excellent signal-to-noise ratio. HB-1A is particularly useful for investigating materials with weak scattering signals using a wide range of sample environments.

Weaknesses (Limitations)

- 1) HB-1A doesn't have its own beam tube, so the wavelength is fixed at $\lambda = 2.38 \text{ \AA}$. This constraint limits the instrument's capability to perform inelastic scattering experiments.
- 2) The space at the beamline is very limited, so this puts severe constraints on instrument upgrades and new capability developments.
- 3) Data collection is confined to the horizontal scattering plane, which means that significant sample alignment effort is required to set up an experiment in some cases. This scattering geometry, coupled with the lack of a wide-angle horizontal field magnet, limits the instrument's ability to investigate field-induced phenomena in quantum materials.
- 4) Data reduction, visualization, and analysis tools provided by ORNL or the user community are old and not maintained. A triple axis software package to replace Graffiti that also includes the functionalities of the user community packages (i.e. Rescal, Reslib) is highly desired.

Opportunities

The ongoing backend upgrade is an excellent opportunity to make HB-1A a world-class instrument for studies of weak scattering signals in quantum materials and beyond. The flexibility of the instrument can

also be significantly enhanced by adding an area detector option at the analyzer position for diffraction experiments, a four-circle option at the sample position for increased reciprocal space coverage down to 4 K, and the development of a polarized beam with full polarization analysis capability. The procurement of a wide-angle horizontal field magnet would also enable a completely new class of experiments on the instrument.

Threats

One possible threat to the instrument is a lack of future funding for new sample environments and capabilities. An additional threat is the inability of the directorate to maintain sufficient sample environment staffing to support all of the complex sample environment equipment that is so critical to HB-1A's science mission.

4.15 EXECUTIVE SUMMARY

HB-1A is a fixed-incident-energy triple-axis spectrometer that has been widely recognized by the condensed matter and materials science communities for its impressive instrument strengths, including high flux, a clean beam, an excellent signal-to-noise ratio, and compatibility with a large variety of sample environments. The instrument complements the current suite of diffractometers and spectrometers available at ORNL very well. HB-1A was a very productive instrument from CY17 – CY19, which culminated in 56 publications during this time. It is noteworthy that the number of publications remained nearly constant compared to the three-year period CY14 – CY16, despite the instrument not running for nearly a year due to the long, unplanned outage at HFIR spanning CY18 and CY19. The monochromator upgrade completed in Nov. 2019 has increased the flux at the sample position by a factor of 3, and the ongoing backend upgrade will further enhance the signal-to-noise ratio and improve the flexibility of the instrument. Moving forward, HB-1A will be known as a one-of-a-kind instrument continuously producing world-class science, which aligns well with the overall mission of NScD.

4.15.1 Comparison of instrument specifications to similar instruments worldwide

	HB-1A	BT7	PUMA	TAIPAN
Monochromator crystals	PG002 double monochromators with vertical focusing	Double focusing PG002, PG004, Cu220	Double focusing PG002, Cu220, Cu111, Ge311	Double focusing PG002, Cu200
Flux at sample (n cm⁻² s⁻¹)	4.2x10 ⁷ @ 14.5 meV	3.4x10 ⁷ @ 14.7 meV with PG002 vertically focused	1x10 ⁸ @ 14.7 meV with PG002 vertically focused 4.5x10 ⁸ with PG002 double-focused	2x10 ⁸ @ 50 meV with PG002 double-focused
Incident energy	14.5 meV fixed	5 to 500 meV	5 to 160 meV	5 to 70 meV (PG002) 14 to 200 meV (Cu200)
Scattering angles	-5° to 135°	-5 to 120°	-70° to 120°	-128° to 115°
Analyzer crystals	PG002, Be002, Si111	PG002 flat, horizontally focused, or configs with PSD	PG002 and Ge311	Double focusing PG002
Analyzer angles	-60° to 120°		-120° to 120°	-110° to 110°
Detector type	He-3 single detector	He-3 single detector, He-3 detector groups, or PSD	He-3 detector groups or PSD	He-3 single detector
He-3 Single Detector Dimensions	50 mm x 150 mm	50 mm x 150 mm	25 mm x 150 mm	25 mm x 100 mm or 50 mm x 100 mm
Beam Size (FWHM)	39 mm x 24 mm	38 mm x 50 mm	Dependent on mono configuration	Dependent on mono configuration
Polarized beam	None	He-3 polarizers	None	He-3 polarizers

Comparison of sample environment capabilities with similar instruments worldwide

	HB1A	BT7	PUMA	TAIPAN
Temperature range	0.05 K to 1773 K	0.05 K to 1873 K	0.05 K to 2200 K	0.05 K to 1873 K
Max magnetic field	8 T vertical field	15 T vertical field	12.5 T vertical field	12 T vertical field
Max pressure	2 GPa (CuBe clamp cell)	2.5 GPa (ZrO ₂ clamp cell)	10 GPa (Paris-Edinburgh cell)	10 GPa (Paris-Edinburgh cell)

Data and computing capabilities

	HB-1A	BT7	PUMA	TAIPAN
Data acquisition	SPICE	NICE	NICOS	SICS/Gumtree
Data visualization	Graffiti, DAVE	DAVE	NICOS	Graffiti
Data analysis packages	Matlab (Reslib)	Matlab (Reslib), DAVE	Python-based packages	Restrax
Data Modeling	Matlab (SpinW), FullProf	Matlab (SpinW), DAVE	Matlab (SpinW), Python-based packages	Matlab (SpinW), Restrax
Simulation and data correction tools	Matlab (Reslib)	Matlab (Reslib), DAVE	Takin	Restrax
Planning tools	Graffiti, DAVE, Matlab (Rescal)	DAVE, Matlab (Rescal, SpinW)	Takin, Matlab (SpinW)	Graffiti, Restrax, Matlab (SpinW)

4.16 REFERENCES

- [1] Tian W., Li J., Lynn J.W., Zarestky J.L., Vaknin D., Spin dynamics in the magnetoelectric effect compound LiCoPO₄, *Physical Review B*, **78**, 18, 184429 (2008).
- [2] Ma J., Delaire O., May A.F., Carlton C.E., McGuire M.A., VanBebber L.H., Abernathy D.L., Ehlers G., Hong T., Huq A., Tian W., Keppens V., Shao-Horn Y., Sales B.C., Glass-like phonon scattering from a spontaneous nanostructure in AgSbTe₂, *Nature Nanotechnology*, **8**, 445–451 (2013).
- [3] Cai L., Toulouse J., Luo H., Tian W., Anisotropic phonon coupling in the relaxor ferroelectric (Na_{1/2}Bi_{1/2})TiO₃ near its high-temperature phase transition, *Physical Review B*, **90**, 054118 (2014).
- [4] Dhital C., Yamani Z., Tian W., Zarestky J.L., Sefat A.S., Wang Z., Birgeneau R.J., Wilson S.D., Effect of uniaxial strain on the structural and magnetic phase transitions in BaFe₂As₂, *Physical Review Letters*, **108**, 087001 (2012).
- [5] Kimchi I. and Vishwanath A., Kitaev-Heisenberg models for iridates on the triangular, hyperkagome, kagome, fcc, and pyrochlore lattices, *Physical Review B*, **89**, 014414 (2014).
- [6] Cook A.M., Matern S., Hickey C., Aczel A.A., and Paramakanti A., Spin-orbit coupled $j_{\text{eff}} = 1/2$ iridium moments on the geometrically frustrated fcc lattice, *Physical Review B*, **92**, 020417 (2015).
- [7] Reig-i-Plessis D., Casavant D., Garlea V.O., Aczel A.A., Feyngenson M., Neuefeind J., Zhou H.D., Nagler S.E., and MacDougall G.J., Spin transition and orbital glass physics in near-itinerant CoV₂O₄, *Physical Review B*, **93**, 014437 (2016).
- [8] Banerjee A. *et al*, Proximate Kitaev quantum spin liquid behavior in a honeycomb magnet, *Nature Materials* **15**, 734 (2016).
- [9] Banerjee A., Yan, J.-Q., Knolle J., Bridges C.A., Stone M.B. Lumsden M.D., Mandrus D.G., Tennant D.A., Moessner R., and Nagler S.E., Neutron scattering in the proximate quantum spin liquid α -RuCl₃ *Science* **356**, 1055 (2017).

5. HFIR CG4-C COLD NEUTRON TRIPLE-AXIS SPECTROMETER BEAMLINER STATUS AND PLANNING SUMMARY

5.1 OVERVIEW/CURRENT STATUS

The cold neutron triple-axis (CTAX) instrument is a conventional triple-axis spectrometer with variable incident energy from a cold moderator and variable sample-analyzer distances. The Cold Guide 4 bender and guide hall shielding reduce background levels at CTAX, and the 15-cm-tall guide profile is well exploited by CTAX's vertically focusing monochromator (PG 002). To enhance accommodation of strong magnetic fields at the sample position and simplify future polarization analysis, the amount of ferromagnetic material has been minimized in the construction of this instrument.



CTAX is currently an instrument in the user program, active since 2012. It is a collaboration of the Neutron Sciences Directorate at Oak Ridge National Laboratory and the University of Tokyo, as part of the US-Japan Cooperative Program on Neutron Scattering. The scientific communities that use the CTAX instrument include condensed matter physics and materials science. Typical applications of this instrument include studies of nuclear and magnetic structures, quasi-elastic scattering, and lattice and magnetic dynamics in a variety of materials, including superconductors, transition metal oxides, multiferroics, thermoelectric materials, and low-dimensional quantum magnets. CTAX enables better analysis of low-energy excitations in materials.

The instrument backend was upgraded in 2015. A vertical translation system for the Be/BeO filters was successfully implemented. A 9-blade PG analyzer with variable horizontally focusing capability was successfully installed. Tests performed after the upgrade confirmed that the detector counting rate was increased by a factor of 3-4 for certain materials where the horizontally focusing condition can be implemented, with no measurable increase in instrument background.

Team Structure

CG4-C is part of the Triple-Axis team of the NSD Spectroscopy group. The instrument team consists of the staff Instrument Scientists Jaime Fernandez-Baca (0.33 FTE), Tao Hong (1.00 FTE) and Travis Williams (0.33 FTE), as well as Scientific Associate Mike Cox (0.5 FTE). The computational instrument scientist providing software support for CG4-C is Andrei Savici.

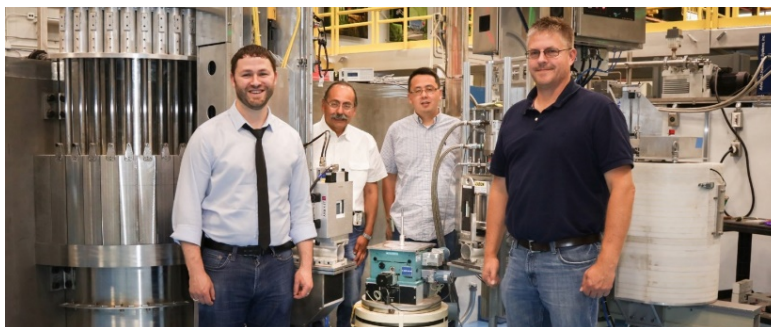


Figure 5.1. Instrument team members (left to right): Travis Williams, Jaime Fernandez-Baca, Tao Hong, and Mike Cox.

5.2 SCIENTIFIC FOCUS

Since 2017, 69 general user proposals were submitted to the CG4-C instrument, of which 46 were selected to run as proposed, resulting in 90 unique users utilizing CG4-C and 35 papers published based on CG4-C data, 1 of which is in 'DOE high impact' journals, and 7 in journals with an impact factor > 7.

The following paragraphs summarize the results of selected science highlights, showcasing the diverse capabilities of the cold neutron triple-axis spectrometer. Examples presented include research on bulk single-crystal and thin film samples/on spin structure and dynamics/with complex sample environments such as a He-3 insert, an 11-T vertical-field and a 6-T horizontal-field cryomagnets.



Figure 5.2. CTAX publication statistics

5.3 SCIENTIFIC HIGHLIGHTS

Field-induced quasiparticle breakdown in a quantum antiferromagnet

Tao Hong, Y. Qiu, M. Matsumoto, D. A. Tennant, K. Coester, K. P. Schmidt, F. F. Awwadi, M. M. Turnbull, H. Agrawal & A. L. Chernyshev, *Nature Communications* 8, 15148 (2017)

Quasiparticles, such as phonons and magnons, have become a fundamental concept in condensed matter physics for interacting many-body systems. However, quasiparticles can break down spectacularly in rare conditions. To date, the phenomenon of the field-induced spontaneous magnon decay in ordered antiferromagnets is much less mature experimentally. A neutron scattering study using the 11-T vertical-field cryomagnet uncovered the field-induced magnon decay and renormalization of magnon dispersion in the single crystal form of an $S=1/2$ coupled two-leg ladders antiferromagnet $C_9D_{18}N_2CuBr_4$. The sample was cooled down to 250 mK and an external magnetic field was applied up to 10.8 Tesla. In combination with linear spin-wave theory calculations, the observed magnon instability at finite fields was shown to originate from the strongly repulsive interaction between the single-magnon state and the two-magnon continuum. This work provides much-needed experimental insight to the understanding of the quantum many-body effects.

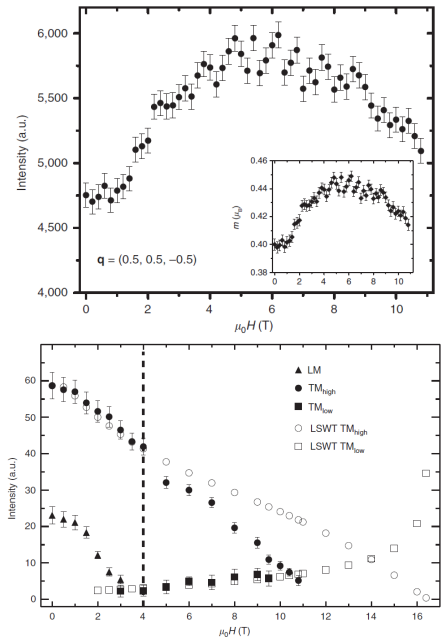


Figure 5.3. Top: Background-subtracted peak intensity as a function of field at $q=(0.5,0.5,-0.5)$. Inset: the size of the staggered moment as a function of field. Bottom: Evidence of spontaneous magnon decays at the magnetic zone center. Data were collected at $T=250$ mK.

Time dependence of the magnetic structure in a triangular lattice magnet $\text{Ca}_3\text{Co}_2\text{O}_6$

Kiyochiro Motoya, Takumi Kihara, Hiroyuki Nojiri, Yoshiya Uwatoko, Masaaki Matsuda, and Tao Hong, *Journal of the Physical Society of Japan* 87, 114703 (2018)

It is unexpected to observe the time dependence of the magnetic structure in a system without randomness or imperfections. $\text{Ca}_3\text{Co}_2\text{O}_6$ is one of the very few known examples. The time and magnetic field evolution of the magnetic structure were determined by single-crystal neutron diffraction measurements using the horizontal-field Mag-G with maximum allowable field of 6 Tesla. The observed long-period magnetic order is attributed to competition between the ferromagnetic intrachain and antiferromagnetic interchain interactions.

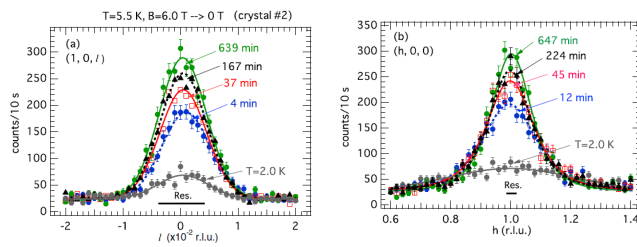


Figure 5.5. Neutron scattering patterns measured in zero field along (a) $(1, 0, l)$ and (b) $(h, 0, 0)$ at various elapsed times in $T=5.5$ K after removing the magnetic field of 6.0 T.

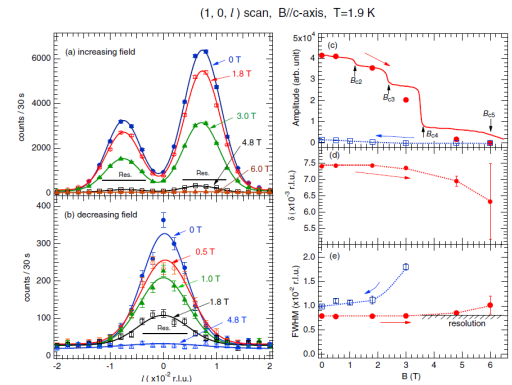


Figure 5.4. Magnetic field variations of neutron scattering intensity along the $(1, 0, l)$ at $T=1.9$ K in the (a) increasing, (b) decreasing field processes and of (c) the integrated amplitude, (d) the peak position δ , and (e) the width (FWHM).

Large spin-orbit torque efficiency enhanced by the magnetic structure of a collinear antiferromagnet in epitaxial IrMn thin films

Jing Zhou, Xiao Wang, Yaohua Liu, Jihang Yu, Huixia Fu, Liang Liu, Shaohai Chen, Jinyu Deng, Weinan Lin, Xinyu Shu, Heng Yau Yoong, Tao Hong, Masaaki Matsuda, Ping Yang, Stefan Adams, Binghai Yan, Xiufeng Han and Jingsheng Chen, *Science Advances* 5, eaau6696 (2019)

Antiferromagnetic materials hold numerous interesting features that are strongly preferred for future spintronic applications. It is notoriously challenging to underpin the atomic-scale spin structures of antiferromagnetic thin films, although they are crucial for functional properties, such as spin-transfer torque that provides a promising path for switching magnetization for energy-efficient magnetic memory. High-resolution neutron diffraction experiments have found that epitaxial $L1_0$ -IrMn thin films can host an unconventional spin structure at room temperature, which consists of twin domains with the spin axes orientating toward $[111]$ and $[-111]$, respectively, and thus causes a very large spin-orbit torque as observed in ferromagnetic resonance experiments. This work reveals the critical roles of spin structure on large spin-orbit torques generated by metallic antiferromagnets that hold great potential for future spintronics.

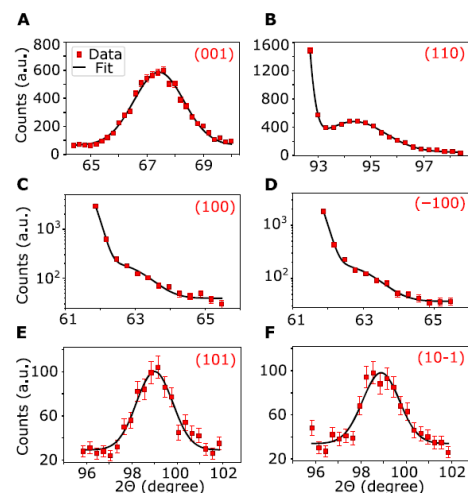


Figure 5.6. Neutron diffraction θ - 2θ scans for several nuclear and magnetic reflections in the epitaxial IrMn thin film. (A) (001). (B) (110). (C) (100). (D) (-100). (E) (101). (F) (10-1).

Novel excitations near quantum criticality in geometrically frustrated antiferromagnet CsFeCl₃

Shohei Hayashida, Masashige Matsumoto, Masato Hagihala, Nobuyuki Kurita, Hidekazu Tanaka, Shinichi Itoh, Tao Hong, Minoru Soda, Yoshiya Uwatoko and Takatsugu Masuda, *Science Advances* **5**, eaaw5639 (2019)

The investigation of materials that exhibit quantum phase transition provides valuable insights into fundamental problems in physics. The ground state of a triangular lattice antiferromagnet CsFeCl₃ is quantum disordered in the low-pressure phase and has a noncollinear magnetic structure in the high-pressure phase. The neutron excitation spectrum continuously evolves through the applied hydrostatic pressure: a single mode in the disordered state becomes soft with increasing pressure and it splits into gapless and gapped modes in the ordered state. Extended spin-wave theory reveals that the longitudinal and transverse fluctuations of spins are hybridized due to nature of the non-collinear ground state. This work is of primary importance to discover a novel quantum hybridized state and to advance the physics of the interplay between the geometrical frustration and the quantum criticality. The results were published in *Science Advances* **5**, eaaw5639 (2019).

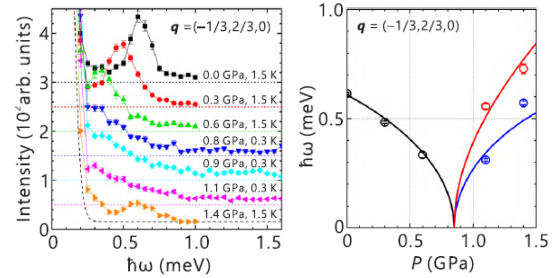


Figure 5.7. Left: Constant- q scans at $(-1/3, 2/3, 0)$ showing evolution of the gap energies as a function of applied hydrostatic pressure. The black dashed curve is a Gaussian function of the incoherent scattering at 1.4 GPa with the FWHM of 0.17 meV. Right: Pressure dependence of the excitation energies at $(-1/3, 2/3, 0)$ calculated by the extended spin-wave theory. Above 0.9 GPa, the blue and red curves are the excitations of gapless and gapped modes, respectively. The circles are peak energies obtained from the above constant- q scans.

5.4 GENERAL USER PROGRAM

CG4-C has proven to be an instrument with a solid user base. There are now active user groups performing experiments on the instrument in the research areas of condensed matter physics, energy materials, functional materials, and thin film heterostructures.

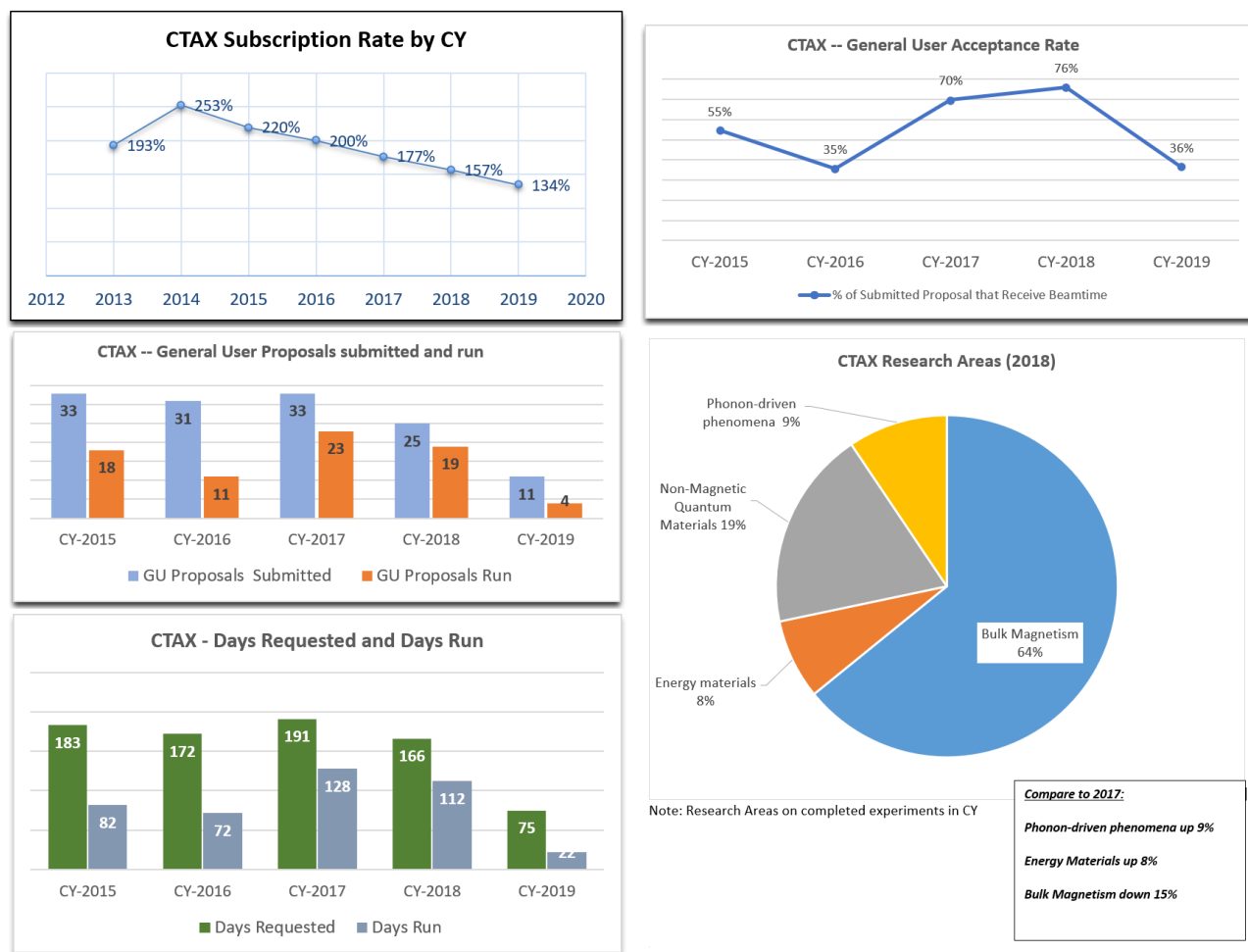


Figure 5.8. CTAX user program statistics

5.5 UPDATE ON INSTRUMENT DEVELOPMENT ACTIVITIES

The Neutron Science Directorate plans to build a next-generation cold-neutron multi-analyzer triple-axis spectrometer (MANTA) at CG1, HFIR with the installation coupled to the re-optimization of the HFIR cold guide hall in 2023 or 2024 during the Be reflector replacement.

5.6 SAMPLE ENVIRONMENT

The measurements can be performed at a variety of different temperatures (0.03-1800 K), vertical-

magnetic fields (0-8 T), horizontal-magnetic fields (0-6 T) and hydrostatic pressures up to 1.5 GPa.

5.7 SOFTWARE

The data acquisition software is SPICE. Graffiti has been used for the CG4-C data reduction and some analysis can be done on the computer cluster analysis.sns.gov. Various users have also developed their own software and scripts for analyzing and fitting CG4-C data.

5.8 UPDATE ON IMPACT OF DISCRETIONARY BEAMTIME

Discretionary beamtime is used to build collaborations, to attract new users and new research projects, to test new instrument capabilities, and further the science program of NScD staff. Half of the discretionary beamtime is allocated through ORNL Neutron Sciences sciences initiatives, with the majority of that time on CG4-C being given to proposals within the Quantum Materials initiative.

Outreach and Expansion Activities. CG4-C has participated in the National School on Neutron and X-ray Scattering (<http://neutrons.ornl.gov/nxs>) every other year for the past 6 years. This outreach effort is important to help grow a skilled user community.

Experiments on CG4-C have contributed to five Ph.D. theses from US Universities since 2012.

5.9 VISION

Near-term Vision (1-3 years)

Ensure CG4-C reaches its full potential by providing a stable, low background, cold neutron triple-axis spectrometer with reliable software to visualize and analyze data.

Strategic Vision (3-10 years) and Alignment with NScD/ORNL Strategic Plans

The Neutron Science Directorate plans to build a next-generation cold-neutron multi-analyzer triple-axis spectrometer (MANTA) at HFIR with the installation coupled to the re-optimization of the HFIR cold guide hall in 2023 or 2024 during the Be reflector replacement.

5.10 FUNDING/RESOURCE NEEDS

The next-generation cold-neutron multi-analyzer triple-axis spectrometer (MANTA) at CG1, HFIR has an estimated cost of ~\$10 M.

5.11 FUTURE FUNDING OPPORTUNITIES

In addition to advocating for internally funded instrument upgrades, the instrument team is actively seeking external funding for this project.

5.12 SELF-ASSESSMENT

Strengths

Neutron diffraction/inelastic neutron scattering measurements under variable sample environment conditions including T (4-1800 K), vertical H (0-8 T), horizontal H (0-6 T) and P (0-1.5 GPa). Instrument configurations with high energy-resolution (0.1 meV) and high q-resolution (0.01\AA^{-1}) can be achieved.

Weaknesses (Limitations)

- 1) Low neutron flux due to the misalignment of the CG4-C guide.
- 2) Low data collection efficiency due to the single He-3 detector.

Opportunities

The guides of HFIR cold guide hall is planned to be re-optimized in 2023 or 2024, at which time a new cold triple-axis instrument, MANTA, will be constructed to overcome the limitations listed above.

Threats

Lack of resources (funding), lack of added staff (second, 1.0 FTE instrument scientist), and the possible inability to retain staff.

5.13 EXECUTIVE SUMMARY

The productivity of the HFIR CG4-C cold neutron triple-axis spectrometer has been increasing markedly each of the past three years. Six of these papers were in journals with high impact factors (>7). CG4-C already supports a good diversity of sample environments, such as temperature, pressure and magnetic field.

5.13.1 Comparison of instrument specifications with similar instrument worldwide

	CG-4c	RITA II (PSI)	TASP (PSI)	SPINS (NIST)	MACS (NIST)
Velocity Selector	No	No	No	No	No
Avg. Flux ($n\text{ cm}^{-2}\text{ s}^{-1}$)	$5 \cdot 10^6$	$8 \cdot 10^6$	$5 \cdot 10^6$	$8 \cdot 10^6$	$5 \cdot 10^8$
Beam size	40mm (W)*30 mm (H)				40 mm(W)*20 mm(H)
Scattering angles	-15° to 115°	≤120°	≤125°	-4° to 120°	-120° to 120°
Incident energy	2.2 to 18 meV	2.5-20 meV	2.3-25 meV	2.4-14 meV	2.3-17 meV
Final energy	≥3.0 meV	≥2.5meV	≥2.5 meV	≥2.6 meV	≥2.5 meV
Analyzer	Fixed vertical and variable horizontally focusing	A flexible 9 blades analyzer	Fixed vertical and variable horizontally focusing	11 blades for either flat or variable horizontally focusing	20 fixed vertically focusing analyzers
Resolution	0.1-1 meV at elastic line	0.04-1 meV at elastic line	0.04-1 meV at elastic line	0.05-1 meV at elastic line	0.02-1.4 meV at elastic line
Detector type	Single He ³ detector	Position sensitive He ³ detector	Single He ³ detector	Single He ³ detector	Multi He ³ detector
No. of detectors	one	one	one	one	40
Polarized beam	No	No	Bender	Supper mirror	He ³ polarizer

5.13.2 Data and computing capabilities

	CG-4c
Data reduction	SPICE
Data visualization	SPICE/Graffiti
Data analysis packages	MATLAB
Data Modeling	SPINW

Simulation and data correction tools	
Planning tools	
Computing resources	Analysis.sns.gov

5.13.3 Comparison of sample environment capabilities with similar instruments worldwide

	CG-4c	RITA II (PSI)	TASP (PSI)	SPINS (NIST)	MACS (NIST)
Temperature range	0.05 to 1400 K	0.05 to 1400 K	0.05 to 1400 K	0.05 to 1400 K	0.05 to 1400 K
Max magnetic field	8 T	15 T	12 T	10 T	10 T
Max pressure	1.5 GPa	1.5 GPa	1.5 GPa	1.5 GPa	1.5 GPa

6. SNS BL-18, THE WIDE ANGULAR-RANGE CHOPPER SPECTROMETER (ARCS): BEAMLINE STATUS AND PLANNING SUMMARY DOCUMENT

6.1 OVERVIEW/CURRENT STATUS

The wide angular-range chopper spectrometer ARCS at the Spallation Neutron Source (SNS) BL-18 is optimized to provide a high neutron flux at the sample position with a large solid angle of detector coverage. This enables studies of various types of excitations in condensed matter systems, such as phonons or magnons, in both powder and single crystal samples.

Thermal and epithermal neutrons from the ambient temperature water moderator are transported to the sample by a tapered neutron guide system. A large, vertical axis T₀ chopper blocks the prompt pulse background radiation from the target as well as other neutron energies that may cause background in the spectrometer. A short pulse of neutrons of the desired incident energy is selected by a Fermi chopper, which may be chosen from two mounted on a translation table. The sample vacuum chamber accommodates a variety of sample environment equipment and also houses an oscillating radial collimator to reduce background. The collimator may be moved into place or removed via a motorized vertical lift. An array of 920 linear position-sensitive ³He detectors arranged in a 3m-radius cylindrical geometry is located in the detector vacuum chamber. To facilitate rapid changes of the sample and associated equipment, a curved gate valve can isolate the detectors from the sample position so that only the smaller volume needs to be vented. The gate valve is opened to allow a windowless path for the scattered neutrons to the detectors to reduce background. Data are collected by an event-based acquisition system, providing maximum flexibility for data analysis and filtering.

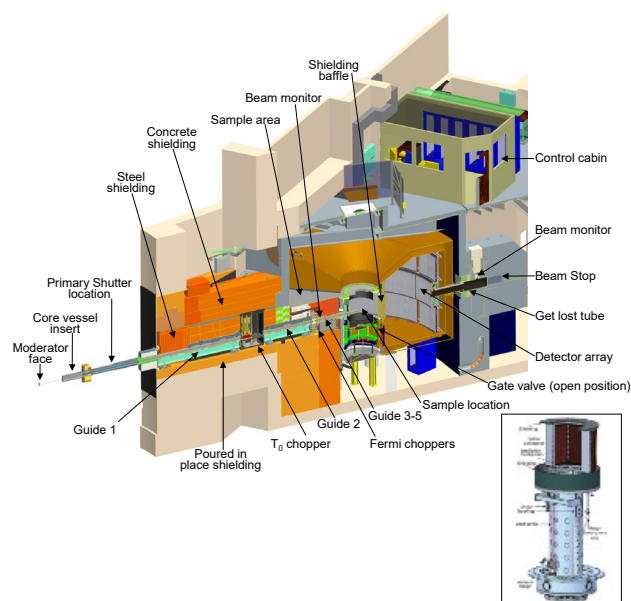


Figure 6.1. Schematic view of the ARCS layout. Inset: Radial collimator on lift

ARCS started first user experiments in 2008 after a successful Instrument Development Team (IDT) construction project funded by DOE (PI: Brent Fultz, Caltech). This engagement by active users provided valuable design input as well as early users and groups interested in technique development. The last IDT designated experiment ran at ARCS in 2016, and the IDT beam days transitioned to discretionary time managed by the Neutron Sciences Directorate. Since approximately 2012 ARCS has maintained a fairly steady publication rate of over 20 per year and averaged about 2.2 experiments per article. The over-subscription rate for ARCS is typically around 3, though the number of proposals submitted to ARCS more recently has decreased. This could be due to the maturation of the direct geometry instrument suite at the SNS. Proposals now go to the instrument best suited to their needs, so ARCS proposals are more directly aimed at using the high flux at moderate resolution with thermal and epithermal energies combined with the wide angular coverage. These numbers compare favorably to other inelastic

instruments at ORNL and other institutions and indicate that ARCS has a strong technical performance compared to equivalent instruments around the world.

A large majority of user experiments at ARCS continue to be accommodated by three sample environment capabilities: a bottom-loading closed-cycle refrigerator (CCR) with low background (5K – 300K/450K hot stage), a top-loading CCR (5K – 700K) and an ILL-style vacuum furnace (300K – 1500K(V)/1800K(Nb)). ARCS can accommodate low temperature options, e.g. Orange cryostats, and magnets but these sample requirements are not typically well matched to the energy resolution and range of ARCS. The Neutron ElectroStatic Levitator (NESL) runs routinely at ARCS and facilitates studies of the dynamics of containerless, super-cooled liquids. A variety of other options are available, from gas loading to pressure cells.

Software at ARCS is adequate but expected to undergo continuing improvements. The instrument switched to the current standard using CSS and EPICS in the spring of 2018. This provides new capabilities as well as brings all of the SNS direct geometry spectrometers to a common DAS system. Data is automatically reduced to a standard format (nxspe) that is compatible with traditional time-of-flight inelastic visualization and analysis software (Mslice, Horace). Often no other reduction is needed. A growing number of groups are using newer visualization and analysis tools available within Mantid which provide more statistically correct binning of single crystal data. Additional analysis to meaningful physical quantities, such as extracting the neutron-weighted phonon density-of-states with appropriate corrections, is provided by locally developed codes. Jupyter notebooks provide users with some guidance to combine multiple incident energies for DOS studies, for example. External user groups are also developing codes, for example to explore single crystal phonon dispersions with specialized background modeling and capabilities for combining data from multiple Brillouin zones.

Team Structure

Management responsibilities for ARCS lie in the Direct Geometry Spectroscopy Team in the Spectroscopy Group, Neutron Scattering Division (NSD). Neutron scattering scientists Doug Abernathy (1 FTE) and Garrett Granroth (1 FTE) are members of this team. The ARCS Scientific Associate (SA) is Rick Goyette (0.5 FTE) who also supports Corelli.

Additional SA support is provided by Victor Fanelli, the SEQUOIA SA, as needed. Current software support comes from the Direct Geometry Computational Instrument Scientist Andrei Savici. Previously, Andy Christianson and Arnab Banerjee served as neutron scattering scientists supporting ARCS, Lacy Jones provided SA support, and Jiao Lin provided embedded software support for data reduction, visualization, and analysis.



Figure 6.2. The ARCS instrument team. From left to right: Doug Abernathy (point-of-contact), Garrett Granroth (neutron scattering scientist), Rick Goyette (scientific associate) and Victor Fanelli (SEQUOIA SA). Not shown – Andrei Savici (computational instrument scientist).

Publications. In the calendar years of 2017 to 2019, there were a total of 61 publications and 8 theses utilizing ARCS. Of the journal publications, 19 have a journal impact factor greater than 7 and 10 are in the list of “DOE high impact” journals.

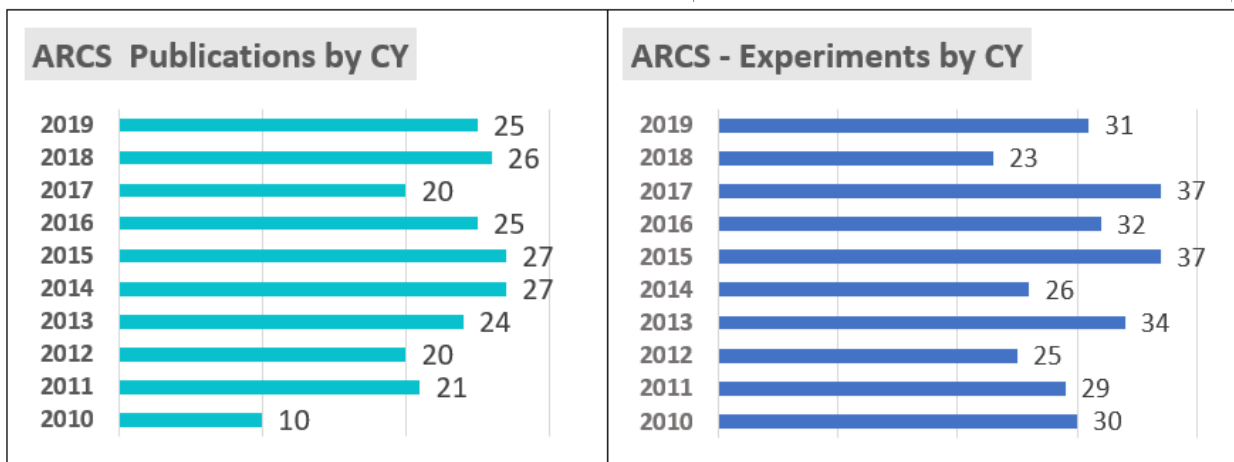
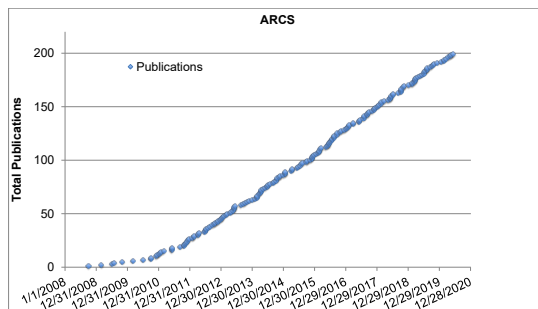


Figure 6.4. ARCS publication and experiment statistics

SCIENTIFIC FOCUS

ARCS provides a high flux with moderate energy resolution and a broad momentum coverage, which allows it to address an extensive list of scientific topics in dynamics of materials. In 2019 the topics identified in the Instrument Proposal Tracking System included Phonon-driven phenomena, Bulk magnetism, Energy materials, Superconductivity, Fluids, and Nanoscale/disordered materials. Experiments are roughly divided evenly between vibrational and magnetic spectroscopy, and also divide approximately evenly between single crystal and powder samples. The highlights included below are selected to demonstrate the range of topics studied at ARCS as well as the high impact of the results.

6.2 SCIENTIFIC HIGHLIGHTS

Beyond quasi-harmonic theory: Silicon anharmonicity and quantum effects

D. S. Kim, O. Hellman, J. Herriman, H. L. Smith, J. Y. Y. Lin, N. Shulumba, J. Niedziela, C. W. Li, D. L. Abernathy, B. Fultz, Proceedings of the National Academy of Sciences of the United States of America 115(9), 1992-1997 (2018)

Silicon has a peculiar negative thermal expansion at low temperature. This behavior has been understood with a “quasiharmonic” theory where low-energy phonons decrease in frequency with volume contraction. Inelastic neutron scattering measurements of phonon dispersions over a wide range of temperatures taken at ARCS (Kim, PNAS 2018) cast doubt upon quasiharmonic theory, which predicts the wrong sign for most phonon shifts with temperature.

A high-purity single crystal of silicon (mass ~ 28.5 g) was machined into a tube for optimal neutron scattering properties. The sample was rotated in a closed-cycle refrigerator and a furnace, and at each temperature the 4D $S(\mathbf{Q},E)$ data were reduced and multiphonon scattering was subtracted to give all phonon dispersions in the irreducible wedge of the first Brillouin zone (Figure 6.5). The multiphonon scattering produces a relatively smooth background between the phonon dispersions and was determined to produce the majority of the background intensity. The “folding” technique of summing all of the $S(\mathbf{Q},E)$ data (from >100 Brillouin zones) into an irreducible wedge increases the signal strength and suppresses polarization effects that alter intensities in some Brillouin zones. Data were analyzed to find the shift in individual phonon modes as a function of temperature.

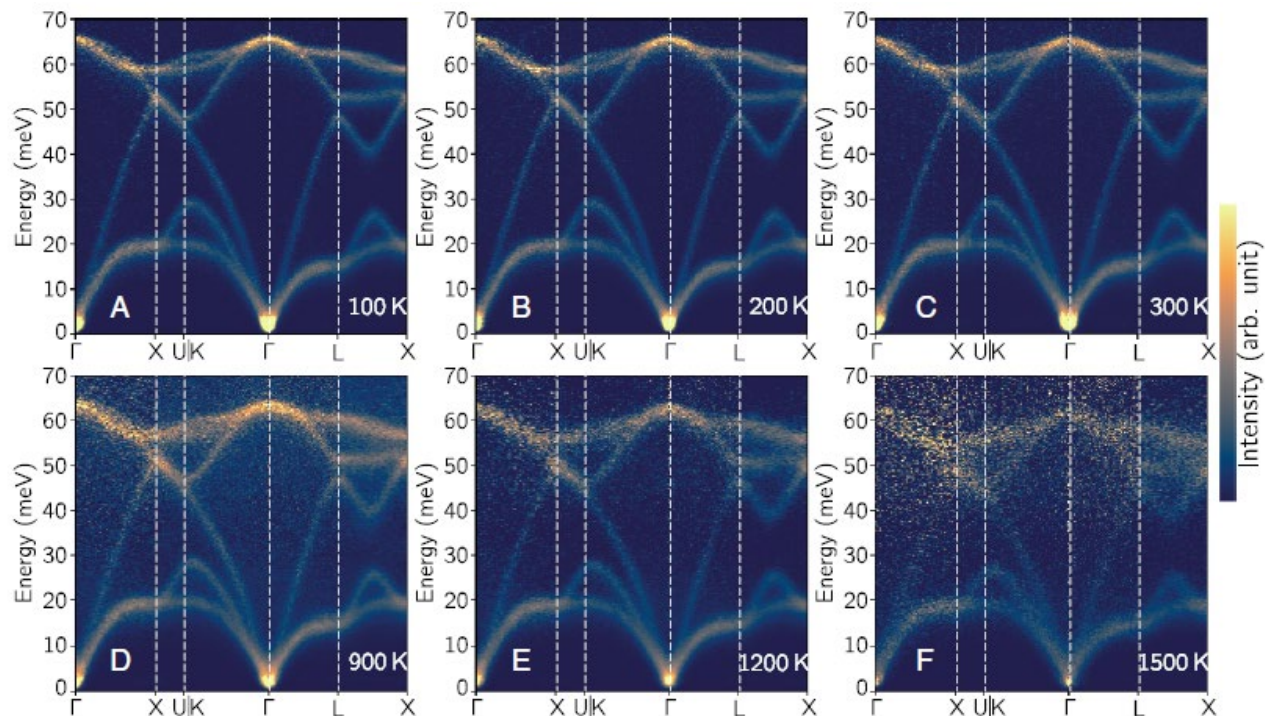


Figure 6.5. Experimental phonon dispersions of silicon. Inelastic neutron scattering data of silicon were measured on ARCS at (A) 100 K, (B) 200 K, (C) 300 K, (D) 900 K, (E) 1,200 K, and (F) 1,500 K. The 4D phonon dynamical structure factors, $S(\mathbf{Q},E)$, were reduced, multiphonon-subtracted, and “folded” into one irreducible wedge in the first Brillouin zone. Phonon dispersions are shown along high-symmetry lines and through the zone $L-X$.

To correctly predict the phonon shifts and thermal expansion, fully anharmonic *ab initio* calculations were required. The stochastically initialized temperature-dependent effective potential (s-TDEP) method samples and fits the phonon potential landscape and can accurately describe highly anharmonic systems. This includes higher-order contributions of the lattice dynamic Hamiltonian, which intrinsically includes the phonon–phonon interactions as well as nuclear quantum effects. Pure phonon anharmonicity, i.e., phonon–phonon interactions, dominate the phonons in silicon from low to high temperatures, altering the effective interatomic potential and causing both positive and negative shifts of phonon energies. At low temperatures, the zero-point quantum occupancies of high-energy vibrational modes alter the energies of low-energy modes through anharmonic coupling. This nuclear quantum effect with anharmonicity (and quasiharmonicity) is the essential cause of the negative thermal expansion of silicon. The crystal structure, anharmonicity, and nuclear quantum effects all play important roles in the thermal expansion of silicon.

Vibrational studies of ionic transport materials

J. Ding, J. Niedziela, D. Bansal, J. Wang, X. He, A. F. May, G. Ehlers, D. L. Abernathy, A. H. Said, A. Alatas, Y. Ren, G. Arya, O. Delaire, *Proc Natl Acad Sci USA* 117, 3930 (2020)

J. Niedziela, D. Bansal, A. F. May, J. Ding, T. Lanigan-Atkins, G. Ehlers, D. L. Abernathy, A. H. Said, O. Delaire, *Nature Physics* 15, 73 (2019)

T. Krauskopf, S. Mui, S. P. Culver, S. Ohno, O. Delaire, Y. Shao-Horn, W. G. Zeier, *Journal of the American Chemical Society* 140(43), 14464 (2018)

S. Mui, J. C. Bachman, L. Giordano, H. H. Chang, D. L. Abernathy, D. Bansal, O. Delaire, H. Satoshi, R. Kanno, F. Maglia, S. Lupart, P. Lamp, S. H. Yang, *Energy & Environmental Science* 11, 850 (2018)

Unveiling the unusual atomic dynamics in ionic conductors is critical for the design of energy conversion, storage and battery materials, for example to rationalize their thermal transport properties in thermoelectric applications or their fast ionic conductivity in solid-state electrolytes. ARCS provides efficient measurement of the phonon density of states and can contribute to fundamental understanding of how lattice dynamics influences ion transport.

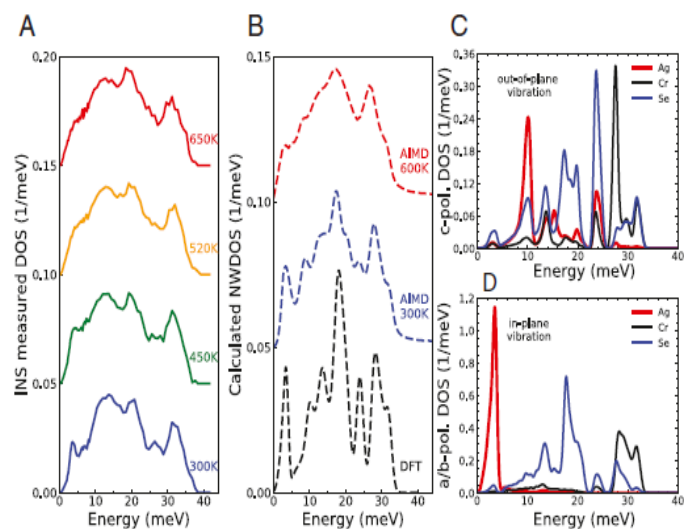


Figure 6.6. AgCrSe₂ phonon DOS from experiments and simulations. (A) INS powder measurements at ARCS with $E_i = 20$ and 80 meV. Blue, green, orange, and red lines are measured at 300, 450, 520, and 650 K. (B) Calculated neutron-weighted DOS. Black dashed line is labeled as DFT, and AIMD at 300 and 600 K are blue and red dashed lines. (C and D) Site-projected DOS from DFT for the c-axis polarized (C) and in-plane (D) motions in the a–b plane. Ag motions mainly contribute the strong peak around 3.5 meV for the in-plane vibration and a weaker peak near 10 meV for c polarizations.

In a comprehensive study of the anharmonic lattice dynamics and superionic transition in AgCrSe₂ (Ding, PNAS 2020), measurements of the phonon density of states as a function of temperature at ARCS were used to elucidate the relationship between in-plane vibrations and stochastic diffusion. As shown in Figure 6.6, at 300 K, a sharp peak is seen at 3.5 meV, broadening at 450 K and smearing out completely once AgCrSe₂ enters the superionic regime (between 450 and 520 K). However, an overall milder broadening can be seen on warming for all features above 5 meV, which is a consequence of anharmonicity and increasing atomic vibration amplitudes. The overall crystalline framework remains stiff through the transition. Density functional theory (DFT) and ab initio molecular dynamics (AIMD) capture the features seen (Figure 6.6B), and the simulations closely reproduce the extreme damping of the 3.5-meV peak as temperature increases. Decomposition of the atomic motions along and perpendicular to the c-axis (normal to the Ag ion planes in the layered structure) as seen in Figure 6.6C/D shows that the low energy feature is a result of “2D rattler modes.” These modes explain the low lattice thermal conductivity in the low temperature phase of AgCrSe₂. In the superionic regime, the in-plane Ag vibrations are strongly disrupted and damped, leading to the smearing of the 3.5-meV peak in the vibrational spectrum.

Vibrational results from ARCS have been used in several other studies of ionic dynamics. As with the AgCrSe₂ results, in the superionic phase of CuCrSe₂ (Niedziela, Nat. Phys. 2019), long-wavelength acoustic phonons capable of heat conduction remain largely intact, whereas specific phonon quasiparticles dominated by the Cu ions break down as a result of anharmonicity and disorder. The weak bonding and large anharmonicity of the Cu sublattice are present already in the normal ordered state, resulting in low thermal conductivity even below the superionic transition. These results demonstrate that anharmonic phonon dynamics are at the origin of low thermal conductivity and superionicity in this class of materials. Other studies of ionic transport look for ways to correlate various methods of characterizing phonon behavior in a material with the observed conductivity. Investigation of the lattice dynamics of the superionic conductor Na₃PS_{4-x}Se_x (Krauskopf, JACS 2018) by Raman spectroscopy, inelastic neutron scattering at ARCS and computations shows the evolution of multiple local symmetry reduced polyhedral species likely affect the local diffusion pathways, while experimental and calculational evaluation of the average vibrational energies for the mobile ion and anion framework are important to assess and screen for ionic conductors. A study of lithium ion conductors (Muy, Energy Environ. Sci. 2018) relates the trend in ionic mobility and electrochemical oxidation stability of lithium ion conductors to one common physical origin, the atomic vibrational frequencies of ion conductor constituents, thus highlighting the critical role played by the lattice dynamics in governing the lithium ion conductivity and stability of lithium-ion conductors.

These studies collectively illustrate the importance of combining the efficient collection of lattice dynamics data at ARCS over a wide temperature range to results from other instruments and techniques. CNCS provided data on low energy excitations and quasi-elastic neutron scattering results. X-ray elastic and inelastic also provided information about the structures and dynamics. Raman scattering and a broad range of computational techniques all contributed to a more detailed understanding of ion transport in important classes of energy-related materials.

Single crystal magnetism: Highly frustrated square-lattice itinerant magnet CaCo_{2-y}As₂

A. Sapkota, B. G. Ueland, V. K. Anand, N. S. Sangeetha, D. L. Abernathy, M. B. Stone, J. Niedziela, D. C. Johnston, A. Kreyssig, A. I. Goldman, R. J. McQueeney, *Physical Review Letters* 119, 147201 (2017).

ARCS continues to provide a high flux and moderate resolution for single crystal studies of magnetic excitations at thermal and epithermal energies. Magnetic frustration arises when competing interactions between magnetic moments cannot be mutually satisfied. It suppresses the development of long-range magnetic order and often creates enhanced spin fluctuations, which can lead to a variety of novel phases. Often the geometry of the lattice leads to frustration. However, in the case of a square lattice system, the frustration can arise from competing nearest-neighbor (NN) and next-nearest-neighbor (NNN) interactions. A study of the itinerant antiferromagnet CaCo_{2-y}As₂ at low temperature reveals two orthogonal planes of scattering perpendicular to the Co square lattice in reciprocal space, demonstrating the presence of effective one-dimensional spin interactions (Sapkota, PRL 2017).

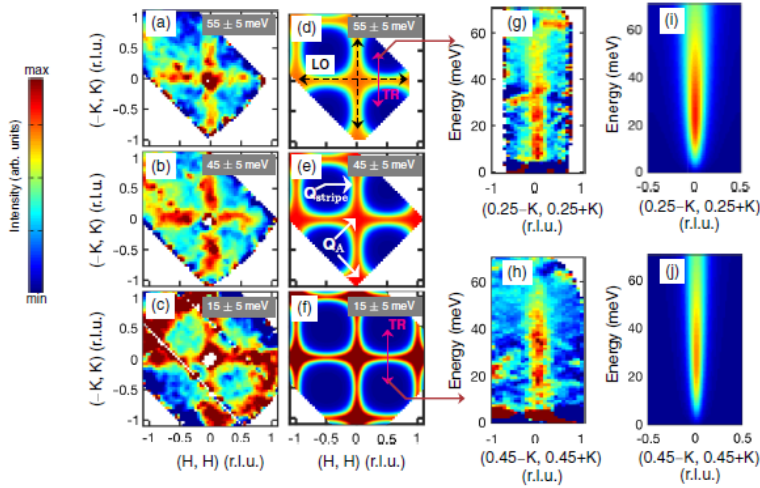


Figure 6.7. Spin fluctuations in $\text{CaCo}_{2-y}\text{As}_2$: Experimental INS data ($E_i = 75 \text{ meV}$) vs diffusive model. (a)–(c) Constant-energy slices of the background-subtracted data averaged over the energy ranges of 50–60, 40–50, and 10–20 meV, respectively. (d)–(f) Corresponding constant-energy slices calculated using the diffusive model. (g),(h) Transverse slices of the background-subtracted data. (i),(j) Corresponding energy dependence of the scattering obtained using the diffusive model.

The presence of the very striking spin fluctuations in $\text{CaCo}_{2-y}\text{As}_2$ is seen in the inelastic neutron scattering data from ARCS (Figure 6.7). $\text{CaCo}_{2-y}\text{As}_2$ has A-type antiferromagnetic order at low temperatures and the low-energy spin fluctuations are expected to originate at $Q_A = [(0,0),(1,1)]$. However, constant energy slices of the data (Figure 6.7a-c) show that the scattering from the spin fluctuations extends along the longitudinal direction, crossing positions including $Q_{\text{stripe}} = [(1/2,1/2)]$ at all accessible energies from ~ 10 –120 meV. In contrast, the scattering along the transverse direction is sharp (Figure 6.7g-h). A model more appropriate for itinerant systems close to magnetic order than the standard Heisenberg model was developed. Results from fitting to the ARCS data (Figure 6.7d-f,i-j) indicate that there is extreme frustration in $\text{CaCo}_{2-y}\text{As}_2$, as seen by the value of a frustration parameter $\eta = J_1/2J_2 \sim -1$, where J_1 and J_2 are the NN and NNN magnetic interactions. These results are shown to arise from near-perfect bond frustration within the J_1 - J_2 Heisenberg model on a square lattice with ferromagnetic J_1 and hence indicate that the extensive previous experimental and theoretical study of the J_1 - J_2 Heisenberg model on local-moment square spin lattices should be expanded to include itinerant spin systems.

6.3 GENERAL USER PROGRAM

For the years of 2017 through 2019, 178 general user proposals were submitted to ARCS, of which 91 were selected to run, resulting in ~ 65 unique ARCS users per year. A breakout of the science areas covered is shown in Figure 6.8. These categories are broadly aligned with the ORNL and NScD strategic plans for studies of quantum and energy materials.

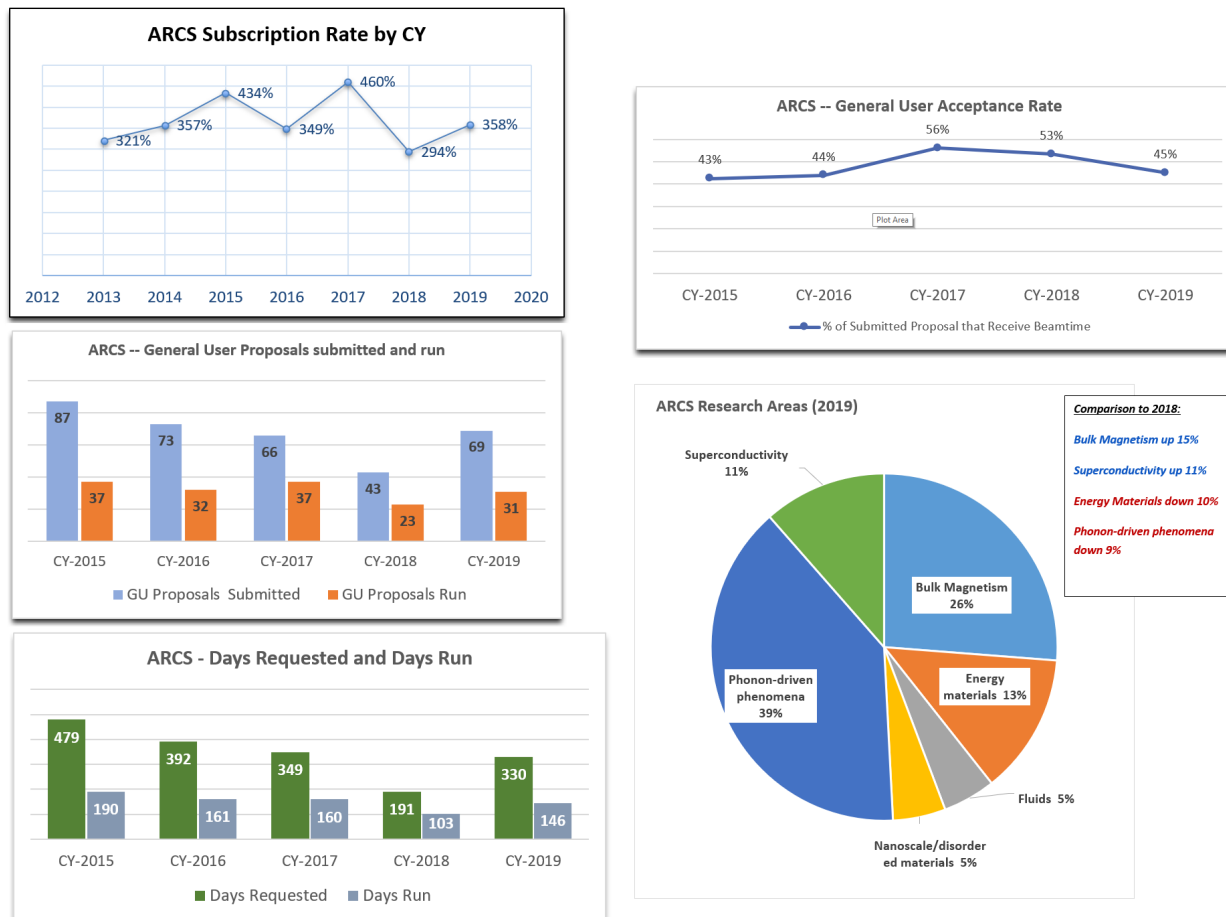


Figure 6.8. ARCS user program statistics

6.4 UPDATE ON INSTRUMENT DEVELOPMENT ACTIVITIES

ARCS has completed or initiated a number of projects since 2017 to enhance the instrument capabilities and address operational issues.

ARCS detector array upgrade

The changeout of the detector electronics and controls for the ARCS ^3He linear position-sensitive detector array was completed in the spring of 2018 during the long Inner Reflector Plug exchange outage. This project replaced all electronics boards with current standards, reconfigured the high voltage for external supplies and replaced all cabling. A new design of pre-amp boards is more resistant to damage during unexpected vacuum venting. All detector packs are individually powered so that specific ones may be recovered more easily if there is a communication issue. The new electronics allow for finer control of the discrimination for neutron detection, which reduced the variation in apparent efficiency across the detector array tubes and gained ~15% in overall count rate as determined by the standard high-intensity vanadium calibration runs.

New DAS controls

ARCS switched to the new data acquisition system in spring 2018. The system is based on EPICS instrument control with Control System Software (CSS)/Phoebus GUIs. The DAS provides a common look and feel across the SNS instruments suite and improves the utility for our user base in term of single crystal

alignment and scripting/queueing. ARCS has implemented an incident energy selection tool that includes an automatic mode to select the appropriate Fermi chopper and speed for a requested incident energy. Two look-up tables based on measured flux and resolution data are used to select settings emphasizing “Resolution” or “Flux”. Manual control of all chopper settings is also allowed, along with modes for TO chopper only operations (used for high intensity vanadium calibration) and white beam data collection. All standard sample environment equipment controls are incorporated in the system. Most typical experiments at ARCS can be run using the supplied Table Scan, which controls the EPICS process variables and places automatic data collection scans on a data collection queue. A prototype python-based scripting for data collection has been used, and refinements of that system are underway to provide an alternative way to script experiments.

Optimized CCR

A new medium bore (70mm) top-loading CCR optimized to the requirements of ARCS and SEQUOIA was approved through the Mid-level Procurement process and is scheduled for delivery in 2020. The new device combines the best of the two CCRs currently in use at ARCS through optimizing the background while allowing for user sample changes and high temperature operations. This should reduce stress on the SA and sample environment teams for equipment changes and limit the need to local contact intervention for sample changes (required currently for the bottom loading CCR due to crane training limits). The reduced bore compared to the current device will decrease the cooling time for sample changes.

Automatic helium exchange gas handling

A system to control the exchange gas in top-loading CCRs used at ARCS is under construction. It is designed to automate the pump/purge and backfill process done when a sample is changed. Computer control will allow the exchange gas to be pumped out when transitioning from low temperature operations to heating of the sample above room temperature. This will eliminate the need for manual intervention by users or requests for the Instrument Hall Coordinator to perform the task.

Multi-sample stick

ARCS has finished a design and is waiting for manufacturing to implement a multi-sample changer that would use the existing large bore CCR and add a motorized 6 sample stick. One rotation and one vertical translation will allow samples to be positioned in the ARCS beam. To fit within the existing CCR and use the entire ARCS detector array without interference, the design uses a new 3D printing technology to make the sample mount from a B₄C/ aluminum composite. This combines the support and heating requirements with neutronic shielding for a compact design. The initial temperature range is planned for 10K to 450K and testing of a mock-up holder is underway to understand the thermal impact on cooling and heating of the larger holder in the CCR.



Figure 6.9. Prototype six sample holder.

Software

ARCS participates in the overall direct geometry spectrometer discussions concerning new methods for data visualization and analysis of the large 4-dimensional datasets collected. Some specific efforts for ARCS include:

1. **Phonon DOS:** One of the major uses of ARCS is to measure the phonon density-of-states in materials. Code for converting neutron scattering data into DOS has been incorporated into more user-friendly Jupyter notebooks by the computational data analysis group (Jiao Lin). The algorithms allow multiple

incident energies to be combined with appropriate joining of the intensities. Further work is planned to allow a more scripted use of the methods to incorporate into other data analysis workflows.

2. **Resolution characterization and modeling:** Vanadium scattering data from ARCS taken with an expansive set of chopper parameters were analyzed to provide detailed information about the flux and energy resolution available for users (J. Y. Y. Lin, A. Banerjee, F. Islam, M. D. Le, D. L. Abernathy, *Physica B: Condensed Matter* **562**, 26 (2019)). The data were compared to the PyChop model for direct geometry energy resolution available in Mantid. The results of these studies are available to users through the website <https://rez.mcvine.ornl.gov> and incorporated into the automatic energy setting feature of the ARCS DAS system.
3. **Super-resolution:** ARCS collaborated with the computational data analysis group (F. Islam, J. Lin) to explore methods to extract higher resolution information from inelastic scattering measurements. The super-resolution concept, where multiple measurements of the same object are combined to improve the knowledge of the original, was explored in relation to a phonon DOS measurement of graphite (F. Islam, J. Y. Y. Lin, R. Archibald, D. L. Abernathy, I. I. Al-Qasir, A. A. Campbell, M. B. Stone, G. E. Granroth, *Review of Scientific Instruments* **90**, 105109 (2019)). The ARCS energy resolution was parametrized, and various convolution methods were tested in the analysis.

6.5 UPDATE ON THE IMPACT OF DISCRETIONARY BEAM TIME

Since 2016, ARCS has allocated discretionary time through the SNS standard practice within NSD. The time has gone to encourage collaboration among local students (UTK), postdocs and other ORNL staff. Discretionary time supported the involvement of ARCS in studies of resolution correction and the super-resolution concept. Discretionary time at ARCS is used to test the suitability of samples and ideas before competing for beamtime through the regular General User allocations, and to complete data collection for ongoing collaborations to enable publications. A recent example of intra-ORNL collaboration supported by discretionary time is the collection of scattering cross-section data for moderator materials for the Transformational Challenge Reactor, a DOE funded research project at ORNL to design a modular 3D printed reactor. The measurements of YHx across a variety of compositions and temperatures were made at ARCS and SEQUOIA, and subsequently have been supported through the General User program.

By NSD policy ARCS has allocated some discretionary time through the various science initiatives. This has not been a large source of proposal for ARCS since many potential users are from the Quantum Materials Initiative, where the use of cold neutrons and magnets are often required. More recently proposals from the High Pressure Initiative have been allocated at ARCS.

6.6 OUTREACH AND EXPANSION INITIATIVES

ARCS has a large percentage of repeat users, presumably due to the specialized nature of inelastic neutron scattering. Outreach to non-expert user groups will need to be enabled by improving the ease of using software and making better connections to modeling capabilities. The ARCS team has been participating regularly in DOE's National School on Neutron and X-Ray Scattering, recently alternating years with SEQUOIA. Hands-on experiment and data reduction/analysis sessions that are given during the workshop provide graduate students and post-doctoral researchers a great opportunity to become familiar with inelastic neutron scattering. ARCS has a strong record of enabling student theses with 8 in the period of 2017 to 2019 and 35 overall.

6.7 ARCS VISION

Near-term Vision (1-3 years)

Complete instrument projects to ensure the most reliable and efficient operation of ARCS and enable a mail-in program. Develop user software to enhance the scientific output of the instrument. Investigate additional longer-term instrument developments.

ARCS is a mature instrument and had benefited from recent investments in key systems to improve operational reliability. The next stage of investment will be focused on improvements in efficiency in running the majority of user requested experiments. The new CCR will reduce time spent on changing sample environment equipment. Completion of the multiple sample stick and automatic exchange gas handling will improve efficiency for data collection and allow the establishment of a mail-in program for powder inelastic neutron scattering at ARCS. The new DAS should enable more complete information to be passed to reduction software to speed up data visualization and analysis.

User software for direct geometry instruments continues to lag. While new projects are underway, often developments are at the cutting edge and do not get implemented in methods that users can easily access. ARCS will work on powder software in the near term, since that is a major part of the science done with the instrument. Better tools for resolution are needed and should help ensure the maximum is gained from the measurements done.

ARCS was built by design as an almost complete instrument. There is no more space for detectors, and additions like the oscillating radial collimator are done. One last upgrade foreseen in the design is something to fill a gap in the beamline at the T0 chopper position. By default, this could be an additional T0 chopper to reduce background for high incident energy measurements. Some study will be done to address what gains would come from an additional Fermi (or Fermi-like, e.g. magic chopper using supermirrors) chopper to serve as a pulse-shaping, resolution-enhancing chopper. This would address concerns with resolution that are limiting application of dynamic PDF or other Fourier transform methods.

Strategic Vision (3-10 years) and Alignment with NScD/ORNL Strategic Plans

ARCS will enable a complete scientific approach to understand excitations in materials incorporating advanced computing and enhanced analysis of the neutron scattering data. New capabilities in energy resolution from hardware and software will open new regimes.

ARCS will continue to study quantum and energy related materials. Larger scientific gains in productivity are expected to come from coupling the neutron scattering information with advanced modeling. New methods to correct or model the instrument resolution will allow more detailed studies, and advances in data reduction to address unavoidable background will open more opportunities in advanced sample environment. Resolution may also be enhanced by new chopper hardware to push ARCS into new territories.

6.8 FUNDING/RESOURCES NEEDS

Personnel: As an inelastic instrument, ARCS runs well with the standard complement of two instrument scientists and one scientific associate and should remain at that level. New instrumentation additions to enhance productivity, such as the multi-sample changer, should be accommodated by efficiencies gained

from improving DAS and analysis software. Standardization across the direct geometry spectrometer suite will help smooth over times when help is needed by easing cross-training.

Sample environment: ARCS has pursued a concept for a multi-sample changer that would use an existing large bore CCR and add a motorized 6 sample stick. An automatic exchange gas handling system will ease requirements for user intervention for large temperature range experiments. Other sample environment needs are being address through NScD processes and collaboration with other instruments.

Software: New data reduction, visualization and analysis software is a large ongoing need for ARCS and the direct geometry spectrometer instruments. Full use of the event data is still being implemented, and various levels of resolution need to be defined and implemented at all points of the process, e.g. experiment planning, data analysis, comparisons to simulations. The ability to more seamlessly chain together advances in simulation and modeling will be key; and of course, the advances must be accompanied by efforts to make the software user friendly and well documented.

Future funding opportunities. ARCS will continue to work through NScD processes to get funding for new sample environment, upgraded beamline equipment and access to students/postdocs. Collaborations for LDRD funding will continue.

6.9 SELF-ASSESSMENT

Strengths

ARCS is a high flux, moderate resolution instrument that accommodates a large variety of scientific topics and sample types. It has proven to be stable over the long term in performance as an instrument, as well as in productivity of papers. The technology incorporated into ARCS was by design well understood and remains at or near the leading edge of current practice.

Weaknesses

As with other direct geometry instruments, data visualization and analysis software currently slow down ARCS productivity. Maintenance and upgrade projects have been done but there remain many places that could fail as ARCS ages. In several instances the design does not allow easy access, such as the incident beamline guides (risk of vacuum leaks) and the sample chamber (many components, e.g. sample isolation gate valve, collimator and lift, slits, internal shielding). There remain some unexplained sources of background that affect standard measurements like the phonon DOS.

Opportunities

There are still improvements to be made in efficient data collection by incorporating a multi-sample changer and enabling better flow of the data through reduction to visualization and analysis. This may in turn attract non-traditional inelastic neutron scattering users, particularly with better coupling to scientific modeling of the sample under study. Novel analysis methods using Fourier transforms may provide more accessible data as well. Given the flux at ARCS, there may be more that can be done with stroboscopic or time-dependent measurements.

Threats

As ARCS ages, certain failures would involve significant down time. For example, the incident beam guide access would require shutting down multiple beamlines and unstacking shielding for ARCS and SEQUIOA.

As a practical matter ARCS could be out of the user program until the next long shutdown. Even if ARCS maintains its advantage for data collection speed, since new sources being constructed or proposed focus on lower energy neutrons, scientific productivity also involves new software and modeling. Other comparable instruments (see the appendix) may gain advantages through advanced computing. A variety of x-ray inelastic scattering techniques (resonant and non-resonant) are competing with inelastic neutron scattering. While these techniques continue to evolve, they are often complementary to what ARCS can do, for example extending the kinematic range for measurements or using very small single crystals. Neutrons will continue to have the advantage in the measurement of absolute scattering cross-sections, so the tools for enabling that must be further developed and deployed.

6.10 EXECUTIVE SUMMARY

ARCS provides a high flux and large momentum coverage to enable a broad range of science. The instrument team and the facility are dedicated to continued high productivity by investing in maintenance and development activities. New areas will be opened up by innovation in sample environment, additional beamline instrumentation and advancements in software. Continuing improvements in user visualization and analysis software, coupled to advanced modeling and resolution corrections, will provide a solid platform for highly productive investigations.

6.10.1 Comparison of instrument specifications to similar instrument worldwide

	ARCS	MERLIN (ISIS)	MAPS (ISIS)	4SEASONS (JSNS)
Moderator	Decoupled water	Gd poisoned water	Gd poisoned water	Coupled hydrogen
Source frequency	60 Hz	50 Hz	50 Hz	25 Hz
Avg. Flux ($n\text{ cm}^{-2}\text{ s}^{-1}$)	$3 \times 10^5\text{ n cm}^{-2}\text{ s}^{-1}$ @ 1MW	$6 \times 10^4\text{ n cm}^{-2}\text{ s}^{-1}$	$2 \times 10^4\text{ n cm}^{-2}\text{ s}^{-1}$	$1 \times 10^5\text{ n cm}^{-2}\text{ s}^{-1}$ @ 1MW
Flight Path	$L_1+L_2 = 13.6\text{ m}$ $L_3(\text{min})=3.0\text{ m}$	$L_1+L_2 = 11.8\text{ m}$ $L_3(\text{min})=2.5\text{ m}$	$L_1+L_2 = 12\text{ m}$ $L_3(\text{min}) = 6$ (~8m of m=3 guided added 2018)	$L_1+L_2 = 18\text{ m}$ $L_3(\text{min}) = 2.5\text{ m}$
Beam size	$5 \times 5\text{ cm}^2$	$5 \times 5\text{ cm}^2$	$5.5 \times 5.5\text{ cm}^2$	$4.5 \times 4.5\text{ cm}^2$
Scattering angles	$3^\circ - 135^\circ$	$3^\circ - 135^\circ$	$3^\circ - 60^\circ$	$3^\circ - 130^\circ$
Incident energy	15 - 1500 meV	7 - 2000 meV	15 - 2000 meV	5 - 300 meV
Elastic $\Delta E/E_i$	2 - 5%	3 - 5 %	2 - 5%	> 5 %
Detector type	1m ^3He LPSD	3m ^3He LPSD	~1m ^3He LPSD	2.5m ^3He LPSD
No. of detectors	920	270	574	350
Detector solid angle	2.5 sr	3.1 sr	0.45 sr	2.5 sr

6.10.2 Comparison of sample environment capabilities with similar instruments worldwide

	ARCS	MERLIN (ISIS)	MAPS (ISIS)	4SEASONS (JSNS)
Temperature range	30mK – 1900K	30mK – 800K	30mK – 800K	100mK – 1900K
Max magnetic field	5T (SlimSAM), 8T	4T	3T	3.5T
Max pressure	4.2 kbar (Al autofretage cell),	5.6 kbar TiZr 10kbar gas cells	5.6 kbar TiZr 10kbar gas cells	

6.10.3 Data and computing capabilities

	ARCS	MERLIN (ISIS)	MAPS (ISIS)	4SEASONS (JSNS)
Data reduction	Mantid	Mantid	Mantid	Utsusemi (MLF/J-PARC)
Data visualization	Mslice/Horace/Mantid	Horace, MSlice, Tobyfit, Mantid	Horace, MSlice, Tobyfit, Mantid	Utsusemi
Data analysis packages	Tobyfit	Tobyfit	Tobyfit	
Data Modeling	None (some effort in McStas/McVine)	No public software available	No public software available	
Simulation and data correction tools	Mantid (absolute units vanadium standard); DAVE Mslice (GDOS,absorption)	Mantid (absolute units vanadium standard);	Mantid (absolute units vanadium standard);	
Planning tools	Horace, Mantid DGSPanner & PyChop	Horace, PyChop	Horace, PyChop	Utsusemi
Computing resources	ARCS1, ARCS2 (~32 nodes)			Workstation (CPU: 2.3 GHz x 18 cores (36 threads), Memory: 256 GB, OS: Ubuntu 16.04)

7. SNS BL-17, THE SEQUOIA FINE-RESOLUTION FERMI CHOPPER SPECTROMETER: BEAMLINE STATUS AND PLANNING SUMMARY DOCUMENT

7.1 OVERVIEW/CURRENT STATUS

The SEQUOIA Fine-Resolution Fermi Chopper Spectrometer (SEQUOIA) is located on BL-17 at the Spallation Neutron Source (SNS). The instrument is a time-of-flight direct geometry chopper spectrometer. The incident energy neutrons typically used at SEQUOIA range from 8 meV up to 2000 meV. The SEQUOIA instrument was built to provide good wave-vector and energy resolution for thermal neutron spectroscopy measurements. SEQUOIA has been fully in the user program since 2010.

An illustration of the instrument and its components is shown in Figure 7.1. Guides transport neutrons from the decoupled ambient water moderator of the SNS to the sample along a 20-meter incident flight path. A vertical axis t-zero (t_0) chopper is installed close to the shutter to block the prompt pulse of neutrons and gammas. Two Fermi choppers are installed on a translation table to allow one to switch between chopper configurations quickly. These choppers are specified to provide both high neutron flux and high energy resolution configurations. SEQUOIA's entire secondary flight path from the sample to the detectors is evacuated to a level of approximately $1E-6$ Torr. A large gate-valve separates the sample vacuum chamber from the detector vacuum chamber allowing for samples and sample environments to be changed from the sample chamber without disturbing the large detector vacuum chamber. A large Helium-3 (^3He) position sensitive detector array surrounds the sample position in a right circular cylinder geometry. This results in a secondary flight path, distance from the sample to the detector which varies between 5.5 and 6.3 meters in length. The energy resolution of the instrument can be tailored between approximately 1 and 5% of the incident neutron energy. The detector coverage includes scattering angles between 2.5 and 60 degrees.

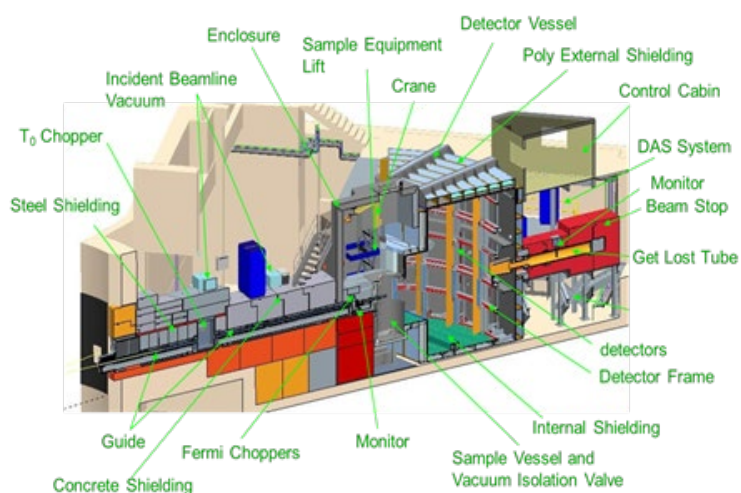


Figure 7.1. Illustration of the SEQUOIA instrument and its components. The flight path of the neutrons travels from left to right in this figure.

SEQUOIA complements the other thermal moderator direct geometry chopper spectrometer at the SNS, ARCS. ARCS is a high flux instrument with coarse energy resolution. SEQUOIA operates with finer energy resolution at the expense of neutron flux. SEQUOIA has large solid angle coverage at low-to-intermediate scattering angles with good wave-vector and energy resolution. See G. E. Granroth, *et al.*, *J. Phys.: Conf. Ser.* **251**, 12058 (2010) and M. B. Stone, *et al.*, *Rev. Sci. Instr.* **85**, 045113 (2014) for detailed information regarding the design and operation of the spectrometer.

The science being examined with SEQUOIA is having an impact on a cross-section of important research areas including unconventional superconductors, quantum magnetism, itinerant magnets, ferroelectrics, thermoelectrics, multiferroics, confined water, metal hydrides, and hydrogen dynamics in various materials. Powder samples and single crystal samples are both measured with the instrument. An instrument specific three position cryogenic powder sample changer has made powder sample measurements with multiple samples very efficient. Single crystal measurements typically are awarded between four and seven days of measurement time. Powder measurements of a single spectrum at a single temperature can be performed in a few hours. Powder measurements are often awarded between one and four days of measurement time depending upon the number of samples and the complexity of the measurement

Team Structure

Management responsibilities for SEQUOIA lie in the spectroscopy group within the Neutron Scattering Division (NSD). The Instrument team is shown in the photograph in Figure 7.2. Lead instrument scientist Matthew Stone and instrument scientist Sasha Kolesnikov are each 1 Full Time Employee (FTE). The SEQUOIA Scientific Associate (SA) is Victor Fanelli, a member of the Scientific Associates Team two in the SNS Instrument Operations Group of the NSD (1 FTE).

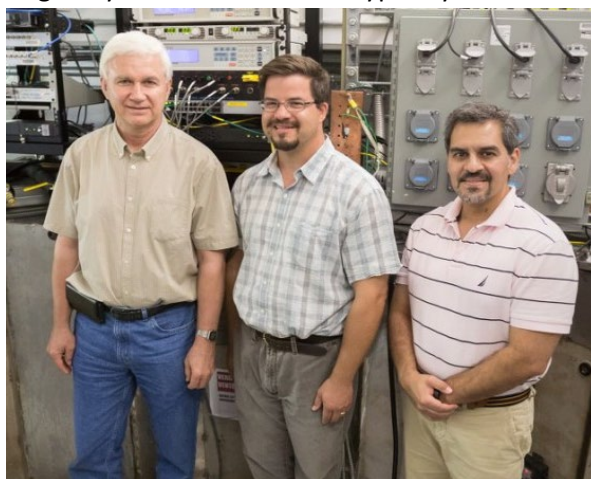


Figure 7.2. The SEQUOIA Instrument team photographed inside the SEQUOIA instrument 'sample cave'. From left to right: Alexander "Sasha" Kolesnikov (Instrument Scientist), Matthew Stone (Lead Instrument Scientist) and Victor Fanelli (Scientific Associate (SA)).

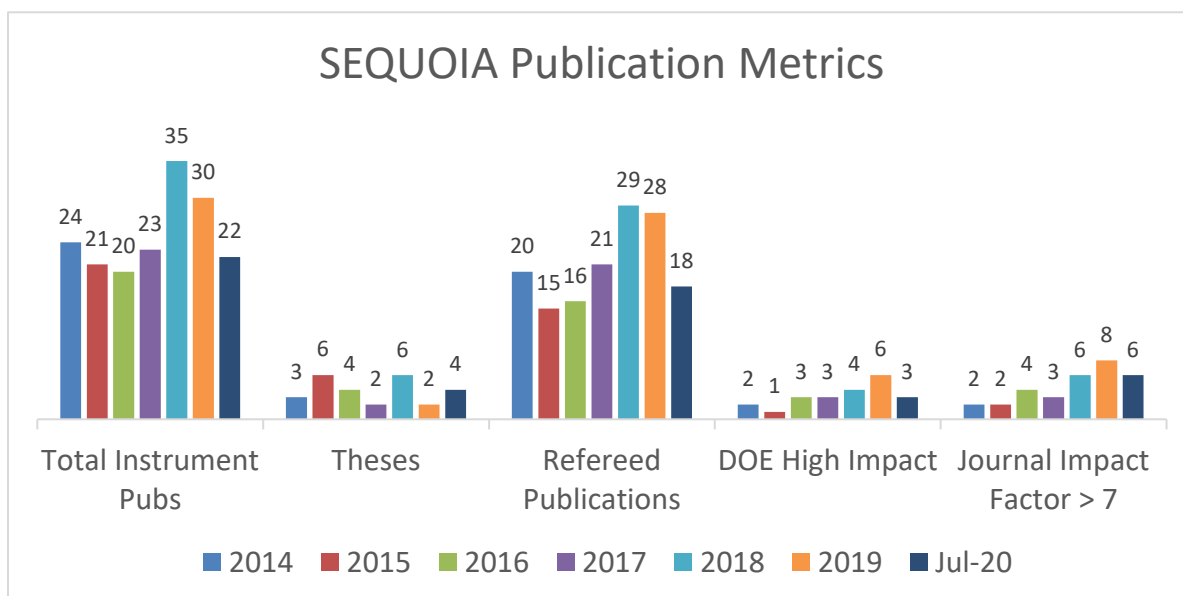


Figure 7.3. SEQUOIA publication metrics from 2014 through July of 2020.

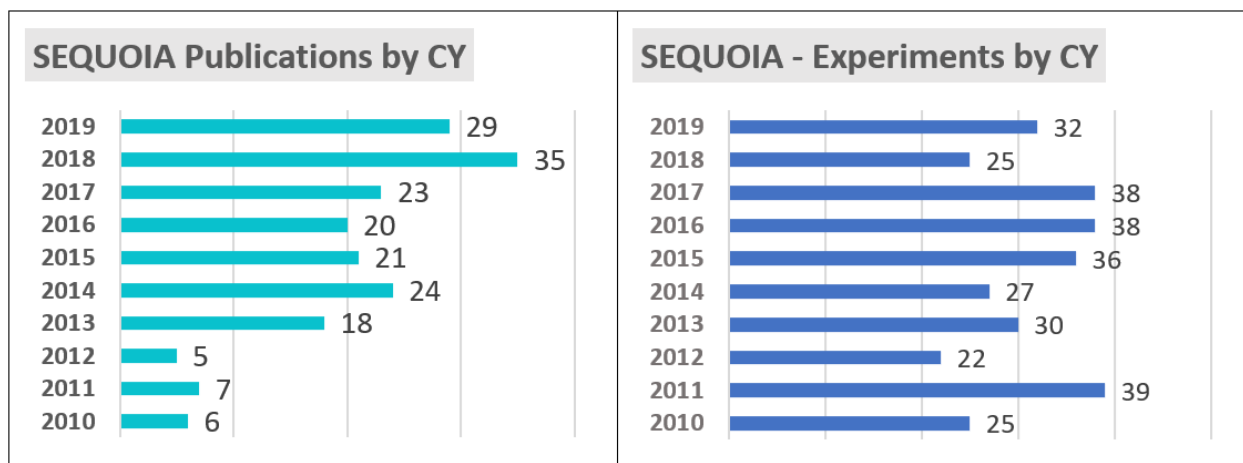


Figure 7.4. SEQUOIA publication statistics

7.2 SCIENTIFIC FOCUS

From 2017-2019, 177 general user proposals were submitted to SEQUOIA, of which 95 were selected, resulting in 156 unique users. As of mid-2020, there have been a total of 177 peer reviewed publications of which 32 have a journal impact factor greater than 7. Twenty-five publications from SEQUOIA are in the list of “DOE high impact” journals. Additional details regarding publications from the SEQUOIA instrument are shown in Figure 7.3 and Figure 7.4.

7.3 SCIENTIFIC HIGHLIGHTS

SEQUOIA is used to study a range of scientific problems. Experiments are performed in the fields of quantum magnetism, frustrated magnetism, hydrogen storage, and conventional and unconventional superconductivity. We provide here several examples to demonstrate the breadth of work being done using the SEQUOIA spectrometer.

Three-Magnon Bound State in the Quasi-One-Dimensional Antiferromagnet α -NaMnO₂

R. L. Dally, A. J. R. Heng, A. Keselman, M. M. Bordelon, M. B. Stone, L. Balents, and S. D. Wilson, "Three-Magnon Bound State in the Quasi-One-Dimensional Antiferromagnet α -NaMnO₂," *Phys. Rev. Lett.* **124**, 197203 (2020)

The compound α -NaMnO₂ is known as a layered system that has potential to be a non-lithium based material for use in electrodes. A Jahn-Teller distortion of the oxygen octahedra around the Mn³⁺ ions leads to quasi-one-dimensional antiferromagnetic chains along the crystallographic b-axis. Measurements of this system were performed at the SEQUOIA instrument to understand the magnetic exchange interactions of the compound. SEQUOIA allowed the team to determine the details of the exchange interactions of the Heisenberg Hamiltonian. The measured spectrum along the K direction in reciprocal space is shown in Figure 7.5.

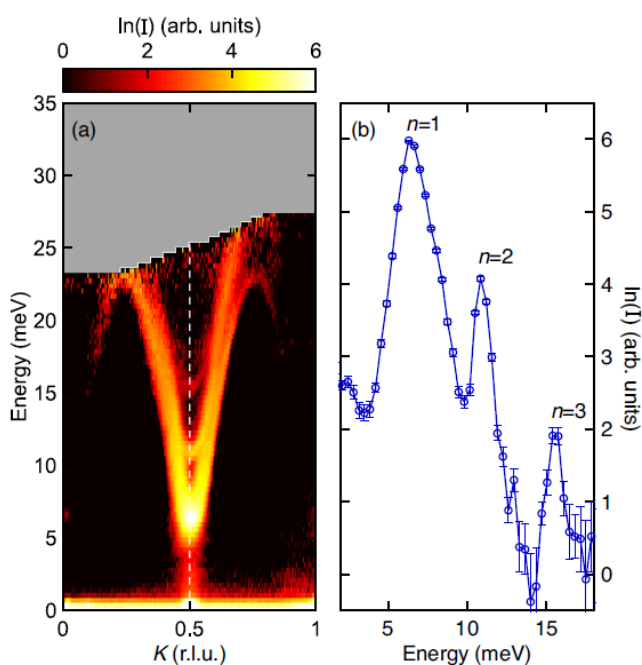


Figure 7.5. Inelastic neutron scattering intensity measured for α -NaMnO₂. Data are shown on a logarithmic intensity scale. (a) spectrum as a function of energy transfer (vertical axis) and wave-vector transfer along the K direction of reciprocal space (horizontal axis). (b) Constant wave-vector scan through the $K=0.5$ position as a function of energy transfer.

The measured spectrum shows a clear gap of approximately 6 meV at the antiferromagnetic wave-vector. This gap is due to a single-ion anisotropy. Upon close inspection, and as shown in Figure 7.5(b), there are indeed three dispersive modes in the measured spectrum. The two higher energy modes are the respective two and three-magnon bound states of the antiferromagnetic chain. Two magnon bound states have been observed previously using neutron scattering techniques. However, this is the first instance of a measurement of a three-magnon bound state using inelastic neutron scattering. The data quality allowed for a refinement of both the quasi-one-dimensional exchange $J_1=5.34(8)$ meV and the Single-ion anisotropy $D=0.46(2)$ meV. The experiment made use of the significant detector coverage of the SEQUOIA chopper spectrometer to integrate the scattering intensity along the orthogonal to chain directions in reciprocal space. This allowed for the observation of the weak three-magnon bound state in α -NaMnO₂.

Frustrated Magnetism in a Mott Insulator

J. C. Leiner, H. O. Jeschke, R. Valenti, S. Zhang, A. T. Savici, J. Y. Y. Lin, M. B. Stone, M. D. Lumsden, J. Hong, O. Delaire, W. Bao, and C. L. Broholm, *Phys. Rev. X* **9**, 011035 (2019).

The phase diagram of V_2O_3 as a function of pressure or substitution with Cr, i.e. $(V_{1-x}Cr_x)_2O_3$, contains both paramagnetic and antiferromagnetic phases as well as both insulating and metallic phases. SEQUOIA was used to map out the complete excitation spectrum of $(V_{0.96}Cr_{0.04})_2O_3$ in both the antiferromagnetic and paramagnetic insulating phases. The refined values of the exchange interactions illustrate that frustrated

magnetic interactions are responsible for suppressing magnetic long-range order. This suppressed order to lower temperatures opens a larger portion of the phase diagram for the paramagnetic Mott-insulator transition to occur in this compound.

$(V_{1-x}Cr_x)_2O_3$ is the first observed system to exhibit a Mott metal to insulator transition [D.B. McWhan, *et al.*, *Phys. Rev. Lett.* **23**, 1384 (1969) and D.B. McWhan and J. P. Remeika, *Phys. Rev. B* **2**, 3734 (1970)], and as such it has been the subject of intense study since the late 1960s. In fact, it is one of the first materials to be examined using the polarized triple axis developed by Moon, Riste, and Koehler at ORNL [R.M. Moon, *Phys. Rev. Lett.* **23**, 527 (1970)]. These early polarized diffraction measurements were able to determine the magnetic structure in one portion of the phase diagram as consisting of vanadium moments ferromagnetically coupled in individual layers, but antiferromagnetically coupled between the layers. However, a detailed description of the exchange interactions between the vanadium moments was been lacking for half a century.

The large pixelated detector coverage, tunable energy resolution and large neutron flux on sample at SEQUOIA were used together to systematically map the magnetic excitation spectrum of $(V_{0.96}Cr_{0.04})_2O_3$. Figure 7.6(c) and (d) illustrate the respective $T=5\text{ K}$ and $T=205\text{ K}$ measured spectrum along high symmetry directions in reciprocal space. A Heisenberg Hamiltonian with single ion anisotropy and nine exchange interactions was required to model the measurements. The results shown in Figure 7.6(a) based upon DFT calculations and Figure 7.6(b) based upon modeling of the neutron

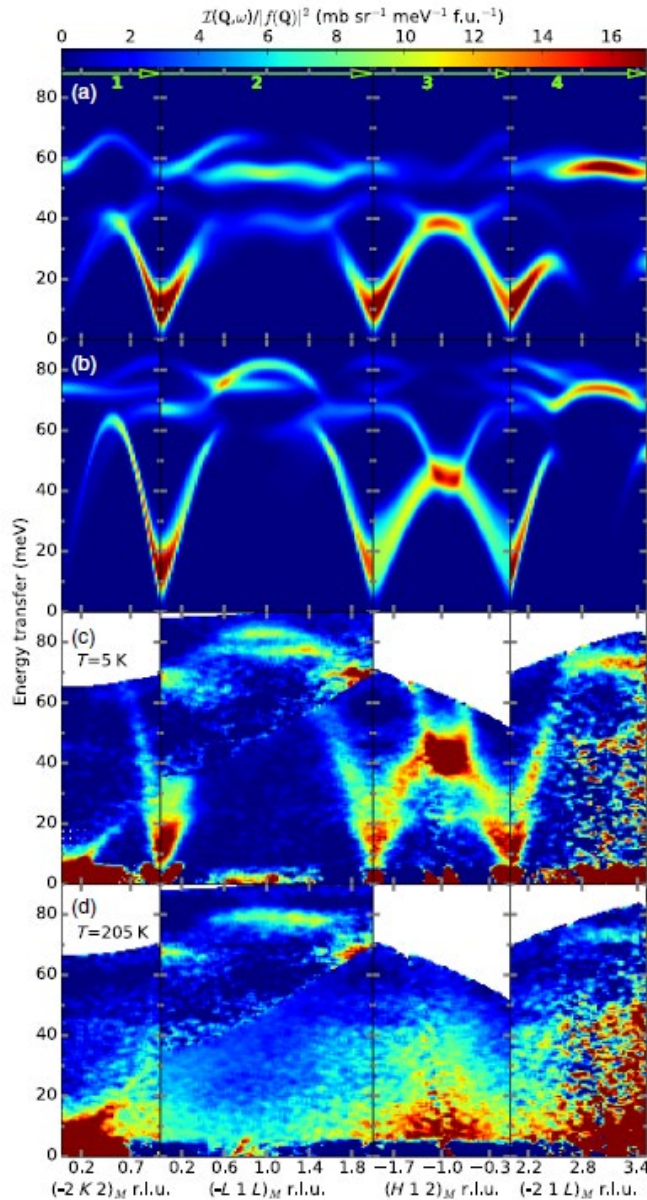


Figure 7.6. (a),(b) Calculated neutron scattering intensity using SpinW[7] for exchange constants determined from the low-temperature $T=5\text{ K}$ measurements (c). Panel (d) corresponds to measurements at $T=205\text{ K}$. Data were acquired with $E_i=100\text{ meV}$ at SEQUOIA and averaged over multiple Brillouin zones and divided by the squared magnetic form factor for presentation with an azimuthally averaged incoherent background subtracted.[8]

scattering measurements are an excellent representation of the measured data. The refinement of the low temperature data allowed for a new understanding of the paramagnetic phase as consisting of a quasi-two-dimensional cooperative paramagnet with frustrated nearest and next nearest neighbor interactions within distorted honeycomb layers.

Complexity of Intercalation in MXenes: Destabilization of Urea by Two-Dimensional Titanium Carbide

S.H. Overbury, A.I. Kolesnikov, G.M. Brown, Z. Zhang, G.S. Nair, R.L. Sacci, R. Lotfi, A.C.T. van Duin, and M. Naguib, *J. Am. Chem. Soc.* **140**, 10305 (2018)

MXenes are a new class of 2D materials with properties that make them important for applications that include batteries, capacitive energy storage and electrocatalysis. Intercalation is known to be possible in these materials and it is critical for many applications, therefore understanding the interaction between MXene and intercalants is crucial for using MXenes as pseudocapacitor electrode materials. We have investigated urea interaction within a titanium carbide based MXene using inelastic neutron scattering (INS) to probe the state of intercalated species [S.H. Overbury, A.I. Kolesnikov, G.M. Brown, Z. Zhang, G.S. Nair, R.L. Sacci, R. Lotfi, A.C.T. van Duin, and M. Naguib, *J. Am. Chem. Soc.* **140**, 10305 (2018)]. IR spectra of the urea-MXene could not be obtained because the MXene materials are black and were strongly absorbing of the IR radiation. To get the best energy resolution, we measured the INS spectra with four incident energies, $E_i = 30, 110, 250$ and 600 meV, selected by the high-resolution Fermi 2 ($E_i < 200$ meV) and high-flux Fermi 1 ($E_i > 200$ meV) choppers. The use of the direct geometry spectrometer (DGS) SEQUOIA is essential in study of materials containing hydrogen (which has a large mean-squared displacement, u_H^2) in order to get information on high energy modes; only a DGS can provide access to low momentum transfer, Q , at high energies, thus resulting in reasonable Debye-Waller factor, $\exp(-Q^2 u_H^2)$. By comparison with reference materials, we found that under intercalation conditions urea decomposes readily in contact with Ti_3C_2 , leading to intercalation of ammonium observable by INS and evolving carbon dioxide detected

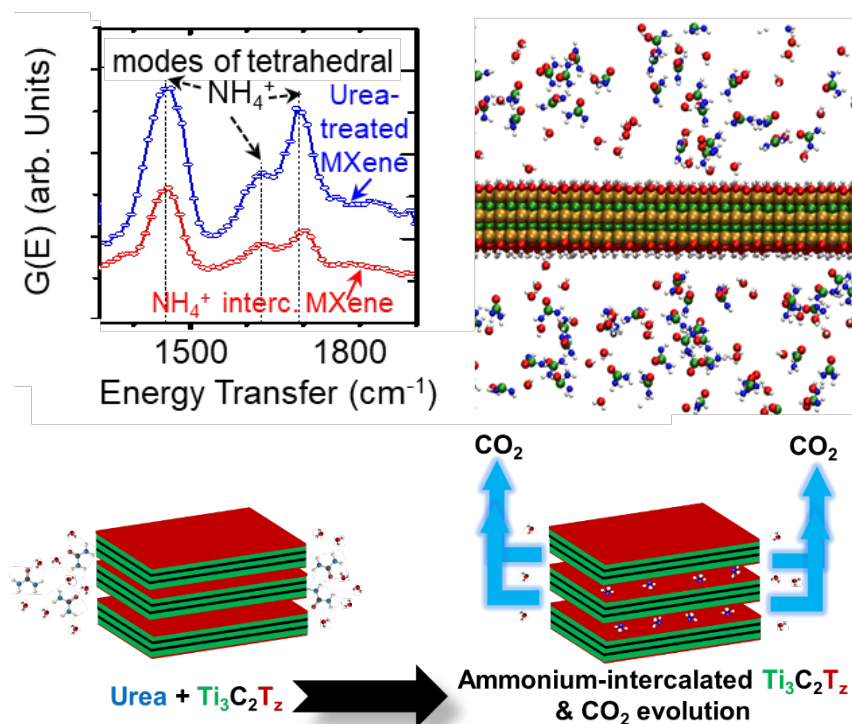


Figure 7.7. INS spectra for Urea treated MXene, and NH_4^+ intercalated MXene reference sample show excellent agreement for the NH_4^+ modes. ReaxFF was used to provide insights for pathways for urea decomposition on MXenes. INS and IR measurements showed that urea interact with MXene results in ammonium intercalation and CO_2 evolution. [S.H. Overbury, et al. *J. Am. Chem. Soc.* **140**, 10305 (2018)]

by IR spectroscopy. Reactive molecular dynamics calculations provided atomistic insights for reaction pathways. These results show that the presence of active metal sites and strongly acidic/basic moieties in MXenes could serve as catalytic centers that destabilize the intercalating species.

Water and Intercalated Protons Exhibit Limited Dynamics in Tungsten Oxide Hydrates for Electrochemical Energy Storage

J. B. Mitchell, N. R. Geise, A. R. Paterson, N. C. Osti, Y. Sun, S. Fleischmann, R. Zhang, L. A. Madsen, M. F. Toney, D.-E. Jiang, A. I. Kolesnikov, E. Mamontov, and V. Augustyn, *ACS Energy Lett.* **4**, 2805 (2019)

There is widespread interest in determining the structural and dynamical features of redox-active electrochemical energy storage materials that enable simultaneous high power and high energy density. Structural water can be found in diverse classes of materials, and it has been hypothesized that proton transport in materials with extended structural water networks may occur via the Grotthuss mechanism, whereby very fast (picosecond time scale) proton transport occurs by hydrogen bonding to adjacent water molecules [X. Wu *et al.*, *Nat. Energy* **4**, 123 (2019)].

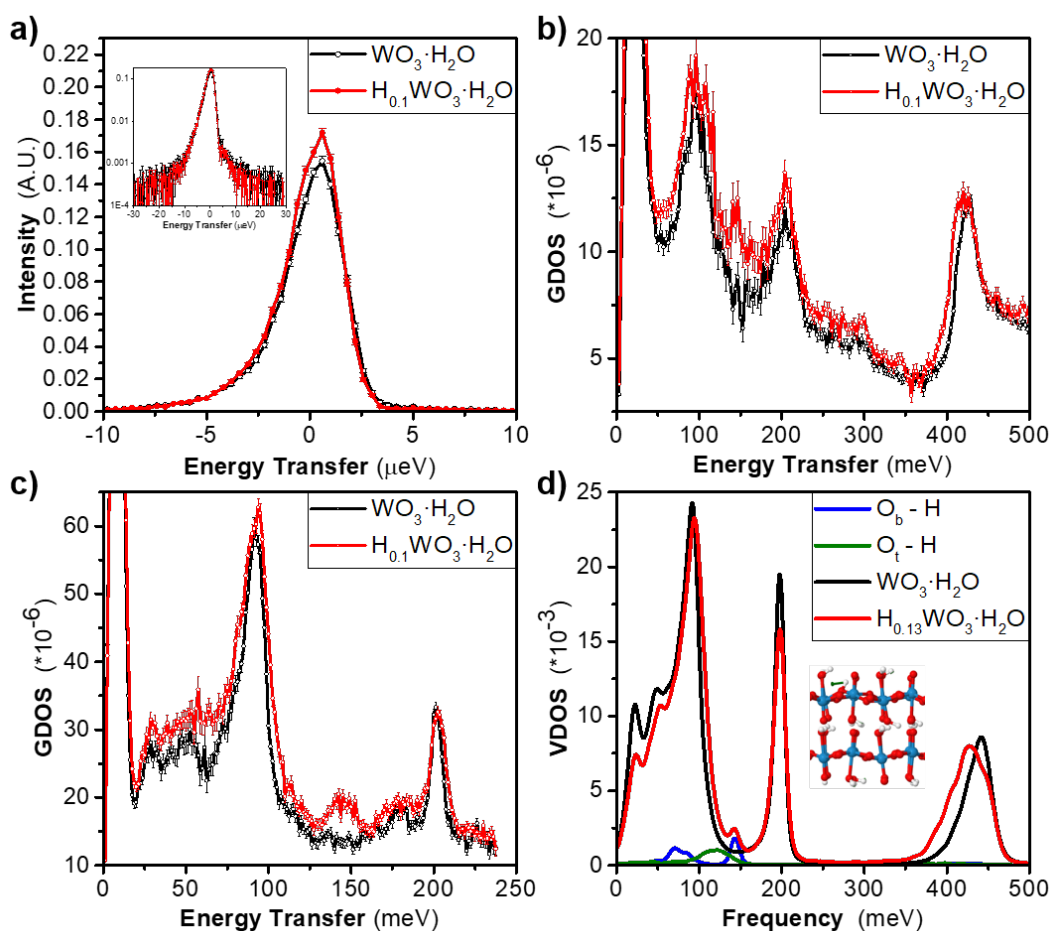


Figure 7.8. (a) QENS in the pristine ($\text{WO}_3 \cdot \text{H}_2\text{O}$, black) and proton intercalated ($\text{H}_{0.1}\text{WO}_3 \cdot \text{H}_2\text{O}$, red) states at $T = 300$ K. INS of the same electrodes at $T = 5$ K with incident energies (b) 600 and (c) 250 meV. Generalized vibrational density of states (GDOS) from INS and ab initio MD simulations of the vibrational density of states (VDOS, (d)) show the effect of intercalated protons at the bridging oxygen atoms to the overall spectrum.

In order to understand the role of structural water during proton transport that is coupled to a faradaic reaction, we investigated de/intercalation of protons in hydrated tungsten oxides, $\text{WO}_3 \cdot n\text{H}_2\text{O}$, by using inelastic (INS) and quasi-elastic neutron scattering, solid-state nuclear magnetic resonance, X-ray diffraction, and ab initio molecular dynamics (AIMD) simulations.

INS was utilized to determine the intercalated proton binding site in $\text{H}_x\text{WO}_3 \cdot \text{H}_2\text{O}$. The intercalated protons lead to the presence of a new peak at ~ 150 meV and a shift in the O–H stretching mode peak to ~ 420 meV, as compared to the pristine electrode, in good agreement with AIMD and DFT calculations, which reveal that the peak at ~ 150 meV is consistent with the W–O–H bending mode of a proton present at the bridging oxygen (O_b) site.

Our measurements reveal that confined interlayer water in crystalline tungsten oxide hydrates, $\text{WO}_3 \cdot n\text{H}_2\text{O}$, enables highly reversible proton intercalation at sub second time scales. We determine that the rapid electrochemical proton intercalation is due to the ability of the confined water layers to isolate structural transformations to two dimensions while stabilizing the structure along the third dimension. As a result, these water layers provide both structural flexibility and stability to accommodate intercalation-driven bonding changes. This provides an alternative explanation for the fast energy storage kinetics of materials that incorporate structural water and provides a new strategy for enabling high power and high energy density with redox-active layered materials containing confined fluids.

7.4 GENERAL USER PROGRAM

From 2017 to 2019, 177 general user proposals were submitted to SEQUOIA, of which 91 were selected, resulting in 156 unique users. The SEQUOIA user community includes individuals with diverse scientific backgrounds. The largest user community would be comprised of condensed matter physicists who study hard or soft condensed matter systems (for a more detailed breakout of the science areas see pie chart in the Appendix). The most used sample environment at SEQUOIA is the bottom loading closed cycle refrigerator (CCR). This operates both in a single crystal and a powder configuration. In the powder configuration, three samples can be loaded onto a sample changer. Other commonly used sample environments include a top-loading CCR, a liquid helium-based cryostat, and the vertical field superconducting magnets available in the sample environment suite.

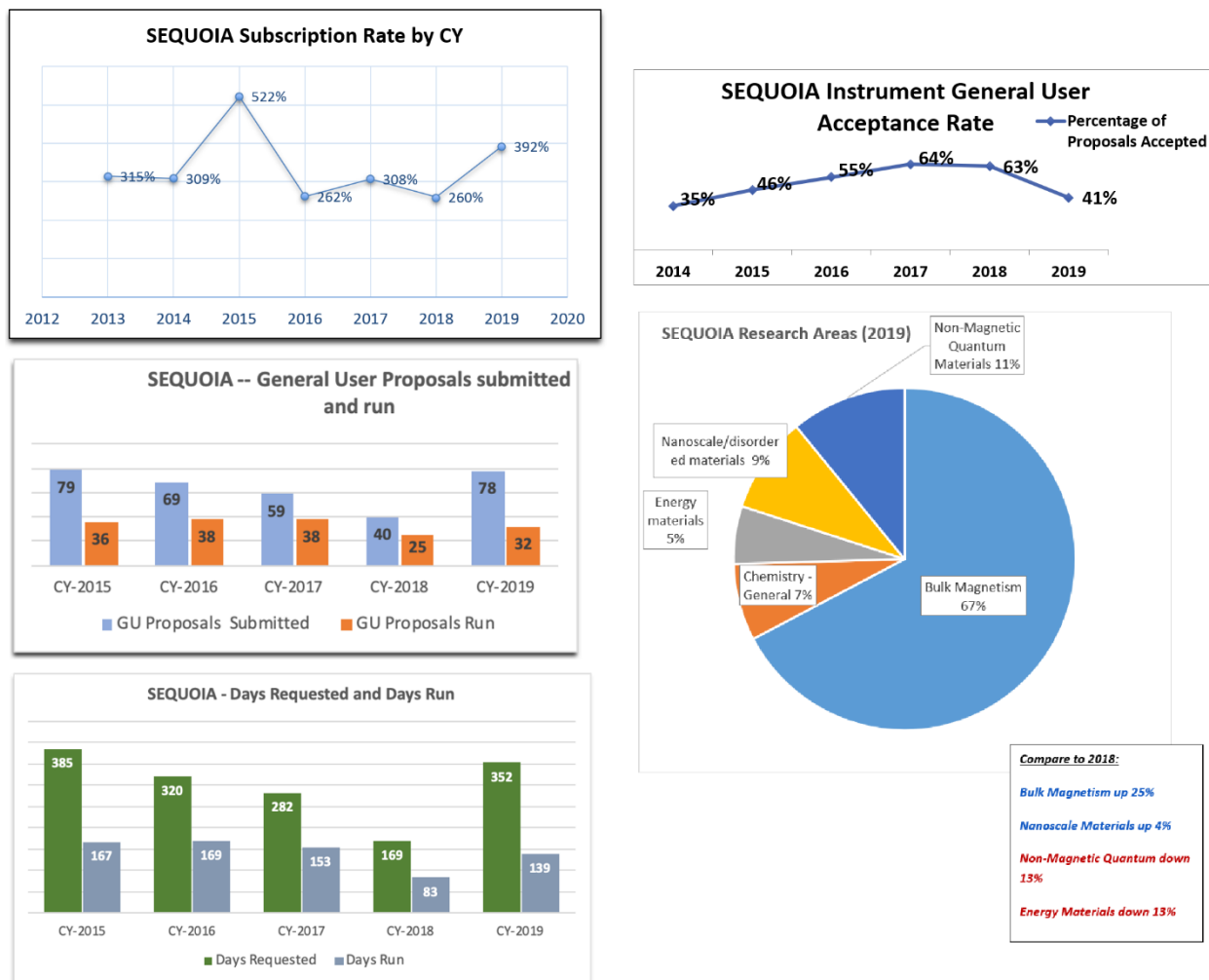


Figure 7.9. SEQUOIA user program statistics

7.5 UPDATE ON INSTRUMENT DEVELOPMENT ACTIVITIES

There have been three upgrades during the past three years. The capabilities of the vacuum system have been improved, additional detector coverage at SEQUOIA has been acquired, and the three-sample changer of the bottom loading CCR has been redesigned for more rapid deployment in the field.

In 2015, an effort was made to identify weaknesses in the vacuum system at SEQUOIA. These included having no back-up or redundancy in the high vacuum system on the sample chamber, having a control system that was different from other in-house systems and difficult to maintain by the local groups, and safety concerns regarding the cabling within the high vacuum control panels. In 2016 funding was awarded to solve these issues. A superior roughing pump was installed on the detector chamber, a turbo pump capable of a full pump down sequence was added to the sample chamber, two turbo pumps were added to the detector chamber for further redundancy and to provide a means of leak checking, vendors have supplied a new cabinet with separate power and controls sections, and a new control interface has been installed. Installation and testing were completed in May of 2018. There has been no loss of beamtime due to vacuum system failures at SEQUOIA since this installation. Pump down time for the detector tank has improved from 15 hours to 9 hours under ideal conditions. This is the time it takes to bring the

detector tank from atmosphere to a pressure below $9E-5$ Torr. Base pressures have decreased in both the detector and sample chambers due to the operation of the turbopumps. The Turbopumps are not able to replace the performance of the cryopumps, but they are additional pumping capacity and redundancy. The sample chamber pump down times were previously between 15 and 30 minutes. Sample chamber pump down times are now regularly less than 7 minutes.

SEQUOIA has also begun a slow acquisition of additional detector coverage. Four 8-packs have been installed below the beam stop in row one of the instrument in 2019. An additional 8-packs is purchased and will be installed in the winter 2020 outage. Another 8-pack will be installed in the summer 2021 outage. This will complete one segment of the bottom row of the SEQUOIA detector array.

We have also redesigned the three-sample changer for the bottom loading CCR. Previously, installation of the changer sample mounts would require detaching and attaching portions of the CCR cold finger and thermometry. This process was time consuming and often resulted in broken wires. We have incorporated the three-sample changer into the cold finger so that only the attachment of a single piece of shielding with one fastener is able to place the CCR in the three-sample configuration.

7.6 UPDATE ON IDT AND DISCRETIONARY BEAM TIME

The SEQUOIA IDT has officially ended in 2018. Since this time up to 25% of the beamtime has been awarded to discretionary proposals. The publication rate for Ph.D. dissertations and publications has been maintained through this transition. Discretionary time requires a full written proposal to be submitted. This request is reviewed by the Direct Geometry Spectroscopy group leader and the division director. Neutron Scattering Division staff are eligible to submit proposals for discretionary beam time.

7.7 OUTREACH

The SEQUOIA chopper spectrometer and the experiment team participates every two years in the Department of Energy's National School on Neutron and X-Ray Scattering. The instrument and team provide hands-on experience in using the instrument and the examination and treatment of measured data provided by the instrument. This school provides graduate students and post-doctoral researchers an excellent learning opportunity in the field of inelastic neutron scattering. Some of the students which participate in this school become users of the instruments later in their career path.

The SEQUOIA team has published a 2016, 2017, and 2019 issue of an instrument newsletter called *The Syllabary*. SEQUOIA's namesake is a native American member of the Cherokee tribe who invented a written language of syllables (i.e. a syllabary) of the Cherokee nation in the early 19th century. The newsletter (example front page shown in Figure 7.10) is sent to a mailing list of more than 300 individuals that are users, potential users, and stake holders of the SEQUOIA instrument. The newsletter provides information concerning the instrument development, how to apply for time at the facility, recent scientific highlights and a list of recent publications and theses which feature SEQUOIA measurements.

Team members from SEQUOIA have participated in and helped organize workshops to grow the user community. These include the Quantum Materials Young Investigator's workshop in 2018 and 2019 at ORNL. SEQUOIA team members have also presented webinars discussing the "First Experiments at the Second Target Station." In addition, in April of 2018, a SEQUOIA team member has participated in discussions with United States Senate and House of Representatives staff concerning the science done with neutron scattering at the SNS and HFIR at ORNL.

Team members from SEQUOIA have also presented results of instrument measurements at national and international conferences in both contributed and invited talks. One member of the SEQUOIA team has worked at the *science trailers* organized by the neutron scattering directorate and ORNL. These events occur at public functions and serve to educate the community concerning the scientific activities occurring within the neutron directorate and within ORNL.

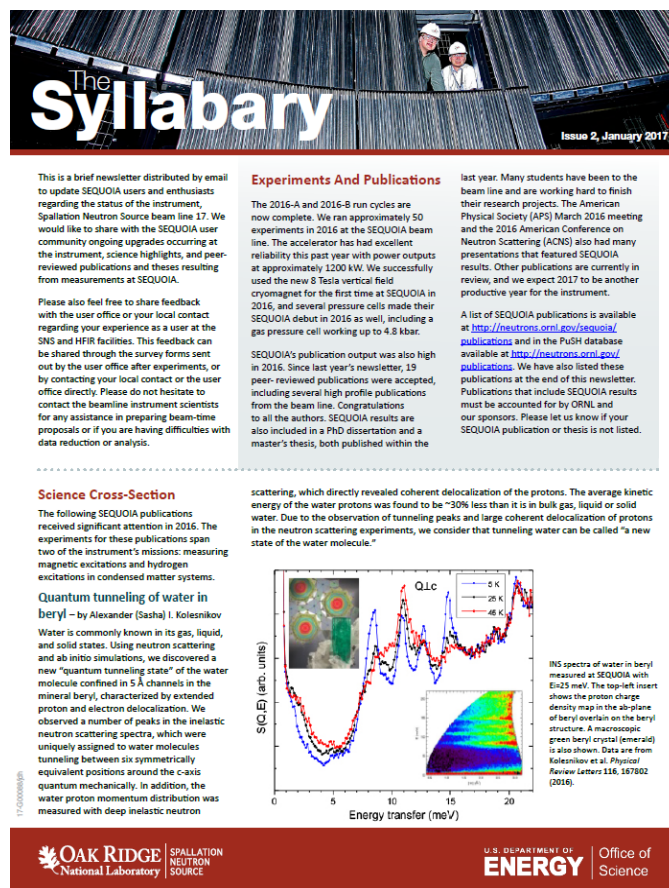


Figure 7.10. First page of issue 2 (January 2017) of the SEQUOIA newsletter, *The Syllabary*. The newsletter is sent by email to more than 300 SEQUOIA stakeholders. It contains information on recent science at the instrument, publications, and how to apply for beamtime at the instrument.

7.8 VISION

Near-term Vision (1-3 years)

SEQUOIA is now a well-established and highly in-demand instrument among the inelastic neutron scattering community. It is SEQUOIA's goal to become the world-wide chopper spectrometer of choice for the study of correlated electron and hydrogen dynamics at thermal neutron energies. In our 2017 instrument review, the near-term vision was to eliminate or minimize the potential failure points that have been apparent in past operation of the instrument while designing longer-term hardware upgrades that will expand the scientific capabilities. We have achieved the goal of minimizing failure points in the instrument operation, and we have begun longer-term hardware upgrades for the instrument. We will continue to have the near-term goal of expanding instrument capabilities with hardware investments. We will be adding the goal of maximizing efficient use of the instrument to take full advantage of the increase in neutron flux as the power of the SNS is increased.

These two goals are to be performed while maintaining the operation and scientific output of the SEQUOIA instrument. There are also significant opportunities that exist in the realms of data management, reduction, standardization and analysis. We list here goals of the instrument team for SEQUOIA over the next three years.

- Contribute to further improving the instrument DAS with the Instrument Data Acquisition and Controls (IDAC) group in the Neutron Technologies Division.
- Request and receive funding for design, purchase and installation of neutronic shielding for the floor and lower rear wall of the detector tank. There is a significant vertical dependence in the instrument background. There is more background in the detectors nearest the floor of the detector chamber. We believe this is due to the lack of shielding on the floor behind the detector array, and the lack of significant shielding on the rear interior walls of the detector chamber. Shielding these areas will improve the anisotropic background and increase the signal-noise ratio for the entire instrument. The ARCS instrument has observed a similar anisotropic background to a lesser degree.
- Procure funding for and perform the design of the Brillouin scattering option for SEQUOIA. Please see the Brillouin scattering option subheading for further details.
- Procure funding for the preliminary design of a radial collimator for the scattered beam at SEQUOIA. SEQUOIA has no radial collimator. We have gone through a preliminary design considering placement of the collimator. The current location of choice for such a collimator is in the SEQUOIA sample chamber. We previously considered a radial collimator in the detector tank; however, this installation would limit the range of scattering angles out of plane and the collimator would need to remain permanently installed. A preliminary design needs to be done to make certain the collimator would fit within the boundary conditions of the sample chamber and allow its use with both small and larger sample environments.
- A 14 T magnet has been delivered to the SNS. SEQUOIA will test operation of this large magnet at the beamline in August and September of 2020. Suitable preliminary measurements will be considered for this test.

- Creating a rapid mail-in system for SEQUOIA measurements. Guidelines are being developed within the Neutron Science Directorate for establishing and maintaining a mail-in research program. SEQUOIA would like to begin the establishment of a mail-in system in order to provide users rapid access for emerging studies in the community. We anticipate devoting approximately 5% of the general user beam time to mail-in rapid access proposals.
- A new top loading CCR is to be acquired in 2020 with the ARCS instrument. This CCR will have the convenience of a top-loader with the fast-cool down times and low backgrounds associated with a bottom loading CCR. This will allow measurements to be done where users are allowed to change samples and the low background of the bottom loading CCR is preserved. It will include a gas handling system that will automatically pump-out exchange gas when the temperature of the CCR increases above 325 K. This will save measurement time and allow for more consistent gas loading of the CCR (i.e. a fixed volume of gas at room temperature will be used for every measurement below 325 K).

Brillouin Scattering Option: SEQUOIA’s energy scale and large secondary flight path make it well suited for Brillouin Spectroscopy measurements. The SEQUOIA team is proposing upgrades to allow for an increase in scattering coverage of the first Brillouin zone of condensed matter systems. This project leverages an intersection of capabilities at ORNL and the neutron scattering facilities.

The addition of small angle detectors at SEQUOIA will extend the kinematical region for neutron scattering to low momentum transfer (Q) while keeping energy transfer relatively large. Fig. 6.9 compares the Q - E relations for scattering angles 0.5 and 5 degrees for different values of incident energy, E_i . The current minimum scattering angle for SNS spectrometers is approximately 3 degrees. An incident beam collimator and a third Fermi chopper (high energy, high resolution) would also need to be added to the instrument to allow SEQUOIA to operate as a Brillouin spectrometer. This technique is currently used at the HRC instrument at JPARC with success [S. Itoh, *et al.*, J. Phys. Soc. Jpn. **82**, SA033 (2013)]. Accessing the additional kinematical region will allow new experimental studies in condensed matter systems, e.g.

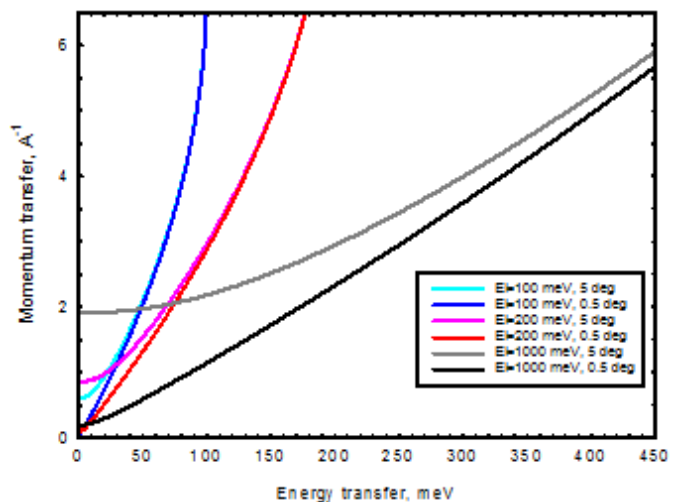


Figure 7.11. Kinematically accessible region of momentum transfer and energy transfer space for several incident energies. Lines are shown for detectors located at 5 degrees and at 0.5 degrees scattering angle. The region above each line is the portion accessible by inelastic neutron scattering. The current proposal is to extend the detector coverage at SEQUOIA to 0.5 degrees in scattering angle.

- i) To study the magnetic excitation spectrum of correlated electron materials with ferromagnetic fluctuations. A ferromagnet’s cross-section is greatest around $Q \sim 0$ wave-vector transfer. Accessing lower values of Q allows for accurate measurements of ferromagnetic excitations [S. Itoh, *et al.*, J. Phys.: Conf. Ser. **502**, 012043 (2014)]. With the ability to directly measure the first Brillouin zone in a ferromagnet, we will be able to quickly determine fundamental parameters concerning the ferromagnet behavior without the need for single crystal measurements.

- ii) To measure collective dynamics in hydrogen bonded materials (not only water) in solid, liquid (supercooled) and supercritical states (see e.g. F. Sacchetti, *et al.*, Phys. Rev. E **69**, 061203 (2004) and A. Consolo, Adv. Cond. Matter Phys., Article ID 137435 (2015));
- iii) To investigate transport of small molecules through biological membranes mediated by phonons [F. Sacchetti, *et al.*, Phys. Rev. E **69**, 061203 (2004)];
- iv) To study the effect of “phononic propagation and localization in liquid noble gases and the existence of both low- and high-frequency phononic gaps at THz scale” [M. Zhernenkov, *et al.*, Nature Comm. **7**, 11575 (2016).]. This research will “support the developments of sound control and heat management through phononic gaps manipulations at meso- and nanoscales. In particular, the phononic gap manipulation can be realized by immersing nanoparticles (with directional bonds between them) in liquids and aqueous solutions of interest. Tuning size, shape and material of the nano-blocks is the key factor for the emerging technology of phononic harvesting nano-clusters and for the phononic gaps engineering with controllable sound output, ... and “will advance the field of metamaterials at the THz scale” [D. Bolmatov, *et al.*, Sci. Reports **6**, 19469 (2016).].
- v) To access clearly the magnetic cross-sections of 4d/5d/4f magnetic materials. The magnetic form-factor of these ions is shifted to very low wave-vectors, making accurate measurements difficult at currently available scattering angles [S. Calder, *et al.*, Nature Comm. **6**, 8916 (2015)].

Detector Installation Path: SEQUOIA has installed four additional 8-pack detectors since 2017. SEQUOIA now has 61.8% of its detector array installed. There are five rows available for detectors to be installed at SEQUOIA, and only three of these rows currently are populated substantially with detectors. Two additional 8-pack detectors will be installed between 2020 and 2021 to raise the percentage to 63%. We propose an upgrade path to fill out the entire detector array. Note that 35 8-packs is approximately \$600,000 (This estimate was verified by K. Berry on 6/13/2017). Seventy-six 8-packs are not installed. The detector upgrade path also includes a redesign of the area around the beam-stop to allow for measurements to smaller scattering angles. This would require the purchase of between 2 and 4 8- or 16-packs. 16-packs near the beam-stop may improve wave-vector resolution of features in this vicinity for thermal wavelengths.

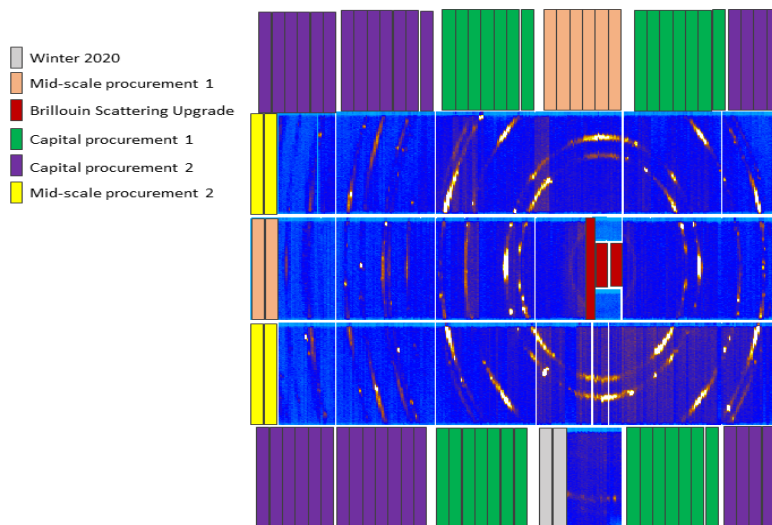


Figure 7.12. : Detector upgrade path for SEQUOIA, BL17, at the SNS. The Brillouin Scattering upgrade will add detectors in the vicinity of the beam-stop, shown in red

Figure 7.12 illustrates the detector upgrade path and locations of detectors for each phase.

Winter 2020 – Two 8 packs will be installed to complete the section in the first row below the beam stop.

Mid-scale procurement – A midscale procurement proposal for eight 8-packs is being submitted in July of 2020. These detectors will be placed in the fifth row above the beam stop and at the highest scattering angles of the middle row.

Brillouin upgrade – a high density of pixelated detectors will be placed inside the beam stop.

Capital Procurement 1– twenty-eight (28) 1.2 m long, 1-inch diameter 8 packs installed at the smaller scattering angles available in the top and bottom detector rows of the instrument. These would be arranged immediately above and below the beam stop and improve the low-angle coverage of the detector array. This is especially useful for measurements of magnetic excitations in single crystals.

Capital Procurement 2 – twenty-six (26) 1.2 m long, 1-inch diameter 8 packs - Install 8-packs in the remaining top and bottom row positions of the instrument. This will provide additional powder averaging of data for powder samples at larger wave vector transfers as well as an increase in out of plane reciprocal space coverage for single crystal samples.

Mid-scale procurement 2 – A midscale procurement proposal for four (4) 8-packs to be placed at the highest angles of the second and fourth rows of the detector coverage.

Strategic Vision (3-10 years) and Alignment with NScD/ORNL Strategic Plans

The longer-term vision of the SEQUOIA instrument is to perform selective hardware installations and upgrades that will improve the efficiency of the instrument, improve the ratio of signal to noise and allow for additional scientific capabilities that are not available elsewhere within the neutron scattering facilities at ORNL. It is the goal of the SEQUOIA beamline staff to make SEQUOIA the fastest (greatest scattering intensity) inelastic instrument in the world with the best signal to noise to perform measurements over the range of 10 meV to 2000 meV incident energy. The proposed upgrades are also chosen to transition well to the capabilities being promoted for the inelastic instrument suite at the second target station of the SNS. We provide here a list of these instrument upgrades which will have the greatest scientific impact on the SEQUOIA instrument.

7.9 FUNDING/RESOURCES NEEDS

To increase the scientific throughput measured in the number of publications from the instrument there are three investments that should be made. Opening up the bottle neck from experiment to publication (i.e shortening this time) is crucial to the output of the instrument. One way to shorten this time frame is to improve the software which users use to visualize and analyze their measurements. The majority of users at the instrument are using software provided by other neutron scattering facilities (Dave-Mslice from the NIST Center for Neutron Research is used most often for powder samples, Horace from the ISIS facility is used in some cases for single crystal measurements). This software was not intended for examining the large datasets which are created from single crystal measurements at SEQUOIA. However, users use this software because it is more documented, easier to use, and operates more clearly with less crashes than any other software available. The lack of appropriate visualization and analysis software is a road-block that needs to be cleared.

Another investment that will improve the scientific output of SEQUOIA is in the hardware upgrades for the instrument which have been listed here. These upgrades are chosen and prioritized to yield the greatest impact and improvement in data quality and speed of operation of the instrument. In the case of the Brillouin scattering option, they also expand the scientific mission and therefore the user community of the instrument. The total investments in physical equipment listed here total approximately \$2M. This includes a radial collimator, the Brillouin Scattering spectrometer option, more shielding on the instrument, filling out of the entire detector array, and a change in the final guide optics.

If cost were not a barrier, adding additional FTE instrument scientists would improve the scientific output of the instrument. This would increase throughput of experiments, provide more individualized assistance to users in data analysis and writing manuscripts, and allow for the instrument scientists to have additional time to concentrate on instrument upgrade projects. However, cost is, of course, a barrier. A reasonable option would be to add a single FTE that would work on both of the thermal chopper spectrometers (ARCS and SEQUOIA). This would result in 2.5 FTE instrument scientists at both ARCS and SEQUOIA and an increase in scientific throughput from both of these instruments.

7.10 FUTURE FUNDING OPPORTUNITIES

The excellent past performance of the SEQUOIA instrument relative to that of the higher sample throughput instruments in need of upgrades has likely hampered the case for upgrade funding. Past efforts for funding have been made through the LDRD process, the directorate level large procurement process, and the directorate level mid-scale procurement process. The instrument team will continue to pursue these funds at the laboratory and directorate level. LDRD funding will also be pursued by the instrument scientists for scientific projects which will make use of the SEQUOIA beamline. These will often be in collaboration with other ORNL scientific staff.

7.11 SELF-ASSESSMENT

Strengths

A great strength of the SEQUOIA instrument is the ability to provide both high flux and high-resolution modes of operation very quickly over a range of incident energy (20-200 meV) neutrons. It takes less than 5 minutes in most cases to switch modes of operation. Other facilities require craning out the beamline choppers and installation of a different chopper over the course of multiple hours. The large flux of thermal neutrons from the SNS and the large detector coverage of the SEQUOIA instrument together are responsible for the success of the instrument. Another strength of the instrument is the beamline staff at SEQUOIA. The instrument scientists' scientific background couples well with the scientific mission of the instrument. The service minded attitudes of the beamline staff (SA, and Instrument Scientists) has been a significant asset to the instrument. The beamline staff works well together to deal both with the daily operation of the instrument as well as expanding the horizons of the instrument's capabilities.

Weaknesses

The large flux of the SNS has made background reduction not a significant priority for instrument development. Users are beginning to demand more of the instruments capabilities as the initial generation of measurements has been accomplished and published. These experiments require improved

signal to noise typically under limited sample conditions. SEQUOIA needs to be funded to improve its background. A scattered beam radial collimator should be installed to reduce the background from complicated sample environments (liquid helium cryostats, cryomagnets, and furnaces). Furthermore, the signal measured can be increased at SEQUOIA through an investment in the approximately 64 8-packs of detectors that can be installed at the instrument. The measurements being performed at SEQUOIA have been skewed toward more correlated electron materials than dynamics in hydrogenous systems. This has been in part due to the VISION beamline taking a portion of this work from SEQUOIA. There is also a large oversubscription rate at SEQUOIA. This leads to the possibility of alienating the instruments user base if the distribution of beam time awarded is not considerate of the scientific backgrounds being represented across the instrument suite at SNS/HFIR and the amount of time awarded to underrepresented research groups. The software available for data acquisition, visualization, and analysis are also all weaknesses that contribute to making it difficult for users to acquire, visualize, analyze and ultimately publish their results.

Opportunities

The development of the Brillouin scattering option for SEQUOIA has the potential to attract a new population of users to the beamline to take advantage of this capability. This option would also be of use to the current user community of the instrument. Any software for visualization and analysis that is stable, fast, has a well-documented manual with examples, and can do whatever the current software is capable of (but better) will result in a greater throughput of scientific publications from the instrument.

Threats

Difficulties with the instrument vacuum components, detector electronics, and the prior DAS have been overcome. There is always a risk of a catastrophic vent of the detector chamber which would result in costly damage to the detector electronics. These *passion vents* have not occurred since approximately 2010 or 2011 at SEQUOIA. We will continue to operate the instrument with this possibility in mind

Competitors of the SEQUOIA beamline include ARCS at SNS, MERLIN and MAPS at ISIS, and 4SEASONS at JPARC. With the exception of the ARCS instrument, SEQUOIA has a greater publication output than the similar instruments at other neutron scattering facilities. Table 1 lists the capabilities of the SEQUOIA, MAPS, MERLIN and 4SEASONS instruments. SEQUOIA compares favorably with these other instruments. However, the instruments at other facilities are considered to have better backgrounds than SEQUOIA.

7.12 EXECUTIVE SUMMARY

SEQUOIA is a high demand thermal chopper spectrometer at the SNS. The scientific output of the instrument compares favorably to that of similar instruments at other international neutron scattering facilities. We have performed upgrades to improve the instruments reliability. There are upgrades planned that will enhance the scientific capabilities and measurement efficiency of the instrument. These are conceptualized but require funding for design and procurement. The SEQUOIA detector array is only 61.8% populated. A capital investment in detectors would provide an expansion of the instrument's capabilities.

7.12.1 Comparison of instrument specifications to similar instrument worldwide

	SEQUOIA	MERLIN (ISIS)	MAPS (ISIS)	4SEASONS (JSNS)
Moderator	Ambient poisoned decoupled water	Gd poisoned water	Gd poisoned water	Coupled hydrogen
Source frequency	60 Hz	50 Hz	50 Hz	25 Hz
Avg. Flux (n cm⁻² s⁻¹)	1.7 x 10 ⁵ @ 1.2 MW	6 x 10 ⁴	2 x 10 ⁴	1x10 ⁵ @ 1MW
Flight Path	L ₁ +L ₂ = 20 m L ₃ (min) =5.5 m	L ₁ +L ₂ = 11.8 m L ₃ (min) =2.5 m	L ₁ +L ₂ = 12 m L ₃ (min) = 6 m	L ₁ +L ₂ = 18 m L ₃ (min) = 2.5 m
Beam size	5 x 5 cm ²	5 x 5 cm ²	5.5 x 5.5 cm ²	4.5 x 4.5 cm ²
Scattering angles	2° - 59.3°	3° - 135°	3° - 60°	3° - 130°
Incident energy	8 - 2000 meV	7 - 2000 meV	15 - 2000 meV	5 - 300 meV
Elastic ΔE/E_i	1.5 - 5 %	3 - 5 %	2 - 5%	> 5 %
Detector type	1.2m, 1" diam. ³ He LPSD	3m ³ He LPSD	~1m ³ He LPSD	2.5m ³ He LPSD
No. of detectors	896 1.2 m LPSDs	270	574	350
Detector solid angle	0.864 / 1.44 (60 %)	3.1 sr	0.45 sr	2.5 sr

8. SNS-BL5, CNCS, COLD NEUTRON CHOPPER SPECTROMETER, STATUS AND PLANNING SUMMARY

8.1 OVERVIEW AND CURRENT STATUS

CNCS is a direct geometry inelastic spectrometer designed to operate with cold neutrons. Most user experiments are conducted with <10 meV energy neutrons, but for phonon work one also tends to use higher energy ($\sim 1/3$ of the time overall). CNCS has a wide angle detector array that covers ~ 1.7 sr, which is about standard now for this class of instrument at other facilities. By design (narrow guide) CNCS stands out with finer energy resolution when compared to other in-class instruments. The flux on sample is 2-4 times higher than the best in-class competition (LET at ISIS and IN5 at ILL), at the same energy and the same energy resolution. A detailed comparison with other in-class instruments can be found further below. In standard configuration the beam on the sample is also focused vertically (~ 30 mm tall) and therefore the instrument is suited to studying relatively small samples (as measured by the standards for inelastic scattering).

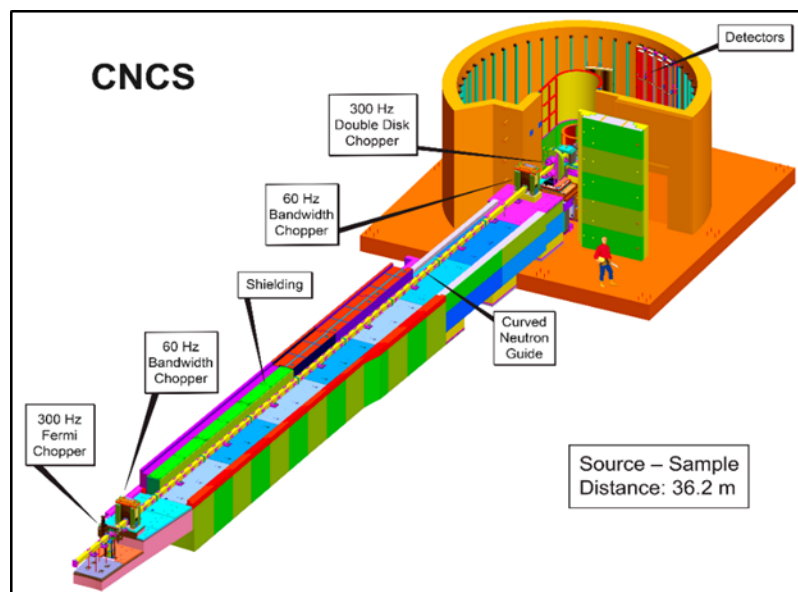


Figure 8.1. CNCS Instrument layout

CNCS is a productive instrument. During the years to review, 2017-2020 (present), 86 papers were published (20 in 2017, 28 in 2018, 20 in 2019, and 18 in 2020 as of July) in peer reviewed journals including Nature Materials, Nature Physics, Physical Review Letters, and Proceedings of the National Academy of Sciences. CNCS has been particularly successful in the areas of low temperature magnetism, heat transport in thermoelectric materials, and the secondary structure and dynamics of proteins with biological function. CNCS has benefited from highly productive collaborative research programs with several ORNL-based groups and this has been critical in some of these areas.

CNCS also hosts a world leading research program for inelastic scattering at pressure, up to 3 GPa, which is due to the focused character of the beam and a strong local interest in science with pressure.

Since the start of user operation in 2009, CNCS has consistently been one of the most oversubscribed instruments at the SNS, with oversubscription rates (requested beam time vs. available beam time) routinely between 3x and 6x. User experiments last 4.3 days on average. To date, more than 280 user experiments have been conducted and more than 182 papers have been published from this research in peer reviewed scientific journals.

The workhorse sample environment equipment is an Orange flow cryostat that operates in a 1.8 K – 360 K range, which can be extended with a ^3He insert down to 0.3 K and with a dilution insert down to 50 mK. The SNS 5 T and 8 T cryomagnets are also often used for which dilution inserts are available as well. For higher temperature, there is a bottom loading CCR that covers the temperature range 10 K – 750 K with a

100 mm sample space diameter, and a top loading CCR with a similar temperature but a 50 mm sample space diameter that causes and increased background. Most experiments (~50% – 70%) study collective excitations in single crystal materials with the sample rotation method.

A key to efficient and successful instrument operation are data acquisition and data reduction/analysis software. On the acquisition side, CNCS has been on the forefront testing and upgrading CSS/EPICS/Phoebus. The acquisition software has proven to be robust and user friendly. As the graphical user interface was written first, lower-level command-line operation is not yet implemented, but scripting has been implemented successfully with all experiments during the time of this review using scripting as the control method. Planning tools are within MANTID, and while increased synergy between MANTID and CSS/EPICS/Phoebus would increase efficiency the current model has been working without failures. Auto-reduction has been undergoing changes, and the system is generally robust. All users have been relying on the online catalogue ONCat, to help understand their experiments. While historically, data visualization and analysis has been done with either Horace or Mslice, MANTID has been increasing in share to currently stand at around 30%. Users of the single crystal MANTID software based on events have been generally pleased, but the time to generate a plot from such algorithms is typically between 30 minutes to 2 hours, so quick single-crystal plots with pre-determined user bins is needed for real-time decision making.

Team Structure

2017: Georg Ehlers (point-of-contact instrument scientist), Andrey Podlesnyak (instrument scientist), Gabriele Sala (post-doc working with Georg Ehlers), Chris Schmitt (primary scientific associate CNCS, supporting scientific associate role on HYSPEC and ARCS), Andrei Savici (embedded software scientist for HYSPEC and CNCS)

2018: Daniel Pajeroski (point-of-contact instrument scientist), Andrey Podlesnyak (instrument scientist), Gabriele Sala (post-doc working with Georg Ehlers), Chris Schmitt (primary scientific associate CNCS, supporting scientific associate role on HYSPEC and ARCS), Andrei Savici (embedded software scientist for HYSPEC and CNCS)

2019: Daniel Pajeroski (point-of-contact instrument scientist), Andrey Podlesnyak (instrument scientist), Chris Schmitt (shared primary scientific associate on BASIS and CNCS)

2020: Daniel Pajeroski (point-of-contact instrument scientist), Andrey Podlesnyak (instrument scientist), Chris Schmitt (shared primary scientific associate on BASIS and CNCS)

While the beam power at the SNS has been increasing, the staffing level at the CNCS has been decreasing.

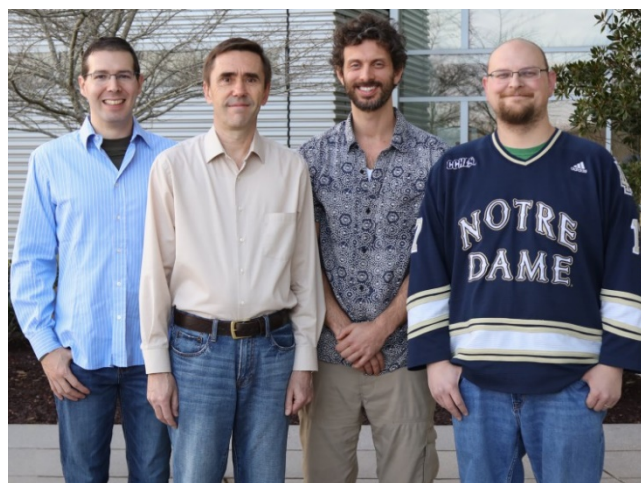


Figure 8.2. CNCS team (left to right): Gabriele Sala (postdoc working on CNCS - transitioned to STS in 2019), Andrey Podlesnyak, Daniel Pajeroski, Chris Schmitt.

8.2 SCIENTIFIC FOCUS

Research at CNCS focuses on studying collective excitations in hard and soft matter materials in the 0-10 meV range. This typically includes magnetic excitations and phonons in quantum magnets, geometrically frustrated magnets, multiferroics, and thermoelectric materials. CNCS provides an excellent complement to BASIS for quasielastic studies and frequently measures polymers, protein, or molecules in confined geometries.

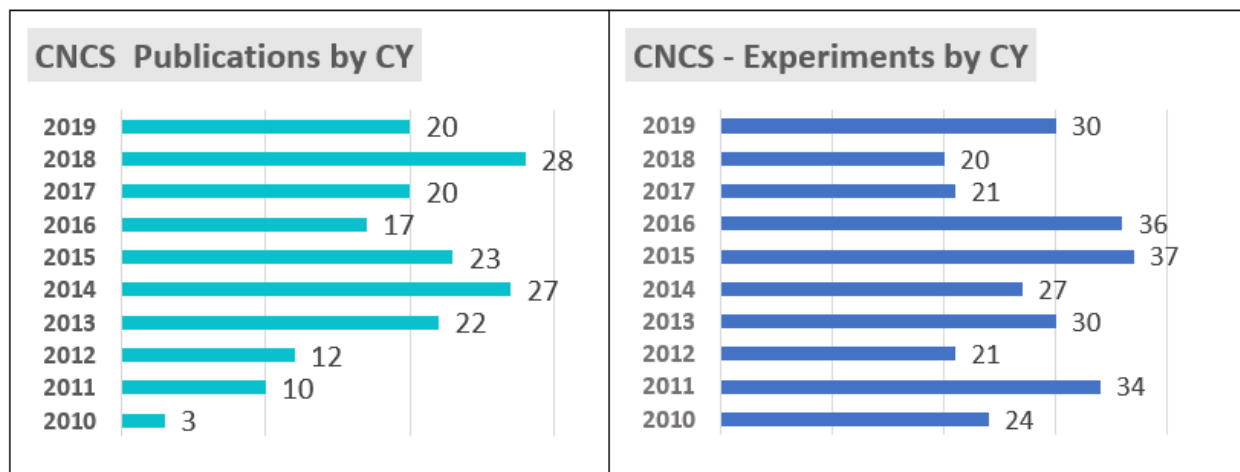


Figure 8.3. CNCS publication statistics

8.3 SCIENTIFIC HIGHLIGHTS

Anharmonic lattice dynamics and superionic transition in AgCrSe₂

Ding J., Niedziela J., Bansal D., Wang J., He X., May A.F., Ehlers G., Abernathy D.L., Said A.H., Alatas A., Ren Y., Arya G., Delaire O., *Proceedings of the National Academy of Sciences of the United States of America*, 117, 3930-3937 (2020) DOI:10.1073/pnas.1913916117.

Superionic conductors are solids that host highly mobile ions, and have applications in energy storage, energy collection, and sensing. Inelastic neutron scattering may be used to better understand the lattice dynamics in such materials to increase fundamental understanding of their useful properties. AgCrSe₂ is a thermoelectric material that has a superionic phase transition at $T_{OD} = 475$ K. The crystal structure of AgCrSe₂ is highly planar in character, whereby Ag ions intercalate between planes of CrSe octahedra and ionic conduction is within these planes. The CNCS was used to interrogate the acoustic phonons of the lattice and the Ag ion diffusion (the ARCS spectrometer was also used complementarily to investigate higher energy phonons). Using incident energies of 12 meV and 4 meV that have different Q-E ranges and resolutions, a series of temperatures were measured across the phase transition. A non-dispersive phonon branch was revealed around 3.5 meV in the 300 K data, which damps and merges with the elastic line above T_{OD} , Figure 8.4 (A-C). Superionic diffusion of the Ag ions is observed in the quasi-elastic portion of the data, Figure 8.4 (D). These results illustrate the mixed lattice dynamics inherent to superionic conductors, as the dispersive acoustic phonons persist above T_{OD} but the non-dispersive acoustic phonons are damped out. Moreover, the phonons in AgCrSe₂ as measured by neutron scattering show large anharmonicity, which also contributes to the intrinsically low lattice thermal conductivity.

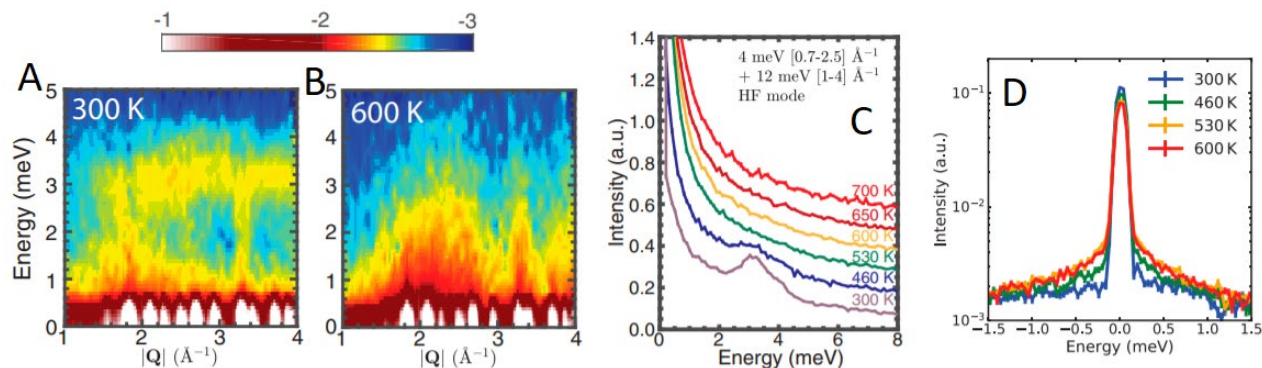


Figure 8.4. $S(|Q|, E)$ maps of AgCrSe₂ from CNCS in the (A) ordered phase and the (B) superionic phase. (C) Integration over momentum shows the temperature dependence of the flat phonon. (D) Quasi-elastic scattering shows the activated hopping.

Competing Magnetic Interactions in the Antiferromagnetic Topological Insulator MnBi₂Te₄

Li B., Yan J.Q., Pajerowski D.M., Gordon E.E., Nedic A.M., Sizyuk Y., Ke L., Orth P.P., Vaknin D., McQueeney R.J., *Physical Review Letters*, 124, 167205 (2020) DOI:10.1103/PhysRevLett.124.167204.

Topological insulators generically have an insulating interior and conducting surface fermions that are symmetry protected from scattering processes. Aside from the rich physics, there are potential applications for topological insulators as high efficiency devices or frameworks for fault-tolerant quantum computers. There are many potential twists on topological insulators, and one example is magnetic topological insulators that break time-reversal symmetry. MnBi₂Te₄ has been proposed as an antiferromagnetic topological insulator. The MnBi₂Te₄ is related to Bi₂Te₃ topological insulators, but with the insertion of magnetic Mn triangular layers. Inelastic neutron scattering is sensitive to magnetic excitations, which may be modeled to extract a magnetic Hamiltonian that in turn provides understanding of the electronic structure. Powder samples of MnBi₂Te₄ were measured on the CNCS with incident energies of 12 meV and 3.32 meV. Spin waves were observed below the magnetic ordering transition temperature and a J_1 - J_2 - J_4 model could reproduce the data, Figure 8.5 (A-C), where J_1 is the 1st neighbor superexchange in the Mn-plane, J_2 is the second neighbor superexchange in the Mn-plane, and J_4 is the 4th neighbor superexchange in the Mn-plane. Refined values of $SJ_1 = 0.30$, $SJ_2 = -0.083$, $SJ_4 = 0.023$, $SJ_C = -0.055$, and $SD = 0.12$ ($J > 0$ is ferromagnetic) were found to be qualitatively reproduced by DFT+U calculations. So, these neutron scattering experiments show that MnBi₂Te₄ has magnetic frustration, Ising anisotropy, metamagnetism, and long-range exchange interactions in the Mn-planes.

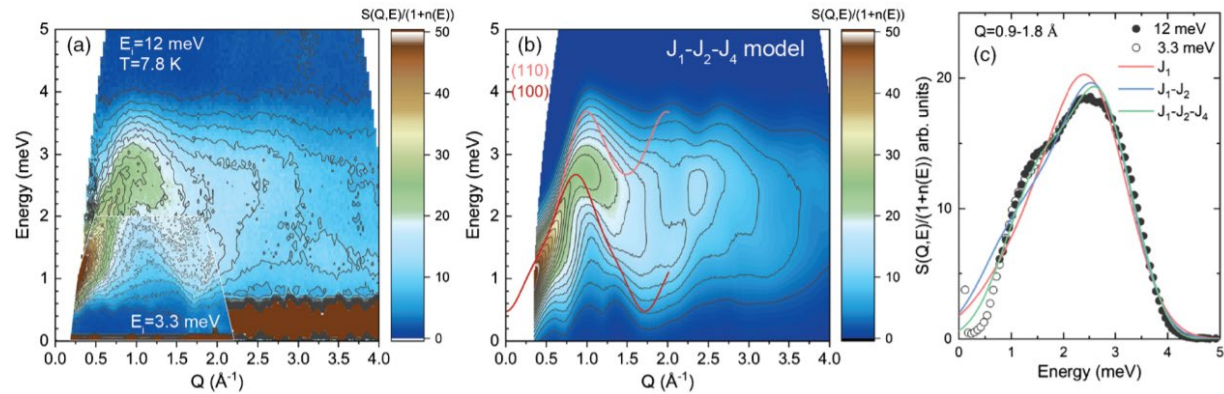


Figure 8.5. (a) Inelastic neutron scattering data from CNCS of MnBi₂Te₄ and (b) model calculations. (c) Less parameterized models (e.g. J_1 or J_1 - J_2) are unable to reproduce the experimental data.

Novel Strongly Spin-Orbit Coupled Quantum Dimer Magnet: $\text{Yb}_2\text{Si}_2\text{O}_7$

Hester G., Nair H.S., Reeder T., Yahne D.R., DeLazzer T., Berges L., Ziat D., Neilson J.R., Aczel A.A., Sala G., Quilliam J.A., Ross K.A., *Physical Review Letters*, 123, 027201 (2019)
 DOI:10.1103/PhysRevLett.123.027201.

Quantum magnetism has been surging due to the promise of quantum computation. Quantum dimer magnets are the simplest system where entanglement is required to explain experimental observations. Antiferromagnetic coupling between two $S = \frac{1}{2}$ spins results in an $S = 0$ ground state and triplet excited states. $\text{Yb}_2\text{Si}_2\text{O}_7$ is a pyrosilicate compound in which the crystal-field around the Yb^{3+} ions stabilizes them into a ground state Kramers' doublet that is well separated from the first excited state doublet. Then, there are many similarities between an $S = \frac{1}{2}$ system and the Yb^{3+} ground state doublet (often called an 'effective $S = \frac{1}{2}$ '). Inelastic neutron scattering can measure the magnetic excitations in quantum magnets like $\text{Yb}_2\text{Si}_2\text{O}_7$, and model magnetic Hamiltonians to test quantum theory. An array of crystals was measured on the CNCS using an incident energy of 1.55 meV. The crystal array of $\text{Yb}_2\text{Si}_2\text{O}_7$ was mounted in a dilution refrigerator inside of a magnet, to allow for a minimum temperature of less than 50 mK and a maximum vertical field of 8 T. In zero field, there is a single dispersive branch associated with a propagating triplon, Figure 8.6 (A). Above the first critical field ($H_{c1} = 0.4$ T for $T \sim 0$ K), antiferromagnetic long-range order is stabilized as the triplon splits and the lower branch begins to merge with the elastic line, Figure 8.6 (B-C). At 1.2 T, bulk measurements suggest the possibility for an additional phase. Finally, above the second critical field ($H_{c2} = 1.4$ T for $T \sim 0$ K) the system is field polarized, Figure 8.6 (D). The inelastic neutron scattering shows $\text{Yb}_2\text{Si}_2\text{O}_7$ to be a quantum dimer ground state, suggests Bose-Einstein condensation of triplons with applied field, and opens avenues for future study to explain the differences in quantum dimers when comparing the canonical $S = \frac{1}{2}$ to rare-earth 'effective $S = \frac{1}{2}$ ' materials.

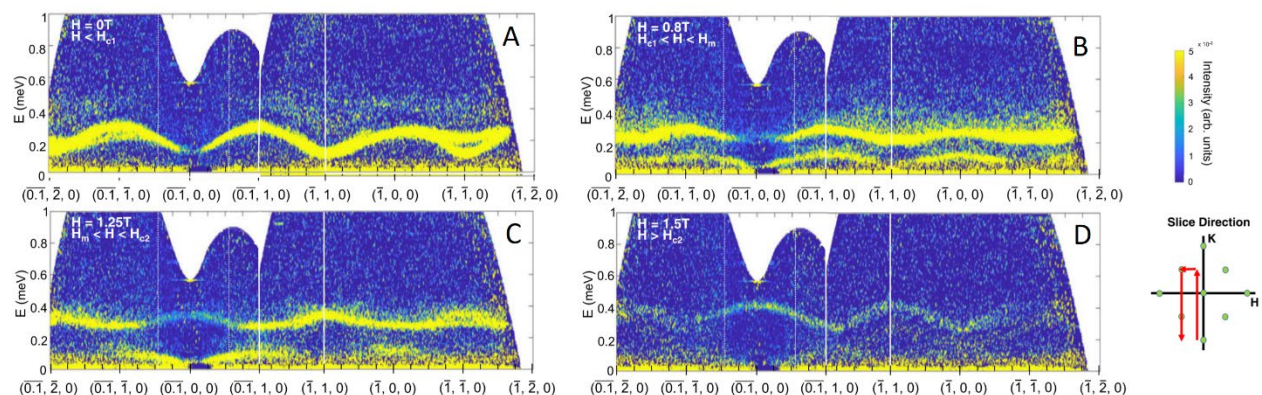


Figure 8.6. Inelastic neutron scattering data from CNCS for $\text{Yb}_2\text{Si}_2\text{O}_7$ at $T = 50$ mK and the magnetic field along the c -axis. Slices are integrated ± 0.1 reciprocal lattice units in the perpendicular direction.

Tomonaga–Luttinger liquid behavior and spinon confinement in YbAlO₃

Wu L.S., Nikitin S.E., Wang Z., Zhu W., Batista C.D., Tselik A.M., Samarakoon A.M., Tennant D.A., Brando M., Vasylechko L., Frontzek M., Savici A.T., Sala G., Ehlers G., Christianson A.D., Lumsden M.D., Podlesnyak A.A., *Nature Communications*, 10, 698 (2019) DOI: 10.1038/s41467-019-08485-7

Decreasing magnet dimensionality from three-dimensions has profound effects on the ground state and excited states, tending to suppress long range order and reveal exotic phases. One-dimensional $S = \frac{1}{2}$ spin chains are highly quantum and have been studied heavily with neutron scattering and other probes. In the pseudo-perovskite YbAlO₃, the Yb³⁺ ions are highly Ising, with a ground state doublet well separated from the excited doublets, supporting an ‘effective $S = \frac{1}{2}$ ’ description. The magnetic interactions in YbAlO₃ are highly one-dimensional, and long-range magnetic order occurs at $T_N = 0.88$ K. A single crystal of YbAlO₃ was measured on the CNCS with incident energies of 1.55 meV and 3.32 meV, using a superconducting magnet cryostat ($H_{\max} = 8$ T) along with a dilution refrigerator insert ($T_{\min} < 50$ mK). Above the Néel temperature, neutron spectra similar to $S = \frac{1}{2}$ spin chains is observed with dispersive fractionalized excitations, Figure 8.7(a). Below T_N at $T = 50$ mK, Bragg peaks appear and the spinons develop a gap, Figure 8.7 (b), becoming confined by the antiferromagnetic, staggered exchange field (B_{st}). By comparison with density matrix renormalization group theory, Figure 8.7 (c-d) spin Hamiltonian parameters were extracted to yield the intrachain interaction $J = 0.21$ meV, $B_{st}/J = 0$ above T_N , and $B_{st}/J = 0.27$ below T_N . Once in the ordered state, the application of external magnetic fields to YbAlO₃ can close the gap and induce quantum phase transitions, as shown in Figure 8.7 (e-f). These inelastic neutron scattering experiments show that f -electron materials may provide additional experimental realizations to explore one-dimensional magnetism, and that YbAlO₃ itself is well modeled as a Tomonaga-Luttinger liquid.

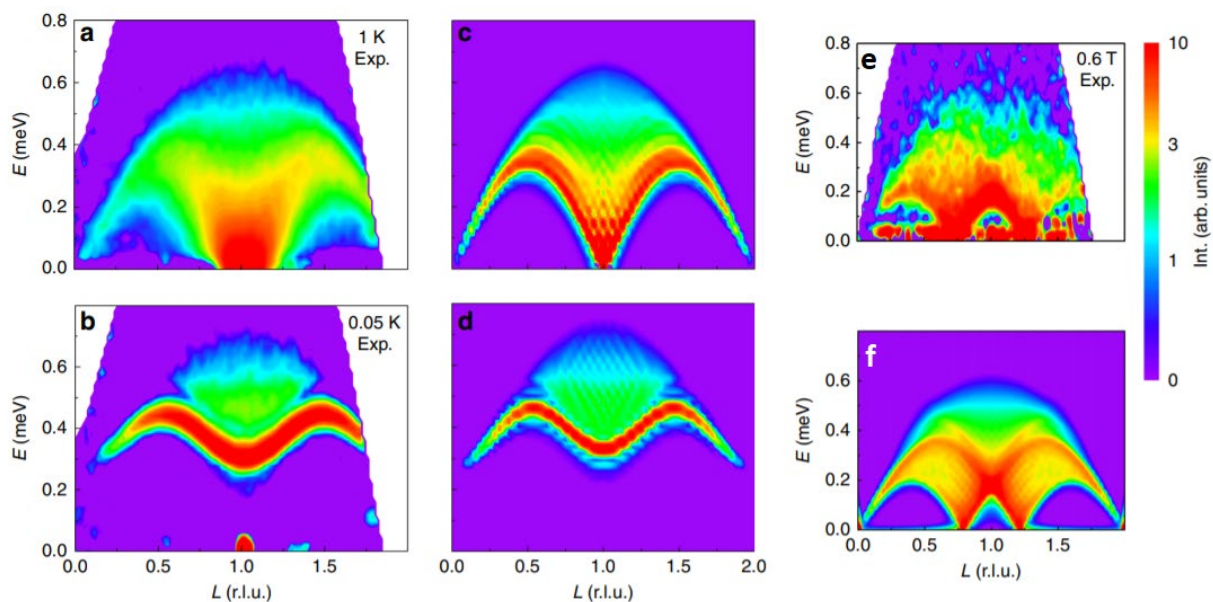


Figure 8.7. Inelastic neutron scattering data from CNCS for YbAlO₃ at (a) $T = 1$ K and (b) $T = 50$ mK, compared to density functional renormalization group calculations in (c and d). At $T = 50$ mK with an applied field of 0.6 T, the (e) experimental data and (f) density functional renormalization group calculations are shown.

Fast Rotational Diffusion of Water Molecules in a 2D Hydrogen Bond Network at Cryogenic Temperatures

Prisk T.R., Hoffmann C., Kolesnikov A.I., Mamontov E., Podlesnyak A.A., Wang X.P., Kent P.R., Anovitz L.M., *Physical Review Letters*, 120, 196001 (2018). DOI:10.1103/PhysRevLett.120.196001

Liquids confined by geometric constraints at the nanoscale are dominated by the interface and may show different phases than bulk liquids. Water is the most studied confined liquid, and its material properties are intimately connected to hydrogen bonding. Molecules in bulk water diffuse translationally and rotationally with picosecond relaxation times, while in confined geometries these diffusion times are slowed. These dynamics may be probed by quasi-elastic neutron scattering experiments. The mineral hemimorphite ($\text{Zn}_4\text{Si}_2\text{O}_7(\text{OH})_2 \cdot \text{H}_2\text{O}$) contains water molecules and hydroxyl groups that form a two-dimensional hydrogen bonded network. Diffraction experiments showed two phases: phase I) at $T > 100$ K where the water molecules orient symmetrically in the crystal towards hydroxyl groups, and phase II) at $T < 100$ K where there is a static rotation of water molecules that doubles the period of the crystal lattice along the c -axis. The CNCS was used to probe the quasi-elastic dynamics in the picosecond range (complemented by measurements on the BASIS spectrometer for dynamics at lower energies). Using an incident energy of 3 meV, spectra in temperature ranges across the phase transition were collected. Two relaxation times were observed at $T = 100$ K, Figure 8.8(a), one “slow” and the other “fast.” Both processes persist across the structural phase transition with no observable change at the transition temperature, Figure 8.8(b). The “slow” relaxation process is associated with breaking of hydrogen bonds between the confined water hydrogens and the framework oxygen atoms. The “fast” process was assigned to an orientational relaxation. These results suggest that the hydrogen bonding is intimately connected to the diffusion processes, and other two-dimensional hydrogen bonded structures would exhibit similar

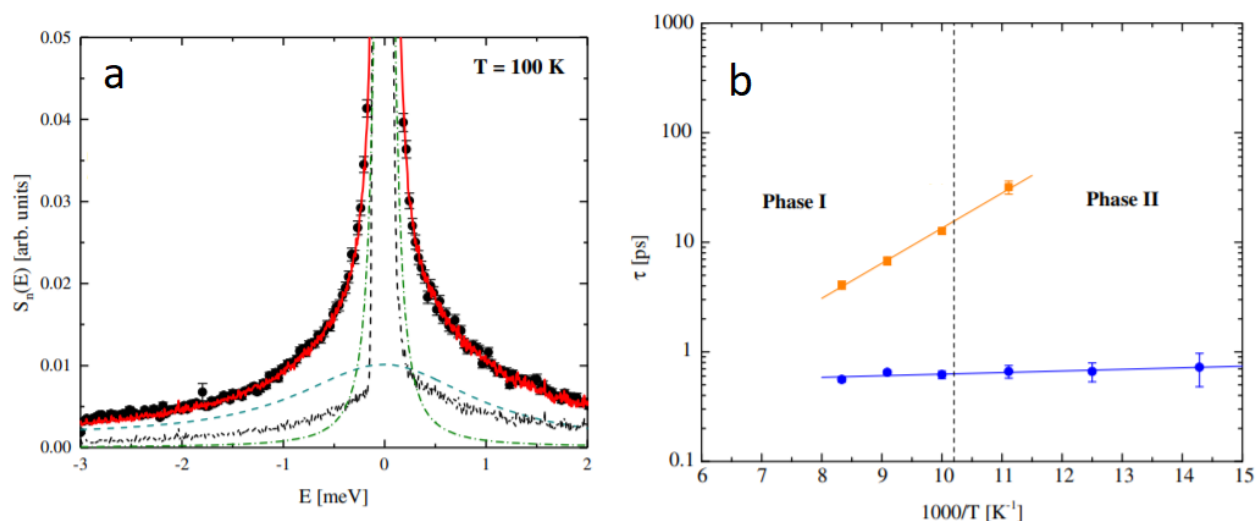


Figure 8.8. (a) The quasi-elastic scattering of $\text{Zn}_4\text{Si}_2\text{O}_7(\text{OH})_2 \cdot \text{H}_2\text{O}$ measured at CNCS with the data as black circles, the “fast” process as blue dashed line, the “slow” process as green dash-dotted line, and the solid red line being all components plus a linear background. (b) An Arrhenius plot of the proton relaxation times, with the “fast” process as blue circles and the “slow” process as orange squares. dynamics.

8.4 GENERAL USER PROGRAM

During calendar years 2017-2019, a total of 1063 beam days were requested for the general user program at CNCS. During the same time, 372 days were allocated for the general user program (35% of the demand). The user base is diverse and includes 37% U.S. government laboratories, 50% US academic institutions and 2% industry, and 11% users from foreign institutions.

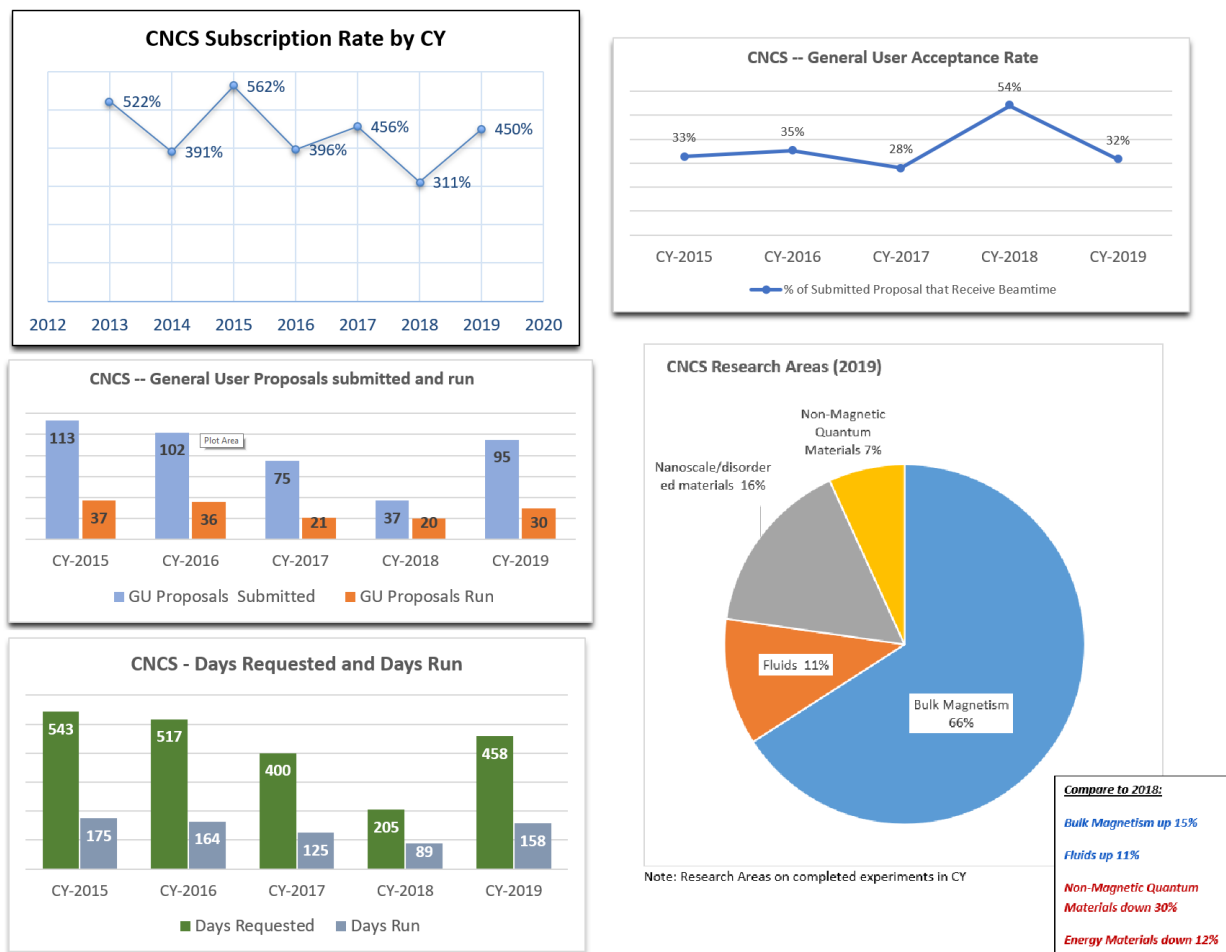


Figure 8.9. CNCS user program statistics

8.5 UPDATE ON INSTRUMENT DEVELOPMENT ACTIVITIES

Several instrument development or upgrade projects are underway at CNCS or are being discussed/planned. Broken down to different aspects of the instrument, some of these are listed in Table 3, and then detailed in the following.

Table 3. CNCS instrument developments

Incoming beam	<ul style="list-style-type: none"> • Solid-state collimator • Band-width chopper upgrade
Sample area	<ul style="list-style-type: none"> • Radial collimator • Sample stick holder in radiation area • Additional instrument control computer
Sample environment	<ul style="list-style-type: none"> • 14 T magnet • Neutron electrostatic levitator • Permanent magnet sample holder • Vertical translation stick • Rotational 3 sample changer • Vertical sample changer cells • Ruby fluorescence pressure determination
Detectors	<ul style="list-style-type: none"> • Additional beam monitor after sample • Argon management system upgrades • Detector window re-sealed
Hutch area	<ul style="list-style-type: none"> • New flooring • Window treatments • Additional cabinet space
Data acquisition	<ul style="list-style-type: none"> • CSS Phoebus • Python scripting
Data reduction	<ul style="list-style-type: none"> • t-zero methods • MANTID
pursuing	<ul style="list-style-type: none"> • New top loader CCR • Automated gas exchange system
potential	<ul style="list-style-type: none"> • End-guide elevator • Completely new guide system • Additional out-of-plane detector coverage

Solid-state collimator: In order to measure smaller scatter angles, a solid-state collimator is being tested for the incoming beam.

Band-width chopper upgrade: After changing the Fermi chopper slit package, additional spurious inelastic signals were found to present in CNCS data. The timing diagram suggested fast neutrons (>100 meV) to be the source, which are not efficiently blocked by the gadolinium absorber of the band-width choppers. Therefore, boron absorber bandwidth choppers have been installed, which reduced the spurious inelastic signals.

Radial collimator: The new oscillating radial collimator was purchased and installed, greatly reducing the background for magnet experiments and allowing detection of previous indiscernible signals.

Sample stick holder in radiation area: An additional sample stick holder has been installed, which allows for workers at the beamline easy access to the holder and to safely place potentially radioactive samples instead of removal to the radiation buffer area.

Additional instrument control computer: An additional OPI computer that controls the instrument was installed directly next to the sample environment pit, which allows workers at the beamline access to read-back and control equipment while in the sample area, thereby increasing efficiency.

14 T magnet: The CNCS has been part of the core instruments testing the new 14 T cryomagnet and has been undergoing planning of stray-fields affecting choppers, quench protection, and the mounting stage.

Neutron electrostatic levitator (NESL): The NESL provides a containerless sample environment to study

metals and reactive materials at temperatures challenging to conventional furnaces, up to 3000 °C. An emerging field, focused on the dynamics of molten and undercooled metals and the fundamental physics governing their properties, promises advances in applications ranging from the design of new castable alloys to demystifying the glass transition. Recently, a significant effort was made to commission NESL at CNCS, and several user experiments have followed. By combining their results with data from ARCS, users can rapidly extract the dynamic pair distribution function (DyPDF) of materials at ultra-high temperatures. In addition, QENS enables direct measurements of diffusion coefficients in the melt. Combined with the energies and resolution available at CNCS, these capabilities are leading edge among neutron user programs, and are driving new advancements in the field.

Permanent magnet sample holder: A 0.9 T max field permanent magnet assembly has been fitted to a standard cryostat sample stick.

Vertical translation stick: For magnets that are too heavy to allow usage of the sample stage elevator, the vertical translation stick allows for optimization of vertical sample position within the beam.

Rotational 3 sample changer: A heater was added to the existing rotational 3 sample changer, which drastically reduced the amount of time required to heat up from base-temperature to 300 K. Currently, planning is underway to re-design in a manner that decreases the specific heat of the stick to further optimize changing sample temperature.

Vertical sample changer cells: CNCS instrument developments. The ³He refrigerators, Triton NANO dilution refrigerator, CCRs, and orange cryostat have windows that are larger enough to allow multiple samples to be stacked and changed with the sample stage elevator. Cylindrical cans, flat plate cans, and single crystal holders have been used for 2 to 3 samples. Especially for ultra-low-temperature systems, this method can save large percentages of beam-time that would otherwise be dedicated to changing samples and temperatures.

Ruby fluorescence pressure determination: A clamp cell with an optical access to the sample chamber allowing in situ pressure determination using ruby fluorescence monitoring has been developed and tested at CNCS. This pressure sensor may currently be used with the wet 4He cryostat.

Additional beam monitor after sample: An additional “direct” beam monitor was installed in the plane of the detector array, behind the sample position. This beam-monitor allows for transmission measurements of samples and for calibrating the energy of the incident beam by using a standard sample along with the upstream beam monitors.

Argon management system upgrades: The addition of a liquid argon Dewar manifold allows for a faster recovery time after a detector tank opening, reduces the external resources load on research mechanics, and allows additional planning during weekends and holidays. The new argon 16-pack manifold allows for two 16-packs of gas bottles to be attached, doubling the length between bottle replacements and further protecting against catastrophic leakage of the gas system.

Detector window re-sealed: The aluminum window that separates the argon detector space from the atmosphere was re-sealed subsequent to increased oxygen presence in the detector space. After re-sealing, holding time was increased compared to the previous 5 years.

New flooring: A new floor was installed in building 8705, which allows for easier transportation of equipment and a cleaner working space.

Window treatments: Users have had difficulty working at the beamline analysis computers when the sun directly shines on their screens, so the installation of window treatments has ameliorated the problem.

Additional cabinet space: Additional cabinets have been installed to increase efficiency by allowing for greater organization at the beamline.

CSS Phoebus: The control software has been undergoing continuous upgrades.

Python scripting: Users may control the CNCS during experiments by using a Python library to send commands to the instrument, which allows for highly customizable control that would be impossible for table scans.

t-zero methods: A series of systematic methods have been developed for determination of the phenomenological timing offset parameter. Currently, the standard practice is to use a look-up table generated by measuring a vanadium calibrant.

MANTID: CNCS has participated in and driven ongoing efforts to improve MANTID, such as for single crystal data reduction and viewing.

New top loader CCR: Currently a top-loading CCR is shared between the CNCS and the BASIS. This is a 50 mm bore top-loading Janis system, which has a high background for the CNCS. The new system would optimize cooling times, allow for low- and high-temperature studies, and look towards the potential of multitudinous sample changers.

Automated gas exchange system: Currently, in order to change between vacuum and inert gas atmospheres, a worker must be on-site within the radiation area. Furthermore, there is no set standard volume of exchange gas. In-house designs and external company's products are being explored to automate the vacuum and exchange gas process associated with changing samples and changing between low- and high-temperature operations.

End-guide elevator: The last section of the guide at CNCS has 3 potential options: no guide, a straight guide, or a focusing guide. The option selected depends upon the needs of the experiment and the constraints of the sample environment. Currently, changing between these options requires a rigging team, which is expensive and also time intensive. If possible, to electronically change between different guide sections would be an improvement of efficiency. Perhaps a 4th option of an incident beam collimator could be included.

Completely new guide system: The guides at the CNCS are now more than 10 years old. Potentially order of magnitude flux increases at the sample position could be upgrading this guide system.

Additional out-of-plane detector coverage: For the past 3 years or more, there have been plans to upgrade the CNCS detector array with the Pharos detectors.

8.6 UPDATE ON IMPACT OF DISCRETIONARY BEAMTIME

Discretionary beamtime in 2018 and 2019 was found to be crucial for scheduling optimization, as unexpected failures of sample environment, failures of user's samples, and scheduling constraints require agility in the scheduling. The inclusion of Science Initiative discretionary time has put an additional strain on the schedule for CNCS.

8.7 OUTREACH AND EXPANSION INITIATIVES

CNCS staff regularly attend workshops and conferences presenting data from CNCS. Andrey Podlesnyak has participated in mentoring the post-doctoral staff members L. S. Wu and T. Xie. Daniel Pajerowski has mentored the undergraduate students Zach Nolan and Rachael Ng.

8.8 VISION

Near term vision (1-3 years)

The CNCS should continue to be world-class in the 1-3 year time window, and expect to host an international community of users. The subscription rate is expected to continue to be high (>2). The requests for complicated sample environment is expected to continue. Ultra-low-temperatures ($T < 1$ K) are inherently suited to cold disk chopper spectrometers, and must be supported in order to keep the

science program and interactions with the community healthy. High temperatures and ranged gas environments are also expected to continue to be important.

The goals of purchasing a new top loading CCR, implementing automated gas exchange systems, and full commissioning the 14 T magnet will be pursued. As the source increases in power, automation will be necessary to make use of the additional flux. Ways to perform in-situ sample changes in ultra-low-temperature systems will continue to be pursued. Multitudinous sample changers for less extreme temperatures will be considered after the commissioning of the NOMAD and VISION multi-sample changers are complete.

The reduction software should continue on the current path, with additional thrust towards user-controlled automation to avoid the pitfalls of long waits for plots to be generated that may hinder experiments and frustrate data-analysts. Support must continue for density of states, multiple scattering corrections, modeling 4-dimensional data with sufficiently accurate energy and momentum resolution.

For CNCS publications to be timely, consideration must also be put into analysis software and user training.

Strategic vision (3-10 years)

In the coming 3 to 10 years, new pulsed neutron sources that are designed more optimally for a cold neutron chopper spectrometer may come online, such as the European Spallation Source (ESS) and the Second Target Station (STS) and the SNS. At ESS, there will be the T-REX (thermal neutrons) and C-SPEC (cold neutrons). At the STS, there will be the CHES (cold neutrons) and HIGGS (thermal neutrons). As the CHES is also at ORNL, it will be the most direct competition of the CNCS.

It may be that CNCS is no longer necessary to the ORNL neutron mission once CHES comes online. Even with 20 new beam lines available at STS, it may be that a different instrument could make better use of the 60 Hz FTS beam that is currently dedicated to the CNCS. It is a possibility that one of the coupled cold moderators at the current SNS will be replaced with a decoupled (cold or thermal) moderator for overall better balance between the sources. In such a scenario, work that would have been performed at CNCS would instead be performed at CHES.

Conversely, it may be that the capital investment associated with creating a new instrument to replace and already mature and productive instrument (the CNCS) is not deemed appropriate. In this situation, experiments would continue at the CNCS. Indeed, the current planning of CHES has a decreased resolution compared to CNCS, in order to maximize flux, and it could be the instruments play complementary roles. If guide upgrades to the CNCS are pursued, the brightness difference between CHES and CNCS would be less extreme (the source being the limiting factor). Moreover, the CHES instrument design does not allow for large equipment at the sample position and the CNCS could still play a role for high magnetic fields, levitators, and similar.

CHES is a concept for a direct geometry inelastic spectrometer that will be built at STS, dedicated to studying small samples. It will receive beam from a cold coupled moderator and take full advantage of the increased peak brilliance of the high brightness STS coupled moderators. The neutron spectrum and scientific mission of CHES and CNCS will overlap to a large extent. Another instrument concept that deserves to be mentioned in this context is HIGGS (High intensity Indirect Geometry Graphite Spectrometer). This is a concept for an indirect geometry spectrometer to be built at BL-8A at the First Target Station at SNS. It will use graphite (002) and (004) reflections to pick final energies in the cold and thermal ranges. Since it is indirect geometry, with (004) the energy resolution will be comparable to CNCS at 4 meV (high flux mode), and early intensity estimates indicate a gain factor over CNCS of 30 at the same resolution (0.15 meV). If HIGGS becomes reality, it will definitely have an impact on how CNCS is best used.

8.9 FUNDING RESOURCE NEEDS

The current level of available funding is adequate for operations. Funding for the “potential” instrument development activities is not secured. Additional funding for software and software documentation will be needed for efficient usage of beam-time.

8.10 SELF-ASSESSMENT

Strengths

CNCS is one of the world’s leading instruments for time of flight spectroscopy (inelastic scattering) with cold neutrons. Presently, the flux on sample is world-class. High-magnetic fields, ultra-low-temperatures, and high-temperatures are routinely supported with low failure rates. For incident energies below 3.5 meV, the background and flux are excellent.

Weaknesses (Limitations)

There is a limit to the sample environment that may be deployed on the CNCS due to resources at ORNL. Scheduling with the constraints of sample environment blocks for a beamline that increasingly requires magnets and dilution refrigerators is problematic. This difficulty leaves a chance for high-impact science to be lost to CNCS and instead performed at another facility. There are sometimes spurious scattering features due to extrinsic features (sample environment, aluminum detector vessel window, beam stop) that can degrade user data analyzability.

Opportunities

Additional tools for users to plan their experiments may increase productivity. For example, if a Monte Carlo simulation of the CNCS was available to users, they may better estimate counting times required in order to observe a hypothesized signal.

Threats

Eventually, new spectrometers will emerge at other sources that offer up to 10 times more neutrons per pulse at the same resolution, which may be further combined with repetition rate multiplication to further boost performance.

8.11 EXECUTIVE SUMMARY

CNCS is a world-leading instrument for time of flight spectroscopy with cold neutrons. The science program conducted at CNCS benefits from its place and immediate environment: one of the leading condensed matter research labs of the country, many materials synthesis and characterization capabilities nearby, many dedicated scientists close, significant and high-performance computing capacity available, and another neutron source (HFIR) with complementing instrumentation within the same organization. CNCS can still be improved in many ways to enhance intensity, reduce background, and make its operation more efficient.

8.11.1 Comparison of instrument specifications to similar instrument worldwide

	CNCS (as of 2014)	IN-5 ILL (as of 2011)	LET ISIS (as of 2011)	DCS NIST (as of 2003)	AMATERAS J-PARC (as of 2011)
Moderator	coupled hydrogen	liquid hydrogen	coupled solid methane	liquid hydrogen	coupled hydrogen
Source frequency	60 Hz	reactor	10 Hz	reactor	25 Hz
Avg. Flux (n cm⁻² s⁻¹)	1.6×10 ⁵ n cm ⁻² s ⁻¹ @ 1MW @ 36 μeV	6.8×10 ⁵ n cm ⁻² s ⁻¹ @104 μeV	5.6×10 ⁴ n cm ⁻² s ⁻¹ @102 μeV	3×10 ⁴ n cm ⁻² s ⁻¹ @67 μeV	1.6×10 ⁵ n cm ⁻² s ⁻¹ @ 1MW @ 36 μeV
Flight Path	L ₁ +L ₂ = 36.3 m L ₃ = 3.5 m	L ₃ = 4 m	L ₁ +L ₂ = 25 m L ₃ = 4 m	L ₃ = 4 m	L ₁ +L ₂ = 30 m L ₃ = 4 m
Beam size	1.5 × 2.5 cm ²	1.5 × 5 cm ²	5 × 4 cm ²	3 × 10 cm ²	1 × 2 cm ²
Scattering angles	3° – 133°	3° – 135°	3° – 140°	5° – 140°	5° – 112°
Incident energy	0.5 - 100 meV	0.5 - 20 meV	0.6 - 80 meV	1 - 50 meV	1 - 80 meV
Elastic ΔE/E_i	1.5 – 5%	1.7 – 5 %	0.8 – 5%	1.5 – 5 %	1 – 5 %
Detector type	2m ³ He LPSD	3m ³ He LPSD	4m ³ He LPSD	0.4m ³ He simple tubes	2.9m ³ He LPSD
No. of detectors	400	384	480	913	266 of 488
Detector solid angle	1.7 sr	1.78 sr	3.1 sr (when completed)	~0.6 sr (estimate)	2.1 sr (when completed)
RRM	no	n/a	yes	n/a	yes

Depending on energy, CNCS has 2-8 times higher detector count rate than IN5 or LET (on the same sample, at the same energy resolution).

The performance factor over DCS is near 100.

8.11.2 Comparison of sample environment capabilities with similar instruments worldwide

	CNCS (as of 2014)	IN-5 ILL (as of 2011)	LET ISIS (as of 2011)	DCS NIST (as of 2003)	AMATERAS J-PARC (as of 2011)
Temperature range	50 mK – 1100 K	30 mK – 1650 K	30 mK – xx K	30 mK – 1100 K	6 K – 700 K
Max magnetic field	5 T	2.5 T	8 T	12 T	
Max pressure	32 kbar (clamp cell)	10 kbar (clamp cell)	5.6 kbar TiZr 10 kbar gas cells		

8.11.3 Data and computing capabilities

	CNCS (as of 2014)	IN-5 ILL (as of 2011)	LET ISIS (as of 2011)	DCS NIST (as of 2003)	AMATERAS J-PARC (as of 2011)
Data reduction	Mantid	LAMP	Mantid	DAVE	Utsusemi
Data visualization	Mslice/Horace/Vates	LAMP	Mslice/Horace/Vates	DAVE	
Data Modeling	Community dependent				
Planning tools	Horace, DAVE			DAVE	
Computing resources	CNCS1, CNCS2 (~32 nodes)				

9. SNS BL-14B, HYSPEC, NEUTRON DIRECT GEOMETRY SPECTROMETER STATUS AND PLANNING SUMMARY

9.1 OVERVIEW / CURRENT STATUS

HYSPEC is a high-intensity, time-of-flight, direct-geometry spectrometer (DGS), optimized for measurement of excitations in small single-crystal specimens with optional polarization analysis capabilities. The incident neutron beam is monochromated using a Fermi chopper with short, straight blades, and is then vertically focused by Bragg scattering onto the sample position by either a highly-oriented pyrolytic graphite (unpolarized) or a Heusler (polarized) crystal array. Neutrons are detected by a bank of ^3He tubes that can be positioned over a wide range of scattering angles about the sample vertical axis. HYSPEC entered the user program in February 2013 for unpolarized experiments, and offered XYZ polarization analysis through the user program since February 2016. Polarization analysis is accomplished by using the Heusler crystal array to polarize the incident beam, and a supermirror wide-angle polarization analyzer, designed and fabricated by the Paul Sherrer Institut and now owned by ORNL, to analyze the scattered beam.

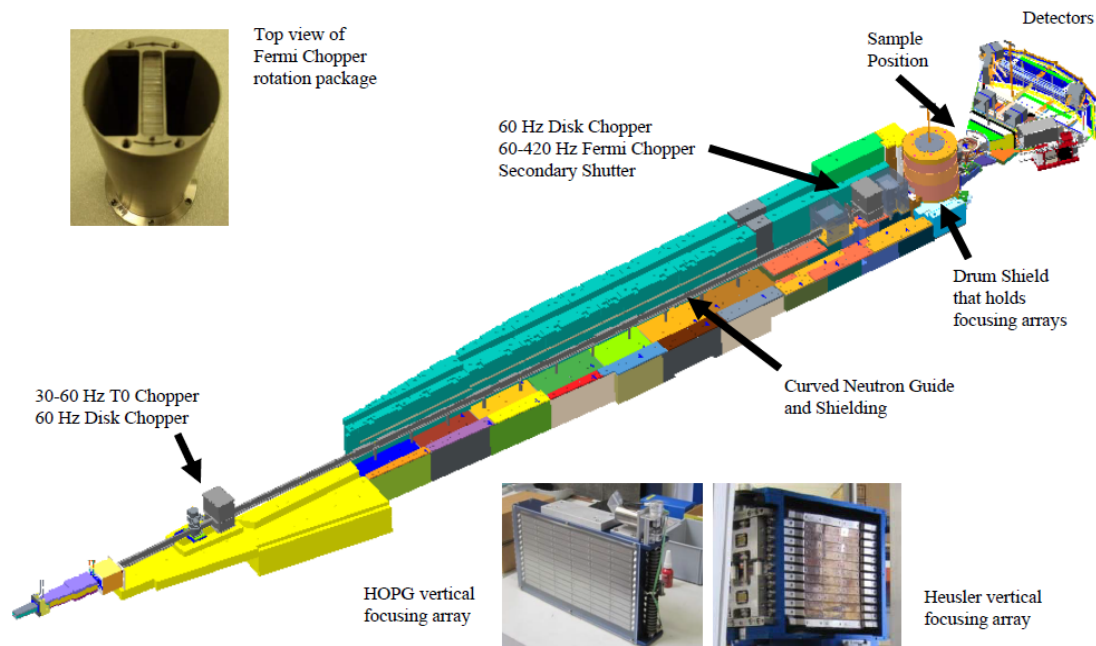


Figure 9.1. Layout of the HYSPEC instrument, with insets showing the Fermi chopper package, and both vertical focusing arrays.

HYSPEC's niche among the family of DGS's at the SNS and the triple axis spectrometers at HFIR includes:

- Polarization analysis option
- Large configurable horizontal angle detector acceptance
- Vertical focusing enables good statistics, for either small single crystals, extreme conditions or lower flux polarized beam configuration
- A cold neutron incident energy range optimized for $3.8 \text{ meV} < E_i < 60 \text{ meV}$ unpolarized and $3.8 \text{ meV} < E_i < 25 \text{ meV}$ polarized

- Moderate energy transfer resolution, between that of CNCS and cold neutron triple-axis spectrometers such as CTAX at HFIR

Team Structure

The HYSPEC instrument is in the Time of Flight Spectroscopy group, within the Neutron Scattering Division. It is staffed by two full-time neutron scattering scientists, Barry Winn (1 FTE) and Ovi Garlea (1 FTE), and is also supported by a scientific associate (0.5 FTE for FY18 and FY19, 1 FTE for FY20), Melissa Graves-Brook. The embedded software support for reduction, analysis and visualization within the Mantid software suite was Andrei Savici for FY17 and FY18, and he returned to the Direct Geometry Spectroscopy team in a Computational Scientist role in the summer of 2020.

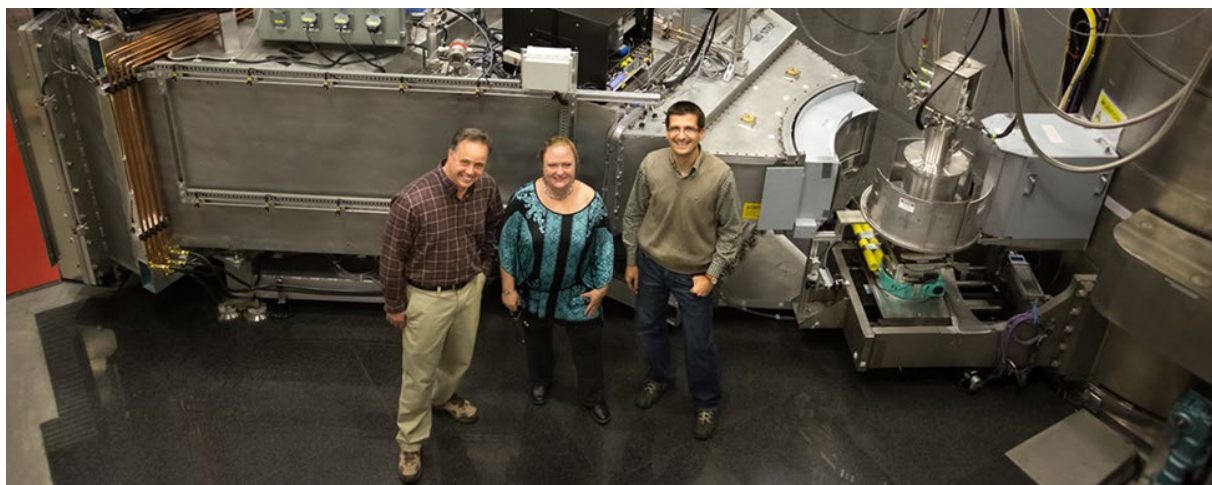


Figure 9.2. HYSPEC team members B. Winn, M. Graves-Brook, and O. Garlea, standing in front of the HYSPEC detector vessel.

9.2 SCIENTIFIC FOCUS

HYSPEC principally studies coherent excitations in single crystal samples of various condensed matter systems using either polarized or unpolarized neutrons. Topics of study include unconventional superconductors; lattice and magnetic dynamics in functional materials including ferroelectrics, memory shape alloys, magnetoresistive and magnetocaloric materials; excitations in geometrically frustrated magnets; phase transitions; itinerant magnets; exotic ground states in quantum magnets and quantum critical phenomena.

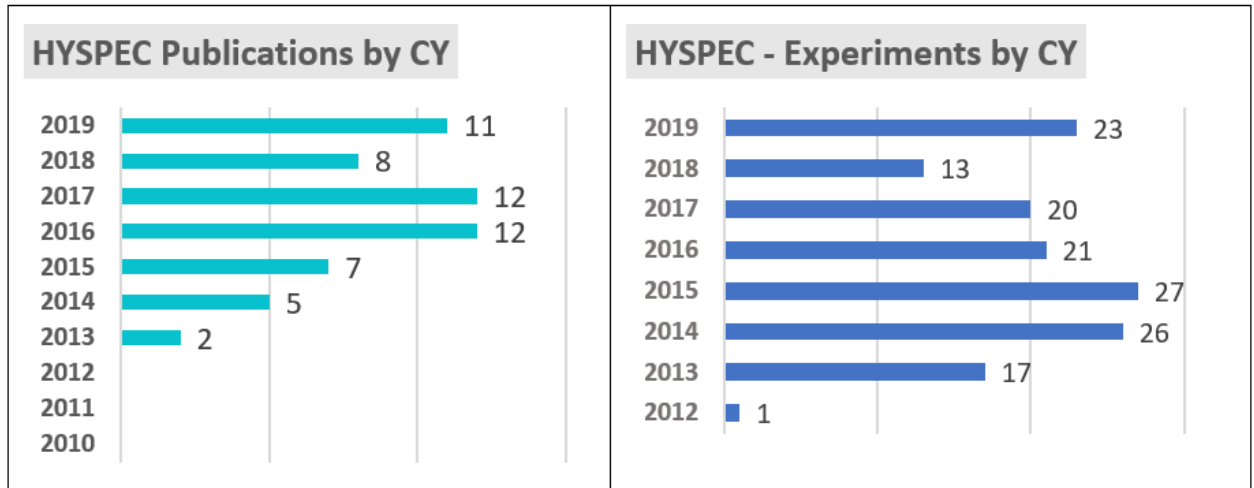


Figure 9.3. HYSPEC publication statistics

9.3 SCIENTIFIC HIGHLIGHTS

The following paragraphs summarize the results of selected highlights, showcasing the diverse science and measurement capabilities of HYSPEC.

Continuum of quantum fluctuations in a three-dimensional $S=1$ Heisenberg magnet

K. W. Plumb, Hitesh J. Changlani, A. Scheie, Shu Zhang, J. W. Krizan, J. A. Rodriguez-Rivera, Yiming Qiu, B. Winn, R. J. Cava & C. L. Broholm, *Nature Physics*, 15, 54-59, 2019

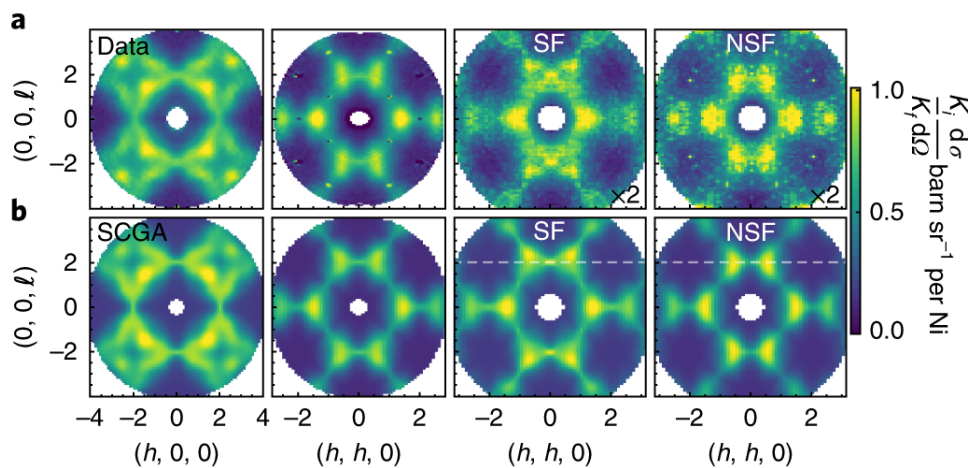


Figure 9.4. Polarized and unpolarized neutron scattering data at 1.8 K (top panels) compared with a calculation (bottom panel) based on self-consistent Gaussian approximation. Polarized neutron measurements labelled by NSF (non-spin-flip) measures components of the dynamic spin correlation function that are perpendicular to the (h,h,ℓ) scattering plane, and SF (spin-flip) measures the component of the spin correlation function polarized within the (h,h,ℓ) scattering plane.

Polarized neutrons scattering measurements performed at HYSPEC were decisive in demonstrating that $\text{NaCaNi}_2\text{F}_7$ material is a 3D $S=1$ Heisenberg antiferromagnet. The ground state of this material appears dominated by quantum fluctuations with a lack of magnetic order and an observed continuum of magnetic excitations consistent with fractionalized excitations. The time-of-flight polarized measurements at HYSPEC complemented earlier MACS data and enabled collecting a comprehensive QE map of the dynamic structure factor that was essential to develop the quantitative understanding of the spatial correlations between spins. Furthermore, the polarized data confirmed the magnetic origin of diffuse scattering and revealed a striking pattern of connected “bow ties” that is characteristic of the emergent electron motion in the quantum spin liquid state. The resulting theoretical model provided critical information on the quantum limit of Heisenberg spins on a 3D pyrochlore lattice.

This is just one of several recent successful polarized neutron experiments performed at HYSPEC, which served in probing realization of exotic quantum magnetic states (e. g. Gao S., et al. , "Manifolds of magnetic ordered states and excitations in the almost Heisenberg pyrochlore antiferromagnet MgCr_2O_4 ", *Physical Review B*, 97, 134430 (2018); Sibille R., et al., "Experimental signatures of emergent quantum electrodynamics in $\text{Pr}_2\text{Hf}_2\text{O}_7$ ", *Nature Physics*, 14, 711-715 (2018)).

Exotic Magnetic Field-Induced Spin-Superstructures in a Mixed Honeycomb-Triangular Lattice System

V. Ovidiu Garlea, Liurukara D. Sanjeewa, Michael A. McGuire, Cristian D. Batista, Anjana M. Samarakoon, David Graf, Barry Winn, Feng Ye, Christina Hoffmann, and Joseph W. Kolis, *Physical Review X*, 9, 011038, 2019

Elastic and inelastic neutron scattering studies provided experimental evidence of new and unexpected magnetic arrangements in the mixed honeycomb-triangular lattice system $K_2Mn_3(VO_4)_2CO_3$. The HYSPEC results indicate that triangular and honeycomb magnetic layers undergo sequential magnetic orderings and act as nearly independent magnetic sublattices. Applied magnetic fields parallel or perpendicular to the c-axis induce exotic ordered phases characterized by various spin-stacking sequences of triangular layers that yield bilayer, three-layer, or four-layer magnetic superstructures. These observations cannot be explained in the framework of quasi-classical theory based only on nearest-neighbor interlayer coupling and raise the possibility that subtle thermal and quantum fluctuations may generate effective interlayer tunneling between the triangular layers separated by honeycomb lattices.

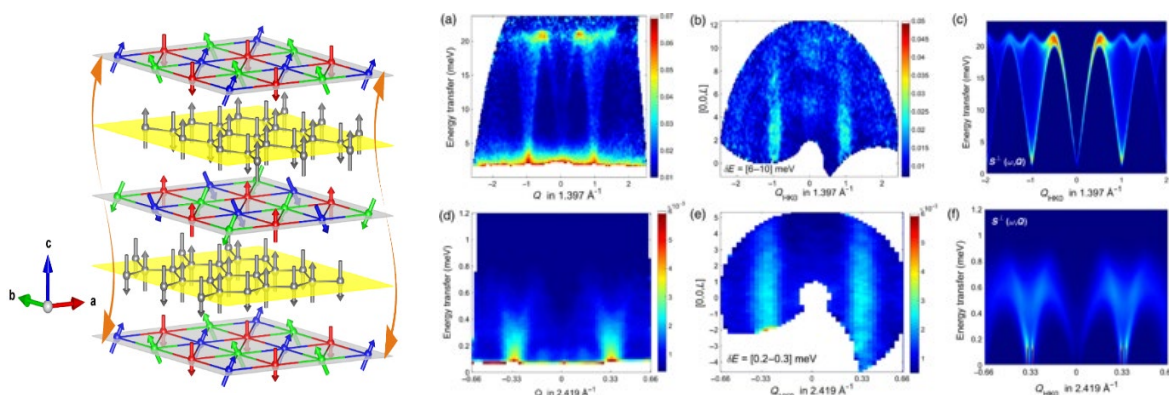


Figure 9.5 Left panel: Models of the static magnetic order in $K_2Mn_3(VO_4)_2CO_3$ compound consisting of alternately stacked triangular and honeycomb magnetic layers. Right panel: INS spectra measured on 0.3 g coaligned crystals to characterize the magnetic interactions of completely different energy scales in the triangular and honeycomb sublattices.

The data in Figure 9.5 illustrates the versatility of HYSPEC, where magnetic excitations at two different energy and momentum scales are measured with the same instrument. In this work, HYSPEC studies in zero and applied magnetic fields (< 8 Tesla) were complemented with neutron diffraction measurements at TOPAS and CORELLI diffractometers and HB-1A triple axis spectrometer, as well as with heat capacity and magnetization measurements at fields up to 16 Tesla using the NHMFL facility. The lead author O. Garlea, who is one of the instrument scientists supporting HYSPEC users, spearheaded this rather comprehensive and thorough look into this material, and brought together an exceptional team to provide fundamental insight into the variety of superstructures observed in this complex magnetic system. This work emphasizes the impressive scientific productivity and expertise of local contacts at HYSPEC, which is an important consideration in user outreach and support.

Intrinsic anharmonic localization in thermoelectric PbSe

M. E. Manley, O. Hellman, N. Shulumba, A. F. May, P. J. Stonaha, J. W. Lynn, V. O. Garlea, A. Alatas, R. P. Hermann, J. D. Budai, H. Wang, B. C. Sales & A. J. Minnich, *Nature Communications*, 10, 1928, 2019)

This research combines inelastic neutron and x-ray scattering with ab initio simulations to reveal a mechanism for halting vibrational energy that is intrinsic to the thermoelectric PbSe crystal. Lead chalcogenides have exceptional thermoelectric properties and intriguing anharmonic lattice dynamics underlying their low thermal conductivities. Isolated intrinsic local modes in perfect crystals were known to occur in nonlinear physics, but here nonlinear localization of a large fraction of an entire phonon was revealed for the first time and shown to play an important role in the transport properties of a thermoelectric material.

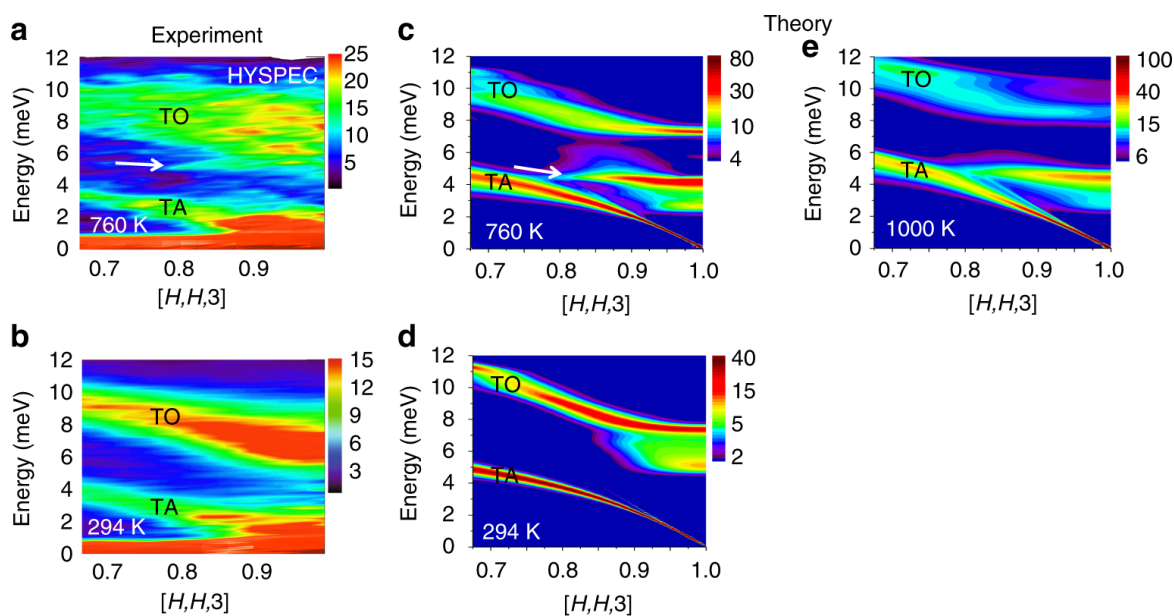


Figure 9.6. Time-of-flight neutron scattering data from HYSPEC (a, b) resolving fine energy structure in the spectral distribution for comparison with the ab initio simulations (c, d, e)

The measurements performed at HYSPEC provided higher energy resolution and larger region in momentum-energy space to complement data acquired using the thermal neutron triple axis spectrometer BT7 at NCNR. The high-resolution measurement proved to be very informative in revealing an additional sharp but nearly dispersionless feature near 5.5 meV (indicated by arrow in Figure 9.6 (a)). The results demonstrated how nonlinear physics beyond conventional anharmonic perturbations can fundamentally alter vibrational transport properties.

Excitations in the field-induced quantum spin liquid state of α - RuCl_3

Arnab Banerjee, Paula Lampen-Kelley, Johannes Knolle, Christian Balz, Adam Anthony Aczel, Barry Winn, Yaohua Liu, Daniel Pajerowski, Jiaqiang Yan, Craig A. Bridges, Andrei T. Savici, Bryan C. Chakoumakos, Mark D. Lumsden, David Alan Tennant, Roderich Moessner, David G. Mandrus and Stephen E. Nagler, *npj Quantum Materials*, 3, 8, 2018

This high-impact result provides evidence that by applying a sufficiently large magnetic field to suppress conventional magnetic order and spin waves in α - RuCl_3 , new unconventional excitations emerge that are consistent with what calculations suggest is a field induced Kitaev quantum spin liquid. If so, then α - RuCl_3 remains a candidate for realization of Kitaev physics and topologically protected quantum computing. In addition to the excitement this generates for this particular material, the demonstration of INS as a useful probe of fractionalized excitations has frankly surprised the quantum computing community, many of whom had only vague and often suppressed recollections of neutron scattering from graduate-level classes in solid state physics. The research team which produced this paper has been deliberate in spreading this good news through the quantum computing community and it is hoped that similar quantum computing candidates will also find their way to HYSPEC.

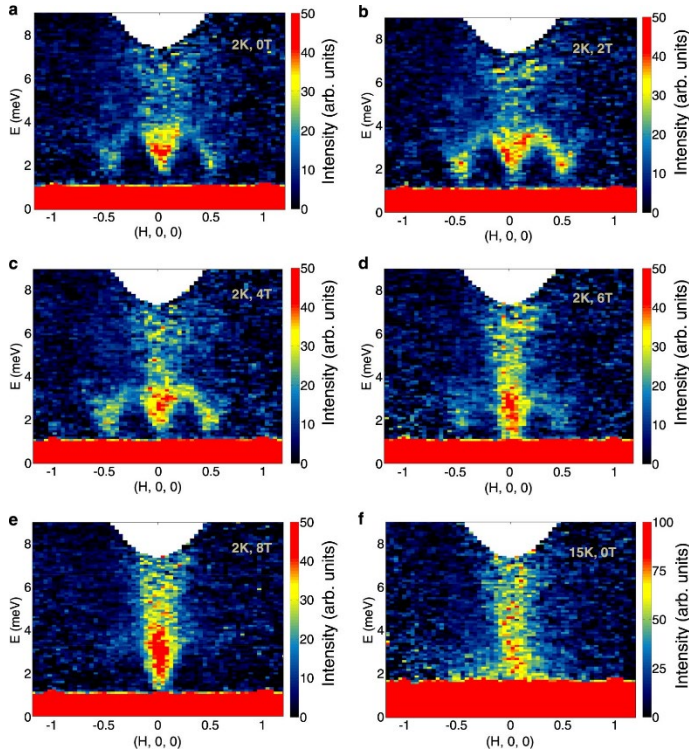


Figure 9.7. Inelastic scattering of α - RuCl_3 along $(H,0,0)$ at 2 K ((a)-(e)) and 15 K (f). At 2 K the field is varied between 0 T and 8 T along the $(-1,2,0)$ direction in the honeycomb plane. The application of a magnetic field suppresses the magnetic order and the spin waves, leaving a gapped continuum spectrum of magnetic excitations.

Because this was a weak signal with slices integrated over a significant region in Q space, a low background contribution from neutrons scattering from the magnet was essential. This experiment was one of the first using a then new 8 tesla vertical-bore split-coil magnet at HYSPEC which employs cadmium-lined wedge supports at the gap in order to reduce attenuation and multiple scattering effects compared to conventional ring-support magnet designs. The exceptionally tight collimation of the HYSPEC radial collimator, combined with the gap geometry and shielding of this 8-tesla magnet, enabled these measurements. For several years following this measurement HYSPEC remained the only DGS at the SNS at which such low background could be achieved with this magnet, until other DGS's installed similarly restrictive collimators.

Anharmonic Eigenvectors and Acoustic Phonon Disappearance in Quantum Paraelectric SrTiO₃

Xing He, Dipanshu Bansal, Barry Winn, Songxue Chi, Lynn Boatner, and Olivier Delaire, *Physical Review Letters*, 124, 145901 (2020)

This study aimed at improving the understanding of the origin of strong phonon anharmonicity in the archetypical perovskite SrTiO₃ (STO) that displays unusual thermal transport properties. By analyzing the temperature dependence of the force constants and the dynamical structure factor, the authors identified how the anharmonic renormalization of eigenvectors, particularly Ti and O motions, is responsible for this effect. They show that the strongly anharmonic modes are primarily determined by the diagonal force constants in the Ti-O interaction. These results establish how a striking T dependence of phonon intensities beyond the harmonic picture can be quantitatively measured with INS mapping of $S(Q,E)$ volumes, providing direct insights into the anharmonic behavior of phonon eigenvectors, and also show how first-principles simulations including anharmonic effects can reproduce and rationalize such effects.

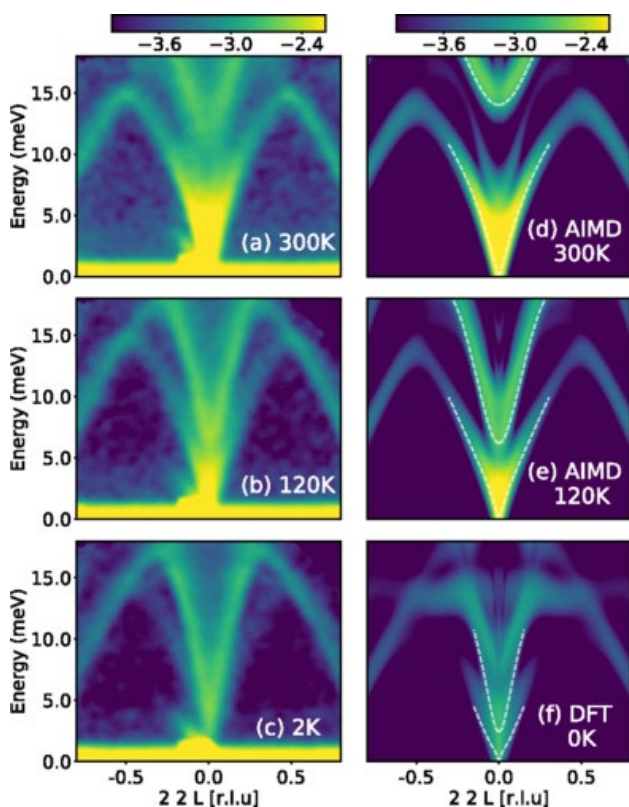


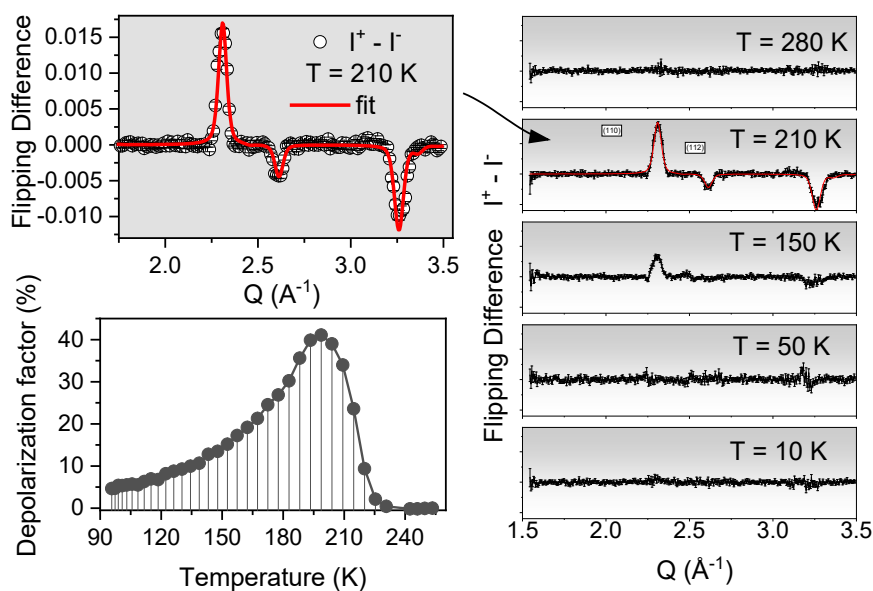
Figure 9.8. $S(Q,E)$ of SrTiO₃ along $Q=[2\ 2\ L]$ directions measured at HYSPEC at 300, 120, and 2 K (d-f) show simulation results obtained from combined ab initio molecular dynamics (AIMD) with the temperature-dependent effective potential (TDEP) method. All are plotted on a log₁₀ scale.

The authors point out several times that although there were hints of these effects when looking at isolated Q-E locations in reciprocal space using a TAX, that they needed in addition DGS measurements at several temperatures to really tease out this effect well. HYSPEC's high flux at incident energies 15 meV and 27 meV made it an obvious choice for the extended Q-E space measurements. It is also worth noting that the HB-3 TAX provided critical complementary information at more temperature points than did HYSPEC. This illustrates one of our common findings concerning good publications, which often benefit from complementary INS measurements from different kinds of spectrometers as well as diffractometers. This high impact result also highlights the need to couple INS measurements with excellent theoretical and modeling studies.

Reentrant spin glass state induced by structural phase transition in $\text{La}_{0.4}\text{Ce}_{0.6}\text{Co}_2\text{P}_2$

Judith K. Clark; Xiaoyan Tan; Alexandra A. Arico; Arthur P. Ramirez; Vincent Yannello; Corey M. Thompson; Kirill Kovnir; V. Ovidiu Garlea; Michael Shatruk, *Phys. Rev. Matt* (2020) -in press

For this study half-polarized and full-polarized elastic scattering measurements were carried out at HYSPEC on pelletized powder of $\text{La}_{0.4}\text{Ce}_{0.6}\text{Co}_2\text{P}_2$ to probe the gradual dissipation of a weak ferromagnetic ordering and onset of a glassy state occurring simultaneously with the structural collapse corresponding to a decreasing of the unit-cell volume by about 3.6%. The studied material belongs to the $\text{La}_{1-x}\text{Ce}_x\text{Co}_2\text{P}_2$ series with a layered ThCr_2Si_2 -type structure and appears at the borderline between the ferromagnetic ($x < 0.6$) and antiferromagnetic ($x > 0.65$) behavior. The observed behavior is analogous to that reported for so-called reentrant spin glasses.



Flipping difference profiles were obtained at selected temperatures by successive measurements with polarized beam parallel and anti-parallel to the external magnetic field produced using a permanent magnet yoke, without performing a polarization analysis of the scattered beam (so-called “half-polarized” method). Measurements showed a clear signature of FM ordering in the spectrum recorded at 210 K (Figure 9.9). At 150 K, however, the FM signal became substantially suppressed

Figure 9.9. The flipping difference of neutron scattering ($I^+ - I^-$) recorded on a powder sample of $\text{La}_{0.4}\text{Ce}_{0.6}\text{Co}_2\text{P}_2$ at different temperatures and the temperature dependence of the neutron depolarization factor by the sample.

and essentially vanished at 50 K. The 210 K spectrum was successfully fit with a soft FM model where magnetic moments align parallel to the applied magnetic field, regardless of the crystal grain orientation. The model fit of the 210 K data yields an ordered moment of $0.15(1) \mu_B$ per Co atom and negligible $-0.01(1) \mu_B$ per Ce atom. We note that such a low detection limit of ordered moment is only possible by polarized measurements by taking advantage of a nuclear-magnetic interference term. The depolarization of the neutron beam by the sample was evaluated from the change in the intensity of the spin-flip signal (I^+), employing the supermirror analyzer. The depolarization increases abruptly at ~ 235 K, in agreement with the onset of FM ordering of the sample. Below 190 K, the depolarization factor steadily decreases, as the sample magnetization vanishes.

9.4 GENERAL USER PROGRAM

HYSPEC is aligned with the NScD 2014 Strategic Plan and the 2020 Neutron Sciences Annual Plan priorities to study quantum materials, and the current user community is a subset of those who perform experiments at either direct geometry or triple axis spectrometers.

Between the start of CY2017 and now, the XYZ polarization analysis or half-polarized modes of operation have occupied 44% of the available beamtime. Experiments that employ these polarized techniques require more time due to lower statistics and multiple measurements (spin flip, non-spin flip, and sometimes multiple field directions at sample). Users are encouraged to complete unpolarized neutron scattering experiments prior to submitting proposals at HYSPEC for polarized experiments.

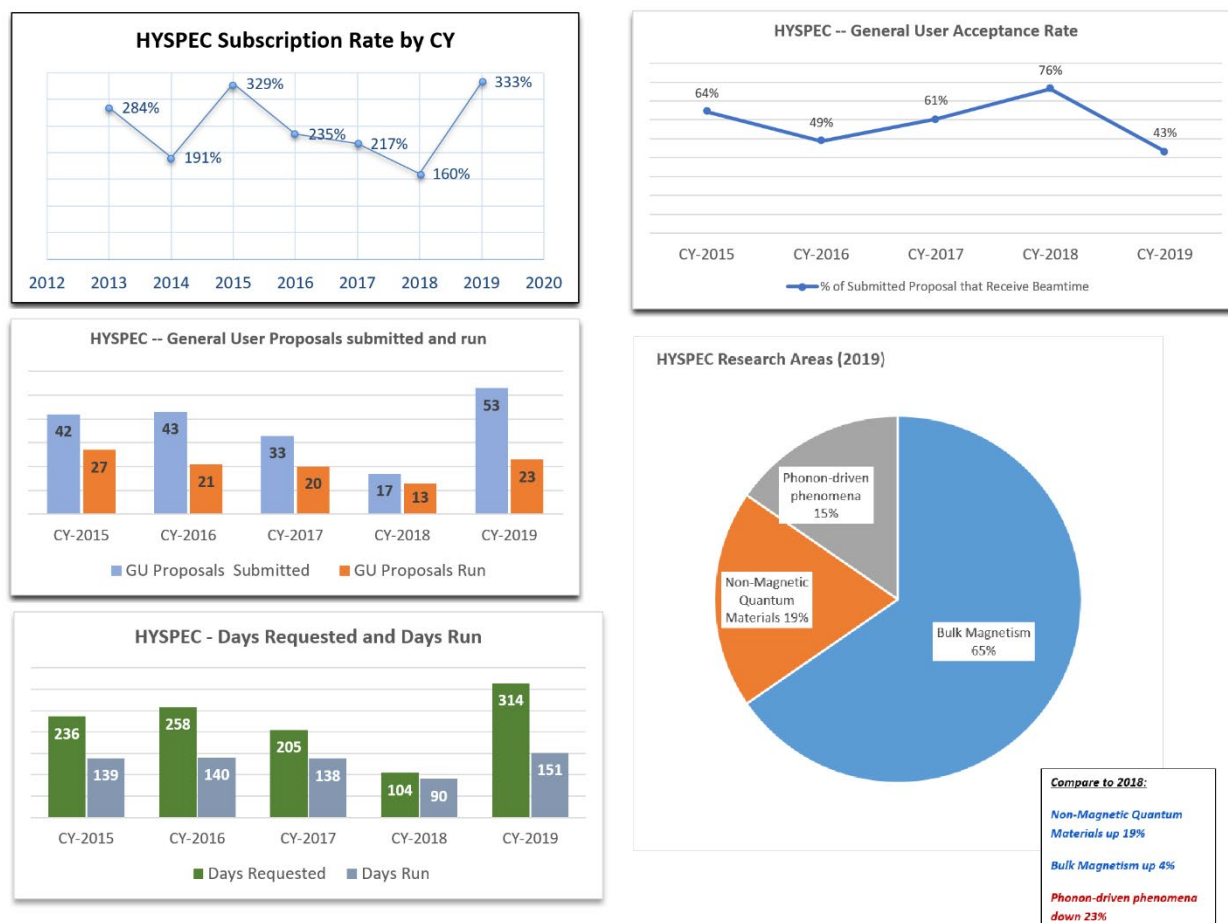


Figure 9.10. HYSPEC user program statistics

9.5 UPDATE ON INSTRUMENT DEVELOPMENT ACTIVITIES

Following are some developments to improve instrument performance since initial commissioning, within the 2017-2020 period.

- (a) **Half-Polarized experiments:** Half polarization technique (polarized incident beam but no polarization analysis) is extremely useful for studying magnetic form factors, magnetization density distribution and spin dynamics in saturated ferromagnets, ferrimagnets and paramagnets

under applied magnetic field. The ease of switching between HOPG and Heusler monochromators to polarize the incident beam and using permanent magnet yokes with vertical and horizontal field directions to enable half-polarized elastic and inelastic measurements using close-cycle refrigerators or Helium cryostats, have enabled initial attempts at half polarized measurements.

One of the harder lessons we have learned [Y. Nambu, *et al.*, "Observation of Magnon Polarization," *Phys. Rev. Lett.* **125**, 027201 (2020)]. was when performing measurements with a horizontal permanent magnet yoke, that we obtain the best performance when using a weak vertical guide field instead of a horizontal guide field. Confusing results when using YIG were clarified when repeating these measurements with a TiZr rod (isotopic incoherent non-spin-flip scattering only) and using the same yoke, where we observed depolarization when the incident beam came close to the permanent magnet poles. This effect was negated when using a weak vertical guide field, presumably because the nodes of the permanent magnet yoke no longer had zero field. This re-emphasizes our need for a superconducting horizontal field magnet with an open geometry at beam elevation for wider scatter angle range, in which poles are further from the sample and a larger open scatter range is possible.

(b) XYZ Polarization Analysis using the supermirror array analyzer and 3D coils at sample:

The supermirror array which was on loan from the Paul Scherrer Institut was purchased by ORNL in the summer of 2020; this is the largest investment at HYSPEC in the 2017-2020 period. Despite slight damage observed on the front edge of some supermirrors in 2017 (which is now routinely protected against), the array has performed admirably since the summer of 2015. The original set of water-cooled 3D coils shown in Figure 9.11 are still in use and routinely generate fields up to 20 Gauss at the sample position. Commissioning was assisted by colleagues from Brookhaven National Laboratory and a detailed description of the supermirror array performance can be found at reference [Zaliznyak *et al.*, "Polarized neutron scattering on HYSPEC: the HYbrid SPECTrometer at SNS", *Journal of Physics: Conference Series* **862**, 012030 (2017)]. This mode has been used at HYSPEC extensively over the past three years, and our ability to capture diffuse inelastic features with polarization contrast distinguishes HYSPEC worldwide.

(c) Elevator / Oscillator for radial collimator and polarizing supermirror array:

The biggest change since the 2017 review was the installation of the oscillator / elevator system in August of 2018. This system was approved in fall 2016 and managed by the Neutron Technologies Division through NScD's scientific productivity upgrade program. The oscillator significantly smoothed out transmission (supermirror reflection) for the supermirror array. Also, despite already uniform transmission through our radial collimator, many users were also pleased to use this same oscillation for the radial collimator when doing unpolarized or half-polarized studies. The oscillator mount for the supermirror enabled modest alignment corrections, which is regularly revised when the supermirror array had to be removed, remagnetized and reinstalled (around 8T or 14 T cryomagnets block time). The main correction we made with these adjustments was to set the center / sample position at the location for highest polarized transmission instead of highest polarization, which we found to be more effective for our users. This also permits us to use sample environments like our workhorse bottom-loading closed cycle refrigerator with the Huber rotation stage underneath (before we had to employ stick rotation and translate the sample to the optimal position for the supermirror array). Finally, the elevator feature both simplifies and speeds up our transition from unpolarized to polarized and back, which has enabled users intending to leverage polarization capabilities to quickly convert to unpolarized as needed, and has simplified the block scheduling process since we no longer have to block polarized experiments

together. We still remove the supermirror array once or twice a year to magnetically recharge the remnant supermirror layers, and to date have been reluctant to keep the supermirror on the oscillator assembly when working with uncompensated magnets.

The oscillator has altered some of HYSPEC operations. The oscillator has restricted the detector vessel range; while we were once able to reach $s_2 = \pm 110^\circ$ at some incident energies before, the oscillator / collimator now restricts us to $s_2 = \pm 88^\circ$. The higher detector vessel angles were rarely used before, and now when higher Q is required users merely employ a higher incident energy with only a modest worsening in energy resolution and flux-on-sample. Another incidental effect of the new use of the elevator is the more constrained access to the Huber rotation / tilt / translation stage used for most sample environments. The cabling was reconfigured, but sample rotation is still constrained when the detector vessel is at $s_2 = -88^\circ$. Finally, the oscillator precludes the use of a motorized translation stage which used to permit the focus-array to sample distance to vary between 1.4 m and 1.8 m. We have rarely used the 1.4 m position to date due to the use of optics between drum shield and sample environment and all magnets requiring the 1.8 m position, so this last restriction is no great loss. Finally, the new 3D coil table is slightly more restrictive than the previous support was concerning tilt of our wider tail cryostats (tilt motors interfere with the bottom of the new coil table) and leveraging block scheduling we tend to leave that table in place. This means that users are now recommended to bring samples that are better aligned to a symmetry plane than before (limiting tilt to 2.5°), or simply plan to not tilt as we already do for magnets. Furnaces and magnets are not compatible with the 3D coils.

In addition to the physical improvements for polarization analysis, we have also improved the reduction workflow, building on his earlier work [Savici, A.T. et al., "Data processing workflow for time of flight polarized neutrons inelastic measurements", Journal of Physics: Conference Series, 862, 012023 (2017)].

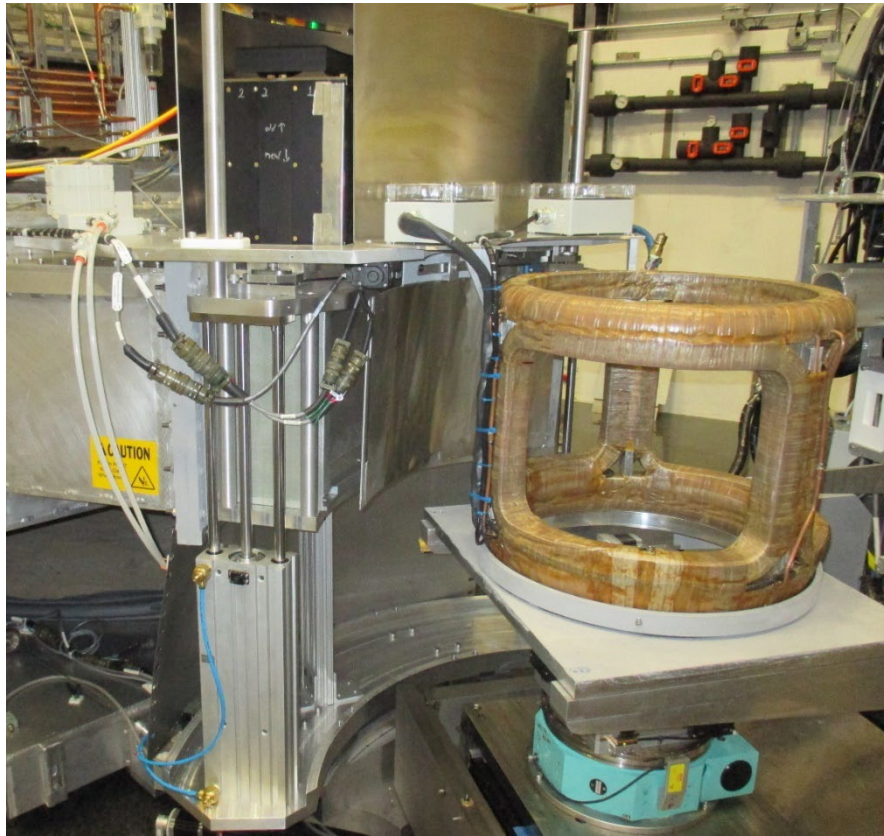


Figure 9.11. The new elevator / oscillator assembly with radial collimator at beam elevation and the supermirror above it. Side shielding has been removed to show the pneumatic lift system. This assembly includes a new table and rotary bearing underneath the 3D coil system, which is loosely mechanically connected to the oscillator assembly.

- (d) Time independent background mitigation:** While pushing the performance limits of HYSPEC for polarization analysis we recognized that although the time independent background (TIB) is subtracted in our reduction, it introduces a noise factor which reduces the signal to noise ratio and either requires longer acquisition times or precludes the detection of weak signals. For polarization analysis where the signal is significantly reduced due to attenuating polarization optics, and for weak-moment systems we were not able to obtain sufficient signal given the TIB. For polarization analysis where we subsequently perform operations on the data sets (sums, scalings, etc.) the noise of the initial measurement gets worse. Specifically, one of our users experienced with polarization analysis (Philippe Bourges, Laboratoire Leon Brillouin) encouraged us to mitigate the time-independent background.

This encouragement led us to a detailed examination of the TIB, where we first confirmed that our sensitivity to gammas is low with current detector thresholds and gain, and then we began a systematic study using a new portable detector platform which employs the same acquisition electronics and software as all SNS instruments. This project was led by M. Graves-Brook who built the mobile cart and coordinated with both Detector and Data acquisition support teams to assemble the rest of the system. This system is based on a platform recently developed by our Data acquisition support team. The detectors themselves are also ^3He linear position sensitive detector tubes arranged in the standard SNS 8-pack configuration and have similar response to the HYSPEC detectors. Our SA took measurements at several locations about the HYSPEC

experiment room, with beam both on and off and shutters both open and closed, and employed a variety of shielding materials and thickness, all in an effort to determine what additional shielding on the detector vessel would reduce TIB.

We found that 5 mm of the shielding product Mirrorbor® reduces TIB by 75%, and are now identifying funds in order to procure sufficient material to cover most of the HYSEPC detector vessel.

- (e) Spherical Neutron Polarimetry demonstration:** In support of LDRD 8824: “Portable High-Tc Wide-angle Spherical Neutron Polarimetry Device” led by P. Jiang and with B. Winn as collaborator, a spherical neutron polarimetry system (SNP) intended for use at both PTAX and GP-SANS at HFIR was tested at HYSPEC in December 2019. This commissioning experiment followed an initial direct beam configuration test at the University of Missouri Research Reactor. The HYSPEC test demonstrated the use of both variable scattered beam directions and successful operation with a narrow tail wet cryostat. This test was performed at HYSPEC for two reasons: (1) the HFIR had experienced an extended shutdown so the availability of HYSPEC enabled SNP commissioning to proceed, and (2) a variant of the HFIR system has been proposed which would enable SNP with a wide-angle scattered beam. Because the future variant would use much of the same support equipment as the HFIR system, so at HYSPEC we integrated these systems with the EPICS control system in use at SNS instruments. In addition to demonstrating SNP, this test enabled the LDRD team to identify several improvements which will enable the SNP to operate more robustly at HFIR. Finally, the success of this LDRD motivated a successful application for a young researcher award for P. Jiang, in which O. Garlea served as mentor / scientist.
- (f) Incident beam RF Flipper:** The HYSPEC team used instrument-specific M&S funds and support from NSD and RAD staff (Y. Kang and A. Parizzi) to design and build an optic-rail mounted RF flipper for the incident beam. In addition to the improved transmission, anticipated improved flipping ratio and simplicity (no flip current optimization required for different incident energies) compared to the currently-used Mezei flipper, it also affords the opportunity to cross calibrate both the Mezei and the RF flippers and to determine the polarization of the other HYSPEC optics. Finally, it aligns with our near-term vision of developing similar optics for the wide-angle scattered beam. Offline testing is immanent and neutron testing is planned for Spring 2021.
- (g) Compact 3D coils:** The HYSPEC team used instrument-specific M&S funds to fabricate a second 3D coil system which is initially only compatible with our narrow tail bottom loading closed cycle refrigerator. This investment was made because it was recognized that some polarization optics require space that the larger 3D coil system does not provide, including possible scattered beam flipping optics. Investing in these coils enables significant flexibility when planning for future polarization developments. These coils are in-hand and neutron testing is planned for Spring 2021.
- (h) Sample Environment:** Sample environments are generally shared with CNCS and CORELLI, and to a lesser extent with ARCS and SEQUOIA, although a dedicated bottom-loading closed cycle refrigerator system (CCR-19) and a dedicated 100 mm bore liquid helium cryostat (CRYO-09) remain highly used sample environments at HYSPEC. The HYSPEC instrument team is actively engaged with the steering committee for sample environments that focuses on high magnetic field and low temperature (B. Winn of HYSPEC is the chair).

The following are sample environment developments completed between January 2017 and June 2020:

- A 14 T vertical-bore split-coil magnet with wedge support at the gap instead of conventional concentric aluminum ring support, has been delivered and tested in the sample cage and at HYSPEC. HYSPEC will be able to host user program experiments in fields up to 14 T and temperatures as low as 300 mK in the 2021A cycle
- An 11 T uncompensated magnet has been used at HYSPEC but has since been moved to HFIR for permanent operation.

The following are sample environment developments in progress in July 2020:

- The 14 T uncompensated vertical-bore magnet will be commissioned at field at HYSPEC in July 2020.
- Delivery of a third 100 mm bore ^3He insert compatible with HYSPEC's dedicated wet cryostat is imminent.
- Procurement of a 50 / 35 mm bore ^3He insert compatible with several magnets is ongoing.
- A procurement specification is in preparation for a dry top loading cryostat which employs new technologies which enable rapid cooling and warming of samples.

(i) Software Improvement: The following are software improvements completed between January 2017 and July 2020, that most directly impacted HYSPEC operation:

- A user-friendly editable reduction script / library workflow that accounts for the XYZ polarization analysis mode. This workflow started from one developed for unpolarized reduction which also works for the other DGS instruments. A. Savici has hosted tutorials to instruct users how to use it. These tutorials have been both internal to ORNL and as part of the 2019 Polarization workshop.

The following are software improvements in progress during July 2020:

- Schärpf angle correction for single crystal XYZ polarization analysis. A prototype analysis script is available but not yet user friendly.
- The IDAQ group is aggressively implementing upgrades which facilitate remote participation during the 2020 pandemic.
- An acquisition scripting control approach for instrument automation, which was first developed as a prototype by then PostDoc G. Sala, is now being developed through IDAQ with collaboration with two other DGS instrument teams. Once beta testing has been completed, we anticipate more users will employ the scripting interface than the currently used table scan interface.

(j) Other improvements: There were several operational and performance related upgrades during this time:

- In order to leverage new operational restrictions of the oscillator/elevator and to remedy the cabling restrictions with the Huber stages under the sample environment, we reconfigured the sample arm. In March of 2020 we removed the linear stage that is no longer useful, attached the detector vessel rotation stage directly to the arm instead of the stage, and lowered the sample rotation stage relative to the tilt stages. This last step

enables us to eventually reconfigure the cabling so that it no longer interferes with the oscillator assembly at $s_2 = -88^\circ$. This upgrade is mostly complete, and we find as a bonus that the detector vessel air pads 'sing' significantly less than before.

- Utility improvements include a chilled water manifold and leak sensor system, and an additional AC transformer and receptacles which have proven necessary as the scope for both polarization optics and sample environments have expanded since initial operation.
- A quench-driven coil failure of the 14 T magnet prior to repair and acceptance at ORNL led to the realization that non-ferrous metal components like aluminum support plates, when in the presence of a quench, can create eddy currents sufficiently strong to mechanically damage a magnet's coils. This prompted an aggressive modeling and fabrication / modification process which has resulted in new slotted plates and other components in preparation for the 14 T magnet testing at HYSPEC.
- In March 2017 the HYSPEC instrument and team experienced a major operational failure. The detector vessel and rotation stage detached from the sample arm during a detector vessel move. It was found that the bolts which attached the rotation stage to the sample arm's then translation stage had all sheared at the interface between the two. A combination of a prudent and swift response by Ovi Garlea and a bit of luck minimized the damage to this disconnection. An excellent response by both our Scientific Associate Melissa Graves-Brook and multiple support teams in NSD and NTD enabled a relatively short downtime of a few weeks and identified several future improvements that we implemented in April 2018.
- To increase the amount of information extracted from XYZ polarization studies on single crystals, one needs to control the magnetic domains present in the samples. For this, we revised a design of a uniaxial pressure device that could be adapted to sample geometry to limit the number of contributing magnetic domains. A test was successfully performed using a MnO crystal.

9.6 UPDATE ON IMPACT OF DISCRETIONARY BEAMTIME

The HYSPEC Instrument Development Team continued to review and sponsor discretionary beamtime experiments at HYSPEC through the fall cycle of 2018. In September of 2018 the IDT agreement was up for its triennial review. NScD management chose to stop using IDT's as an instrument-specific community engagement mechanism at that time in favor of agreements with other specific facilities, formalizing agreements through NScD science initiatives instead of specific instruments. Through the fall cycle of 2018 most of the Discretionary Beamtime was allocated through the IDT – a partial list of IDT supported publications is included below.

Discretionary beamtime allocation changed in July 2019 to enable 50% of this beamtime to be reviewed internally through the new science initiatives. For HYSPEC this resulted in one experiment in the fall of 2019 and one in the spring of 2020, both of which were reviewed through the Quantum Materials Initiative. Other discretionary proposals reflected collaborations both within ORNL and outside of ORNL.

Partial list of IDT supported publications:

[a] Merritt A.M., Reznik D., Garlea V.O., Gu G.D., Tranquada J.M., "Nature and impact of stripe freezing in $\text{La}_{1.67}\text{Sr}_{0.33}\text{NiO}_4$ ", *Physical Review B* **100**, 195122 (2019).

[b] Ran K., Zhong R., Chen T., Gan Y., Wang J., Winn B., Christianson A.D., Li S., Ma Z., Bao S., Cai Z., Xu G., Tranquada J.M., Gu G.D., Sun J., Wen J., "Unusual phonon density of states and response to the

superconducting transition in the In-doped topological crystalline insulator $\text{Pb}_{0.5}\text{Sn}_{0.5}\text{Te}$ ", *Physical Review B* **97**, 220502(R) (2018).

[c] Sibille R., Gauthier N., Yan H., Hatnean M.C., Ollivier J., Winn B., Filges U., Balakrishnan G., Kenzelmann M., Shannon N., Fennell T., "Experimental signatures of emergent quantum electrodynamics in $\text{Pr}_2\text{Hf}_2\text{O}_7$ ", *Nature Physics* **14**, 711-715 (2018).

[d] Savici A.T., Zaliznyak I.A., Garlea V.O., Winn B., "Data processing workflow for time of flight polarized neutrons inelastic measurements", *Journal of Physics: Conference Series* **862**, 012023 (2017).

[e] Xu Z., Schneeloch J.A., Wen J., Winn B., Granroth G.E., Zhao Y., Gu G.D., Zaliznyak I.A., Tranquada J.M., Birgeneau R.J., Xu G., "Surprising loss of three-dimensionality in low-energy spin correlations on approaching superconductivity in $\text{Fe}_{1+y}\text{Te}_{1-x}\text{Se}_x$ ", *Physical Review B* **96**, 13, 134505 (2017).

[f] Zaliznyak I.A., Savici A.T., Garlea V.O., Winn B., Filges U., Schneeloch J.A., Tranquada J.M., Gu G.D., Wang A., Petrovic C., "Polarized neutron scattering on HYSPEC: the HYbrid SPECtrometer at SNS", *Journal of Physics: Conference Series* **862**, 012030 (2017).

[g] Zhong R., "Investigations of Quantum Materials: from Topological Insulators to High Temperature Superconductors", Ph.D. Dissertation, State University of New York at Stony Brook (2017).

[h] Zhong R., Winn B., Gu G.D., Reznik D., Tranquada J.M., "Evidence for a Nematic Phase in $\text{La}_{1.75}\text{Sr}_{0.25}\text{NiO}_4$ ", *Physical Review Letters* **118**, 17, 177601 (2017).

9.7 OUTREACH AND EXPANSION INITIATIVES

The polarized technique of separating spin-incoherent scattering is well established, but we are only starting to demonstrate it and have not yet socialized it aggressively, unlike the LET [G. Cassella, *et al.*, "Polarization analysis on the LET cold neutron spectrometer using a ^3He spin-filter: first results," , *Journal of Physics: Conference Series* **1316**, 012007 (2019)] and MACS [W. Chen, *et al.*, "Wide-angle polarization analysis on the multi-axis crystal spectrometer for the study of collective and single particle dynamics of methanol at its prepeak," *Physica B: Condensed Matter* **564**, 166 (2019)] teams. How we will socialize this capability is described in the near-term vision section below.

For unpolarized work, we have observed increased proposal, experiment and publication rates from some internal ORNL groups since the 2017 review (M. Manley & R. Hermann).

(a) Workshops, Talks: The 2019 tutorial workshop "Polarized Neutron Diffraction and Spectroscopy: Applications to Quantum Materials" educated, encouraged and broadened the user base for polarization analysis. Led by O. Garlea, it included hands-on experience with a HYSPEC experiment and an exercise in using the reduction scripts for polarization analysis. The talk "Magnetic Ground States of Manganese Vanadate Systems with 2D Striped Triangular Lattices" was given by O. Garlea at the ACNS 2018 conference. The talk "Polarization Developments at the Direct Geometry Spectrometer HYSPEC" was given by B. Winn at ICANS 2019. An introduction to neutron scattering talk was presented to Physics faculty and undergraduate students at Tennessee Technological University in 2018.

(b) Student Training, Theses, Tutorials, and Schools: O. Garlea sponsored the undergraduate HERE student Liam Ritchie from Georgia Tech, who was recommended by M. Mourigal. Mr. Ritchie began work on the development of spin wave excitation catalogue. Dr. Garlea is currently sponsoring Judith Roth of Florida State University, who is advised by Dr. Michael Shatruk, on the project "Understanding Unconventional Magnetic Behavior with Neutron Scattering". This project's objectives are: 1) Investigation of the magnetic phase diagram of reentrant spin-glass materials by elastic and inelastic neutron scattering techniques and 2) Investigation of frustrated

magnetism and complex spin textures in ternary chalcogenides with triangular arrangements of magnetic moments.

HYSPEC hosted student experiments for the Neutron and X-ray Scattering School (NXS) in 2017 to demonstrate DGS on a powder with 6-point polarization analysis. HYSPEC had planned to host an experiment during the 2020 NXS but the pandemic changed the format and instruments were not actively part of this year's NXS.

Two dissertations leveraged results from HYSPEC data (M. Zhu and R. Zhong). Although not related directly to HYSPEC, B. Winn hosted in 2020 the SCGSR student Marcus Daum of Georgia Tech, advised by M. Mourigal; his training in the use of McVine was in part to enable modeling of some HYSPEC data, but the primary purpose of his appointment was to support MANTA development efforts (MANTA is a cold neutron triple axis spectrometer proposed for the HFIR guide hall).

9.8 MAPPING RECENT ACTIVITIES TO THE PREVIOUS 3-YEAR VISION

Activities of the HYSPEC team over the last few years align well with our previous near-term vision. Software for polarization analysis advanced sufficiently that we chose to host the first polarization analysis workshop in the fall of 2019. We have made progress towards polarization analysis of magneto-elastic excitations in the construction of miniature 3D coils. The elevator / oscillator system for the supermirror array and radial collimator has been functioning well since the fall of 2018. Wide angle scattered beam flipping capability is currently being assessed via two routes: RF and cryo-flipper capabilities. Early assessment suggests that both are viable approaches. Initial SNP tests at HYSPEC occurred in December 2019 and an ambitious wide-angle SNP design concept is making considerable progress. Finally, both vertical-bore split-coil magnets have made considerable progress. The 11 T magnet has been used in an experiment at HYSPEC and the 14 T magnet will soon be commissioned without neutrons at HYSPEC.

Where we did not meet the goals of the near-term vision include the following. Software for polarization analysis still needs to move beyond flip ratio correction. The use of students and post-docs to build our polarization competency was limited by the change in emphasis for postdocs into science initiatives. The movement towards polarization analysis of magneto-elastic excitations as well as SNP were slower than desired. We have yet to demonstrate linear polarization analysis using a compensated asymmetric vertical-bore split-coil magnet, mainly due to the preferred use of MAG-01 on other instruments and the lack of a specific general user program proposal which requires this capability.

9.9 VISION

Near-term Vision (1-3 years)

HYSPEC will refine and promote its polarization capabilities.

Building and sustaining collaborative in-house research that can benefit from our neutron polarization capability will further stimulate and facilitate the development of advanced algorithms for more efficient data processing and analysis. Software / algorithm for XYZ polarization analysis of single crystals beyond flip corrections shall be developed and beta-tested in parallel, using data from HYSPEC and users who have employed a 6-point (or more) measurement approach.

We intend that the inaugural polarization workshop of 2019 be repeated on a biannual basis indefinitely (2021, 2023, etc.), alternating years with the magnetic structure determination workshop which O. Garlea also co-organizes.

A new research direction will explore the hybridized magneto-elastic excitations appearing in systems with strong spin-lattice coupling, by unambiguously distinguishing between the structural and magnetic scattering features. Evidences of magneto-elastic excitations exist in materials such as the magnetocaloric compound MnFe_4Si_3 [N. Biniskos, “Inelastic neutron scattering on magnetocaloric compound”, PhD dissertation, RWTH Aachen (2018); S. Raymond, N. Biniskos, K. Schmalzl, J. Persson and T. Brückel, “Total interference between nuclear and magnetovibrational one-phonon scattering cross sections,” *J. Phys.: Conf. Ser.* **1316**, 012018 (2019)], but comprehensive studies of phonon-magnon coupling over a wide momentum-energy space are still missing. This direction requires the development of a wide-angle scattered beam flipper; the HYSPEC team has prepared an advanced draft for a SEED proposal and is currently evaluating the feasibility of two different flipper technologies for this flipper. If successful we will then have the first wide-angle white-beam flipper anywhere compatible with a polarizing supermirror array.

As part of a young researcher award for P. Jiang, for development of a wide-angle spherical neutron polarimetry (SNP), the HYSPEC team will support the development of experiment planning and preliminary analysis algorithms for several potential modes of operating this wide-angle SNP device. The commissioning for this wide-angle SNP system is expected to take place towards the end of this 3-year period.

Longitudinal (Z-only) polarization analysis employing a compensated asymmetric magnet (SLIM-SAM, maximum field 5 T) will be commissioned within the next three years at HYSPEC. The polarizing supermirror array was designed to accommodate such a magnet and this mode of operation, but we have not yet tested it with neutrons. In addition, since the new 14 T magnet has an asymmetric mode for polarization analysis studies, we will oversee careful model studies that consider the forces generated between this uncompensated magnet and the polarizing supermirror array, in order to determine what maximum field is safe for operation. We are hopeful that we will be able to operate the 14 T with the array in place, to a maximum field significantly higher than 5 T. As with the previous 3-year plan, these tests and calculations are contingent on both block scheduling and a scientific case for such an experiment.

With the completion of the EPICS data acquisition upgrades at the SNS, and the recent analysis support staff reorganizations, NScD is now well positioned to standardize systems across the DGS suite. Work is already progressing towards similar acquisition interfaces and scripting for instrument control. With the MANTID commitment to a new GUI structure `mantidWorkspace` using the latest QTPy version, the GUI development path for new reduction and analysis platforms is finally very clear. In addition, we intend to leverage the ICEMAN platform which has already been used to analyze some HYSPEC results and compare them to e.g. density functional theory (DFT) model estimates.

Five recent realizations have motivated new directions for our new 3-year plan. The first is that we must reduce our time-independent background and so we intend to invest in detector vessel shielding, as already described in the Activities section above. One side effect of this improved shielding is a reduced prompt pulse signal and possibly more narrow tail in our background, which may extend our ranges of useful incident energies. An unfortunate side effect for the facility is that HYSPEC will become less sensitive to changes in background conditions at the FTS, but the nED on Wheels cart will continue to be used and hopefully will now serve the purpose that HYSPEC has inadvertently done to date.

The second realization is that our current magnet-access path between the HYSPEC rolling door and the POWGEN rolling door will no longer be available by December 2020, due to the addition of another external building at BL-13. Therefore, our strategic 3-year plan includes a newly dedicated path.

The third realization is that longitudinal polarization analysis may provide an attractive capability for an entirely new scientific user community. At HYSPEC, users study either phonons or magnetic excitations. It is rare for users to study any systems with hydrogenous materials due to the large isotropic spin-incoherent scattering contribution. Polarization analysis provides a mechanism (besides deuteration and dynamic nuclear polarization) to separate coherent nuclear scattering from incoherent spin-incoherent scattering. Our colleagues at LET [G. Cassella, J.R. Stewart, G.M. Paternò, V. García Sakai, M. Devonport, P.J. Galsworthy, R.I. Bewley, D.J. Vonshen, D. Raspino and G.J. Nilsen, "Polarization analysis on the LET cold neutron spectrometer using a ^3He spin-filter: first results," *Journal of Physics: Conference Series* 1316, 012007 (2019)] and MACS [W. Chen, S. Watson, Y. Qiu, J.A. Rodriguez-Rivera, A. Faraone, "Wide-angle polarization analysis on the multi-axis crystal spectrometer for the study of collective and single particle dynamics of methanol at its prepeak," *Physica B: Condensed Matter* 564, 166 (2019)] are developing their polarization analysis for this specific community. HYSPEC has recently conducted initial measurements of both normal and deuterated water with colleagues from BNL, the results of which we intend to socialize as we recruit another niche community of HYSPEC users.

The fourth new direction combines renewed concern about liquid helium cost and availability with new and newly integrated technologies which enable high-cooling-power dry cryostats. We are therefore considering investing in a top-loading dry cryostat. This cryostat would be the first or one of the first such cryostats in use at either SNS or HFIR, providing our sample environment group much-needed experience with these new technologies. This investment also represents part of a new broad ORNL strategy to limit and recycle helium.

As applications for cryostats have diversified, we now envision a new approach towards operating this cryostat, with a set of interchangeable tails. The workhorse tail will remain a broad-tail system, but other tails will be optimized with narrow tails for SNP or the new mini 3D coils or be made compatible with optical windows for a new class of optically pumped / neutron probed experiments. We have also been impressed by the performance of dry warm-bore magnets like MAG-I, and are considering investing in both compensated vertical-bore split-coil and a multi-coil horizontal-field magnets which would also be compatible with this new top-loading cryostat, as described below in our strategic long-term vision.

The fifth realization is our pandemic. How can we work safely? How can we host a viable user program? We are fortunate that much of HYSPEC operation is automated, and that our sample turnover is low (~1-4 samples per week) so that onsite activities can be minimized. New developments primarily in IDAQ software are further simplifying this process for all instruments, including HYSPEC.

Finally, we view the current BES emphasis on quantum materials as well aligned to the polarization analysis capability of HYSPEC, especially when exploring fractional excitations with diffuse inelastic scattering. Therefore, we shall persistently advocate for post-doctoral appointments which emphasize these kinds of polarized measurements. That HYSPEC is the optimal instrument at ORNL to study such excitations is incidental to the general scientific need in the context of the Quantum Materials Initiative.

Strategic Vision (3-10 years) and Alignment with NScD / ORNL Strategic Plan

HYSPEC will maximize its scientific impact and pioneer new capabilities for new science.

The HYSPEC team has grown to appreciate in the past three years that the phrase ‘polarization analysis’ does not represent a single technique, but ideally a suite of techniques from which a user selects the optimal approach for a given sample, sample conditions and scientific question. We intend to aggressively develop user-friendly analysis software and new polarization optics in order to build out this suite, leveraging the open and modular HYSPEC sample geometry and its already production-level polarization optics. We also intend to continue the bi-annual polarization tutorial workshops in a concerted effort to build and educate the polarization analysis user community.

For inelastic half-polarized experiments to really mature at HYSPEC requires a horizontal field magnet with an open geometry at beam elevation for wide scatter angle range. Experiments performed to date at HYSPEC partially saturate moments via permanent magnets and steel yokes. Such assemblies can depolarize the neutron beam near the poles, occlude much of the desired horizontal scatter angular range, slow heating and cooling by adding mass. and are limited to ~1000 Gauss at the sample position. Quadrupole magnets at other facilities mitigate all those problems, enabling better results for half-polarized experiments. We currently envision this magnet to be a warm-bore dry magnet compatible with a narrow-tail variant of the dry cryostat described in the 3-year vision.

Building on success of the wide-angle SNP described in the 3-year vision, the HYSPEC team will offer wide-angle SNP as a viable technique through the user program. The narrow tail variant of the new cryostat described in the 3-year vision is compatible with the narrow working diameter of the current wide-angle SNP design concept.

Beyond polarization analysis, HYSPEC’s niche within the unpolarized suite of DGS instruments at the SNS will continue to play a major role in its scientific productivity. Although no new investments are planned to enhance unpolarized capability specifically, we will benefit from investments in both detector shielding and new sample environments. The detector shielding improvements implemented during the first 3 years will not only permit measurements of weak moment samples, but also of smaller and more absorbing samples for unpolarized measurements. For example, we expect iridates will become significantly more accessible for inelastic neutron scattering.

High-field next-generation magnets that employ composite conductors with high temperature superconducting materials (HTS) are on the horizon. Critical current density at high ambient field and liquid helium temperatures for these conductors is inherently greater than that achievable with low temperature superconducting coils, and a 32 Tesla solenoidal magnet is being commissioned at the National High Magnetic Field Laboratory now, whose development and lessons learned will provide guidance for constructing comparable-field magnets for neutron scattering. With greater current density comes the promise of more compact coils with lower stray fields for the same field-at-sample, but the stray fields for uncompensated magnets at higher field will need to be modeled and possibly compensated. HYSPEC’s use of cold neutrons for spectroscopy matches well the scientific demand for high-magnetic-field at sample, and its largely non-magnetic drum shield and sample arm hold out the promise for reasonable compatibility with stray fields. As ambitious plans for an incredibly high field magnet continue to stall, the need for intermediate stepping-stone magnet which (1) accepts a lower field, (2) provides higher steady-state field than currently available at the SNS, and (3) informs the technology and reduces risk for even higher field magnets, motivates us to explore the procurement of such a magnet.

In addition, moderate field HTS dry magnets are already commercially available, in operation at several neutron and x-ray scattering facilities worldwide and have received accolades from both facilities and users. Most of these magnets have been warm bore which is consistent with our proposed narrow-tail cryostat, and potentially also compatible with narrow tails with optical windows. We propose to purchase similar magnets, in part to train our sample environment staff with this new technology, but also to prepare for higher field magnets using similar technology. One such magnet may well be the multipole horizontal field magnet already described. Another magnet would be a new compensated asymmetric vertical-bore split-coil magnet needed to replace the 5 T SLIM SAM magnet, which is nearing end-of-life.

By separating the sample temperature conditions using a warm-bore configuration, we transition to more compact magnet assemblies which no longer require access via the HYSPEC rolling door. Avoiding the rolling door is critical to the long term implementation of magnet experiments at HYSPEC, since it's unlikely that the new 14A magnet path would remain after installation of a new (and as-yet undetermined) instrument at 14A, and since STS construction activities would preclude alternative access paths.

The strategic vision for HYSPEC aligns with and accounts for the 3-source strategy being developed for HFIR, the SNS First Target Station (FTS), and the proposed Second Target Station. HYSPEC has already established itself among the DGS instruments as the cold-neutron, moderate-resolution option, and along with the HB-1 triple axis we provide the additional optional capability of wide-scatter-angle polarization analysis. The complementary nature of DGS's and TAX's is clear, both by operation and by publication, where it's common to find high-impact publications that include results from both TAX's and DGS's for the same system. From an operational perspective DGS's tend to acquire at a few fixed sample environment conditions but leverage both ToF and wide area detectors for rapid acquisition of large volumes of reciprocal space, while TAX's often leverage their higher average monochromatic flux-on-sample by performing parametric studies with much finer steps in temperature, magnetic field. In particular, the polarization analysis capabilities of PTAX complement those of HYSPEC, where PTAX can reach higher energy transfers more easily than HYSPEC, but HYSPEC is more adept at capturing inelastic diffuse scattering. DGS's are also the instrument-of-choice for studies of powder samples when single crystals of sufficient size are not yet available.

HYSPEC will complement capabilities of proposed instruments within the 3-source strategy. In about 5 years at HFIR, we hope to be commissioning the new triple axis spectrometer MANTA. With Rowland focusing at sample, a newly optimized guide system, and a multiplexed and wide-angle analyzer / detector system, MANTA is expected to provide a complementary instrument to HYSPEC by performing studies in a more limited momentum and energy transfer regime. In about 10 years, the Second Target Station will be under construction with instruments in commissioning. The final instrument selection for STS is not complete but there are concepts in development that will enable high brightness cold neutron spectroscopy. Current concepts include an instrument optimized for extreme environments including high magnetic fields and polarization analysis using ^3He polarizers (like the MACS implementation at NCNR).

However, so long as the first target station supports coupled cold moderators, HYSPEC will remain a viable and incredibly useful DGS, and play a key role within the 3-source strategy, for the following reasons:

- HYSPEC will remain the only DGS with polarization analysis achieved via a polarizing supermirror array, enabling large sample environments and compensated magnets (as compared to ^3He filters).
- HYSPEC is currently very scientifically productive, which will not change in 10 years. The niche identified for HYSPEC will remain solid justification for future work.

- HYSPEC has the most potential for development of new capabilities for new science. HYSPEC's configurable region around the sample environment, similar to that of a triple axis spectrometer, make it the DGS-of-choice for prototyping and testing new sample environments, polarization optics, and other techniques.
- HYSPEC is the ideal place to test polarization optics intended for future instruments such MANTA at HFIR or those eventually selected for STS.

9.10 FUNDING / RESOURCE NEEDS

Sample environment: We intend to purchase a top-loading dry cryostat with interchangeable tails, as well as dry warm-bore magnets, as described above.

Software: At HYSPEC, we require an engaged and active community of users and developers to contribute to the development of open source tools. These tools will improve modeling of sample response, polarization analysis, resolution function prediction and convolution, multiple scattering and multiphonon scattering corrections, and publication-quality figure generation, in order to streamline and accelerate the path between data acquisition and publication, as well as to improve the decision-making ability for users as they perform their experiments. In order to achieve this, resource requirements include coding-savvy postdocs who can work closely with the new Computational Instrument Scientist.

Future Funding Opportunities: In addition to seeking internally funded instrument upgrades, the instrument team is committed to endorsing, partnering and leading funding proposals to advance the science mission of HYSPEC using lab-funded LDRD and SEED projects, DOE-sponsored SBIR and EFRC calls, and other funding opportunities from other agencies.

9.11 SELF-ASSESSMENT

Strengths

The magnetic scattering cross section afforded by the magnetic moment of neutrons remains the most direct means to study magnetic structures and excitations in quantum materials. HYSPEC's high flux in the cold-neutron regime, its compatibility with high magnetic field at sample, and its several modes of polarization analysis all position this instrument very well for long-term scientific productivity. Currently, the HYSPEC spectrometer is a leading instrument worldwide in enabling polarized INS measurements of the independent scattering components over a broad range of Q - ω space.

Weaknesses (Limitations)

HYSPEC is only partly compatible with high-field uncompensated magnets. Ferromagnetic components (like rebar in the floor, steel casings for concrete blocks, and chopper and stepper motor systems) and the supermirror array near the sample position will experience significant forces. No instrument at the FTS was designed with uncompensated magnets in mind, in part due to an earlier preference for procuring compensated magnets. HYSPEC is also straddled by the Fundamental Physics Beamline (BL-13) and the Neutron Spin Echo (BL-15) beamline, the two most stray-field-sensitive instruments at the FTS. To best leverage the use of the new 14 T magnet, and to potentially use next generation HTS magnets, modeling, measurements and possible modifications at HYSPEC may be required.

An limitation associated with the use of the polarizing supermirror array is the limited view permitted by the analyzer, especially for energies above 15 meV. Our scattered beam analyzer is much more

constraining than the radial collimator, and limits the effective sample diameter to about 6 mm for energies above 15 meV. Users requiring polarization analysis are encouraged to prepare their samples accordingly.

A longer-term limitation may arise if the FTS moves to better realize the 3-source strategy, by transitioning to all-water moderators. Those instruments currently benefiting from our coupled cold source (BL's 13-15) would require a drastic new design and different scientific objectives in order to leverage different spectral and timing emphasis. This change is not planned for the next changeout of the inner reflector plug, but no plans have yet been made beyond that.

Opportunities

The continued development of polarization capabilities at HYSPEC, as well as the development of data acquisition and analysis software for processing polarized neutron measurements, offers key information for enabling polarized neutron capabilities at the STS.

Threats

One kind of threat is via friendly competition from similar neutron scattering spectrometers worldwide. Unpolarized DGS's like DCS (NCNR), and AMATERAS (J-PARC) are already scientifically productive. Spectrometers that do or will employ wide angle supermirror analyzers include D7 (ILL), DNS (MLZ), FOCUS (SINQ) and POLANO (J-PARC). Spectrometers that do or will employ wide angle ^3He analyzer cells include MACS (NCNR), LET (ISIS), PELICAN (ANSTO) and TOPAS (MLZ). All these instruments and their operational parameters are listed in the appendix.

9.12 EXECUTIVE SUMMARY

HYSPEC is established as a scientifically productive, cold-neutron, intermediate resolution direct geometry spectrometer using either unpolarized or polarized neutrons.

9.12.1 Comparison of HYSPEC polarized capabilities to other instruments

Polarization	HYSPEC	MACS	D7
Unpolarized	User program	User program	User program
Half polarized			
Polarization Analysis	User program for XYZ	User program Z only	User program for XYZ
Polarizer	Heusler focus array	³ He drop-in cell	Focusing bender supermirror (Co/Ti, m=2.8)
Pre-sample flipper	Mezei	Flip nuclei ³ He via AFP	Mezei
Analyzer	Wide angle polarizing supermirror array, remanent	³ He drop-in banana	Wide angle polarizing supermirror array, induced

DNS	PELICAN	FOCUS	POLANO
User program	User program	User program	Under construction
	In commissioning		
User program for XYZ			
Focusing polarizing supermirror array m=3	Bender supermirror polarizer		³ He SEOP in-situ
	RF		Flip nuclei ³ He via AFP
Wide angle polarizing supermirror array, induced	³ He cell, MEOP	Wide angle polarizing supermirror array, remanent	Wide angle polarizing supermirror array, remanent

TOPAS	LET	DCS	AMATERAS
Under construction	User program	User program	User program
	User program Z only	Not scoped	Not scoped
³ He SEOP in-situ, tested at POLI, E _i < 150 meV	Two-channel m=5 FeSi transmission V-cavity		
Flip nuclei ³ He via AFP	Current-ramped precession coil, 99% efficient, to leverage rep-rate multiplication		
Pastis / ³ He donut tested at V20, HZB	³ He drop-in 'banana'		

10. SNS BL-2, THE BASIS BACKSCATTERING SPECTROMETER: BEAMLINE STATUS AND PLANNING SUMMARY DOCUMENT

10.1 OVERVIEW/CURRENT STATUS

The Backscattering Spectrometer (BASIS) is located on BL-2 at the Spallation Neutron Source (SNS). The instrument is a time-of-flight near-backscattering inverted geometry spectrometer, with an energy resolution of ca. 0.0037 meV (FWHM) with Si(111) analyzer crystals and ca. 0.015 meV (FWHM) with Si(311) analyzer crystals. The energy transfer range typically examined at BASIS varies, depending on the incident bandwidth chopper settings, from (-0.1 to +0.1 meV) to (-0.2 to +0.2 meV) to (-0.1 to +0.5 meV) with Si(111) analyzer crystals, and from (-0.66 to +0.66 meV) to (-1.7 to +1.7 meV) with Si(311) analyzer crystals. The corresponding momentum transfer is 0.2 to 2.0 \AA^{-1} with Si(111) analyzer crystals and 0.4 to 3.7 \AA^{-1} with Si(311) analyzer crystals. The BASIS has been in the user program since December 2007.

The BASIS has employed, for the first time in the history of time-of-flight backscattering instruments, silicon analyzer crystals, which provides an opportunity to combine a high energy resolution with a reasonably broad range of energy transfers. To match the high resolution of silicon analyzers, the BASIS faces a decoupled supercritical hydrogen centerline-poisoned moderator with the emission time width of about 60 μsec for the wavelength of 6.3 \AA and utilizes a long incident flight path of 84 m between the moderator and the sample position.

Incident neutrons travel to the sample position through an 83.725 m long supermirror guide. The upstream sections of the guide have a horizontal curvature of 1000 m radius, with the direct line-of-sight ending at about 28 m from the moderator. The curved guide helps eliminate fast neutrons and gamma-rays. At 31 m from the moderator, a straight guide section smoothly joins the curved guide. The coating of the guide sections varies; the last section of the tapered guide has $m = 3.6$. The first sections of the guide are placed inside the core vessel and the primary shutter, thereby providing an increased incident neutron flux. The guide has several gaps to accommodate the primary and secondary shutters and bandwidth selection choppers positioned at 7, 9.25, and 50 m from the moderator. Both the curved and straight guide sections have a rectangular cross-section of 12 cm height and 10 cm width at all distances but the last 8 m of the guide, where tapered supermirror sections compress the beam to 3.25 cm by 3.25 cm at the exit of the guide at 27.5 m upstream the sample position. A part of the last, funnel section of the guide resides inside the spectrometer tank. A system of slits, vertical and horizontal, which allows restriction of the incident beam size, and the incident beam monitor at 23.4 m upstream the sample position, are located between the exit of the guide and the sample position.

The spectrometer tank is evacuated down to below 10 mTorr, as required for the detector operation, and employs extensive background reducing shielding at various locations. The sample chamber, which is typically evacuated to reduce the background (though it is not required for operation), is separated from



Figure 10.1. The BASIS Instrument team. From left to right: Naresh Osti (Instrument Scientist), Niina Jalarvo (Instrument Scientist), Eugene Mamontov (Point of Contact) and Richard Goyette (Instrument Scientific Associate (SA) until 2019. Not shown: Chris Schmitt (current SA).

the main spectrometer tank by a thin aluminum window. This allows quick replacement of sample environment equipment without breaking vacuum in the main tank. The sample chamber opens at the top of the spectrometer tank, from where the sample environment equipment is installed. After exiting the guide and traveling through the system of slits, the incident beam monitor, and the separation aluminum window, the incident neutrons arrive at the sample position. The neutrons that assume wavelength of 6.267 Å after scattering by the sample can be subsequently Bragg-reflected by the Si(111) analyzers toward the detectors. Likewise, the neutrons that assume wavelength of 3.273 Å after scattering by the sample can be subsequently Bragg-reflected by the Si(311) analyzers toward the detectors. On the way from the sample to the analyzer crystals and back to the detectors, neutrons have to pass through a radial collimator with a 4° separation between the vertical blades, which restricts the view of the sample and reduces the background.

On each side of the spectrometer tank (left and right with respect to the incident beam, aka South and North sides), there are upper and lower sets of analyzer crystals panels, Bragg-reflecting neutrons toward the separate detector banks positioned above and below the horizontal plane, respectively. The Bragg angle of about 88° was selected to nearly match the contributions from the primary and secondary spectrometer flight paths. Presently, one quarter of the spectrometer tank is populated with 9 Si(311) analyzer crystal panels, one quarter with 9 Si(111) analyzer crystal panels of the improved design (associated with much improved shape of the spectrometer resolution function), and two remaining quarters with 18 Si(111) analyzer crystal panels of the original design. Each quarter covers about 150° in the horizontal plane and about 22° in the out-of-plane directions, thus providing coverage of about 1 ster, or 8 % of 4π . Two top and two bottom detector arrays, which form circular detector banks above and below the horizontal plane, are comprised of 56 linear position-sensitive He-3 tubes each. Each tube has a diameter of 1.25 cm, an active length of 15 cm, and is filled with He-3 at 8 atmospheres. The total flight path from the sample to analyzer crystals to the detectors, which includes the constant contribution of 2.5 m from the sample-to-analyzer distance, varies between 4.71 m and 4.729 m around a mean value of 4.72 m, depending on the out-of-plane angle of the neutron scattered by the sample. The variations as a function of the detector pixel height in the flight path and, less importantly, in the Bragg angle and the reflected neutron wavelength, are accounted for in the data reduction software, which converts time-of-flight into energy transfer independently for each detector pixel. Since the exact flight path and the final wavelength are known for each detector pixel (assuming a point sample), the incident energy, and, thus, the energy transfer, $E = E_i - E_f$, can be calculated from the total time-of-flight of the detected neutrons. The value of the scattering momentum transfer, Q , can be calculated in a similar fashion, as $Q = (k_i^2 + k_f^2 - 2k_i k_f \cos(2\theta))^{1/2}$. The scattering angles covered by the analyzer panels and the detectors vary between $2\theta_{\min} = 11.5^\circ$ and $2\theta_{\max} = 161.2^\circ$.

Team Structure

Management responsibilities for the BASIS lie in the spectroscopy group within the Neutron Scattering Division (NSD). The instrument team is shown in the photograph in Figure 10.1 (the current restrictions precluded taking a new picture with Christopher Schmitt, who has replaced Rick Goyette in 2019). Three instrument scientists (1 FTE each) are members of the NSD. The BASIS Scientific Associate (SA) is a member of the Scientific Associates Team.

10.2 SCIENTIFIC FOCUS

The range of science areas being studied with the BASIS instrument is unusually broad for a backscattering spectrometer. Soft Matter topics have traditionally dominated the scientific agenda at the BASIS, but lately Energy Materials topics came to prominence. It should be noted, however, that most of Energy Materials studies at the BASIS involve electrolyte fluids, in the bulk state or in confinement (for example, for supercapacitors applications), and thus could be also classified as Soft Matter studies. Other traditional Soft Matter topics addressed at the BASIS are in various areas of biological and polymer sciences. Aside from these, hydrogen confined in various materials is routinely measured at the BASIS. One area which has been repeatedly tried, with substantial effort, but little success, was measurements of single-crystal samples, mostly in search of magnetic excitations. Typical duration of a BASIS experiment is between four and six days.



Figure 10.2. BASIS publication statistics

10.3 SCIENTIFIC HIGHLIGHTS

The BASIS has been used to solve a broad range of scientific problems. We provide herein several examples that demonstrate the breadth of scientific work that was done in 2017-2020 using capabilities of the BASIS spectrometer.

Mixed Ionic Liquid Improves Electrolyte Dynamics in Supercapacitors

N. C. Osti, A. Gallegos, B. Dyatkin, J. Wu, Y. Gogotsi, and E. Mamontov, *Journal of Physical Chemistry C* **122**, 19476-10481 (2018)

Well-tailored mixtures of distinct ionic liquids can act as optimal electrolytes that extend the operating electrochemical window and improve charge storage density in supercapacitors. To this end, quasielastic neutron scattering (QENS) measurements at the BASIS in conjunction with classical density functions theory (cDFT) simulations have explored the electric double-layer behavior near the onion-like carbon electrode surface of mixtures of two room-temperature ionic liquids (RTILs), 1-ethyl-3-methylimidazolium bis(trifluoromethylsulfonyl)imide (EmimTFSI) and 1-ethyl-3-methylimidazoliumtetrafluoroborate (EmimBF₄). Computational results reveal that a mixture with 4:1 EmimTFSI/EmimBF₄ volume ratio displaces the larger [TFSI⁻] anions with smaller [BF₄⁻] ions, leading to an excess adsorption of [Emim⁺] cations near the electrode surface. These findings are corroborated by the QENS measurements that reveal the highest fraction of the cations immobilized near the surface at this mixture composition. Moreover, the cations that remain mobile exhibit the highest diffusivity at this mixture composition, as also revealed by the QENS. Molecular-level understanding of ion packing near electrodes provides insight for design of ionic liquid formulations that enhance the performance of electrochemical energy storage devices. This work was supported as part of the Fluid Interface Reactions, Structures and Transport (FIRST) Center, an Energy Frontier Research Center funded by the U.S. Department of Energy, Office of Science, Office of Basic Energy Sciences.

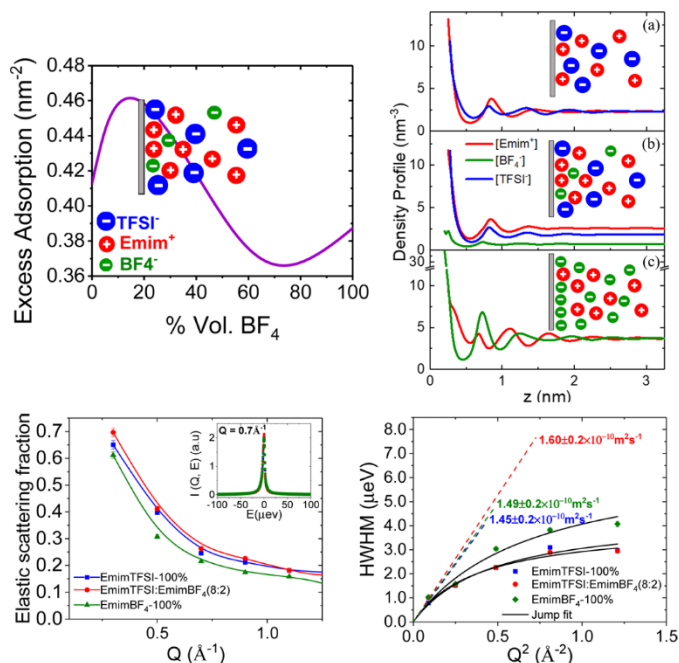


Figure 10.3. Top: classical DFT results. Left panel: excess adsorption of cations near the electrode surface as a function of anion concentration in EmimTFSI-EmimBF₄ ionic liquid mixture. Right panel: ion distributions for 0, 13, and 100 vol. % of EmimBF₄. Bottom: QENS results. The optimal composition is characterized by the highest fraction of the immobile cations (left panel) and the highest diffusivity of the remaining mobile cations (right panel).

Spatial-Temporal Characteristics of Confined Polymer Motion Determine Proton Conduction of Polyoxometalate-Poly(ethylene glycol) Hybrid Nanocomposites

H. Wu, L. Li, M. Tsuboi, Y. Cheng, W. Wang, E. Mamontov, S. Uchida, Z. Wang, and P. Yin, *Journal of Physical Chemistry Letters* 9, 5772-5777 (2018)

As a group of highly charged metal oxide nano-sized clusters, polyoxometalates (POMs) possess appreciable stability against high temperature and significant proton conductivity in ambient environments, which makes them promising candidates for fuel cell devices. POMs can be hybridized with polymers to form nanocomposites, which could significantly enhance POMs' proton conductivity as well as mechanical properties. Specifically, highly efficient proton conductors, polyoxometalate-poly(ethylene glycol) (POM-PEG) hybrid nanocomposites, can be synthesized by encapsulating a single PEG chain

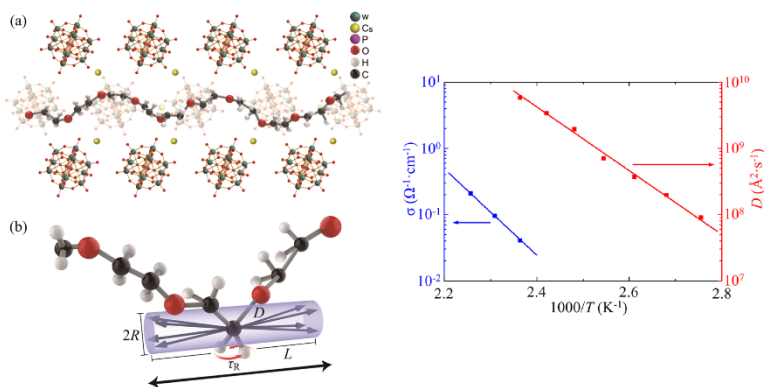


Figure 10.4. Left: conformation of the PEG inside the 1D nanochannel defined by the framework of POMs. Top panel: PEG chain is seen to stay as a distorted helix. Bottom panel: illustration of the meanings of the QENS fitting parameters. The cylinder with a length of L and a radius of R denotes the space that an atom with a diffusivity, D , can explore. The double-headed arrow denotes the direction of the 1D nanochannel. Right: correlation between the diffusivity (red) and conductivity (blue) temperature dependence.

inside the 1D nanochannel defined by the frameworks of POMs. QENS studies at the BASIS have revealed that the PEG segments perform a localized longitudinal random walk and demonstrated a strong correlation between the local motion of PEG and the macroscopic proton conduction of the material. Based on the spatial-temporal characteristics of the encapsulated PEG dynamics, a microscopic picture for the proton conduction process of POM-PEG hybrid materials has been proposed. The localized longitudinal random walk facilitates the proton conduction along the PEG backbones, and the random walk's activation energy is close to that of the proton-conduction process, suggesting that the local dynamics of the PEG chain dominates the proton conduction process of the POM-PEG hybrid materials. These results provide an instructive picture for the rational design and optimization of POM-PEG structures for highly efficient proton conductors with enhanced mechanical and stability performance.

Elucidating the Mobility of H⁺ and Li⁺ Ions in (Li_{6.25-x}H_xAl_{0.25})La₃Zr₂O₁₂ via Correlative Neutron and Electron Spectroscopy

H. Liu, Y. Chen, Z. D. Hood, C. Ma, S. Yu, A. Sharafi, H. Wang, K. An, J. Sakamoto, D. J. Siegel, Y. Cheng, N. H. Jalarvo, and M. Chi, *Energy & Environmental Science* **12**, 945-951 (2019)

A major challenge toward realizing high-performance aqueous lithium batteries (ALBs) is the utilization of a metallic lithium anode. An ideal solid electrolyte that can protect metallic lithium from reacting with aqueous solutions while still maintaining a high lithium ion conduction is not currently available. One obstacle precluding advances in this area is the lack of a reliable experimental tool to differentiate the conduction behavior of H⁺ and Li⁺ ions in a solid electrolyte. QENS at the BASIS has been used to quantify the mobility of H⁺ and Li⁺ ions in protonated cubic Li_{6.25}Al_{0.25}La₃Zr₂O₁₂ (LLZO). The results demonstrate that, within the standard operation temperature range of ALBs, H⁺ ions remain immobile, thus highlighting LLZO as a potential effective separation layer for ALBs applications. Even more importantly, this work successfully demonstrates a new methodological approach to probe diffusion behavior of individual ion species in dual-ion solids, an important and growing family of materials for energy storage and various other applications.

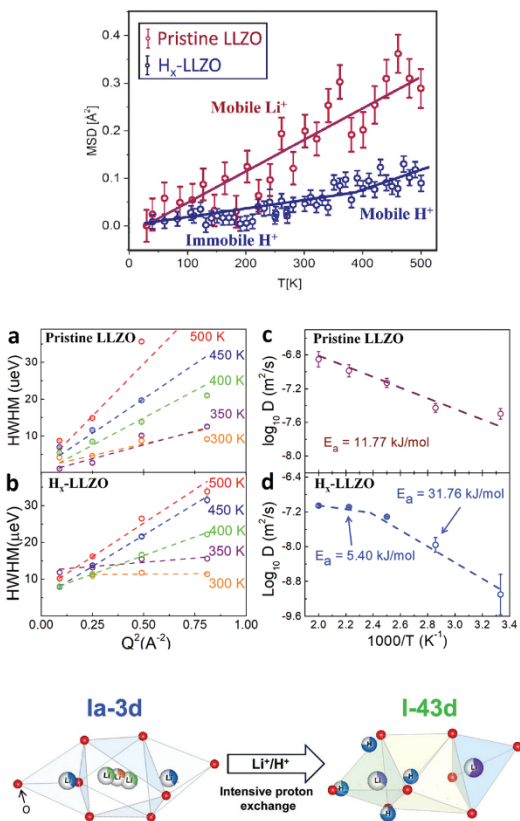


Figure 10.5. Mean-squared displacements (top) and QENS signal broadening (middle) in proton-bearing (Hx-LLZO) and proton-free (LLZO) materials indicating a changing diffusion mechanism for the protons at higher temperatures. Bottom: a schematic illustration of structural and chemical modifications in c-LLZO after intensive proton exchange.

Abnormally Low Activation Energy in Cubic Na₃SbS₄ Superionic Conductors

Q. Zhang, C. Zhang, Z. D. Hood, M. Chi, C. Liang, N. H. Jalarvo, M. Yu, and H. Wang, *Chemistry of Materials* 32, 2264-2271 (2020)

Inorganic Na-ion superionic conductors play a vital role in all-solid-state Na batteries that operate at room temperature. Sodium thioantimonate (Na₃SbS₄), a popular sulfide-based solid electrolyte, has attracted serious attention due to its advantages

of high ionic conductivity at room temperature and impressive chemical stability under ambient conditions. There is limited understanding of the Na ion diffusion mechanisms in Na₃SbS₄ with different crystal structures (e.g., tetragonal and cubic). A combination of electrochemical impedance measurements with DFT simulations and QENS measurements at the BASIS has probed conductive properties of sodium thioantimonate during its phase transition from a tetragonal to cubic structure. Although there is only a slight change in the lattice parameters, the energy barrier for Na-ion diffusion in the tetragonal structure was found to be much larger (by a factor of 5 to 10) than that in the cubic structure from both theoretical and experimental perspectives. The high degree of symmetry in the cubic structure leads to less interatomic correlations between the Na and S(Sb) atoms, a shorter jump distance (2.85 Å), and a larger diffusion coefficient. These results provide insight into understanding the Na-ion diffusion in solid electrolytes with phase transitions and offer fundamental guidance for designing novel solid-state Na-ion conductors.

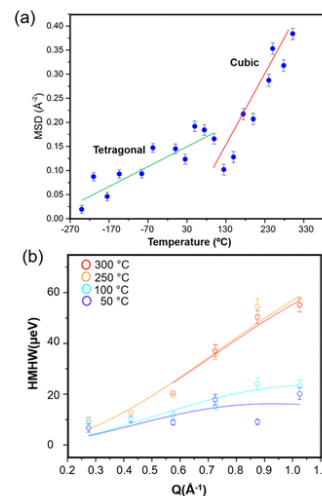
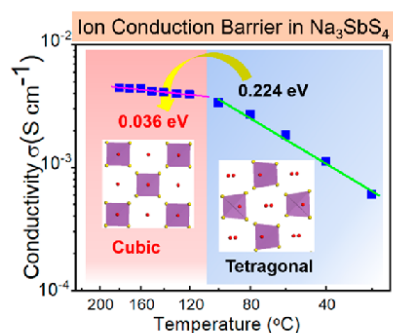


Figure 10.6. Temperature dependence of the conductivity (left) and the mean-squared displacements (top, right) and QENS signal broadening (bottom, right) in Na₃SbS₄

10.4 GENERAL USER PROGRAM

The BASIS user community includes individuals with very diverse scientific backgrounds. Please see pie chart in the Appendix for a detailed breakout of the science areas explored in the BASIS experiments. The most commonly used sample environment at the BASIS would be the top-loading closed cycle refrigerators (CCRs). Other commonly used sample environments include a bottom-loading CCR, a liquid helium based cryostat, a furnace, and a 5 T magnet available in the sample environment suite.

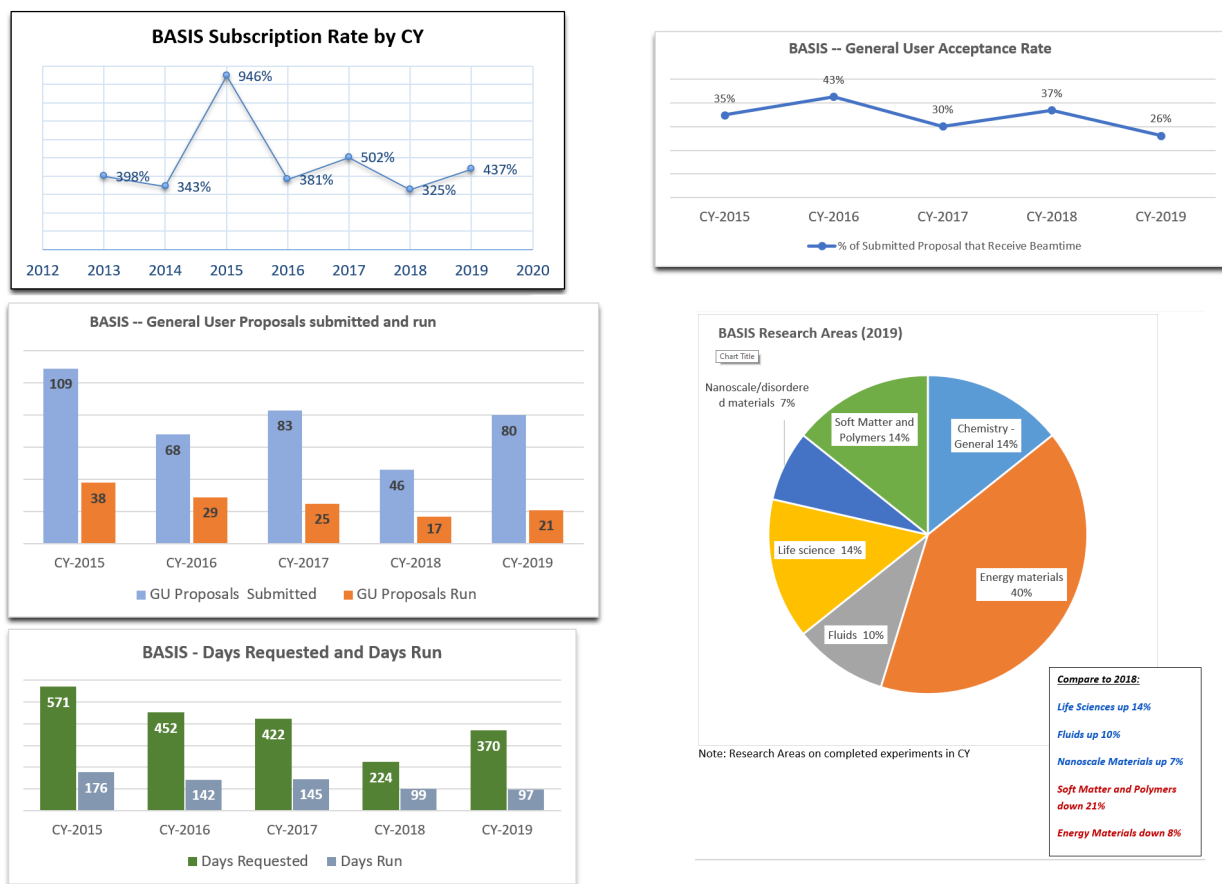


Figure 10.7. BASIS user program statistics

10.5 UPDATE ON INSTRUMENT DEVELOPMENT ACTIVITIES

10.6 UPDATE ON PARTNER AND DISCRETIONARY BEAM TIME.

Since it has entered the user program, the BASIS operated under an agreement with the Juelich Center for Neutron Science (JCNS), where 10 % of the available beam time is awarded to proposal selected by the JCNS. This agreement expired in 2020. Because of the recent expiration of this agreement, 25% of beam time (instead of 15 %) will now be awarded as discretionary time, which requires full written proposals.

10.7 OUTREACH

The BASIS team participates every year in the Department of Energy's National School on Neutron and X-Ray Scattering. The instrument and team provide hands-on experience in using the instrument and the examination and treatment of measured data provided by the instrument. This school provides graduate students and post-doctoral researches an excellent learning opportunity in the field of inelastic neutron scattering. Some of the students which participate in this school become users of the instruments later in their career path.

10.8 VISION

Near-term (1-3 years) and strategic (3-10 years)

The BASIS has become a well-established and highly in-demand instrument among the quasielastic neutron scattering community. It has a fully populated set of crystal analyzers and detectors. When it comes to hardware upgrades, the BASIS faces a competition with the higher sample throughput instruments in need of upgrades, which hampers the case for upgrade funding. The “soft” improvements, as outlined in the previous BASIS review document (2017), could be arguably more attainable. As it was discussed therein, following the recent advances in the QENS analysis software development (qClimax), it is data interpretation rather than data analysis per se that creates the bottleneck for expanding the instrument output. The BASIS review document (2017) featured an elaborate discussion of benefits that would be conferred on the instrument productivity by a postdoctoral researcher who provides (not merely assist with) molecular dynamics (MD) simulation and its full interpretation to the general program users of the BASIS who request it. It was concluded with a statement that *“Furthermore, this is a way to improve the overall quality of BASIS publications and user satisfaction and demonstrate the value of “simulations for users on demand” approach, paving the way to its eventual widespread adoption.”* That mission could possibly be accomplished, in full or in part, by the staff-level personnel filling the recently created positions of the Computational Instrument Scientists, who, in the current implementation, are allocated to the groups rather than individual instruments.

In view of these limitations, the attention may need to be directed to the cost-neutral ways to expand the instrument capabilities. Some advances made towards this goal in the past year are as follows. We have introduced [E. Mamontov, *Nuclear Instruments and Methods in Physics Research A* **949**, 162534 (2020)] the use of a higher-order reflection, Si(333), of the silicon analyzer crystals at a backscattering spectrometer to implement analysis of the relaxation dynamics. This is achieved by monitoring the temperature dependence of the neutron scattering intensity perceived as elastic when measured using Si(111), Si(311), and Si(333) reflections (Figure 10.8). As a test case, we have used a sample with well-characterized, but complex, relaxation pattern, where the non-Lorentzian relaxation function is known to exhibit a set of parameters specific to each temperature point and scattering momentum transfer (Q) value. Even for this very general relaxation pattern, characterized by no constraints on the relaxation function parameters, we have successfully mapped the relaxation times measured using the present approach onto those previously obtained from the full analysis of the quasielastic neutron scattering signal (Figure 9.7). Analysis of the Q -specific activation energies becomes possible for the Q values accessible simultaneously through Si(111), Si(311), and Si(333) reflections (in the present case, $0.9 \text{ \AA}^{-1} < Q < 1.9 \text{ \AA}^{-1}$). While the dedicated neutron spectrometers for this type of analysis are yet to be constructed, we show that the present-day backscattering spectrometers can be employed to analyze temperature dependence of the relaxation time in the samples not amenable to the traditional full analysis of the quasielastic neutron scattering signal (e.g., samples available in very limited amounts). Proposed almost twenty years ago and championed, at various times, by, e.g., Doster, Magazu, and Benedetto, this approach, known by different names, has been broadly discussed in the literature. The novelty introduced herein is in the use of the Si(333) analyzer reflection, which allows this approach to be implemented at high-resolution backscattering spectrometers rather than direct geometry time-of-flight machines.

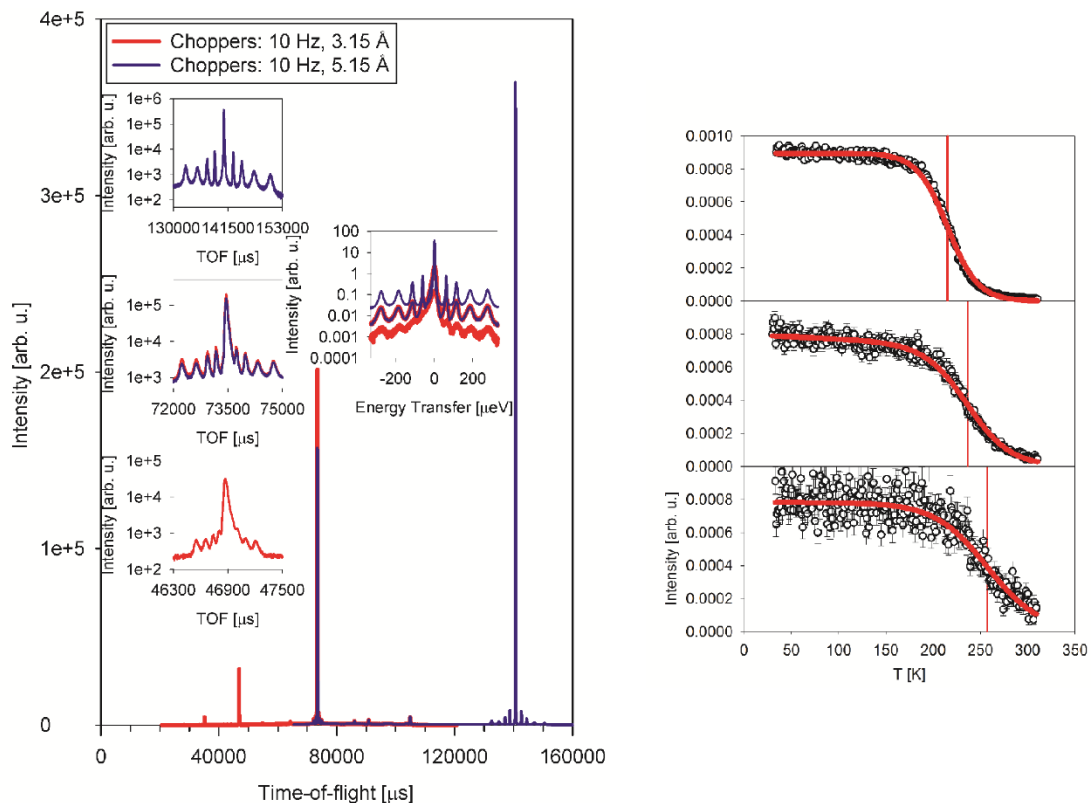


Figure 10.8. Left: the neutron scattering signal from gamma-picoline N-oxide at 9 K as a function of time-of-flight. Red line: choppers operated at 10 Hz with a band center at 3.15 Å, Si(333) elastic reflection at 46,870 μs and Si(311) elastic reflection at 73,450 μs and Si(111) elastic reflection at 140,630 μs . The three insets on the left show zoomed-in TOF ranges near the Si(333), Si(311), and Si(111) elastic peaks to emphasize the quantum tunneling peaks that can be detected using each of these reflections. The inset on the right shows the quantum tunneling data converted from the TOF to energy transfer, where the peaks from different reflections are now at the same positions, but are of different widths due to the variable energy resolution associated with the Si(333), Si(311), and Si(111) reflections. Right: Temperature dependence of the neutron elastic scattering intensity from $(\text{H}_2\text{O})_{0.88}(\text{LiCl})_{0.12}$ (symbols) measured at $Q = 1.3 \text{ \AA}^{-1}$ using Si(333) reflection (bottom), Si(311) reflection (middle), and Si(111) reflection (top). The temperatures of the intensity decay to one-half of its low-temperature value are indicated by the vertical thin red lines. [From: E. Mamontov, *Nuclear Instruments and Methods in Physics Research A* **949**, 162534 (2020)]

Shortly thereafter, we have proposed that the extended Q-range afforded by the use of Si(333) reflection (up to $Q = 5.7 \text{ \AA}^{-1}$), with a reasonably high energy resolution of 0.0336 meV (FWHM), could be used for dynamic pair-distribution function studies of disordered (liquid) systems at the BASIS. The first successful measurement of dynamics PDF from water at the BASIS was performed with Takeshi Egami's group in December 2019; the data analysis is in progress. If successful, we envision many more experiments of this kind at the BASIS in the future.

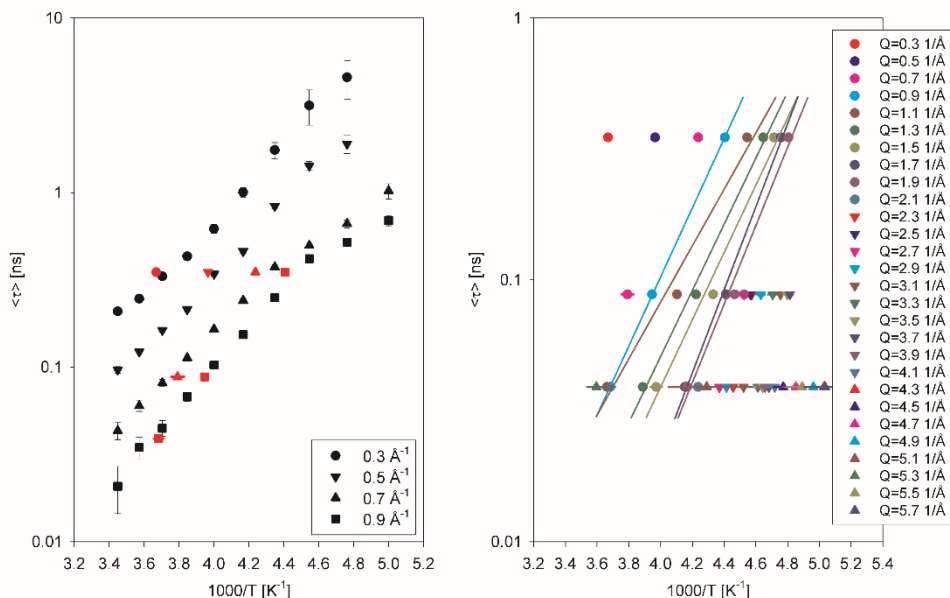


Figure 10.9. Left: Black symbols: average relaxation times previously measured from QENS data for $(\text{H}_2\text{O})_{0.88}(\text{LiCl})_{0.12}$. Red symbols: relaxation times as obtained from the present analysis. Right: relaxation times vs. temperature for $(\text{H}_2\text{O})_{0.88}(\text{LiCl})_{0.12}$ and the corresponding Arrhenius plots (lines) for the Q values accessible through the Si(333), Si(311), and Si(111) reflections. [From: E. Mamontov, *Nuclear Instruments and Methods in Physics Research A* **949**, 162534 (2020)]

10.9 FUNDING/RESOURCES NEEDS

The current staffing level at the BASIS is considered adequate, and it is not anticipated that it would need to be increased in the future.

10.10 FUTURE FUNDING OPPORTUNITIES

The instrument team will continue to pursue future funds at the laboratory and directorate level. These will often be in collaboration with other ORNL scientific staff.

10.11 SELF-ASSESSMENT

Strengths

A great strength of the BASIS instrument is a combination of three factors: a sufficiently high energy resolution combined with a relatively broad range of accessible energy transfers, achieved at a sufficiently high-count rate. These features make the BASIS a highly sought-after instrument among the QENS community.

As outlined in the previous BASIS review (2017), given average experiment duration on the BASIS of 4 to 6 days, which is not substantially different from that at other backscattering spectrometers, the sustained publication history of the BASIS has to be attributed to the service-minded attitude and effort of the BASIS personnel, who actively engage with users in all aspects of experiments, from actual measurement to data reduction/analysis/interpretation to paper writing. We believe that the BASIS can be considered an example of what can be achieved even at a low throughput instrument (high-resolution inelastic) with a sustained concentrated effort.

Weaknesses

The continuing weakness of the BASIS is characteristic of backscattering neutron spectrometers in general; due to the special requirements to the instrument geometry (driven by the energy resolution requirements), they tend to feature a narrow sample environment pit. This restricts the choice of the sample environment equipment compatible with backscattering spectrometers (BASIS is no exception). The only way to mitigate this weakness is to invest in R&D of specialized sample environment equipment of reduced size.

Threats

There are two direct competitors to the BASIS: the proposed MIRACLES backscattering spectrometer at the ESS and the existing DNA backscattering spectrometer at the J-PARC.

The MIRACLES would be an impressive spectrometer, whose actual performance remains to be seen. On the other hand, the DNA is operational. It can be considered a larger version of BASIS (aside from the difference in the means used to define the incident pulse; a decoupled moderator on the BASIS vs. a coupled moderator with a pulsed-shaping chopper on the DNA). With J-PARC attaining the full power, it might be difficult for the BASIS to compete head-to-head with the DNA due to the higher source power and the larger crystal analyzers area of the latter spectrometer. The competitiveness of the BASIS vs. the DNA thus may be determined by the quality of the user experiments and the effort by the instrument personnel.

10.12 EXECUTIVE SUMMARY

BASIS is in high demand and attracts a broad range of users with diverse scientific backgrounds. After a period of rapid growth during the first decade of operation, it has reached the level of maturity characteristic of the established instruments. Although its productivity compares favorably with the productivity of backscattering spectrometers worldwide, a competition from the new backscattering spectrometer at ESS may present a challenge fairly soon. The longer-term development goals at BASIS might involve (1) the expanded use of the opportunities presented by the existing hardware, such as the Si(311) and Si(333) analyzer reflections, and (2) the strategic expansion of the user base to include non-conventional communities of users, such as those who currently perceive their systems of interest as too complex to be probed by neutron scattering.

11. SNS BL-16B, THE VISION VIBRATIONAL SPECTROMETER BEAMLINE STATUS AND PLANNING SUMMARY DOCUMENT

11.1 OVERVIEW AND CURRENT STATUS

Initial configuration: The VISION spectrometer is located on BL-16B at the Spallation Neutron Source (SNS). VISION is an inverse geometry time of flight (ToF) spectrometer used for neutron vibrational spectroscopy, Figure 11.1. The instrument operates nominally at 30Hz and illuminates the sample with the full energy spectrum of neutrons pulses produced by a room temperature water moderator. A T_0 chopper (60 Hz) blocks the gamma flash and reduces the fast neutron background. A bandwidth selection chopper (30 Hz) selects the range of neutron wavelengths incident upon the sample. Neutrons are delivered to the sample through neutron guide ($m=5$) terminated by a 4 m converging section ($m=7$). The nominal beam size at the sample position is $3 \times 5 \text{ cm}^2$. The incident neutron energy is determined by time-of-flight. The final energy of the scattered neutrons is selected by Bragg-reflection on a pyrolytic graphite analyzer. Each of the thirteen analyzers comprises 350 single crystals of graphite, 1 cm^2 each, arranged in a spatially focusing geometry on an aluminum support. These crystals select scattered neutrons with a final energy of approximately 3.5 meV. All thirteen inelastic analyzer/filter/detector banks are operational. After Bragg reflection, the neutrons pass through a cooled (to 20 K) Be filter, which rejects higher orders of Bragg reflection on the graphite single crystals. The instrument dynamic range is -2 to 1000 meV with a constant resolution of above 5 meV. The elastic line has a full width at half-maximum of . The analyzers are arranged in two groups for forward (low Q) and backward (high Q) scattering. The analyzer focussing arrangement allows the use of compact, well shielded detector panels. Each panel (one per analyzer) consists of eight half-inch diameter x eight-inch length ^3He tubes. Two low efficiency ^3He beam monitors, one upstream and one downstream from the sample, record the energy spectrum of the incident and transmitted neutrons. A beam stop completes the beam line configuration. The sample is located 16 m in front of the moderator. The beam line is equipped with a top loading, closed-cycle refrigerator (5 to 700 K, helium exchange gas) in its standard configuration. The description above represents the instrument configuration at the start of its commissioning period in late 2014/early 2015.



Figure 11.1. The VISION spectrometer (BL16B) at SNS.

Commissioning phase: VISION started partial commissioning during the 2014B cycle. Its first complete cycle as an integral part of the SNS user program was 2015A, with significant commissioning activities continuing until the end of the 2015B cycle and into 2016A. Commissioning focused on (a) characterization of the instrument background (b) performance evaluation (flux, resolution, sensitivity, useful dynamic range, ...); (c) testing of the backscattering diffraction detector; (d) solving miscellaneous alignment and background problems; (e) developing the software needed for fast, efficient data reduction; (f) detector calibration; and (g) new sample environment equipment. These activities took place in conjunction with the development of a community of users and the first experiments yielding publishable results.

Update: Tasks (b)-(f) have largely been completed with reliable operation of data acquisition software, detectors, beam monitors, and routine sample environment (CCR, gas handling manifold, sample sticks, and a wide variety of sample holders). Background reduction through the addition of 3D printed blocks filled with B4C, as well as Cd sheets in various locations in the secondary spectrometer has led to a reduction in background by a factor of three compared to the initial configuration. This, in turn, has enabled the easier observation of small signals near the elastic line and facilitated the determination of difference spectra, e.g., in catalysis experiments. Sample environment equipment improvement and development is an ongoing project, largely in response to users' requests. As of 2018, VISION has reached a reliable, steady state mode of operation.



Figure 11.2. VISION team: (left to right) Luke Daemen, Timmy Ramirez-Cuesta, Eric Novak, Yongqiang Cheng.

Team Structure

VISION team: Luke L. Daemen (Lead instrument scientist, 1 FTE), A.J.(Timmy) Ramirez-Cuesta (0.5 FTE), Scientific Associate (Eric Novak, 1 FTE). Yongqiang Cheng is currently the computational instrument scientist for Chemical Spectroscopy – from 2017 until July 2020, he was an instrument scientist on VISION.

11.2 SCIENTIFIC FOCUS

Vibrational spectroscopy is an analytical technique that provides information about molecular structure, chemical bonding, and intermolecular interactions. Infrared absorption and Raman spectroscopies are well-known examples of this widely used form of spectroscopy. VISION uses neutrons rather than photons as a probe of molecular vibrations. This approach has several advantages over optical spectroscopy, including high sensitivity to hydrogen, absence of selection rules, ease of computation of the vibrational spectrum, isotopic sensitivity, no energy deposition in sample, and high neutron penetrability through bulky sample environment.

The science performed on VISION is diverse and encompasses physics, chemistry, geology, biology, and materials science. VISION is particularly efficient at exploiting the large incoherent cross section of hydrogen. The study of hydrogenous materials is therefore a popular research topic on VISION. This includes: water in confinement, hydrogen bonding, hydrogen storage, basic organic chemistry, catalysis and surface chemistry, polymers, batteries and fuel cells, porous materials, hydrous minerals, complex hydrides, proton conductors, and organometallic compounds to give but a few examples. Non-hydrogenous materials can also be studied (and are studied) thanks to the high neutron flux at SNS (source power) and the optimized instrument geometry. The VISION count rate is several hundred times that of its predecessor and competitor, the TOSCA

beam line at the ISIS facility at the Rutherford-Appleton Laboratory. In general, higher count rates promotes faster measurements, permits the use of smaller samples, and enables neutron vibrational spectroscopy experiments not feasible at TOSCA.

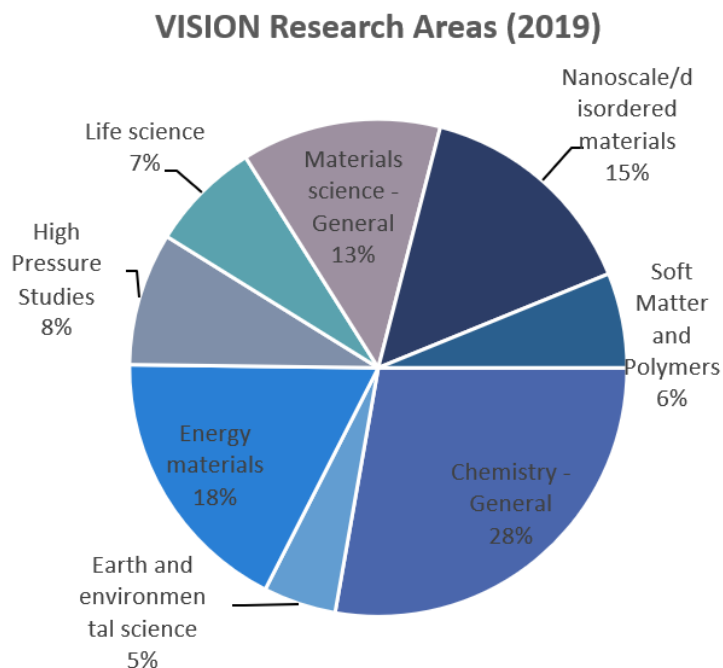


Figure 11.3. The VISION community of users by specialties in 2019

A representative distribution (2019) of proposals among various scientific fields is shown in Figure 11.3. Given the versatility of VISION and the ever-changing nature of the problems and scientific questions of interest to scientists in a particular field, this chart is constantly evolving and changing.

Update: Several new areas of interest have developed in recent years at VISION: (a) Magnetism: The use of VISION to study spin-phonon coupling in *single molecule magnets* through the anomalous temperature dependence of phonon modes strongly coupled to spins. The first experiments in magnetic fields up to 1.2 T were performed during the 2019B cycle; (b) Biochemistry: Several studies of changes in

proteins (e.g., HIV-1 protease) dynamics changes at low frequencies induced by mutations associated with drug resistance issues; (c) Nuclear science and engineering: Renewed interest in *molten salts* driven by DOE's current interest in molten salt reactors and the need for higher quality data for the scattering kernels used in radiation transport codes; (d) Natural materials: Multiple proposals focused on the study of *natural complex materials* such as wood, soot, and coal. These new topics off the beaten path represent healthy developments toward science diversification and the integration of new classes of users at VISION.

11.3 INSTRUMENT PRODUCTIVITY

The number of proposals submitted remained relatively constant over the years. The dip in CY-2018 is due to the Inner Reflector Plug (IRP) replacement project. There was only one call for proposals and one run cycle that year. The year 2019 saw two calls for proposals, but various accelerator problems (RFQ, cryogenic moderators, etc) led to low, 62%, beam availability and a large amount of down time for the user program. The 5-year average number of proposals submitted per cycle is 33. The General User Proposal beam time is 75% of the available number of days per cycle and does not include discretionary beam time, calibration and

instrument development, mail-in programs, proof-of-principle experiments, and other special use of beam time such as the yearly neutron school.

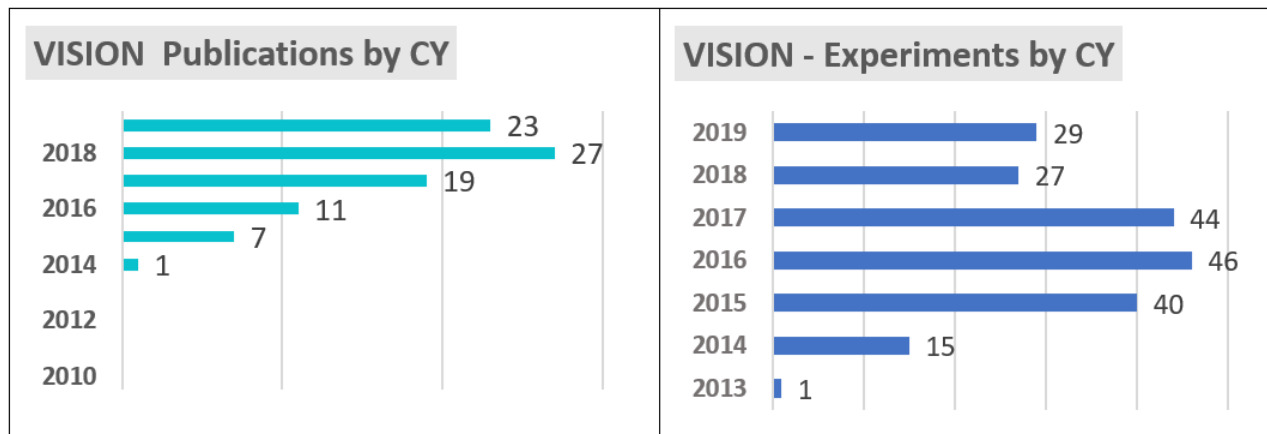


Figure 11.4. VISION publication statistics

Publications trends over the past 5 years reflect the commissioning phase and progressive development of the beam line into a fully operational instrument, as well as the continued growth of the user community over that period. The disappearance of a cycle in 2018 due to the IRP replacement and the accelerator problems in 2019 have led to an anomaly in publication numbers in 2019, but all indications are that 2020 publication numbers will continue the overall upward trend from 2014 that is evident in Figure 11.4. (As of July 2020, VISION has 20 publications + 6 manuscripts accepted for publication.) Until the end of CY19, the total number of publications for VISION is 92.

The number of unique users per calendar year is relatively steady with an average of 40 for the past five years, Figure 11.5. For this same period, data collected at VISION has supported 13 PhD theses at American universities and abroad -an average of 2.6 per year.

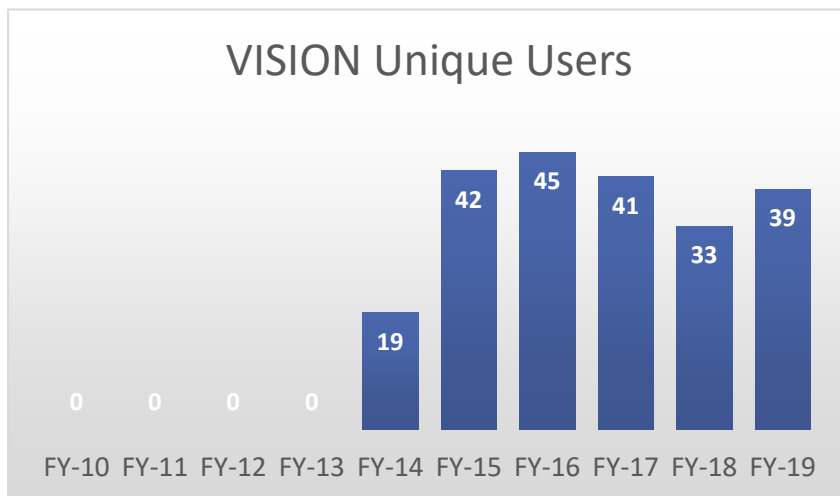
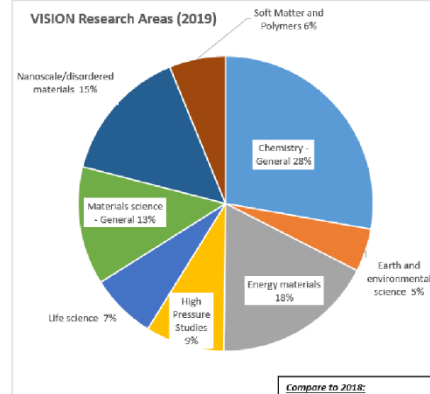
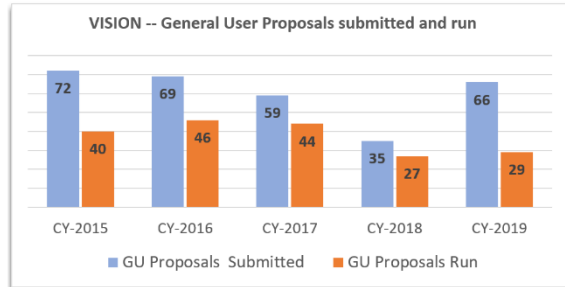
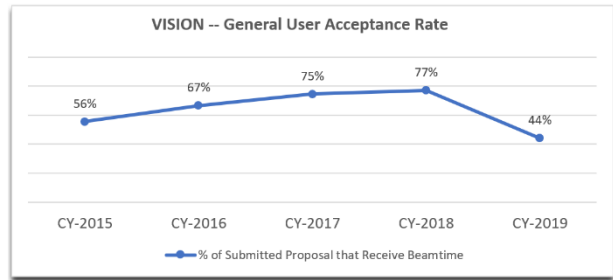
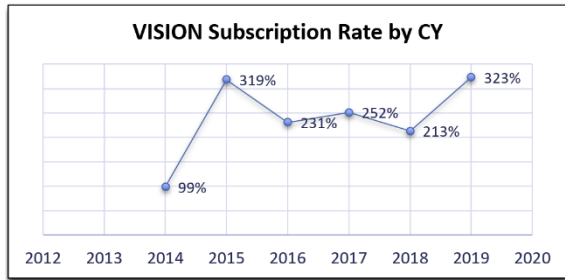


Figure 11.5. VISION unique users. The 2015-2019 (5-year) average is 40.



Compare to 2018:

- Chemistry up 5%
- Materials Science up 13%
- High Pressure Studies up 9%
- Energy Materials down 32%
- Earth and Environmental science down 11%
- Nanoscale Disordered Materials down 9%

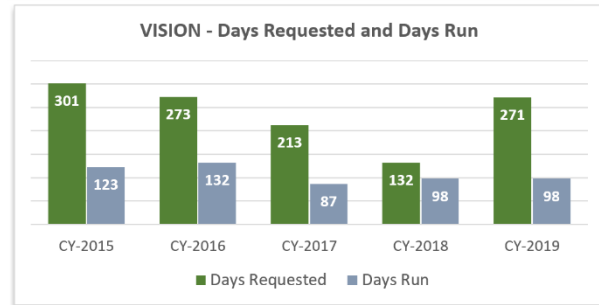


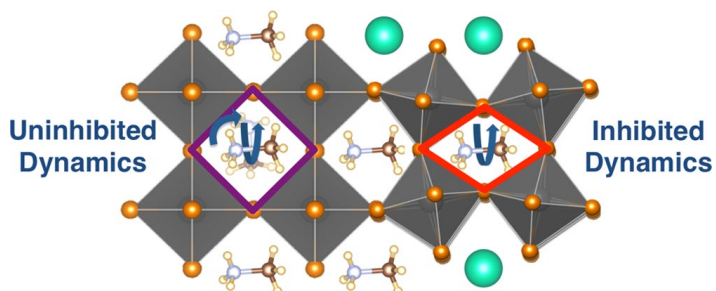
Figure 11.6. VISION user program statistics

11.4 SCIENCE EXAMPLES

Orientalional Glass Formation in Substituted Hybrid Perovskites

Eve M. Mozur, Annalise E. Maughan, Yongqiang Cheng, Ashfia Huq, Niina Jalarvo, Luke L. Daemen, and James R. Neilson, *Chemistry of Materials* 29, 10168 (2017).

Hybrid organic–inorganic perovskites have gained notoriety in the photovoltaic community for their composition-tunable band gaps and long-lived electronic excited states, which are known to be related to the crystalline phase. While it is known that the inorganic and organic components are coupled through



structural phase transitions, it remains unclear as to what role each plays in directing the structure of hybrid perovskites such as methylammonium lead halides ($\text{CH}_3\text{NH}_3\text{PbX}_3$). This group of users presented crystallographic and spectroscopic data for the series $(\text{CH}_3\text{NH}_3)_{1-x}\text{Cs}_x\text{PbBr}_3$, showing that $\text{CH}_3\text{NH}_3\text{PbBr}_3$ behaves as a plastic crystal in the high temperature cubic phase, and substitution of CH_3NH_3 + with Cs^+ leads to the formation of an orientational glass. While the organic molecule exhibits slow, glassy reorientational dynamics, Figure 11.7, the inorganic framework continues to undergo crystallographic phase transitions. These crystallographic transitions occur in the absence of thermodynamic signatures in the specific heat from molecular orientation transitions, which suggests that the phase transitions result from underlying instabilities intrinsic to the inorganic lattice. However, these transitions are not decoupled from the reorientations of the organic molecule, as indicated by inelastic and quasielastic neutron scattering at VISION and BASIS. Observation of a reentrant phase transition in $(\text{CH}_3\text{NH}_3)_{0.8}\text{Cs}_{0.2}\text{PbBr}_3$ permits the resolution of these complex behaviors within the context of strain mediated interactions. Together, these results provided critical insight into the coupled phase behavior and dynamics in hybrid perovskites.

James Neilson has been an associate professor of chemistry at Colorado State University since 2019. His research focuses on functional materials chemistry. He is a recipient of NSF and DOE Early Career Awards and a former Alfred P. Sloan Fellow. This work was part of the Ph.D. thesis of student Eve Mazur.

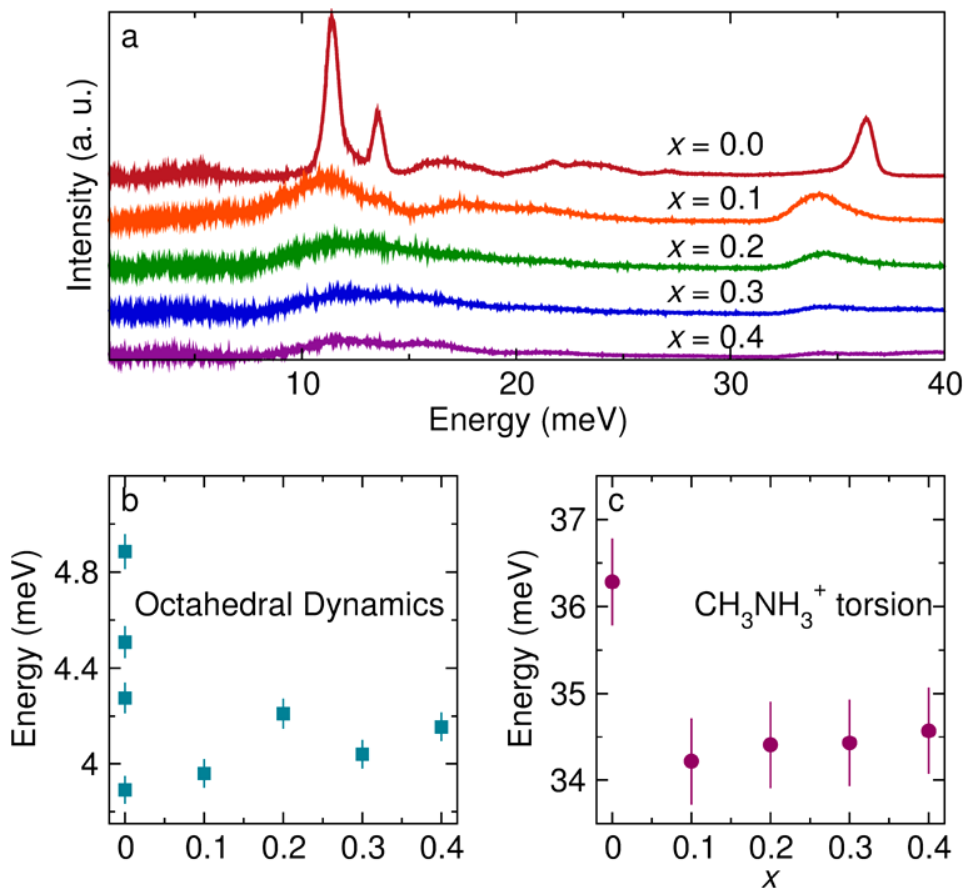


Figure 11.7. Reorientational dynamics of the methylammonium cation as a function of Cs doping as measured at VISION. (a) INS spectra collected at $T = 5$ K of $(\text{CH}_3\text{NH}_3)_{1-x}\text{Cs}_x\text{PbBr}_3$ over the energy range 2–40 meV. (b) The centroid of the low-lying optic phonons (4–5 meV) as a function of x . (c) The average energy of the CH_3NH_3^+ torsion (33–37 meV) as a function of x . Error bars in (b) and (c) are taken from the instrument resolution, respectively. The centroid of the peaks was determined by fitting the peak in the INS spectra to a Gaussian function and extracting the center.

Production of arenes via direct lignin upgrading over a niobium-based catalyst

Yi Shao, Qineng Xia, Lin Dong, Xiaohui Liu, Xue Han, Stewart F. Parker, Yongqiang Cheng, Luke L. Daemen, Anibal J. Ramirez-Cuesta, Sihai Yang and Yanqin Wang, *Nature Communications* 8, 16104 (2017)

Lignin is the only large-volume renewable source of aromatic chemicals. Efficient depolymerization and deoxygenation of lignin while retaining the aromatic functionality are attractive but extremely challenging. Prof. Sihai Yang's group at the University of Manchester reported the selective production of arenes via direct hydrodeoxygenation of organosolv lignin over a porous $\text{Ru}/\text{Nb}_2\text{O}_5$ catalyst that enabled the complete removal of the oxygen content from lignin. The conversion of birch lignin to monomer C7–C9 hydrocarbons is nearly quantitative based on its monomer content, with a total mass yield of 35.5 wt% and an exceptional arene selectivity of 71 wt%. Inelastic neutron scattering at VISION and DFT calculations confirmed that the Nb_2O_5 support is catalytically unique compared with other traditional oxide supports, and the disassociation energy of $\text{C}_{\text{aromatic}}\text{--OH}$ bonds

in phenolics is significantly reduced upon adsorption on Nb₂O₅, resulting in its distinct selectivity to arenes.

Sihai Yang is a professor of chemistry at the University of Manchester, United Kingdom. His academic awards include the Diamond Young Investigator Award (2011), the Honourable Mention Award of International Union of Pure and Applied Chemistry (IUPAC) Prize for Young Chemists (2012), the Institute of Physics B T M Willis Prize (2013), the ISIS Neutron & Muon Source Impact Awards (2019), the CCDC Chemical Crystallography Prize for Younger Scientists (2019), and the RSC Harrison-Meldola Memorial Prize (2020).

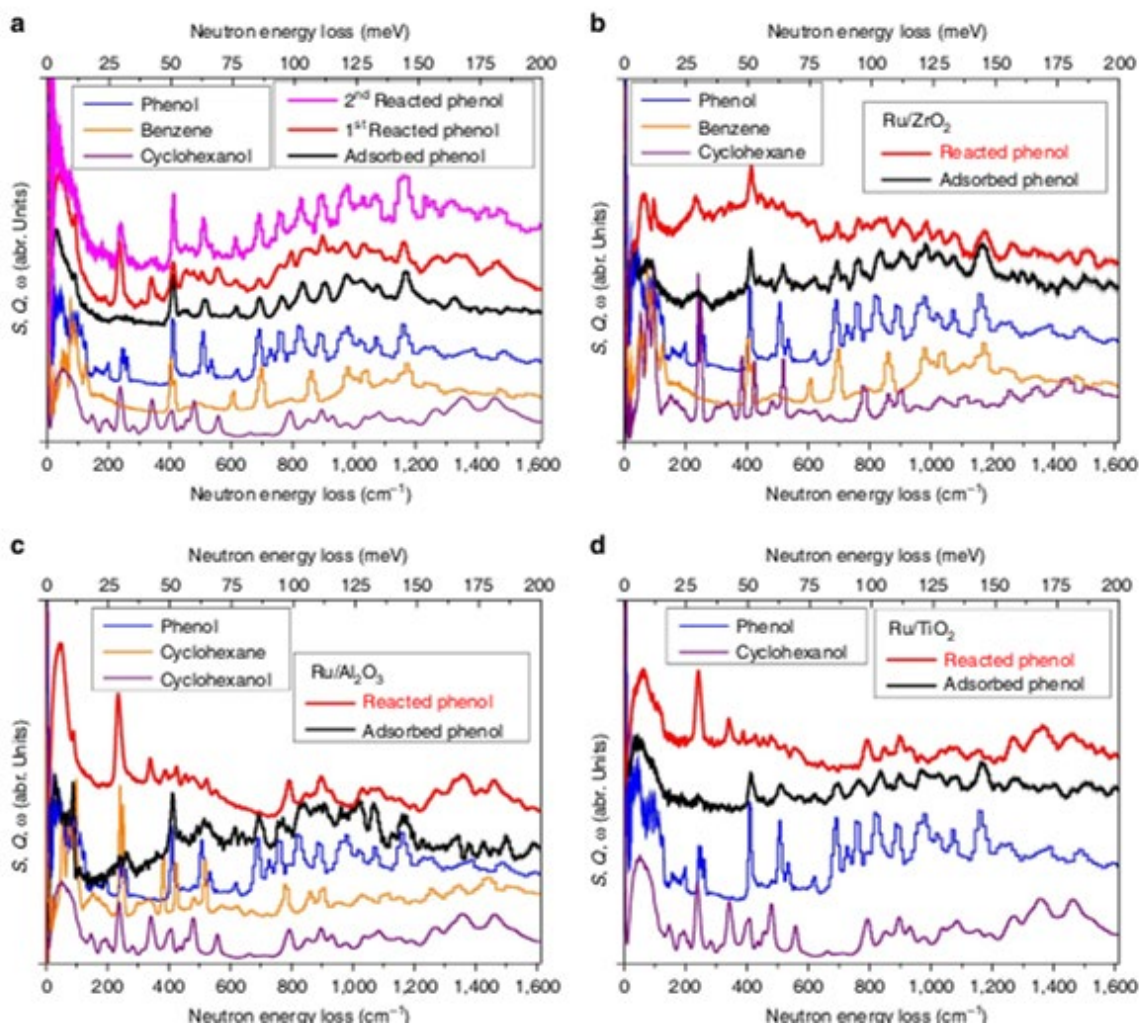


Figure 11.8. Comparison of the INS spectra for the adsorbed and reacted phenol molecules on Ru/Nb₂O₅ (a), Ru/ZrO₂ (b), Ru/Al₂O₃ (c) and Ru/TiO₂ (d). The second reacted phenol curve in panel (a) shows the conversion of phenol to benzene and cyclohexanol, which does not occur on other supports in panels (b)-(d).

Nuclear modes limiting charge mobility in molecular semiconductors

Thomas F. Harrelson, Varuni Dantanarayana, Xiaoyu Xie, Correy Koshnick, Dingqi Nai, Ryan Fair, Sean A. Nuñez, Alan K. Thomas, Tucker L. Murrey, Michael A. Hickner, John K. Grey, John E. Anthony, Enrique D. Gomez, Alessandro Troisi, Roland Faller and Adam J. Moule, *Materials Horizons*, 6, 182 (2019)

Recent theories suggest that low frequency dynamic intramolecular and intermolecular motions in organic semiconductors are critical to determining the hole mobility. So far, however, it has not been possible to probe these motions directly experimentally and therefore no unequivocal and quantitative link exists between molecular-scale thermal disorder and macroscale hole mobility inorganic semiconductors. The charge mobility in molecular semiconductors is limited by significant nonlocal electron–phonon coupling caused by intermolecular vibrations, otherwise known as phonons. To engineer new molecular materials with superior functional properties and performance, a fundamental understanding of how these phonons cause dynamic localization of charge carriers is needed. The users measured the phonon spectrum using high-resolution inelastic neutron scattering (INS) experiments at VISION. INS provides a more complete phonon spectrum than analogous optical experiments, such as FTIR or Raman by averaging the phonon density of states over the entire Brillouin zone, Figure 11.9. Accurate computations of nonlocal electron–phonon coupling parameters for six different molecular semiconductors using density functional theory simulations of phonons over the full Brillouin zone was experimentally validated by inelastic neutron scattering experiments at VISION, Figure 11.10. The coupling parameters were then used to compute charge mobilities which quantitatively agree with literature values, demonstrating the ability to accurately predict functional properties of a variety of molecular semiconductors. The measured results, coupled with

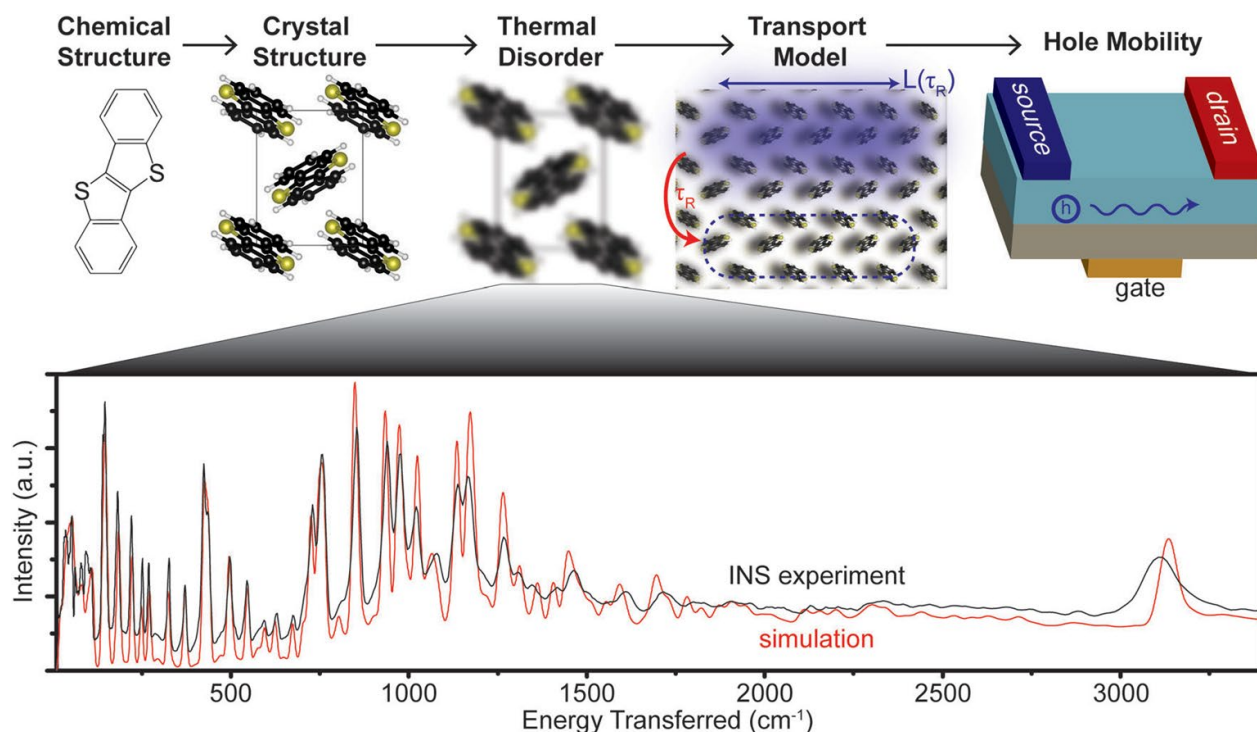


Figure 11.9. Schematic showing the connection between hole mobility, thermal disorder, crystal, and chemical structure in BTBT. The spectrum of motions leading to thermal disorder is measured using inelastic neutron scattering, which agrees with simulated modes over the full energy range measured (410–3500 cm^{-1}).

computational methodology, can be used to screen molecular semiconductors to predict a set of high-performance materials, significantly accelerating the navigation through chemical design space for next-generation materials.

Adam Moule has been a full professor of chemical engineering at the University of California, Davis and is the current titular of the Joe and Jessie Smith Endowed Chair of Chemical Engineering. He is a former Alexander von Humboldt fellow at the University of Cologne.

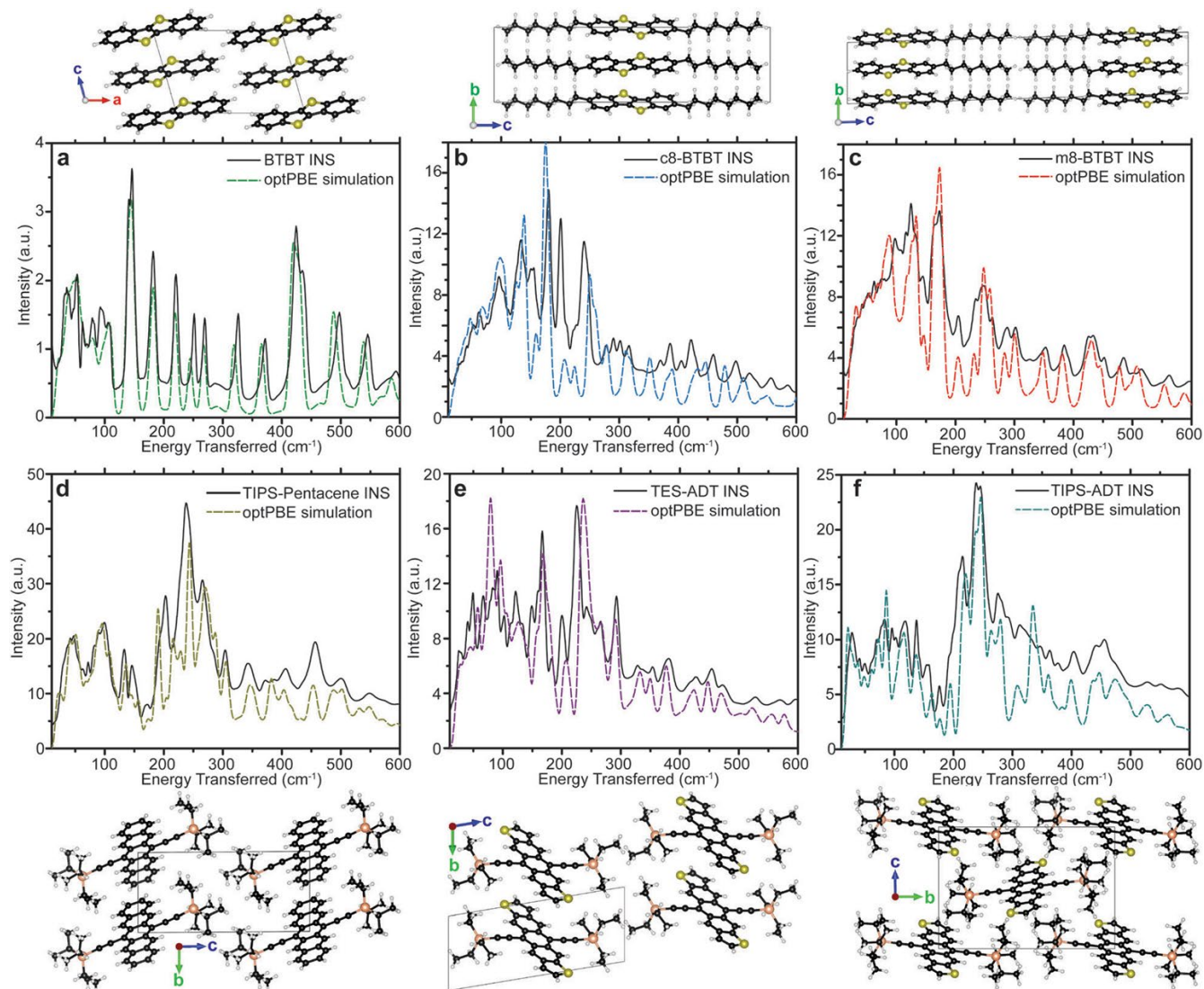


Figure 11.10. (a–f) Experimental INS spectrum, and corresponding optPBE simulation for BTBT, c8-BTBT, m8-BTBT, TIPS-pentacene, TES-ADT, and TIPS-ADT, respectively. Crystal structures used for each simulation are displayed above each plot for the BTBT series. Crystal structures for TIPS-pentacene, TES-ADT, and TIPS-ADT are shown below the plots.

Quantum dynamics of H₂ trapped within organic clathrate cages

Strobel T.A., Ramirez-Cuesta A.J., Daemen L.L., Bhadram V.S., Jenkins T., Brown C.M., Cheng Y.Q., *Physical Review Letters*, **120**, 12, 120402 (2018).

Hydrogen trapped within cage-like, guest-host materials has been of recent interest due to the ideal nature of these systems to understand quantum dynamics and for the possibility of these materials to store hydrogen for energy applications. Clathrate cages provide ideal nanoscale confining potentials for small molecules, and thus provide the rare opportunity to probe the coupled translational-rotational states under model-like conditions. INS experiments at VISION allow direct measurements of the quantum behavior of isolated molecular hydrogen trapped in molecular clathrate cages. The results indicate relatively strong attractive interaction between guest and host with a strikingly large splitting of rotational energy levels compared with similar guest-host systems, demonstrating the first two-dimensional rotation of H₂ in a molecular clathrate.

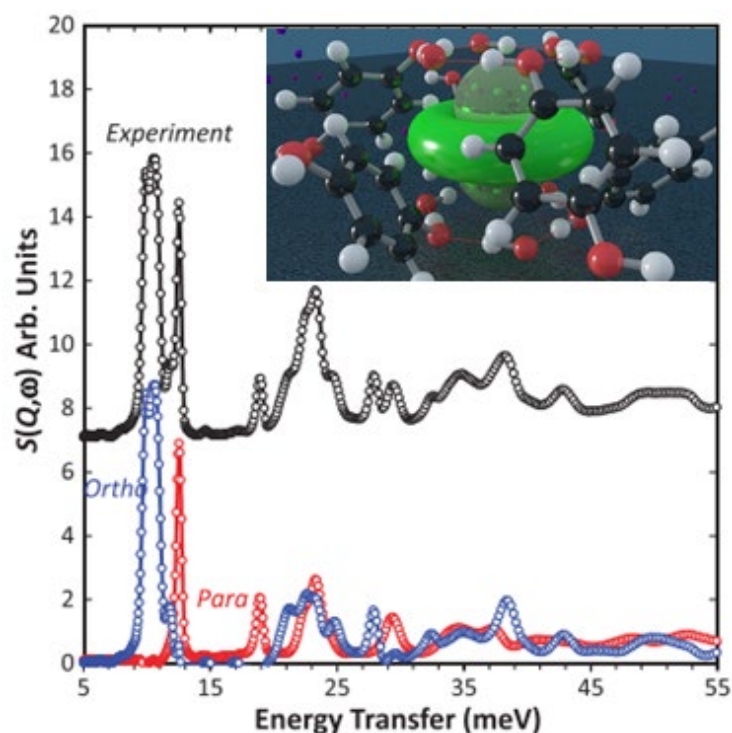


Figure 11.11. Experimental INS spectra collected at VISION from sample formed using n-H₂ recorded at 5 K. Pure ortho and para contributions were obtained by measuring two different samples with known concentrations. Inset shows the probability distribution of a rotating hydrogen molecule trapped inside the organic clathrate cage.

Tim Strobel has been a staff scientist at Carnegie Institution of Washington since 2011. His research focuses on making new materials with advanced properties using high-pressure techniques. He is a recipient of Jamieson Award for outstanding achievement in high-pressure research, Carnegie Fellowship, Carnegie Venture Research Award.

Nature of Reactive Hydrogen for Ammonia Synthesis over a Ru/C12A7 Electride Catalyst

Kammert J., Moon J., Cheng Y.Q., Daemen L.L., Irle S., Fung V., Liu J., Page K., Ma X., Phaneuf V., Tong J., Ramirez-Cuesta A.J., Wu Z., *Journal of the American Chemical Society*, 142, 7655-7667 (2020).

Electride-based catalysts are emerging catalysts that show remarkable reactivity for ammonia synthesis under mild conditions. Ru-loaded electrides composed of a mixture of calcium and aluminum oxides (C12A7) have attracted great attention for ammonia synthesis due to their facile ability in activating N₂ under ambient pressure. However, the exact nature of the reactive hydrogen species and the role of electride support remain elusive for this catalytic system. In this work, Dr. Wu and his colleagues report for the first time that the surface-adsorbed hydrogen, rather than the hydride encaged in the C12A7 electride, plays a major role in ammonia synthesis over the Ru/C12A7 electride catalyst with the aid of in situ neutron scattering techniques at VISION. The results provide a better understanding of the mechanism of ammonia synthesis and N₂ activation using electride catalysts, potentially leading to more efficient catalysis of many difficult hydrogenation reactions.

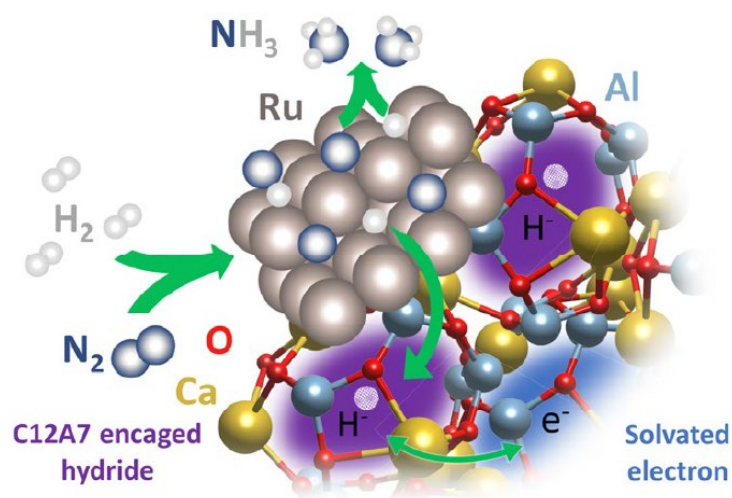


Figure 11.12. Illustration of the reaction of N₂ and H₂ to form NH₃. The reaction is catalyzed by Ru particles atop the C12A7 electride. The encaged H atoms do not play a significant role in the reaction.

Zili Wu is currently the Leader of Surface Chemistry and Catalysis Group at Chemical Science Division, ORNL. His research interests lie in the fundamental understanding of catalytic active sites on the surfaces and interfaces involved in heterogeneous catalysis, photocatalysis and electrocatalysis, establishing structure-catalysis relationships in catalytic solids as a function of time and space, using in situ and operando characterization methods, and fabricating nanomaterials with well-defined structures.

11.5 BEAM LINE DEVELOPMENT ACTIVITIES

Diffraction

In 2018 collimators were designed for the six 90° scattering angle diffraction detector banks at VISION. These collimators were 3D-printed and coated with boron nitride. Testing of the new configuration took place in late 2018/early 2019. New Mantidplot scripts were written for diffraction data reduction and automatic generation of data files in the standard GSAS format. From then on, calibration samples have been run at the beginning of each run cycle to produce an instrument parameter file for Rietveld refinements. The resolution, $\Delta(d)/d = 1\%$, comparable to SNAP.

This new capability is open to all users and permits the simultaneous collection of inelastic and diffraction data for a given sample. Figure 11.13 shows a recent example of the use of inelastic and diffraction data at VISION to study cryolite, $\text{Na}_3[\text{AlF}_6]$, a mineral occurring naturally, but also essential to aluminium production because alumina is readily soluble in molten cryolite.

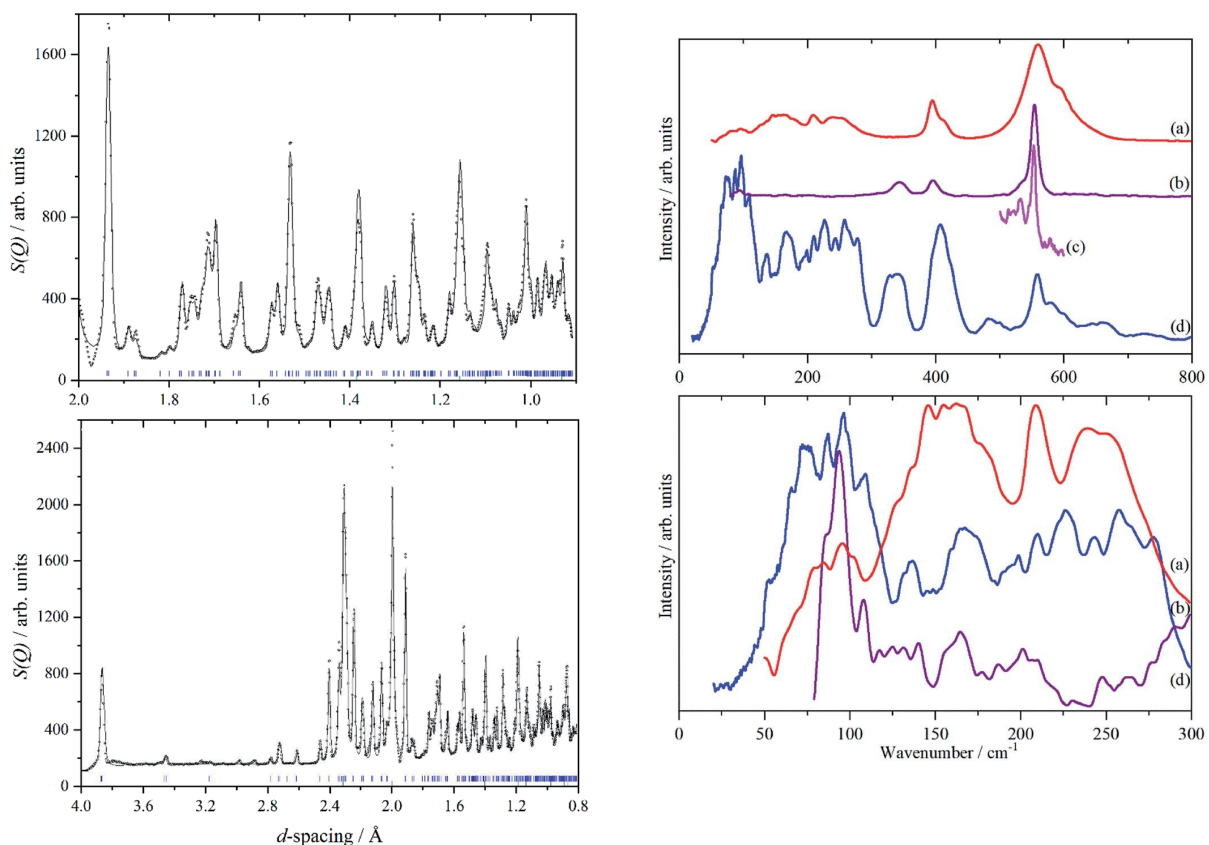


Figure 11.13. Left panel: A two-phase Rietveld fit (solid line) to the VISION neutron data (open circles) in the d-spacing range 2.0 to 0.8 Angstrom (upper panel) and 4.0 to 0.8 Angstrom (lower panel). Blue tick marks indicate the reflection positions for cryolite, whilst green tick marks indicate the reflections associated with the aluminium sample can. An excellent fit to data is obtained, even though the atomic positions and temperature factors of the cryolite have not been refined. Right panel: Vibrational spectra of cryolite: (a) infrared at room temperature, (b) Raman at room temperature (1064 nm excitation), (c) Raman at 13 K (785 nm excitation) and (d) INS at 5 K recorded on VISION. The lower panel shows the lattice mode region on expanded scales. Relative to the top panel the spectra are ordinate expanded: (a) x10, (b) x40 and (d) x1.5. Ref. S. Parker *et al.*, RSC Advances, in press

Pair Distribution Function

Pair distribution function (PDF) analysis continues to emerge as a powerful technique to simultaneously examine both the local and global atomic structures of materials. The most interesting material properties are often a direct result of defects and disorder in the crystal structure. While standard neutron powder diffraction (NPD) yields the long-range atomic structure, PDF analysis is able to probe the local structure, making it an incredibly useful technique to characterize disordered materials. VISION is a unique vibrational spectrometer that takes advantage of an incident white beam to simultaneously measure the elastic and inelastic scattering from a sample. This allows for a direct determination of how structural modifications affect the vibrational dynamics of a material. Many experiments conducted at VISION involve in-situ chemical reactions that produce subtle changes in the local atomic structure, such as order-disorder transitions, which can be difficult to observe with traditional diffraction techniques but could be easily revealed with PDF analysis. In some previous VISION experiments, particularly concerning amorphous or disordered samples, the INS data collected was of excellent quality, but data analysis was difficult due to a lack of structural information. These difficulties can be potentially solved through the combination of simultaneous INS, NPD, and PDF measurements, a combination of which would be a unique capability offered by VISION that would garner significant interest from the scientific user community.

With the new 90° diffraction detector in place (see above), we attempted to obtain pair distribution functions (pdf) on a number of standard materials. The main issues were alignment, background and background subtraction, scattering from sample holders, resolution, and Q-range, as well as data reduction and generation of the pdf, $g(r)$. We solved these issues, partly in collaboration with POWGEN and NOMAD, and we generated pdf for a series of simple materials that have been well characterized and used frequently for the calibration of xray and neutron pdf beam lines. Figure 11.14 shows a comparison of $S(q)$ and $g(r)$ for alpha-quartz for VISION and the LAD spectrometer at ISIS, which was built for the study of liquids and amorphous materials.

Testing continues, but we anticipate making this new capability available to users during the 2021A cycle.

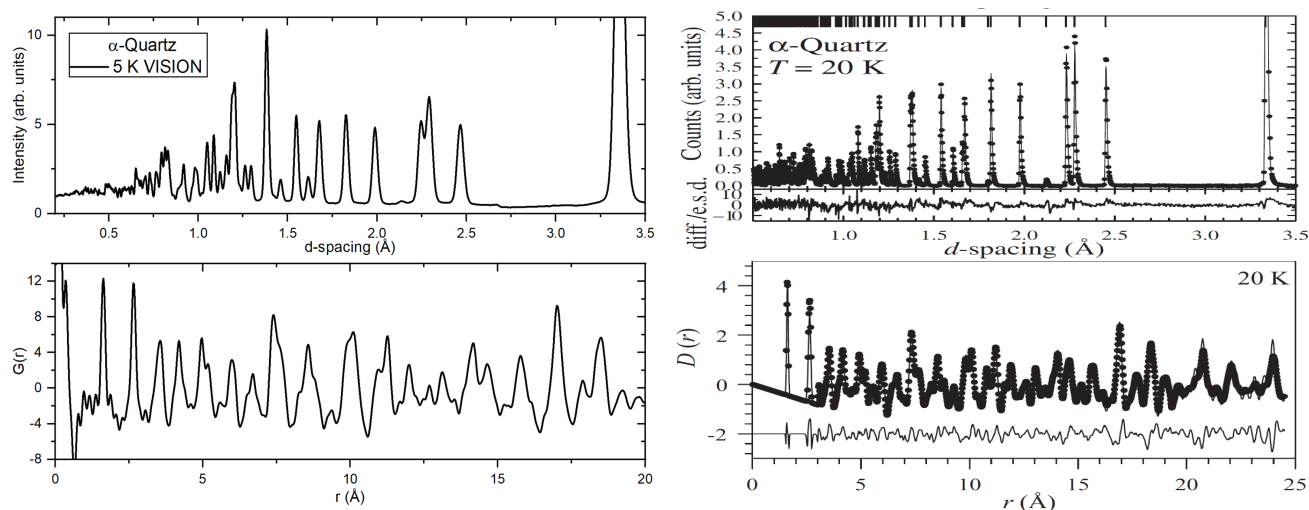


Figure 11.14. Neutron diffraction pattern and PDF $G(r)$ for α -quartz from (left) VISION at 5 K and (right) LAD (ISIS) at 20 K from Ref. 1. Note, $D(r)$ is scaled by a weighted density compared to $G(r)$.

High-pressure cells

The unprecedented flux available on SNS's VISION vibrational spectrometer make it an instrument that is ideally suited to small samples in complex environments. This capability is clearly the key requirement for the successful deployments of various high-pressure experiments as has been done on VISION. In fact, development of high-pressure techniques for VISION was a large part of a special 2015 ORNL LDRD on "Spectroscopy under high pressure" which laid the seed for many of the current high-pressure developments and capabilities.



Figure 11.15. Photos of a CuBe gas pressure capable of 3 kbar available on VISION. The gas pressure cells is also H₂/D₂ compatible

Firstly, an ISIS design for a gas pressure cell was used to purchase hydrogen-compatible gas pressure cells that are capable of 3 kbar (see photos on Figure 11.15). These cells have become a standard fixture on VISION and have been successfully used in the user program such as for example studies on the H₂ as a 2D hindered rotor in organic clathrate cages [T.A. Strobel et al, PRL 120, 120402 (2018)].

Another key effort of high pressure development on VISION has been the development of new diamond anvil cells that allow for sufficient sample volume for vibrational neutron spectroscopy (see Figure 11.16) [B. Haberl et al, **High Pressure Research** 37, 495 (2017) and B. Haberl et al, **Rev. Sci. Instr.** 89 (9), 092902 (2018)]. These cells allow for the necessary large scattering aperture of 120°, use a spring mechanism for temperature-stability of clamped in pressure and are now made from CuBe for faster cooling. Two different types of anvils are used. A form of inexpensive polycrystalline diamond without cobalt, Versimax® can be used for solid samples. Secondly, ultra-large single crystal diamonds grown by chemical vapor deposition (CVD) are used for liquid or gaseous samples such as H₂ or H₂O. In both cases, sample volumes of up to ~1 mm³ are possible. This enables pressure up to 10 GPa. With current increase in power of the facility and upgrades made to the instrument such as new slit system, future developments aim to increase maximum pressures even further.

A major effort in development was thereby focused on methods for reliable repeatable placement of the cell on the beamline (Figure 11.17). This was critical for the accurate background subtractions needed for such small samples inside a complex high-pressure environment. With these improvements in place, it was possible to measure hydrogen up to 2.8 GPa for the first time. These successful measurements suggest tantalizing hints at transitions forbidden at ambient conditions. This work is in progress.



Figure 11.16. CuBe clamped diamond cells with Versimax® anvils.



Figure 11.17. Three images of VISION clamped DAC: (a) mounted on the new sturdy stick, via (b) two bolt holes on the DAC cap and (c) a close-up of the DAC with its cadmium shielding.

In addition to these complex experiments with small samples in expensive diamond cells, it is however also advantageous and of wide interest to perform experiments at a lower pressure (to ~ 5 GPa) but in a cell allowing larger sample volumes. A recent development addresses this by using the McWhan principle of a pre-loaded bicone. A “Mini-McWhan” cell based on new ceramics and polycrystalline diamond pistons has been designed (see Figure 11.18). The cell is constructed of maraging 300 steel and uses four 5/16” screws to provide up to 10 tons preload to the ceramic biconical cylinder (Yttria-toughened Zirconia or Alumina). Once preloaded, the sample volume (3 mm diameter, up to 35 mm³ tall) is externally pressurized with a series of polycrystalline diamond pistons. The pressure on sample is clamped in by transferring load from the external press to the top threaded cap. While the designed maximum pressure is to eventually reach 10 GPa at 7 tons, to date tests have achieved ~ 4 GPa. Additionally, it is possible to also add a Teflon® cup inside the sample opening to allow for liquid samples. This was tested successfully recently on VISION. Good quality spectra were obtained in very short time (in the order of an hour) which makes this type cell very promising for higher through-put high-pressure experiments on VISION.

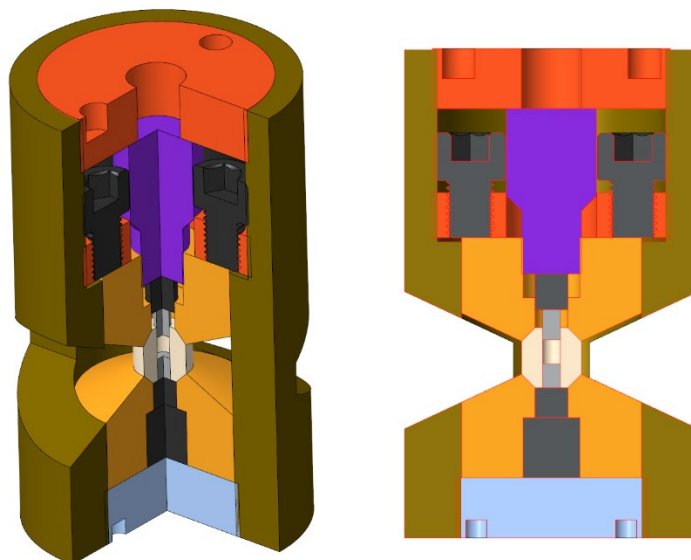


Figure 11.18. 3D model of the new Mini-McWhan cell. The sample is contained inside the (light yellow) ceramic biconical cylinder and pressurized using the (light grey) pistons made from polycrystalline diamond.

Furnace

The MICAS2 vacuum furnace design has proven to be a highly reliable high temperature furnace for SNS. Its larger bore has allowed for many unique experiments to be performed using in-house gas flow inserts. Unfortunately, because of space limitations at VISION the existing MICAS furnaces do not fit at the beam line (as well as on various other beam lines at HFIR). The vacuum shroud hosting all sample environment equipment at VISION is only 13 inches in diameter, compared to 16 inches for most beam lines. All furnaces at SNS are currently designed for the larger size and cannot be re-engineered to accommodate VISION.

The existing VISION CCR (CCR20) is limited to 700K (600K in practice) and this is too low for an increasing number of VISION users to activate, react, or measure samples in situ at higher temperatures. The demand for higher temperatures in situ is particularly significant in the field of catalysis, studies of chemical reactivity (e.g., thermal decomposition), and, more recently for the study of molten salt reactors an area of research actively supported by the US DOE at the time of writing. A mid-level funding, internal proposal to support the design and fabrication of a compact furnace based on the MICAS design was successfully funded in March 2019.

Design work has been completed, fabrication drawings are available, and all commercial parts and materials have been procured. We anticipate fabrication to be complete in late 2020/early 2021 (COVID19 uncertainty) in response to demand from users at VISION.

The new furnace will have a number of sample sticks available for gas loading, rapid cooling, and will be capable of reaching a maximum temperature of 1000°C. The sample environment group at SNS/HFIR is responsible for the design, fabrication, and maintenance of the compact MICAS furnace.

Software

During the FY16 LDRD call, the VISION team together with the NOMAD team and Computer Science and Mathematics Division (CSD) was granted LDRD (Laboratory Directed Research and Development) funding for the development of the ICEMAN project to reduce the barriers to analyze and interpret neutron scattering experiments. One significant outcome of this project is the development of the OCLIMAX code, an updated version of the aCLIMAX software used to calculate neutron vibrational spectra for direct comparison with experimental results. With greatly expanded capabilities, OCLIMAX has the following list of features.

- Powders (coherent, incoherent, elastic, inelastic) and single crystals (coherent, elastic, inelastic)
- Temperature effects (quantum treatment of Debye-Waller factor and phonon populations)
- Multiphonon excitations (powders)
- Arbitrary instrument geometry and resolution
- Arbitrary cuts in 4-dimensional Q-E space (single crystals)
- Interface with atomistic modeling tools (e.g. various DFT codes)
- Interface with neutron scattering data analysis tools (e.g. DAVE and Mantid)
- User-friendly (multiple platform, easy to use, fast on PCs)
- $S(Q,E)$ in absolute unit (barn/energy) (powders)
- Parameter-free calculation of thermal neutron scattering cross-sections
- MD trajectories to neutron scattering spectra (powders)

VISION also has highly streamlined data reduction and analysis workflow, enabled by a series of scripts written for automation and batch processing. These scripts greatly improved the efficiency of data interpretation and DFT modeling, which played an essential role in achieving and maintaining the high throughput of the instrument.

11.6 OUTREACH

VISION participates yearly in the Department of Energy's National School on Neutron and X-Ray Scattering. Hands-on experience in using the instrument and the examination and treatment of measured data provided by the instrument is provided. This school provides graduate students and post-doctoral researchers an excellent learning opportunity in the field of neutron vibrational spectroscopy. Some of the students which participate in this school become users of the instruments later in their career path. VISION also contributes lectures on chemical spectroscopy to the set of formal lectures given to the students.

VISION also hosts a number of students over periods ranging from a few weeks to one year. These students are shared with close U.S. university collaborators with whom VISION has established a collaboration or is trying to develop closer ties.

A number of invited presentations by the VISION team at national and international meetings have contributed greatly to the recruiting of new users. These presentations focus on the VISION capabilities and are occasionally tailored to the scientific interests of a particular audience.

VISION also contributes local meetings (e.g., Joint NSCD/CNMS User Group Meeting) with updates and general presentations (oral/poster) on chemical spectroscopy at VISION.

11.7 STRATEGIC VISION

1. Continue to develop VISION's user community by retaining productive and high visibility users and attracting new user. A realistic goal would be 15-20% of experiments driven by new users each cycle. Engage new types of users rather than seeking new users in established communities. A large number of scientific communities with important and interesting problems that could be addressed by neutron scattering are not routine users of neutron facilities.
2. Continue the development and vesting of new sample environment equipment in the VISION user program. Get feedback from users (feedback form, users group, user group meeting, conferences and workshops) regarding the needs of the community. Work with the sample environment group to achieve these goals.
3. VISION is currently the only multi-functional beam line at SNS (simultaneous diffraction and inelastic neutron scattering). The Second Target Station (STS) at ORNL will have multiple multi-functional beam lines. Exploit and develop VISION with a view to STS operations by identifying new scientific problems and communities that would benefit and how to best utilize a multi-techniques beam line.
4. Consolidate and facilitate multi-instrument collaborations (POWGEN, NOMAD, BASIS, SNAP, SEQUOIA) to have complementary neutron scattering techniques bearing on a problem and provide users with answers more rapidly.
5. Add to the existing complementary techniques (e.g., FTIR or XRD) for sample characterization pre- and post-experiment at the beam line.
6. Campaign for a filter spectrometer for beam line 16A. This beam line would complement VISION very nicely in two different ways: (a) enable neutron vibrational spectroscopy experiments that do not necessarily require the high resolution of VISION, and (b) allow the collection of vibrational spectra at high frequencies where VISION's flux is low. The latter is important to measure stretches for comparison with more conventional techniques such as Raman and IR.

11.8 RESOURCES NEEDED

VISION Staffing

The past year has seen changes in the VISION instrument team. We added a scientific associate to the team who started on March 9th. Of course, this was shortly before the current COVID-19 induced work restrictions which has slowed his integration into the team and the operation of the beam line. Furthermore, Yongqiang Cheng has transitioned to the role of Computational Instrument Scientist for Chemical Spectroscopy and will not be able to provide as much direct support to VISION in the future. While we are still adapting to beamline operations with restrictions on user presence onsite, we would eventually anticipate the need for an additional instrument scientist to support user operations on VISION.

More space for the chemistry lab

Access to a well-equipped chemistry laboratory with sufficient space, equipment, amenities, and utilities remains an issue at SNS. We lag behind most other neutron facilities in that respect. This is particularly important for VISION because numerous experiments require last minute extensive, on site sample preparation. CNMS access through a lengthy, advance approval exercise is wholly inadequate to address the

(often unpredictable) needs that arise in the execution of a neutron scattering experiment from onsite sample preparation to postmortem examination.

Complete BL16A

Compact filter spectrometer beamline to take over the VISION “overflow” and complement VISION at high energy transfers (stretches).

New CCR/cooling system

A custom-made top-loading CCR is being planned (discussion ongoing with Janis) to increase the diameter of the sample chamber and facilitate and enable the development of more complex sample environment equipment (e.g., magnets or larger pressure cells). The design includes a fast pre-cooling of the cryostat that can reduce cooling times from few hours to 20 mins. Built in powerful heating elements can help enable faster sample changes.

Sample Changer

VISION has a sample changer that is currently not operational. The design is complicated, in part due to the constraints in size posed by the current top-loading CCR. The new, larger diameter CCR will enable a simple “chain design” sample changer to be used. The sample changer is required for VISION to improve throughput and enable a mail-in program.

Testing beam time

More beam time reserved to test new sample environment equipment, new techniques, and beam line development in general. Testing new pressure cells or new beam optics takes time to reach a reliable conclusion allowing for integration in the user program.

11.9 SELF-ASSESSMENT

Strengths

VISION is a world-leading instrument; it has the highest flux on sample position and the most extensive solid angle coverage with its focusing analyzers. It can access the elastic line with a resolution of 120 μeV . It also has good diffraction capabilities. Overall, it is a truly multimodal instrument. It is a unique spectrometer that also allows measurements on small and non-hydrogenous samples.

Unlike any other neutron instrument in the world, VISION has dedicated computational resources for modeling of the data and software written to analyze VISION data specifically. The impact is shown in the number of publications, including modeling as part of the interpretation and analysis (over 80%).

Weaknesses (limitations)

VISION can collect data very fast and often throughput is limited by the ability to cool and warm samples. The larger, fast cooling CCR described above will improve the efficiency of VISION. The expanded sample space (both in diameter and length) will help with development of new sample environment capabilities.

The constraints imposed by the current CCR design informed the build of the existing sample changer and, in part due to the size limitations, resulted in a very complex, unreliable sample changer. This sample changer is no longer operational and while we are working on repairs to this changer, a simpler sample changer with improved reliability would enable implementation of a mail-in program.

The diverse science explored on VISION would benefit from additional complementary techniques for pre- and post-irradiation sample characterization.

Opportunities

The capabilities provided by VISION could benefit several communities representing the potential for growth of the user community. Examples include geosciences, environmental sciences, pharmacology, and photochemistry. Expanded sample environments, including high-temperature capabilities, could also broaden the science explored by VISION.

The planned new CCR will allow for a simple design for a simple "chain design" sample changer – an example of such a changer has been in use at the TOSCA spectrometer at the ISIS facility, since 2003. This combination of sample changer and a fast cooling CCR will increase VISION's productivity.

Threats

In terms of neutron vibrational spectroscopy, the main competition for VISION is the TOSCA spectrometer at ISIS in the UK, both indirect geometry spectrometers at pulsed sources. The flux of TOSCA is lower than VISION by a factor of 10-40 depending on energy transfer. However, TOSCA has more instrument staff, and it has an operational sample changer that allows them to run a very efficient mail-in program. The LAGRANGE spectrometer at the hot source at the ILL in Grenoble is also a competitor. In the future, the VESPA spectrometer at the ESS will also serve as competition for VISION (+10 years from now). The design and incident beam characteristics of VESPA may allow it to trade between flux and resolution. How competitive will be VESPA compared with VISION remains to be seen. From the perspective of non-neutron techniques, Nuclear Resonance Vibrational Spectroscopy (NRVS) is a synchrotron-based vibrational spectroscopy technique with unique selectivity for vibrations involving the displacement of Mössbauer-active nuclei; these include ⁸³Kr, ¹¹⁹Sn, ¹⁵⁷Eu, ¹⁶¹Dy, ¹²¹Sb, ¹²⁵Te, and ⁵⁷Fe. This technique is competitive with neutron vibrational spectroscopy in materials containing such elements.

11.10 EXECUTIVE SUMMARY

VISION occupies a unique place in the SNS/HFIR instrument suite and on the worldwide neutron scattering stage. Its competitors are TOSCA at the Rutherford-Appleton (ISIS) facility in the UK and the future VESPA beam line at the ESS.

Since its completion in late 2014 the instrument has grown rapidly in terms of capabilities, science, and user community over the past 6 years. It has reached a level of maturity and reliability comparable to other SNS instruments and has entered a period of relative stability during which its potential will be realized and exploited more fully.

Outreach to conventional and non-conventional communities of users is necessary and healthy for an instrument addressing as wide a variety of scientific topics as VISION.

This must go hand in hand with the development of support labs, sample environment, and data analysis.

12. SNS BL-15, NEUTRON SPIN ECHO SPECTROMETER AT SNS (SNS-NSE)

12.1 OVERVIEW AND CURRENT STATUS

The neutron spin-echo (NSE) method fills the gap between dynamic light scattering and conventional neutron spectroscopy techniques aiming at much slower dynamical processes with typical times up to several hundreds of nanoseconds as they occur in various materials on mesoscopic length scales. The Neutron Spin Echo instrument @ SNS (SNS-NSE) was the first spectrometer of its class by design, is the first spin-echo spectrometer at a Spallation Source and one of the best spectrometers in both resolution and dynamical range in the world. SNS-NSE was built, commissioned, and was operated at SNS until April 2020 by the *Forschungszentrum Jülich* through a common effort of *Jülich Centre for Neutron Science* and *ORNL*. Currently, the SNS-NSE spectrometer is in transition to *ORNL*, and documents are drawn-up to accommodate the transition. NSD has committed to operate the spectrometer and to ensure a continuous, undisrupted and successful NSE user program at SNS. The SNS-NSE spectroscopic design is based on superconducting technology which ensures superior magnetic field homogeneity for a highly effective neutron flux. The design of the NSE spectrometer takes full advantage of recent progress in neutron optics and polarizing supermirror micro-benders, resulting in considerable gains in the polarized neutron flux over a wide wavelength range. The SNS-NSE instrument enables detection of neutron velocity changes of one part per 10^{-5} , whereas the number of neutrons in the velocity band is several times wider than the detected velocity increment, ensuring high neutron intensity. The SNS-NSE provides ultrahigh resolution spectroscopy, with a Fourier time range commonly between 5 ps and up to 150 ns. Due to its wide wavelength span of $2\text{Å} < \lambda < 14\text{Å}$, high magnetic field homogeneity, state-of-the-art field correction elements and novel polarizing benders, with special setup the SNS-NSE can reach Fourier times up to 400 ns, at the expense of neutron flux and the measuring time. The magnetic shielding in the spectrometer enclosure offers reliable and precise operation preventing stray fields from high external magnetic field sources.

Team Structure

The two SNS-NSE instrument scientists Piotr Zolnierczuk and Laura Stingaciu are members of the SANS/Spin Echo Team led by William Heller, part of the Large-Scale Structures Group led by Volker Urban. Mary Odom is member of Scientific Associate Team 3 led by Andre Parizzi, part of the SNS Instrument Operation Group led by Bobby L. Cross. P. Zolnierczuk is directly employed by the *Juelich Centre for Neutron Science*, in transition to *ORNL* during December 2020. L. Stingaciu and M. Odom are employed by *ORNL*.



Figure 12.1. The SNS-NSE Team. From left to right: Piotr Adam Zolnierczuk (Lead Instrument Scientist), Mary Odom (Scientific Associate), and Laura-Roxana Stingaciu

12.2 SCIENTIFIC FOCUS

The SNS-NSE instrument is particularly suitable for the investigation of slow dynamical processes and for unraveling molecular motions at the nanoscopic-to-mesoscopic scale. The instrument is therefore used for research in a variety of fields including, but not limited to: soft-matter research, condensed matter physics, materials science, complex fluids, and biophysics. Investigation of macromolecular assemblies of great importance to human health is one of the important applications of SNS-NSE, attracting users with interest in biophysics and medical research all over the world. For biological problems, NSE can be used to determine the domain dynamics of proteins and enzyme's, studies of lipid systems and biological membranes. In soft matter, dynamics in polymer melts, dynamic-related phenomena in networks and rubbers, interface fluctuations in complex fluids and polyelectrolytes, and transport in polymeric electrolytes and gel systems are also major research subjects addressed by NSE. Recent developments and instrument adaptations have allowed the NSE spectrometer to aid in magnetism studies.

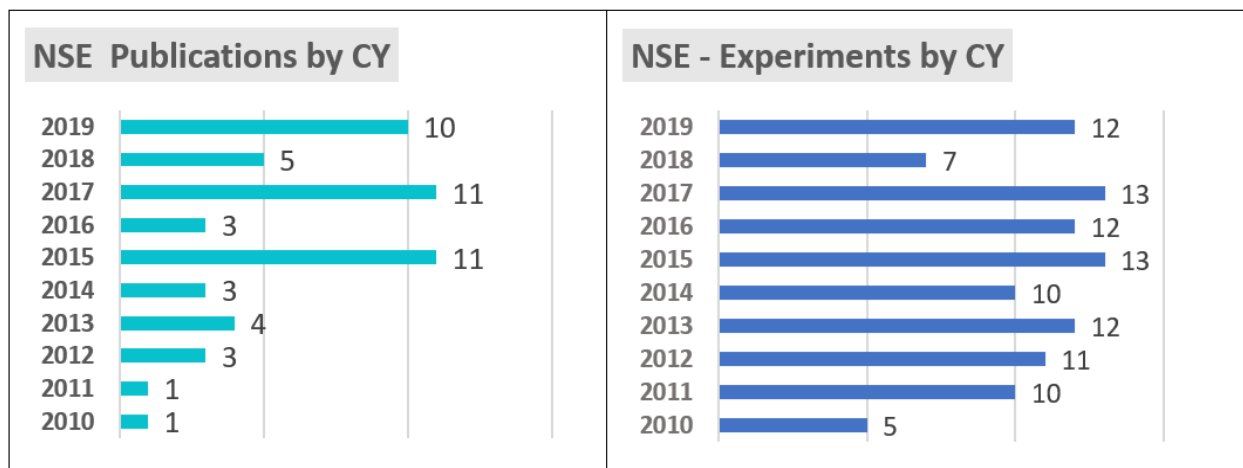


Figure 12.2. NSE publication statistics since entering the User Program.

The SNS-NSE instrument has been consistently oversubscribed in the General User (GUP) program and Partner User (PUP) program. We had **21** research articles published in the past 3 years (2018-2020), in various scientific journals. Full publication list can be found on the [NSE web site](#).

12.3 SCIENTIFIC HIGHLIGHTS

The following summarizes results of selected scientific highlights grouped to exemplify the diverse capabilities of the SNS-NSE spectrometer. The science areas span from soft matter, biology, materials, and quantum condensed matter. Examples include:

Mechanical properties and transport processes in lipid membranes

Dynamics of Phospholipid Membranes beyond Thermal Undulations

Sudipta Gupta, Judith U. De Mel, Rasangi M. Perera, Piotr Zolnierczuk, Markus Bleuel, Antonio Faraone, and Gerald J. Schneider, *J. Phys. Chem. Lett.* 9, 2956 (2018)

Phospholipids play a vital role in cell membranes and are ubiquitous in nature. In aqueous medium, they spontaneously self-assemble to form lipid bilayer vesicles called liposomes. The mechanical properties of the lipid bilayer, in particular its bending modulus, are related to important biological functions like the cellular uptake and release. In this study, Gupta and his collaborators investigated the molecular dynamics of unilamellar liposomes using neutron spin echo spectroscopy. The reported mean squared displacement shows a $t^{0.26}$ dependence in the pico-to-nanosecond region, that points to another process beyond the well-established model of thermal membrane undulation of Zilman and Granek (ZG) which predicts a $t^{0.66}$ and the translational diffusion which is linear with time (Figure 12.3). Comparing the results to molecular dynamics simulations the authors associate that the observed low exponent with a non-Gaussian transient trapping of the lipids. The analysis of the mean squared displacement leads to the important conclusion that the friction at the interface between water and liposomes plays a minor role. Center of mass diffusion of liposomes and transient trapping of lipids define the range in which the ZG model can be applied to analyze membrane fluctuations.

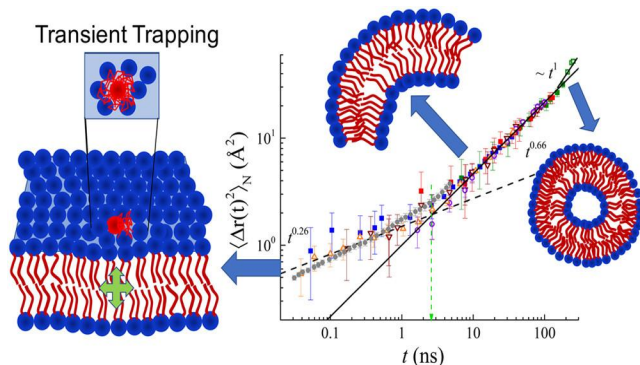


Figure 12.3. Proposed mechanism of transient trapping and mean square displacement $\langle \Delta r(t)^2 \rangle_N$ as a function of Fourier time.

Comparing the results to molecular dynamics simulations the authors associate that the observed low exponent with a non-Gaussian transient trapping of the lipids. The analysis of the mean squared displacement leads to the important conclusion that the friction at the interface between water and liposomes plays a minor role. Center of mass diffusion of liposomes and transient trapping of lipids define the range in which the ZG model can be applied to analyze membrane fluctuations.

Lipid Rafts - Buffers of Cell Membrane Physical Properties

Jonathan D. Nickels, Micholas Dean Smith, Richard J. Alsop, Sebastian Himbert, Ahmad Yahya, Destini Cordner, Piotr Zolnierczuk, Christopher B. Stanley, John Katsaras, Xiaolin Cheng, and Maikel C. Rheinstadter, *J. Phys. Chem. B* 123, 2050 (2019)

Cell membrane picture as a compositionally rich and laterally organized structure has now largely replaced the classical view of a homogeneous fluid mosaic. The lipid raft hypothesis invokes the existence of nanoscopic lateral structures composed of membrane lipids and proteins into distinct domains in the plane

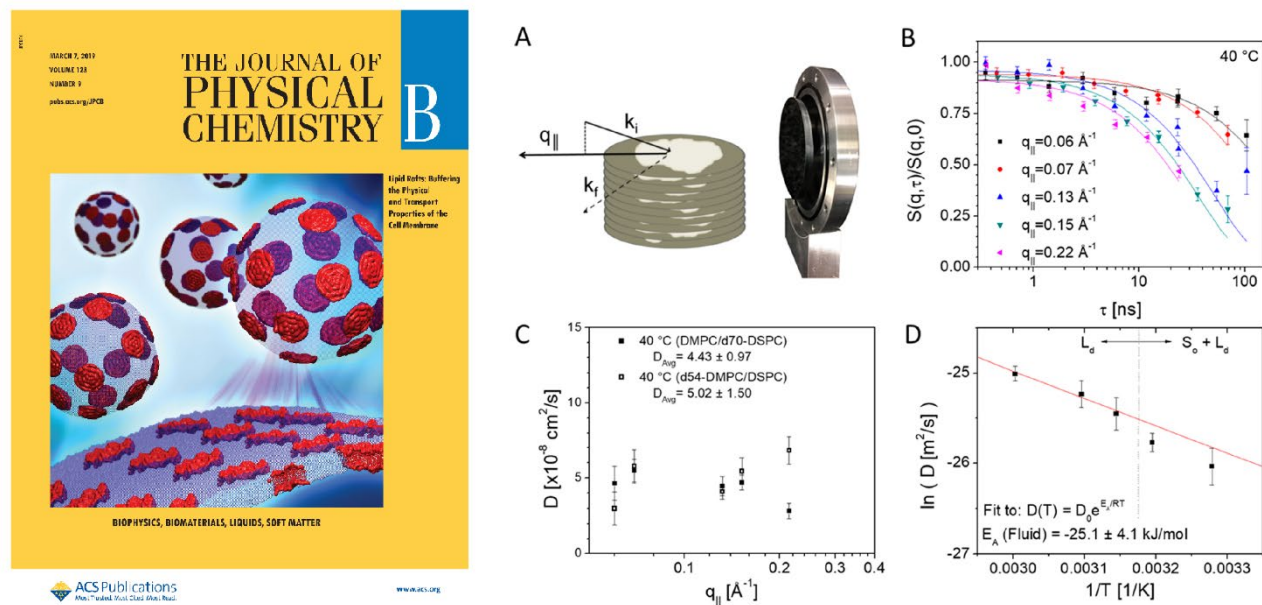


Figure 12.4. Left: The cover of Journal of Physical Chemistry B 123 (2019), issue 9 illustrating J. Nickels *et al.*, research; Right: The lateral diffusion of the lipid DMPC/DSPC bilayer measured using neutron spin echo

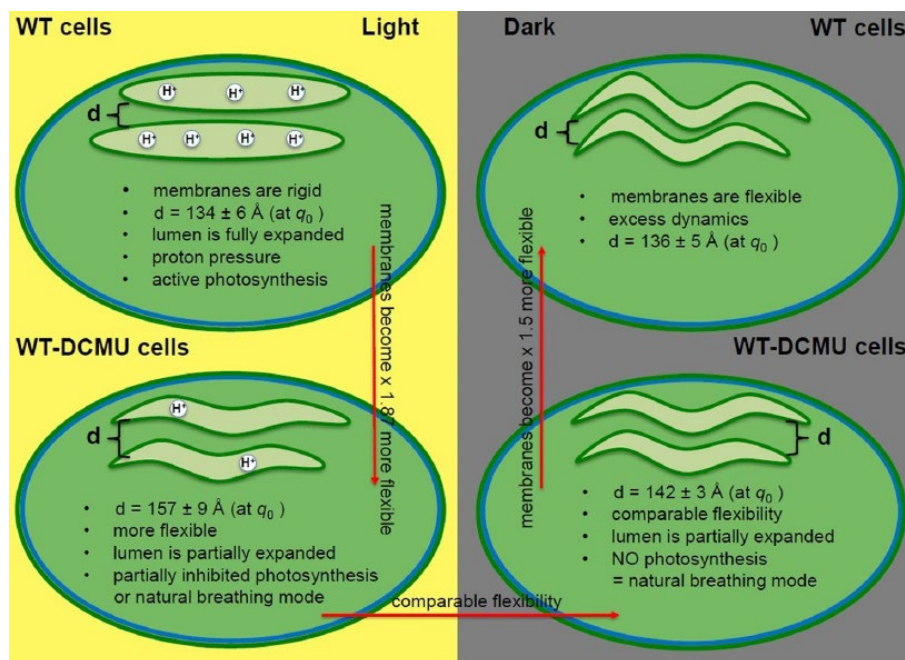
of the membrane that enable organization and regulation of multimolecular protein assemblies. The rafts are being currently understood as platforms for protein partitioning in both eukaryotic and prokaryotic cells. Jonathan Nickels *et al.* propose that the rafts play an additional role of stabilizing membrane physical properties over varying temperatures and other environmental conditions. To provide an example of this phenomenon, the authors have performed neutron scattering experiments and atomistic molecular dynamics simulations on a phase separated model lipid (1,2- dimyristoyl-sn-glycero-3-phosphocholine (DMPC) and 1,2-distearoyl-sn-glycero-3-phosphocholine (DSPC) membrane. The results demonstrate a buffering effect in both the lateral diffusion coefficient and the bending modulus of the fluid phase upon changing temperature. This highlights the potentially advantageous stabilizing effect of complex lipid compositions in response to temperature and potentially other membrane destabilizing environmental conditions. The research was featured also on the cover of *Journal of Physical Chemistry B* (Figure 12.4).

Dynamics of Photosynthetic Membranes in Living Cells under Herbicide Stress

Laura-Roxana Stingaciu, Hugh M. O'Neill, Michelle Liberton, Himadri B. Pakrasi & Volker S. Urban, *Scientific Reports* 9, 5711 (2019)

Cyanobacteria dominated Earth's biosphere for billions of years and are the reason for the oxygen atmosphere of our planet. The photosynthetic machinery in cyanobacterial cells is housed in flattened membrane structures called thylakoids situated in the peripheral part of the cellular cytoplasm. Under photosynthetic conditions these thylakoid membranes undergo various dynamical processes that could be coupled to their energetic functions. High-resolution inelastic neutron scattering experiments performed at SNS-NSE on living cyanobacterium *Synechocystis* sp. PCC 6803 cells, assessed the flexibility of cyanobacterial thylakoid membrane sheets for the first time, the dependence of the flexibility on illumination conditions and the influence of chemically disrupted photosynthesis by herbicidal used on the thylakoid dynamics.

L.-R. Stingaciu and collaborators observed that the membrane relaxation behavior is different between native cyanobacterial cells named WT (wild type) in the Figure 12.5, and herbicide- inhibited cells named WT-DCMU. This supports the hypothesis that photosynthesis plays a role in the expressed dynamics and is affected by the presence of DCMU. The direct comparison between DCMU treated and untreated cells during the light cycle, when the effect of photosynthesis on the rigidity of the system is more observable, shows that by disrupting the electron transfer, DCMU affects the relaxation of the treated membranes as they become 1.87-fold more flexible than the untreated ones. The study strengthens experimentally the hypothesis that the buildup in H⁺ pressure within luminal space during the electron cycle drives important



changes in the *Synechocystis* 6803 thylakoids, and provides a new dynamic dimension to the photosynthetic process in the presence of DCMU herbicide, indicating that photosynthesis can be directly and quantitatively correlated with the mechanical properties of photosynthetic membranes. The study points toward the flexibility of the thylakoids and their active function during energy conversion, rather than a rigid support frame for other photosynthetic components as believed in the past.

Figure 12.5. Diagram of the observed mechanical properties of native WT and inhibited WTDCMU membranes. The green circles represent *Synechocystis* 6803 cyanobacterial cells with one pair of thylakoid membranes, under different illumination conditions. The distance d represents the interthylakoidal distance = the local length scale where thickness and shape fluctuations are sampled. The red arrows show the direction of increase flexibility.

Dynamics of Proteins

Osmolyte Interactions in Intrinsically Disordered Myelin Basic Protein

Laura-Roxana Stingaciu, Ralf Biehl, Changwoo Do, Deiter Richter and Andreas M. Stadler, *Journal of Physical Chemistry Letters*, 11, 292 (2020)

Osmolytes have the power to change the residue's interactions within proteins by altering the ability to move and rearrange in various configurations. Neutron Spin Echo spectroscopy study on the structure and dynamics of the intrinsically disordered myelin basic protein (MBP) denatured by urea showed that osmolyte-denatured MBP is more compact than ideal polymers, while its secondary structure content is entirely lost by denaturation. NSE experiments reveal concomitantly an increase of the relaxation time and of the amplitude of internal motions in urea-denatured MBP as compared to native MBP. When interpreted in terms of the flexible polymers' models, the internal friction parameter decreased ~ 7 fold. Urea seems to not only smooth local energy barriers, reducing internal friction on a local scale, but also significantly reduces the overall depth of the global energy landscape (Figure 12.6). This leads to a nearly complete loss of restoring forces beyond entropic forces and in turn allows for larger motional amplitudes. The noncovalent H-bonds are largely eliminated, driving the unfolded protein to be more similar to a synthetic polymer.

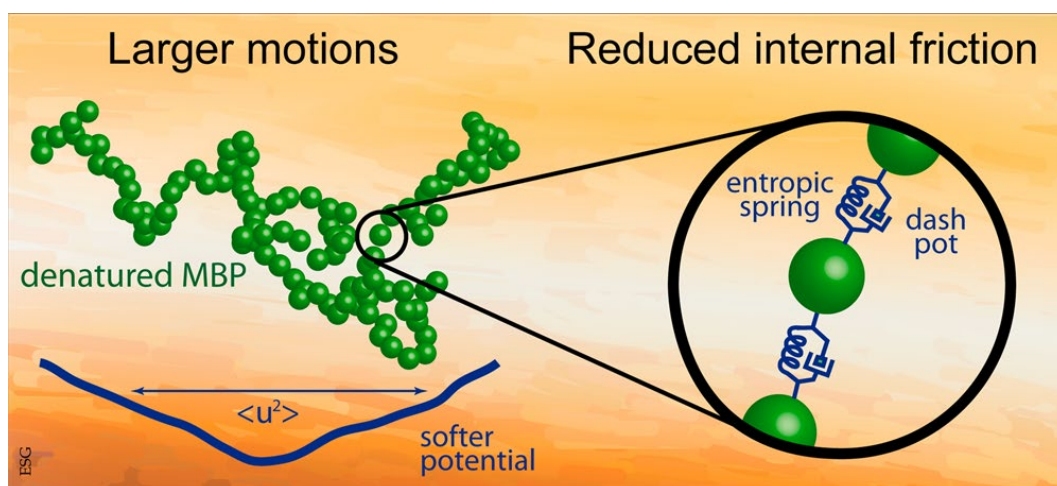


Figure 12.6. Diagram of the assumed protein internal energy landscape and polymer-like dynamics behavior of MBP during osmolyte-denaturation.

Dynamic processes in colloids, polymers and microemulsions

Inner Dynamics of Homogeneously and Heterogeneously Crosslinked PNIPAM Microgels with High Crosslinker Content

Judith Witte, Tetyana Kryey, Jana Lutzki, Anna Margarethe Dahl, Judith Houston, Aurel Radulescu, Vitaly Pipich, Laura Stingaciu, Matthias Krauthammer, Marcus U. Witt, Regine von Klitzing, Olaf Holderer and Stefan Wellert, *Soft Matter*, 15, 1053 (2019)

Microgel particles, especially those with responsive properties such as thermo-responsivity, pH-responsivity or responsivity to ionic strength are the object of numerous scientific investigations due to their large potential for applications such as drug delivery, sensor applications, and biotechnological applications. N-Isopropylacrylamide (NIPAM) is a widely used monomer for the synthesis of microgel particles of poly(N-isopropylacrylamide) (PNIPAM) by tuning the volume phase transition temperature. N,N'-Methylenebisacrylamide (BIS) is a commonly used crosslinker in PNIPAM microgels. It was found that during emulsion polymerization BIS molecules are consumed faster than NIPAM molecules. This results in an uneven distribution of crosslinking and in a denser core and a fluffier shell. To tune the microgel structure towards a more even distribution of crosslinks and polymer, several procedures of introducing the crosslinker and monomers into the network exist today. In this study a thorough and direct comparison of the internal structure and dynamics of microgels is investigated in two kinds of PNIPAM based microgel particles with a high crosslinker content, prepared via classical precipitation polymerization (MG10P) and a continuous monomer feeding approach (MG10F). Dynamics as investigated by neutron spin echo spectroscopy revealed that in MG10P the presence of a dense core region leads to a dominance of the cooperative cooperative density dynamics (Figure 12.7). Zimm-type dynamics could only be observed for MG10F, while a simple Q^2 dependence was observed for the dynamics in MG10P in the entire measured Q -range.

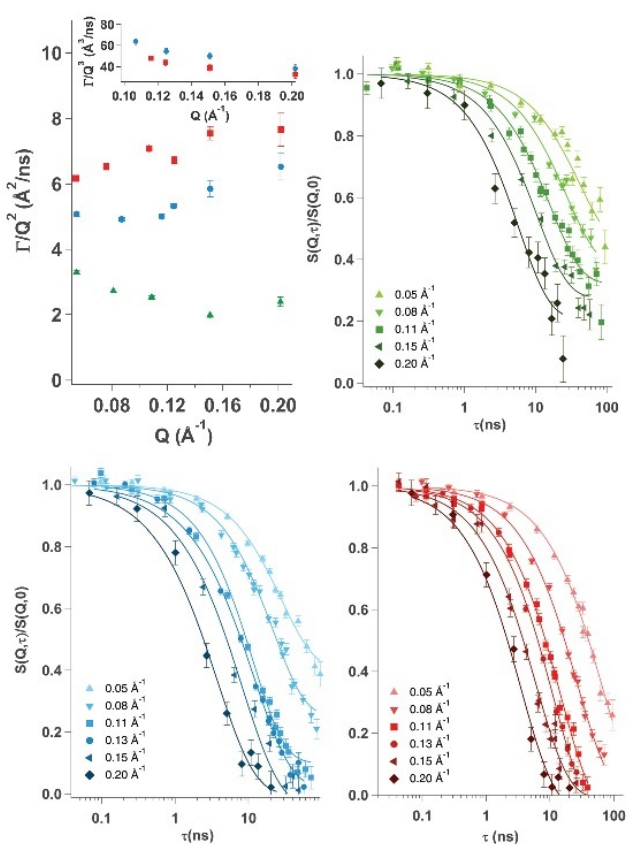


Figure 12.7. Diffusion coefficient as example of dynamics in PNIPAM microgels. While MG10P (green triangles) shows a constant value over the entire Q -range, and the linear PNIPAM solution (red squares) shows a continuous increase, MG10F (blue circles) has a constant value up to $Q = 0.11 \text{ \AA}^{-1}$ and increases afterwards.

Interfacial Fluidity of Bicontinuous Microemulsions

Veerendra K. Sharma, Douglas G. Hayes, Sudipta Gupta, Volker S. Urban, Hugh M. O'Neill, Sai Venkatesh Pingali, Michael Ohl and Eugene Mamontov, *Journal of Physical Chemistry C* 123, 11197 (2019)

Antimicrobial peptides (AMPs) are potentially valuable agents for combating antibiotic-resistant microorganisms. AMPs do not rely upon receptor sites of the infecting microorganisms for their antimicrobial activity, but instead operate by disrupting the molecular packing of biomembranes of prokaryotes through their insertion, leading to pore formation and ultimately death of the microorganism. AMPs possess a broad activity spectrum, including action as anticancer agents and activity against HIV. In this study Sharma and his collaborators evaluated the effect of the antimicrobial peptide, melittin, on the long-range collective and local undulation motions of bicontinuous microemulsions (B μ Es) using NSE in combination with other scattering techniques. B μ Es were isolated from Winsor-III systems formed by mixing aqueous melittin solutions containing sodium dodecyl sulfate with dodecane/1-pentanol mixtures at optimal salinity. An increase of melittin concentration linearly increased the diffusivity of the microemulsions and decreased the bending rigidity up to an aqueous melittin concentration of 2g/L (Figure 12.8), thus indicating an increase of interfacial fluidity. Further increase of melittin concentration above 2g/L did not change the diffusivity and only slightly increased the rigidity. These changes reflect differences of interaction between melittin and B μ E surfactant monolayers at different melittin concentrations. At low concentrations, melittin is highly associated with the surfactant monolayers, likely ion-paired to the sulfate surfactant head groups and perhaps partially penetrating into the surfactant tail region. At high concentrations > 2g/L, an apparent saturation concentration, added melittin is less strongly associated with the monolayers. The bending rigidity here reflects contributions from both the elasticity and saddle-splay moduli and suggests that the bending moduli obtained is not an effective indicator of dynamics for the B μ Es investigated. The study demonstrates overall that amphiphilic solubilizates can have a complex impact on dynamics of surfactant monolayers in microemulsions, with implications for transmembrane diffusion and the kinetics of release from the microemulsion phase, which are important characteristics for the use of B μ Es as delivery vehicles and host systems for bio-chemical reactions.

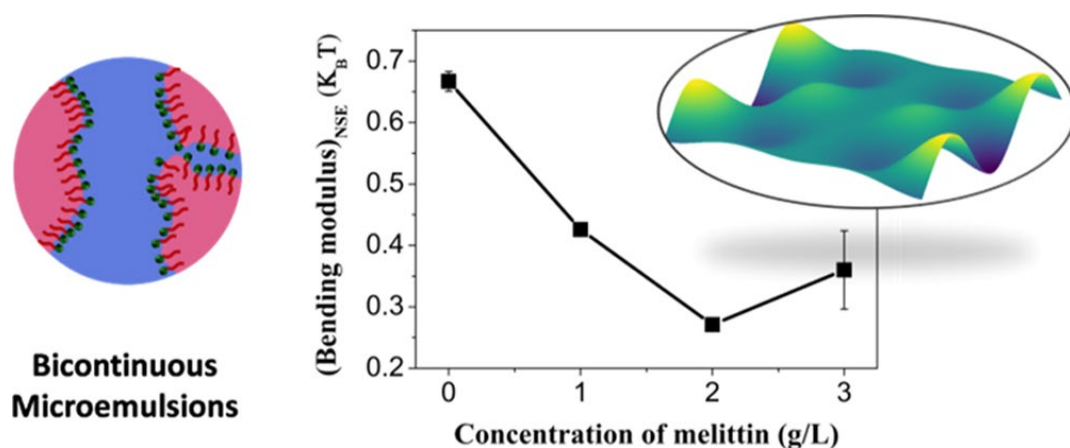


Figure 12.8. Diagram of the bicontinuous microemulsions fluidity and its dependence on the antimicrobial peptide concentration.

12.4 USER PROGRAM OF THE SNS-NSE SPECTROMETER

BL-15, Neutron Spin Echo Spectrometer entered fully into User Program in the year 2011. The average number of days per an NSE experiment is 9-10 days. The SNS-NSE has been constantly oversubscribed with a subscription rate, over 7-year average (Number of requested days/Number of available days) of 359%. Figure 12.9 shows the yearly oversubscription rate as recorded by the SNS User Office.

The SNS-NSE spectrometer addresses a very diverse scientific community over General User Program, the Partner-User Program and recently also thru Discretionary time. The SNS-NSE instrument can be used to answer scientific questions in a variety of fields like: soft-matter research, biophysics, condensed matter physics, materials science, chemistry, complex fluids, etc., being particularly suitable to unravel slow dynamical processes and molecular motions at nanoscopic and mesoscopic scale. Figure 12.9 shows the active research areas as of year 2019.

12.5 GENERAL USER PROGRAM

In the period 2017-2019 the SNS-NSE instrument ran for over 350 neutron production days. The number of General User proposals submitted and ran within this period is displayed in Figure 12.9. The acceptance rate for proposals submitted via the General User program is, on average between 40-50% of the submitted proposals, depending strongly of the total number of proposals submitted.

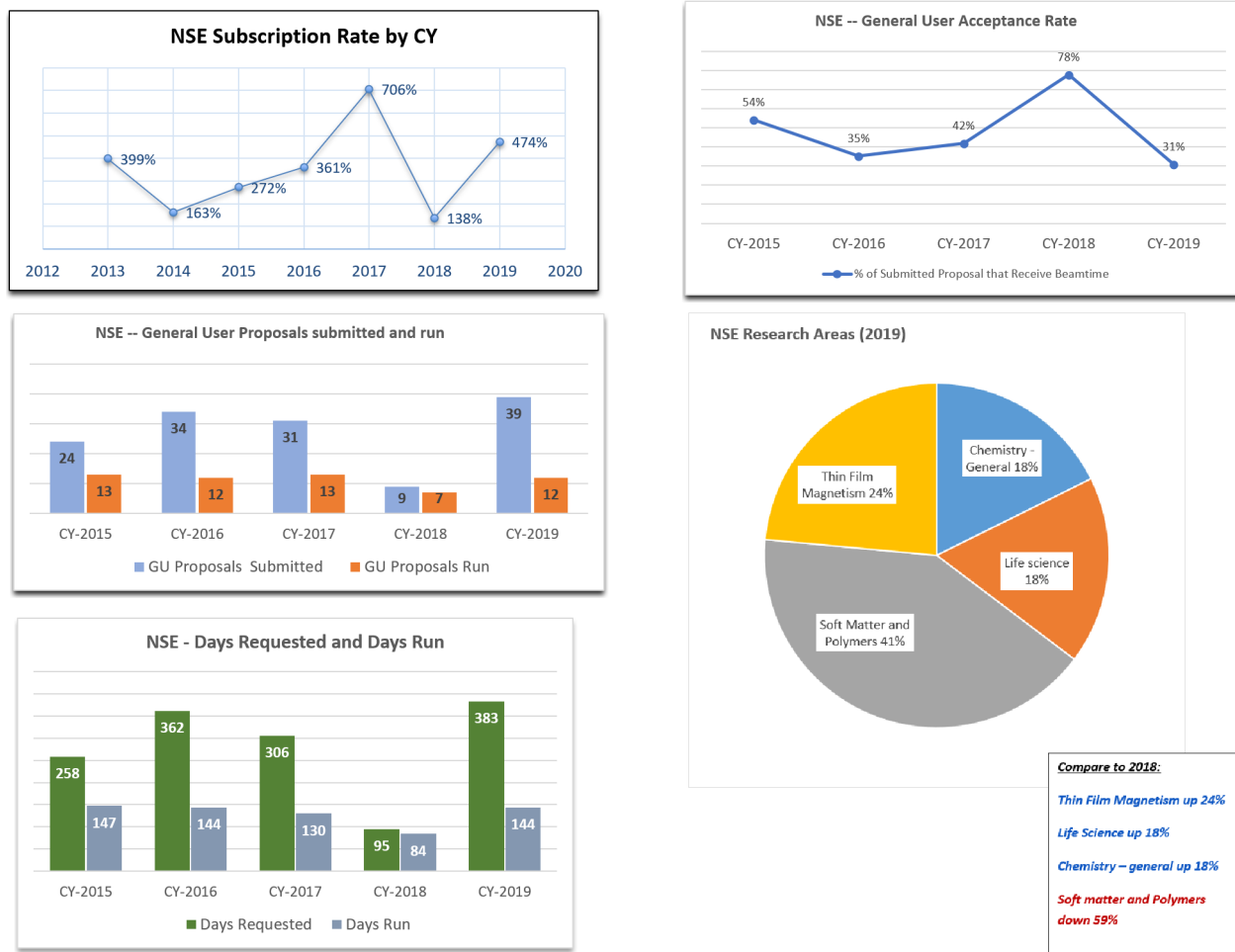


Figure 12.9. NSE user program statistics

12.6 UPDATES ON DISCRETIONARY AND PARTNER-USER PROGRAM

During the review period, the SNS-NSE spectrometer had no discretionary beam time for ORNL program development. 25% of the beam time was made available to users through the Partner User program for the Research Center Jülich in Germany and other German institutions, the main contributor and builder of the SNS-NSE spectrometer. Some of this beam time (up to maximum 10 days every year) is used to expand the instrument capabilities and further the science program of the instrument team members. Many of the SNS-NSE sample environment upgrades projects like *Temperature Forcing System*, *Electric Field Cell*, *Light cell*, *Tumbler*, *High-Pressure Cell*, as well as software upgrades came as a continuous effort of the NSE team and beam time thru Partner User program.

12.7 OUTREACH AND EXPANSION INITIATIVES

The neutron spin echo community, though relatively new in the United States, has enjoyed a healthy growth in recent years, and in particular there are strong needs for training graduate students and postdoctoral associates. The SNS-NSE team participates yearly in the DOE's National School on Neutron and X-Ray Scattering with a lecture on NSE technique: *"Introduction to Neutron Spin Echo Spectroscopy"* and with 3

days of hands-on experiments in order to demonstrate the neutron spin echo technique as well as the instrument capabilities to over 70 registered graduate students. The SNS-NSE team participates also yearly for the past 3 years in the workshop and neutron school in biology “Neutron Scattering Applications in Structural Biology” with invited talks on NSE science in biology, lecture on dynamics: “*Dynamics of soft matter and bio molecules probed by Neutron Scattering*” which is a general introduction in dynamics lecture, with focus on time-of-flight, back-scattering and spin echo spectroscopy techniques, as well as with practical experiments.

In 2018 Stingaciu organized the workshop entitled “*Soft and Bio-Materials Dynamics at the Nano- to Meso-Scale*”. The workshop discussions aimed to understand limitations and gaps between different dynamic techniques (especially Neutron Spin Echo and X-ray Photon Correlation Spectroscopy). The workshop had 63 registered participants with 58 participants present on site over the course of 2 days, representing 12 institutions:

ORNL, University of Cincinnati, NIST, University of Tennessee, BNL, Clemson University, LBNL ALS, APS ANL, Louisiana State University, SLAC Stanford University, Stony Brook University and FZJ-JCNS from Germany. In 2019 Stingaciu was co-organizer of the workshop “*Intrinsically Disordered Protein Regions in the Context of Polymer Physics*” a major research topic in structural biology. The workshop was inspired by questions related to how understanding synthetic polymer structure and dynamics can be useful for understanding IDRs, where NSE technique plays a major role.

Both instrument scientist at SNS-NSE (Stingaciu and Zolnierczuk) participate and present numerous posters and talks in national and international workshops and conferences on application of QENS in soft matter, as part of advertising SNS-NSE capabilities to the world-wide user community.

12.8 UPDATE ON INSTRUMENT DEVELOPMENT ACTIVITIES

The SNS-NSE underwent several upgrades over the past years in order to improve the overall instrument performance and broaden the flexibility and capabilities. The foremost improvements to overall instrument performance are the Support System Improvements. These started with the replacement of the old 120mm polarizing bender with the new kink polarizer from Swiss Neutronics that contributed to an improvement of flux for all wavelengths of ~16.9%. Other major Support System Improvements include:

- Installation of new data analysis workstation and new control workstation (Win10 PC) for supplementary sample environments
- Upgraded chopper 1 disc to carbon fiber
- Upgraded chopper controller PC and software
- Installed air cooling system and temperature sensors to choppers 1 and chopper 2
- Upgraded revolver software with added flexibility for testing of revolver function.

Most of the Sample Environment Improvements done at SNS-NSE over the past years were made for improving accessibility, safety, and accommodate science requests from our users. These include:



Figure 12.10. Group picture of the “Soft and Bio-Materials Dynamics at the Nano- to Meso-Scale” the NSE & XPCS Workshop @SNS.

- Humidity chamber implementation with required non-reactive atmosphere (nitrogen line setup), customized lock box for large quantities of D₂O, setup of computer for the sample environment controls outside enclosure
- Upgrade of cryo-furnace, its heating elements and sample can for reaching temperatures below 5K
- Upgrade of cryo-furnace lifting fixture to improve safety and ease of mounting and dismounting by users
- Upgrade of cryo-furnace storage cart to mitigate safety problems
- New upgraded sample holder for Temperature Forcing System (TFS), for better insulation and improve beam transparency
- New heater arm for TFS
- New mechanical holders fabricated to host grazing incidence cell
- New mechanical holders fabricated to manually adjust alignment of crystals into NSE spectrometer
- Work has begun on a new stretching device for polymer samples in the beam.

As part of the transition to ORNL an extensive effort has begun on Upgrades to Procedures and Oversight of the SNS-NSE spectrometer. These activities include:

- Inventory of all equipment, parts, tools, and supplies into a comprehensive set of online documents
- Set up cataloging system for cabinets and drawers for ease of reference when communicating
- Organize all parts, tools, and supplies, and record their storage locations
- Started detailed maintenance logs for equipment (compressors, choppers, heat exchanger, vacuum pumps, sample cells) to make them available for the SNS support groups
- Migrated maintenance of vacuum systems to the SNS support group. Ongoing projects include
- Migrating chopper support to SNS support group
- Testing new CAENels power supply for upgrades of the entire power system replacement of old Bruker power supplies
- Upgrading of superconducting coils temperature monitoring controls from current unsupported ones to new ones supported by SNS.

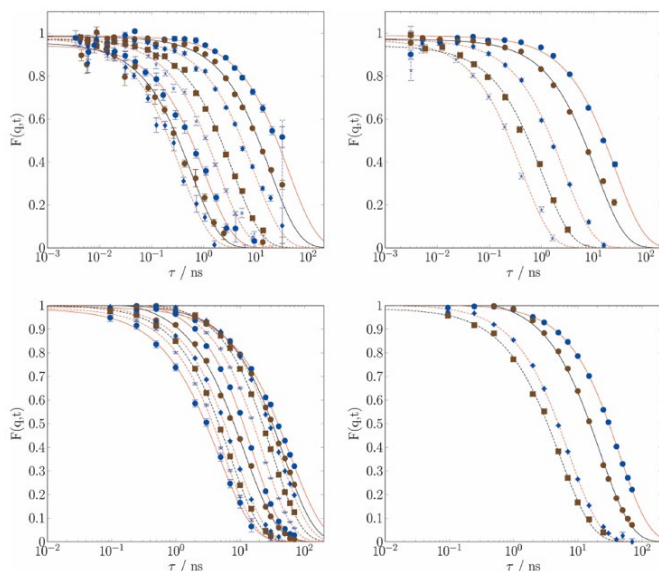


Figure 12.11. Sample reduction data obtained with DrSpine, the new data reduction software at SNS-NSE.

SNS-NSE Instrument Scientist Piotr Zolnierczuk and co-authors created a new dedicated software program called *DrSpine (Data Reduction for Spin Echo)* to address this issue and presented their results in [*J. Appl. Cryst.* (2019) 52:1022-1034]. The algorithms employed in *DrSpine* allow to extract the intermediate scattering function $S(Q,t)$ independent of the selected binning. In addition, the software can also reduce the data from NSE spectrometers installed at a continuous source, like J-NSE Phoenix at FRMII, Garching, Germany. The reduction software is available to users via the SNS analysis cluster with a quick guide, extended manual and help implemented in the program.

12.9 VISION

Near-term Vision (1-3 years)

Ensure that NSE reaches its full potential as a world class neutron spin echo instrument. It is clear that SNS-NSE spectrometer will continue to have a central role in the study of dynamics of soft matter (polymers, biopolymers, membranes, etc.) for the North American neutron user community as the only working NSE instruments in the United States. SNS-NSE team is working hard to expand the capabilities of the instrument. Upgrading, developing and deploying new sample environments is an immediate priority for the entire instrument team. Implementing a shear cell and rheometer, pressure cell, and extreme temperatures capabilities will open new possibilities for research. The hard-matter community has recently expressed great interest to employ SNS-NSE to study magnetic systems which typically require sample environment temperatures in the order of 10-3 K. A new cryostat with the possibility of mounting crystals including independent sample orientation along with development of a more compact software for magnetic data reduction is also part of our vision.

Data reduction and data analysis is also a high priority of the instrument team. The new reduction software *DrSpine* has been deployed to SNS analysis cluster with help from SNS Linux group and made available to users inside and outside ORNL network. Users are encouraged and trained constantly during their experiments at SNS-NSE to learn to reduce data and to get experience in manipulating the data reduction software. On short term, this will create further flexibility into accessing NSE data measured at SNS-NSE, and

New reduction software

Efficient data extraction from neutron time-of-flight spin-echo raw data

Neutron Spin Echo spectrometers operating at pulsed sources like SNS-NSE and employing time-of-flight technique are able to use broad wavelength band neutrons resulting in comprehensive sets of experimental data. With only a few instrumental settings one can cover, in a quasi-continuous way, a large range of wavevector and Fourier time space. Extracting all the information contained in the raw data and mapping them to a suitable physical space in the most efficient way presented a challenge to existing software reduction programs.

the NSE data reduction from, virtually, any part of the world. It will contribute to develop a more experienced and independent NSE user community.

The growing biology and biophysics user's community routinely needs to access instrument resolutions above 50 ns. While it is easily achievable with current SNS-NSE spectrometer capabilities in order to go above 50 ns, one has to operate the spectrometer in the 8 Å - 11 Å wavelength band, which has a flux lower than the most commonly used wavelength band of 5 Å - 8 Å. In order to increase the resolution at higher wavelength, we plan further to look into local technical improvements of the analyzer and polarizer system, as well as the flippers efficiency. Small gain in the polarize flux at the sample area and higher flipper and analyzer efficiency could result in an increase of the instrument productivity: the number of accepted proposals could increase as the time required to take data would shrink, and, in turn the number of publications per year would grow.

Upon full transition to ORNL and with the advantage of local support groups the transition to EPICS, new power supplies and new data acquisition software will also be implemented.

The trusted expertise of the NSE team presents the opportunity of running more and more mail-in type experiments, where users ship samples to SNS-NSE and perform the experiment virtually, by constant on-line chat with the instrument team. This is especially useful under recent developments of the COVID-19 pandemic and helps preserve and encourage our user community. Therefore, a reorientation toward some online form of neutron experiments that will require less physical onsite presence of the users is also part of our future vision.

Strategic Vision (3-10 years) and Alignment with NScD/ORNL Strategic Plans

The NSE will be key to a variety of scientific studies involving the understanding of detailed molecular surface structure. Complemented by the rapidly improving capabilities of molecular dynamics (MD) simulations available at ORNL, the SNS-NSE presents a unique experimental means for investigating slow dynamics in soft matter and biology to unravel molecular motions at mesoscopic length scales, such as molecular rheology of polymer melts, related phenomena in networks and rubbers, interface fluctuations in complex fluids, polyelectrolytes, transport in polymeric electrolytes and gel systems, and the molecular dynamics of proteins, phospholipid membranes and other biomolecules. The high resolution NSE spectrometer at SNS is also ideal for investigating spin-glasses, ferromagnets as well as the phase transitions emerging in the forefront of magnetism, like the quantum phase transitions in solid state physics and magnetism.

Real Space Investigation: Recently, the critical influence of the spatial discreteness at the molecular level on the phase behavior of complex fluids has been identified by computer simulation, confocal microscopy and small-angle neutron scattering measurements. The effect of the spatial heterogeneity on the dynamical characteristics has not been included in the current theories such as mode-coupling theory (MCT) or self-consistent generalized Langevin equation (SCGLE). The structure of a soft matter system can be defined in terms of the topology of molecular connectivity. The structural change occurs when the local topology of a constituent particle is changed by losing or gaining just one nearest neighbor, prompting the system to move from one potential energy landscape (PEL) minimum to another. Moreover, it has been discovered that the macroscopic Maxwell relaxation time is indeed equal to the characteristic time for bond breaking/formation at the microscopic length scale. This observation indicates the close connection between the rheological behavior of highly cooperative soft matter systems and local topological fluctuations.

It has been difficult to characterize such dynamical events using existing scattering techniques. This topological fluctuation is highly localized within a spatial range of around a particle diameter. For these highly localized dynamical processes, the information will be inevitably widely spread out in reciprocal Q space. Within the experimentally accessible Q range, the information on these local collective dynamics not only is partially concealed in the measured dynamical correlation functions, such as $F(Q, \tau)$ measured by NSE, but often also is masked by other dynamical processes such as the phonon-like longitudinal diffusion. In this regard, this newly revealed localized dynamical process is hardest to identify based on the current experimental protocol.

The unique combination of a wide dynamic range with a large spatial range of NSE at SNS provides an ideal tool to investigate the localized dynamical processes occurring at the microscopic length scale. The intermediate scattering function, $F(Q, \tau)$, can be Fourier-transformed to real space into the Van Hove function, $g(r, t)$. Such conversions are possible only today with the NSE which provide data of $F(Q, \tau)$ over a wide enough Q , approximately two orders of magnitude from 0.04 \AA^{-1} to 4 \AA^{-1} , to allow accurate Fourier transformation. Combining the improved instrument hardware such as optimized polarizers and analyzer with advanced data analysis algorithms and theoretical and modeling efforts to take full advantage of instrument capabilities, the at SNS-NSE offers an unprecedented opportunity for experimentally investigating the critical topics of localized dynamics in different fields of condensed matter such as the entanglement dynamics in polymer melts, hydrogen bonding dynamics in water and its confined state, and influence of elastic heterogeneity in the rheological behavior of molecular and metallic glasses.

Driven by the NSD goal to establish and sustain a science culture of innovation and communication that continuously improves neutron scattering scientific impact and productivity, we also strategize and advocate strongly for building an “**Neutron Spin Echo Center of Excellence @ ORNL**” within the next 5 to 10 years, with two high resolution NSE spectrometers, with complementary characteristics separated by scientific applications. Our strategy is divided in two major phases: maintaining and operating the actual SNS-NSE @ BL15 instrument while building a high resolution monochromatic NSE spectrometer @ HFIR, after the new core vessel upgrades. This long-term strategy is already discussed and proposed by the NSE focus group: Stingaciu, Laura R.; Zolnierczuk, Piotr A.; Ehlers, Georg; Urban, Volker S.; Fitzsimmons, Michael R.; Heller, William T.; Chen, Wei-Ren; Herwig, Kenneth W.

12.10 FUNDING/RESOURCE NEEDS

The SNS-NSE operates with a staff of 3 full time employees – two Instrument Scientists and one Scientific Associate. The scientists support an equal number of user experiments. Beyond user support, the instrument scientists pursue their own scientific programs. The scientific associate divides her time among user support, instrument operations, maintenance, repairs, and development. Funding for the instrument and team are still shared between Forschungszentrum Jülich and Oak Ridge National Laboratory, pending a full transition to ORNL by the end of 2020. The instrument, two staff members, all equipment and support for equipment, support for crafts, union work, administrative support, and all other services provided to users are currently supported by ORNL.

For daily operation of the SNS-NSE spectrometer the old Brüker power supply system that supplies current to all the coils of the instrument will need to be upgraded in the near future. The system was built using circuit board technology from the late 1970s and a design based on an inter-device control logic that introduces multiple parallel failure modes, requires a large and complex store of spare parts, and complicates trouble shooting and restoration of operation. In 2013, Brüker sold their power electronics business to SigmaPhi. During this transition, much of the expertise related to this system and components

was lost. In preparation for this event the stock of spare parts at the beam line was increased to extend the operational lifetime for the system in the face of obsolescence. SigmaPhi discontinued the product line and support has also been inadequate. In the past 3 years, many spares have been used, and replacements are now unavailable.

The testing of a new system manufactured by CAENels has recently begun. These power supplies offer stability, resolution, and operational flexibility for the applications demanded by NSE spectrometer equivalent to the highest quality and most expensive units in the world at a very reasonable price. Each unit is a self-contained power supply and controller with digital display that enables quick and simple testing, troubleshooting and restoration of operation. The cost for such a system to be designed, tested, and installed at SNS-NSE should be on the order of \$300,000. This investment would help ensure reliable continuity of operation of the SNS-NSE for the coming years. Both FZJ and ORNL are committed to help with this investment.

12.11 SELF-ASSESSMENT

Strengths

Our biggest strength is the technical uniqueness of the design of SNS-NSE spectrometer and its situation at the Spallation Neutron Source. SNS-NSE is world-wide, the first neutron spin echo spectrometer built on superconducting technology. This ensures a highly homogeneous magnetic field for the neutrons spin precession. SNS-NSE spectrometer encodes tiny velocity changes that neutrons suffer during the scattering process into their spin precession angle. This allows the use of a broad velocity distribution in the incoming beam. Both these unique features of SNS-NSE result in a large flux of polarized neutrons at the sample position. At a pulsed spallation source this property causes a decoupling of the proper spin-echo resolution in terms of Fourier time from the time-of-flight wavelength resolution that depends on the effective neutron pulse duration. A system of 4 choppers ensures that no unwanted neutrons are transmitted at the 60 Hz pulse repetition of the source for any of the variations in instrument length operational position (18 m - 28 m) that are used for a wide angular coverage. In addition to these (and many other) technical advantages, the instrument team of SNS-NSE spectrometer is fully dedicated in utilizing the instrument full potential to advance its scientific mission.

Weaknesses/Limitations

In contrast to direct spectral filtering where only those neutrons with a well-defined energy reach the detector, the Fourier transformation property of the measuring principle of neutron spin echo implies that at any NSE spectrometer settings, virtually 50% of the neutrons that are scattered into the detector direction are counted. As a consequence, weak but rather important spectral features are buried under the counting noise caused by the-integrated neutron flux. Therefore, reasonable performance is expected only for relaxation type scattering contributing at least several percent of the total scattering in the considered direction. This is our bigger limitation that creates a drastic selectivity in the type and volume of the samples and experiments that can be ran at SNS-NSE, limitation which comes mostly from the physics of scattering polarized neutrons rather than from instrumental limitations. Operating software of the SNS-NSE for data acquisition was identified also as a limitation in the overall user experience. The uniqueness and the complexity of SNS-NSE spectrometer is at times frightening to users and the instrument team needs to be full-time involved in almost every user experiment.

Opportunities

By continuous development of the data reduction software, SNS-NSE unique capabilities can be harnessed to enable flexible and robust time-of-flight slicing of the data and reach currently inaccessible time and space domains for most of the other spectrometers. The new dedicated software program called *DrSpine* is constantly updated to keep up with NSE user community needs. A big opportunity lies in the development of a GUI type, user-friendly interface for the data reduction software. Significant opportunities lie also in the technical development of several sample environments to support users in tackling scientific questions that required the use of high voltage electric field, sample tumbling, rheology, magnetic scattering, use of high pressure or extreme temperatures. The general user community could also take great advantage from increasing the polarized flux and the opportunity of using smaller sample volumes. Reaching out to universities, conferences and workshops creates the opportunity to expand our user community and attract new and challenging experiments that will push further the scientific vision of SNS-NSE. Also, the length of an NSE experiment and the trusted expertise of the NSE team present the opportunity of running more mail-in type experiments, where users ship samples to SNS-NSE and perform the experiment virtually, by constant on-line chat with the instrument team. This is especially useful opportunity under recent developments of the COVID-19 pandemic and helps preserve our user community.

Threats

Unforeseen complications in financial support for large technical upgrades will produce significant drawback in serving the well-established US user community. Competing instruments available at JPARC, ILL, FRM2 and NIST, continue constantly their race in technical enhancements and upgrades. Phoenix J-NSE spectrometer at FRM2 has already surpassed our spectrometer by using the same superconducting technology but superior design for the main precession coils. Newly financed upgrade project of the NIST NSE spectrometer and their constant collaboration with FZJ aims to implement the same identical upgrades at NIST as Phoenix J-NSE. The high specificity of some of the SNS-NSE electrical and mechanical components is also one of our biggest concern, since several parts of the spectrometer are built on prototype-like components with less or no number of spares available for immediate replacement. Future priorities of the beam line staff include the implementation of more standard, easy – purchasable technical components into SNS-NSE design to ensure its flexibility and constant functionality at high-standard parameters.

12.12 FUTURE FUNDING OPPORTUNITIES

Upon expiration of the Jülich agreement the SNS-NSE instrument was evaluated for performance, output, as well as unique scientific contributions. Continued operation was determined to be the optimum situation to support the growing user program. ORNL is strongly committed to support SNS-NSE as full-time instrument in the General User program. We also foresee the opportunity to team with users in larger funding efforts to produce more unique and exotic sample environments which may become part of the ORNL sample environment suite. These types of collaborations will position the instrument team to participate in future funding calls.

12.13 EXECUTIVE SUMMARY

The Neutron Spin Echo technique is in high demand and has the potential for increased throughput. The scientific program continues to grow in scope and diversity. With recent technical upgrades, new data reduction software and the development and integration of sophisticated sample environments a more intuitive NSE instrument, for expert and novice users alike is available in the user program. Our scientific

throughput demonstrated the power and potential of the SNS-NSE instrument. Further software developments and technical upgrades will expand the instrument capabilities and reduce data acquisition time. SNS-NSE will continue to be the most important tool for the high-resolution slow dynamics studies of biological, soft matter and even hard condensed systems, for the next several years.